STRUCTURAL BEHAVIOUR OF STEEL FIBRE REINFORCED CONCRETE MEMBERS

Hassan Aoude

Doctor of Philosophy

Department of Civil Engineering and Applied Mechanics

McGill University

Montreal, Quebec, Canada

December 2007

A THESIS SUBMITTED TO THE FACULTY OF GRADUATE STUDIES AND RESEARCH IN PARTIAL FULFILMENT OF THE DEGREE OF DOCTOR OF PHILOSOPHY

DEDICATION

In the name of God, the most merciful, the most compassionate

This thesis is dedicated to my parents who sacrificed all in the pursuit of what is best for their children

ACKNOWLEDGMENTS

Foremost I must thank God for facilitating the completion of this work.

I would like to express my utmost gratitude and appreciation to Professor Denis Mitchell for his guidance, patience and encouragement during this research programme.

The assistance and advice of Dr. William Cook was invaluable and was greatly appreciated.

The research presented in this thesis was carried out in the Jamieson Structures Laboratory at McGill University. I would like to expresses my gratitude to Marek Przykorski, Ron Sheppard, Damon kiperchuk and John Bartczak. The assistance of Dean Macdougall, Rita Menneh, Andrew Salzberg, Lama Baali and Mehdi Belghiti during the construction and testing of the specimens was also greatly appreciated. I would also like to express my thanks to the professors of the Department of Civil Engineering and Applied Mechanics of McGill University. The assistance of the office staff is also gratefully acknowledged.

The donation of materials by Bekaert Steel Wire Co. was appreciated. Thanks are also given to Luc Lemoyne (Bekaert) and Jean-Francois Dufour (King Materials) for their practical guidance during the experimental work.

The financial assistance provided by the Fonds Quebecois de la Recherche sur la Nature et les Technologies (FQRNT) and the Natural Sciences and Engineering Research Council of Canada (NSERC) was highly appreciated.

Finally, I would like to thank my mother, my father and my brothers for their understanding, constant encouragement and tremendous support. This thesis could not have been completed without them.

Hassan Aoude

December, 2007

LIST OF SYMBOLS

A_a	Initial slope of the descending branch of the buckling curve
A_c	Net cross-sectional area of concrete in RC tension member
A_{ch} , A_{core}	Cross-sectional area of RC column core
A_{cover}	Cross-sectional area of the cover in RC column
A_f	Cross-sectional area of fibre
A_g	Gross cross-sectional area of RC column
A_{ineff}	Ineffectively confined core area in RC column
A_{KE}	Effectively confined core area in RC column
A_{net}	Net concrete area in RC column
A_s	Cross-sectional area of steel reinforcement
A_{sh}	Total transverse steel area within the spacing s in RC column
A_{shy}	Total cross-sectional area of transverse reinforcement perpendicular to one direction
A_v	Transverse reinforcement cross-sectional area in RC beam
$\frac{a}{d}$	Shear span to depth ratio in RC beam
b_w	RC beam web width
c_x , c_y	Widths of the concrete core parallel to the x and y axis
d	Effective depth of RC beam
d_b	Nominal bar diameter of steel reinforcement
d_f	Diameter of fibre
d_v	Effective shear depth of the beam
E_c	Modulus of elasticity of plain concrete
E_s	Modulus of elasticity of longitudinal steel reinforcement
E_S	Modulus of elasticity of transverse steel reinforcement

E_{sh}	Initial slope of steel reinforcement strain hardening curve
$f_c^{'}$	Specified compressive strength of concrete
f'_{co}	Peak concrete cylinder compressive strength
$f_{cc}^{'}$	Peak confined concrete compressive strength
f_{cc}	Confined concrete compressive stress at a given strain
f_{cf}	Compressive stress of fibre reinforced concrete at a given strain
f'_{cu}	Peak unconfined concrete compressive strength
f_{cu}	Unconfined concrete compressive stress at a given strain
$f'_{cu\,f}$	Peak unconfined concrete compressive strength adjusted for the presence of fibres in the concrete mix
$f'_{cc\,f}$	Peak confined concrete compressive strength adjusted for the presence of fibres in the concrete mix
f_{cr}	Concrete cracking stress
f_f	Confining pressure provided by the steel fibres
f_{fib}	Effective confining pressure provided by the steel fibres
f_{hcc}	Stress in transverse steel reinforcement at maximum strength of confined concrete
f_{hy}	Yield stress of transverse reinforcement
$f_l^{'}$	Lateral confining pressure
f'_{le}	Effective confinement pressure that acts on column core
$F_{pullout}$	Maximum pullout load of a single fibre
f_r	Modulus of rupture of concrete
f_s	Axial stress in longitudinal steel reinforcement
f_{sp}	Concrete splitting tensile strength
FT	Flexural toughness factor
f_u	Ultimate stress of longitudinal steel reinforcement
f_y	Yield stress of longitudinal steel reinforcement

f_{fy}	Fibre tensile strength
Δf_{cf}	Increase in concrete strength due to fibre confinement
G_{fo}^{Fe}	Fracture energy of plain concrete
G_{f}^{Fe}	Fracture energy of SFRC
h	Height of RC beam
h_c	Cross-sectional dimension of column core
h_o	Fibre dimension which is a function of hook geometry
h_x	Maximum horizontal centre-to-centre spacing between longitudinal bars on all faces of column that are laterally supported by seismic hoops or crosstie legs
I'_E	Ratio of effective confinement pressure that acts on the RC column core
I_{Eo}	Earthquake importance factor
k	Parameter that controls the slope of ascending branch of the stress-strain curve of confined concrete
k_1 , k_2	Parameters that control the curvature of descending branch of the stress-strain curve of confined concrete
K_e	Confinement effectiveness coefficient
k_{f1} , k_{f2}	Parameters used to define the descending branch of SFRC stress-strain curve
k_n	Factor accounting for the number of longitudinal bars in RC column
k_o	Fibre dimension which is a function of hook geometry
k_p	Factor accounting for compression in column or wall
L	Unsupported length of longitudinal steel reinforcing bar
L/d	Unsupported length-to-bar diameter ratio of longitudinal steel reinforcing bar
L_f	Length of fibre
$L_{f,straight}$	Length of straight portion of fibre neglecting the hooks
M_f	Factored moment applied to RC member

M_v	Factor that accounts for higher mode effects on base shear
n	Parameter that describes the shape of SFRC stress-strain diagram
η_l	Length factor that accounts for variability in fibre embedment length
n_l	Total number of longitudinal bars in a cross-section that are laterally supported by the corner of hoops or seismic crossties
n_2	Factor that accounts for half the fibres crossing the cracking plane
N_c	Axial load carried by concrete during tensile test
N_{fibres}	Effective number of fibres per unit area
N_s	Axial load carried by steel reinforcement during tensile test
N_{total}	Total number of fibres in concrete cross-section
P_1	Load at onset of complete debonding during fibre pullout
P_2, P_3	Load plateau at end of first hook contribution during fibre pullout
P_4	Load plateau at end of second hook contribution during fibre pullout
P_c	Axial load carried by concrete
$\frac{P_{c,cover}}{P_{co}}$	Normalized axial load carried by cover
$P_{c,nc}$	Axial load carried by the concrete in columns constructed without cover
P_{calc}	Peak load capacity of column computed using analytical equations
P_{crit}	Load that causes debonding to commence during fibre pullout
P_e	Volume percentage beyond which the efficiency of the fibres is improved due to a positive group effect
P_{exp}	Peak load capacity of column from experiment

P_f	Maximum factored axial load on column for earthquake loading cases
P_{fm}	Volume percentage beyond which the efficiency of the fibres ceases to improve
P_{ineff}	Load contribution of fibres at a given strain in the ineffectively confined core area of RC column
P_n	Normalised axial load carried by RC column ($\frac{P_c}{P_{co}}$)
P_o	Nominal axial resistance of the column at zero eccentricity
P_{total}	Peak axial load sustained by RC column
$\Delta P'$	Mechanical pullout load contribution of hook due to the formation of two plastic hinges
$\Delta P''$	Mechanical pullout load contribution of hook due to the formation of one plastic hinge
R_o	Over-strength related force modification factor
R_d	Ductility-related force modification factor
r_f	Fibre radius
RI	Steel fibre reinforcing index
s	Center-to-center spacing of transverse steel reinforcement in RC member
s'	Clear spacing between transverse reinforcement
S_x	Longitudinal spacing of transverse reinforcement
s_{ze}	Effective crack spacing parameter
$S(T_a)$	Design spectral response acceleration
T_a	Fundamental period of building
T_{fib}	Fibre tensile load contribution in SFRC tension member
TR_{cf}	Toughness ratio of fibre reinforced concrete
TR_c	Toughness ratio of plain concrete
V	Lateral earthquake force
V_c	Concrete contribution to shear resistance

V_{exp}	Experimentally obtained shear resistance
v_f	Volume fraction of fibres in the concrete mix
V_f	Factored shear applied to RC member
V_{fib}	Fibre contribution to shear resistance
$V_{fib,eff}$	Effective fibre contribution to shear resistance
V_m	Maximum shear capacity sustained by beam
V_n	Nominal shear resistance
$V_{n\,CSA}$	Shear resistance of beam neglecting the effect of the fibres as computed using the CSA general method
V_{nf}	Shear resistance of the beam including the influence of the fibres
$V_{n\,MCFT}$	Shear resistance of beam neglecting the effect of the fibres as computed using the MCFT
V_{no}	Shear resistance of beam neglecting the effect of the fibres
V_r	Factored shear resistance
V_s	Transverse steel contribution to shear resistance
W	Dead load on the building, including snow and partition load effects
w_f	Weight fraction of fibres in the concrete mix
$\sum w_i^2$	Sum of the squares of the clear spacings between adjacent longitudinal bars
Δ_1	Slip of the fibre at full-debonding.
Δ_3	Slip of the fibre at load P_3 during pullout
Δ_4	Slip of the fibre at load P_4 during pullout
Δ_{cr}	Displacement corresponding to elastic cracking strain of the concrete
Δ_m	Beam mid-span deflection at ultimate shear capacity
Δ_{max}	Beam mid-span deflection at failure
Δ_{tra}	Transverse displacement during buckling of longitudinal steel reinforcing bar

Δ^{*}_{tra}	Constant equal to 4% of the unsupported length of the longitudinal steel reinforcing bar
α	Fibre orientation factor
α_{eff}	Effective fibre orientation factor
α_{v}	Shear factor used to scale pullout resistance of fibres in combined tension and shear
β	Factor accounting for shear resistance of cracked concrete
β_{1}	Material parameter that controls shape of SFRC stress-strain diagram
β_{t}	Tension stiffening factor
ε_{avg}	Average axial strain in longitudinal steel reinforcement
ε'_{c50c}	Post-peak strain measured at 50% of maximum confined stress
ε'_{c50u}	Post-peak strain measured at 50% of maximum unconfined stress
ε'_{cc}	Peak confined concrete compressive strain
ε_{cc}	Confined concrete compressive strain at a given stress
ε_{cf}	Compressive strain of fibre reinforced concrete at a given stress
$\varepsilon_{c,i}$	Initial member strain for the condition of zero axial load
ε_{cr}	Elastic strain in concrete at cracking
ε'_{cu}	Peak unconfined concrete compressive strain
ε_{cu}	Unconfined concrete compressive strain at a given stress
ε_{s}	Average axial strain due to axial stress in longitudinal steel reinforcement
ε_{shr}	Free shrinkage strain in concrete
ε_{sh}	Strain corresponding to the commencement of strain hardening
ε_{spall}	Strain at which SFRC cover spalling is effectively complete
ε_{tf}	Idealized concrete strain caused by a given tensile stress

ε_{tra}	Average axial strain due to transverse displacement in longitudinal steel reinforcement
ε_u	Ultimate strain of longitudinal steel reinforcement
ε_x	Average longitudinal strain at mid-depth of beam
κ	Parameter that determines if yielding of transverse reinforcement occurs
κ_{eff}	Empirical fibre participation factor to shear resistance
η	Normalized SFRC compressive stress
ρ	Reinforcing steel ratio in tension member
ρ_c	Ratio of longitudinal steel reinforcement in concrete column core
ρ_{sey}	Effective sectional ratio of confinement reinforcement in the y direction
τ_{bond}	Bond shear strength
μ	Frictional coefficient of fibre-matrix interface
θ	Angle of inclination of diagonal compressive stresses to the longitudinal axis of the member
θ_a	Parameter used in the computation of ε_{tra}
ϕ_c	Material resistance factor for concrete
ϕ_s	Material resistance factor for steel
λ	Factor that accounts for the use of light-weight concrete
σ_c	Post-cracking stress in the concrete at a given tensile strain
σ_{fib}	Fibre tensile stress contribution in SFRC member
σ_{sfrc}	Stress in SFRC at a given tensile strain
Ψ	Cover spalling factor in SFRC
Ω	Pullout factor
$\Omega_m, \Omega_1, \Omega_2, \Omega_3, \Omega_4$	Normalized loads defined in the fibre pullout curve

TABLE OF CONTENTS

LIST OF TABLES

LIST OF FIGURES

ABSTRACT

A series of full-scale axial compression tests was conducted on RC and SFRC columns. The specimens, which were detailed with varying amounts of transverse reinforcement, were cast using a self-consolidating concrete (SCC) mix that contained various quantities of fibres. The results demonstrate that the addition of fibres leads to improvements in load carrying capacity and post-peak response. The results also show that the addition of steel fibres can partially substitute for the transverse reinforcement in RC columns, thereby improving constructability while achieving significant confinement. Analytical models for the prediction of the load-strain response of SFRC columns are presented and validated with the experimental results.

The tensile behaviour of SFRC members reinforced with a single reinforcing bar was also studied. The results indicate that the addition of fibres leads to improvements in tension stiffening and crack control. A procedure for predicting the response of tension members, accounting for the presence of fibres, is presented.

Experimental investigations were carried out on a series of RC and SFRC beams. The effects of steel fibres on shear capacity, failure mechanism and crack control are studied. The results show that the addition of steel fibres leads to improvements in load carrying capacity and can lead to a more ductile failure. A simple procedure that can be used to predict the ultimate shear capacity of SFRC beams is introduced and validated using results from other researchers.

ABRÉGÉ

Une série d'essais a été réalisée sur des poteaux de taille réelle soumis à des charges axiales. Les échantillons, qui avaient des quantités variables d'armature transversale, ont été construits en utilisant un béton auto-plaçant qui contenait une quantité variable de fibres métalliques. Les résultants de cette étude expérimentale démontrent que la présence des fibres influence positivement la capacité portante des poteaux. De plus, les résultats montrent que l'utilisation d'un béton renforcé de fibres métalliques (BFM) peut s'avérer une solution appropriée pour assurer une ductilité adéquate aux poteaux. L'auteur propose des modèles analytiques pour prédire le comportement de poteaux chargés uniaxialement.

Le comportement sous tension d'éléments en BFM armés d'une seule barre a été étudié. Les résultats montrent que la présence de fibres améliore la résistance en tension. Une procédure pour la prédiction de la réponse des éléments soumis sous tension, prenant en compte la présence de fibres métalliques, est présentée.

Des recherches expérimentales furent entreprises afin d'étudier le comportement de poutres sans étriers. L'influence de la présence de fibres sur le développement de fissures ainsi que les mécanismes de ductilité et de rupture est discutée. Les résultats montrent que l'ajout de fibres améliore la capacité portante et la ductilité des poutres. Une procédure est suggérée afin de déterminer la capacité portante de poutres construits avec BFM.

Chapter 1 Introduction

1.1 Introduction

Research has shown that the addition of steel fibres can improve many of the properties of concrete elements including tensile resistance, fracture toughness and crack control. These enhancements in performance result from the influence of the randomly oriented fibres in arresting cracks and the resulting improvements in the post-cracking resistance of the concrete. Although a large body of research on the structural applications of steel fibre reinforced concrete (SFRC) exists, the potential of using this material in load-carrying structural elements has yet to gain wide acceptance in construction.

One of the possible applications of SFRC is in reinforced concrete (RC) beams that are shear critical. The addition of fibres can potentially partially substitute for conventional shear reinforcement.

Another possible application involves the use of SFRC in reinforced concrete columns. In the case of RC columns, modern design codes impose stringent requirements for confinement with transverse reinforcement in order to ensure ductile performance. For seismic design, these requirements often result in highly congested columns that may cause problems during construction. The use of SFRC in such columns may allow for a reduction in the amount of transverse reinforcement, leading to improved constructability.

One of the drawbacks associated with SFRC is that the addition of fibres to traditional concrete can cause problems in workability when high fibre quantities are used (1% and above) and in situations where high ratios of steel reinforcement are used. One innovative approach may lie in the combined use of SFRC and a highly flowable self-consolidating concrete (SCC) to improve workability and facilitate placement.

This thesis reports the results of a research program that was undertaken in order to investigate the potential benefits that can arise from the use of steel fibre reinforced concrete in structural elements such as RC columns and beams. One of the innovations involved the combination of steel fibres with a highly flowable SCC mix.

1.2 Research Program Objectives

The purpose of this research program is to perform an experimental and analytical study on the performance enhancements that can be gained from the use of steel fibres in reinforced concrete members. An additional objective is to examine if the provision of steel fibres would permit a reduction of transverse reinforcement in the key regions of RC elements.

1.2.1 Experimental Program

In the experimental program, the objectives are to investigate the following behavioural aspects:

(i) the influence of steel fibres on the axial response of RC columns, including:
- peak load carrying capacity
- post-peak ductility
- delay of cover spalling

(ii) the influence of steel fibres on the tension stiffening response of concrete

(iii) the influence of steel fibres on the shear response of RC beams, including:
- shear resistance
- crack control

1.2.2 Analytical Program

In the analytical program, which complements the experimental results, the objectives are the following:

(i) to develop a model that can predict the compressive load-strain response of columns constructed with SFRC

(ii) to develop a model that can predict the influence of fibres on tension stiffening

(iii) to develop a simple procedure that can predict the maximum shear resistance of beams constructed with SFRC

1.3 Thesis Organization

The thesis first begins with a state-of-the-art review of the various topics that are treated in the thesis (Chapter 2). Thereafter, the thesis details the three main phases of the research program:

1. The first phase of the research program investigates the behaviour of steel fibre reinforced concrete columns subjected to axial loading:
   - Chapter 3 summarizes the various aspects of the testing program
   - Chapter 4 presents the results from 21 full-scale column specimens tested under pure axial loading
   - Chapter 5 analyzes the results and details the benefits that result from the use of SFRC in columns
   - Chapter 6 presents an analytical model that can be used to predict the complete load-strain response of columns constructed with SFRC
2. The second phase of the research program investigates the behaviour of steel fibre reinforced concrete members subjected to pure tension:
   - Chapter 7 summarizes the various aspects of the testing program
   - Chapter 8 presents and analyzes the results from 3 specimens tested under pure tensile loading
   - Chapter 9 presents an analytical model that can be used to predict the tension stiffening response of SFRC
3. The third phase of the research program examines the behaviour of steel fibre reinforced concrete beams subjected to shear:
   - Chapter 10 details the various aspects of this phase of the experimental program
   - Chapter 11 presents and analyzes the results from tests on 3 full-scale beam specimens
   - Chapter 12 presents an analytical model that can be used to predict the shear resistance of SFRC beams

Chapter 13 provides some concluding remarks regarding the experimental and analytical work.

Chapter 2 Literature Review

2.1 Chapter Overview

This chapter presents a comprehensive review of the literature regarding the various topics that will be studied in this thesis.

The literature review will begin with a description of the concept of using steel fibre reinforced concrete as a structural material and will summarize some of the mechanical properties (Section 2.2).

Section 2.3 will introduce the concept of using steel fibres in combination with self-consolidating concrete (SCC).

Section 2.4 will summarize some of the methods that can be used to predict the behaviour of RC columns and will present a summary of some of the past research that has focussed on the use of steel fibres in RC columns.

Section 2.5 reviews past research on the use of steel fibres to improve the shear resistance of beams.

2.2 Steel Fibre Reinforced Concrete

Plain unreinforced cement based materials such as concrete are brittle and are prone to cracking when subjected to relatively small tensile stresses. Since the advent of modern construction this deficiency has been solved with the use of continuous steel reinforcing bars which are strategically placed to withstand tensile and shear stresses in the structural member, resulting in an efficient composite system that can be used to build our structures.

The brittle nature of traditional concrete has also fuelled the interest in developing fibre reinforced concretes since the random orientation of the discrete fibres in a cement based matrix can lead to improved toughness and tensile properties.

This section of the literature review begins with an introduction to the concept of using steel fibre reinforced concrete for structural applications (Section 2.2.1). Section 2.2.2 presents some of the methods that can be used to account for fibre pullout in SFRC. Sections 2.2.3 and 2.2.4 present a summary of the behaviour of SFRC in tension and compression respectively. Finally, Section 2.2.5 outlines some of the current standardized methods for characterizing SFRC toughness.

2.2.1 Introduction to SFRC

2.2.1.1 Definition of SFRC

Steel fibre reinforced concrete (SFRC) is a composite material whose components include the traditional constituents of Portland cement concrete (hydraulic cement, fine and coarse aggregates, admixtures…) and a dispersion of randomly oriented short discrete steel fibres.

The development of steel fibre reinforced concretes began in the early 1960s (Li, 2002). Since then, the use of SFRC has gathered great interest, with research demonstrating the potential benefits that may lie in the use of the material in both structural and non-structural applications.

2.2.1.2 Main advantages associated with the use of SFRC

Steel fibres were originally developed in view of trying to strengthen the concrete matrix, however it is now understood that fibres do not typically alter the strength properties of the matrix (Li, 2002). Rather, the major role of the fibres is to improve the crack control and to alter the post-cracking behaviour of the cement based matrix (Banthia and Mindess, 1995). Hence, the main benefit that arises when fibres are added to the matrix is with respect to improvements in the energy absorption properties of the material and the ability of the material to carry tensile stresses after crack initiation. Other advantages associated with SFRC include improved impact resistance, improved fatigue resistance and improved durability against shrinkage cracks (Li, 2002).

2.2.1.3 Current applications of SFRC and code guidance

There is a wide range of possible structural applications for SFRC including the use of fibres to improve shear resistance. Other possible applications include the use of fibres to enhance the seismic resistance of structural members such as RC columns. Figure 2.1 highlights some of the potential structural and semi-structural applications for SFRC.

Although there has been much research into the potential use of SFRC in structural members, the current use of steel fibres has been limited to non-structural applications. For instance, fibres are used for controlling cracks in structures such as industrial slabs, pavements and concrete containers (Li, 2002). Another current application involves the use of steel fibres with shotcrete in tunnel mining applications.

There is limited use of SFRC in structural applications, partly due to the increased cost of steel fibres and the conservative nature of the construction industry (Li, 2002). Furthermore, despite extensive research and development, to this point, most modern design codes do not provide guidance for structural engineers with respect to the use of SFRC as a structural material. The lack of design specifications makes it difficult for engineers to use SFRC in structural applications.

2.2.1.4 Factors affecting fibre efficiency

The types of steel fibres available on the market vary in shape and size. Figure 2.2 shows some typical fibres. Fibres are normally deformed at their ends or crimpled along there length in order to improve their pullout and bond characteristics. Among the most popular steel fibre typologies are hooked-end fibres such as those produced under the Dramix brand (see Fig. 2.3).

Typical fibre lengths are in the range of 10 to 60 mm. Cross-sections are normally round while rectangular cross-sections are sometimes used. For round fibres, the cross-section diameter is typically in the range of 0.4 to 1 mm (Minelli, 2005).

The fibre content in traditional concrete mixes is usually in the range of 20 to 120 kg/m^3 or 0.25% to 1.5% by volume (Johnston, 2001), with lower fibre dosages used in the present industrial applications such as in the case of slabs on grade, while structural applications usually require fibre contents greater than 0.5% by volume.

The main characteristics that will influence the mechanical properties of fibre-reinforced composite are (Minelli, 2005):

- Type of fibre (cross-sectional shape, anchorage properties…)
- Aspect-ratio (L_f / d_f)
- Fibre dosage
- Strength of the concrete matrix

2.2.1.5 Mixture proportioning and factors affecting workability

It should be noted that for the type of concrete mix that is used (size of coarse aggregate and gradation, water cement ratio, etc…) there will be a limiting fibre content in order to ensure proper dispersion of the fibres in the concrete mix (Minelli, 2005). Hence in the choice of fibre content and fibre properties one must balance the required level of performance with the needed level of workability.

For instance, with traditional concrete mixes, a fibre volume greater than 1% will usually lead to an unworkable material that will lead to problems during placement.

2.2.2 Pullout strength of steel fibres

2.2.2.1 Pullout strength based on shear bond strength

For straight round fibres, the average pullout force can be approximated using Eq. 2-1 if one assumes a constant bond shear strength, τ_{bond}, along the length, L_f, of the fibre (Hannant, 1978).

$$F = \tau_{bond} \times \pi \times d_f \times \frac{L_f}{2} \qquad \text{2-1}$$

The parameter d_f is the diameter of the fibre and τ_{bond} is the bond-shear strength, which is a function of the matrix properties.

It should be noted that deformed or hooked-end fibres will have an improved pullout resistance when compared to straight fibres due to a mechanical contribution during pullout (Alwan et al., 1991). Hence, for such fibres, one should include a way of accounting for the mechanical work of the fibre during pullout. For instance, one approach is to use a bond factor to scale the contribution depending on the typology of fibre that is used (for example see Imam et al. (1997)).

2.2.2.2 Mechanical contribution to pullout resistance

For the case of hooked-end steel fibres, the mechanical clamping of the hook plays a significant role in increasing the pullout load as well as the pullout energy of the fibre from the matrix (Alwan et al., 1991).

For smooth straight steel fibres, the pullout response is affected by the interfacial bond properties between the matrix and the fibre (Nammur and Naaman, 1989). Alwan et al. (1991) found that a new parameter comes into play in the case of deformed fibres, namely the geometric properties of the fibre (in the case of hooked end steel fibres; mechanical clamping action due to the hook geometry). In the case of hooked-end fibres, Alwan et al. postulated that the mechanical contribution of the hook is a function of the load needed to straighten the fibre as it is being pulled out from the matrix.

Figures 2.4 and 2.5 describe the various stages in the pullout process (Alwan et al., 1991). During the first stage ("elastic" stage), the response is elastic with P_{crit}

representing the load that causes debonding to commence. During the second stage ("partial debonding" stage), the pullout contribution would be due to elastic shear stresses and interfacial frictional stresses along the length of the fibre. At the end of this stage (at load P_1) the fibre is assumed to be completely debonded from the matrix.

The third stage is referred to as the "mechanical clamping" stage in which the fibre hook starts to deform, straighten and pullout (loads P_2 through P_4). From the experimental data, Alwan et al. suggest that this phase is primarily a function of the mechanical contribution of the hook. Hence, the pullout resistance from this stage would be a function of the hook geometry and would be independent of the matrix strength.

Lastly, in the fourth stage ("frictional pullout" stage), the fibre is pulled out from the matrix due to the decaying interfacial frictional stresses.

Alwan et al. suggest that stages 1, 2 and 4 can be predicted using the model presented by Naamur and Naaman for smooth fibres.

In order to compute the values P_3 and P_4, Alwan et al. propose using the relationships in Eq. 2-2 to 2-5. These equations were derived based on assumptions regarding the number of plastic hinge locations that form in the hook during the various load stages.

$$P_3 = P_1 + \Delta P' \tag{2-2}$$

$$P_4 = P_1 + \Delta P'' \tag{2-3}$$

$$\Delta P' = \frac{\left[\dfrac{f_{fy}\pi r_f^{\,2}}{3\cos\theta}\right]\left[1 + \dfrac{\mu\cos\beta}{(1-\mu\cos\beta)}\right]}{[1-\mu\cos\beta]} \tag{2-4}$$

$$\Delta P'' = \frac{\left[\dfrac{f_{fy}\pi r_f^{\,2}}{6\cos\theta}\right]}{[1-\mu\cos\beta]} \tag{2-5}$$

In these relationships, P_1 is the load at the onset of complete debonding while P_3 and P_4 are the first and second pullout load plateaus, respectively (see Fig. 2.4). The value $\Delta P'$ represents the mechanical pullout load contribution due to the formation of two plastic hinges, while $\Delta P''$ represents the corresponding value due to the formation of one plastic hinge. The values f_{fy}, r_f and μ are the fibre yield strength, fibre radius and the frictional coefficient of the fibre-matrix interface. The values θ and β are a function of the fibre geometry.

The values Δ_3 and Δ_4 that are shown in Fig. 2.4 can be computed using Eq. 2-6 and 2-7, where k_o and h_o are a function of the hook geometry of the fibre as illustrated in Fig. 2.5. The value Δ_1 represents the slip of the fibre at full-debonding.

$$\Delta_3 = \Delta_1 + k_o \qquad \text{2-6}$$

$$\Delta_4 = \Delta_3 + h_o \qquad \text{2-7}$$

2.2.2.3 Fibre orientation factor

The "effective" number of fibres per unit area, N_{fibres}, can be calculated using Eq. 2-8 for fibres randomly oriented in three dimensions (Hannant, 1978, Lee, 1990):

$$N_{fibres} = \frac{v_f}{A_f} \times \alpha \times \eta_l \qquad \text{2-8}$$

Where A_f, is the cross-sectional area of the fibre, while v_f is the volume fraction of fibres in the matrix.

The orientation factor, α, is used to account for the random orientation of the fibres crossing any arbitrary cracking plane (Dupont, 2003). For a fibre that is not limited by any boundary conditions (fibre in "bulk"), several authors have suggested using a value of 0.5 for this parameter by integrating the fibre pullout length over all possible orientation angles (Hannant, 1978, Dupont, 2003). For a graphical representation of α for this scenario see Fig. 2.6. For fibres with one or two boundary conditions, Dupont (2003) suggests using values of 0.6 and 0.84 respectively for α.

The length factor η_l is used to account for the variability in the fibre embedment length across the cracking plane. The fibre embedment length can vary between $L_f / 2$ and 0 (see Fig. 2.7). If pullout occurs from the side with the smaller embedment length, one can assume that the effective embedment length is $L_f\ /\ 4$ (therefore the factor $\eta_l = 0.5$).

2.2.3 Behaviour of SFRC in tension

As was noted earlier, when subjected to tensile stresses, concrete is a material that fails in a brittle manner at the onset of cracking. The random orientation of fibres greatly enhances the post-cracking resistance thereby ensuring a more ductile failure.

There are several methods that are proposed in the literature to study the tensile behaviour of SFRC. These include direct tensile tests on small dog-bone specimens and “variable diameter” specimens (Cassanova, 1996). Another procedure involves the testing of notched specimens where the stress is measured as a function of the crack opening displacement (COD). An example is the proposed method for the uniaxial testing of SFRC (RILEM, 2002) in which a notched cylinder that has a height and diameter of 150 mm is tested under uniaxial tension.

2.2.4 Behaviour of SFRC in compression

Several authors report that the effect of fibres on the compressive strength is not very substantial (Minelli, 2005, Dupont, 2003, Nataraja et al., 1999). However, the addition of fibres significantly enhances the descending branch of the compressive stress-strain curve. During the uniaxial compressive test, lateral swelling of the concrete takes place resulting in a combination of shear and tensile stresses in the concrete section and hence an improved toughness results due to the improved post-cracking resistance of the steel fibre reinforced concrete (Johnston, 2001). Several investigators have proposed models for the characterization of the compressive stress-strain behaviour of SFRC.

2.2.4.1 Nataraja et al. model

Nataraja et al. (1999) proposed a model for the complete stress-strain curve for SFRC. The model was derived based on an experimental program in which round crimpled fibres were used at volume fractions ranging from 0.5% to 1.0%. The model defines the various parameters of the stress-strain curve based on a parameter called the steel fibre reinforcing index, RI (where RI is obtained using Eq. 2-9). Equations 2-10 and 2-11 define the peak compressive stress and strain of the SFRC based on this index as follows:

$$RI = w_f \frac{L_f}{d_f} \qquad 2\text{-}9$$

$$f'_{cf} = f'_{cu} + 2.1604(RI) \qquad 2\text{-}10$$

$$\varepsilon'_{cf} = \varepsilon'_{cu} + 0.0006RI \qquad 2\text{-}11$$

The parameters f'_{cu} and ε'_{cu} as well as f'_{cf} and ε'_{cf} are the peak compressive strength and strain of the plain and fibre reinforced concretes, respectively.

The toughness ratio of the steel fibre reinforced concrete, TR_{cf} is obtained using Eq. 2-12, where TR_c is the toughness ratio of the plain unreinforced concrete.

$$TR_{cf} = TR_c + 0.0978RI \qquad 2\text{-}12$$

In addition, the authors propose Eq. 2-13 to predict the complete stress-strain curve for SFRC. Where f_{cf} and ε_{cf} are the stress and strain values and β_1 is a material parameter that controls the shape of the stress-strain diagram and is computed using Eq. 2-14.

$$\frac{f_{cf}}{f'_{cf}} = \frac{\beta_1 \left(\varepsilon'_{cu} / \varepsilon'_{cf} \right)}{\beta_1 - 1 + \left(\varepsilon'_{cu} / \varepsilon'_{cf} \right)^{\beta_1}} \qquad 2\text{-}13$$

$$\beta_1 = 0.5811 + 1.93RI^{-0.7406} \qquad 2\text{-}14$$

2.2.4.2 Hsu and Hsu model

Hsu and Hsu (1994) proposed some empirical expressions for the stress-strain relationship of high-strength SFRC. The authors tested a series of cylindrical specimens to arrive at the model. Hooked-end steel fibres were used at a volume fraction of 0.25% to 1%. They proposed Eq. 2-15 and 2-16 to characterize the stress-strain curve:

$$\eta = \frac{f_{cf}}{f_{cu}^{'}} = \frac{n\beta_1 x}{n\beta_1 - 1 + x^{n\beta_1}} \qquad \text{for } 0 \le x \le x_d \qquad 2\text{-}15$$

$$\eta = \frac{f_{cf}}{f_{cu}^{'}} = \eta_d \, exp\left[-k_d \left(\frac{\varepsilon_{cf}}{\varepsilon_{cu}^{'}} - x_d \right)^a \right] \qquad \text{for } x_d \le x \qquad 2\text{-}16$$

Where β_1 and n are material parameters that describe the shape of the stress-strain curve. The parameters η and $\frac{\varepsilon_{cf}}{\varepsilon_{cu}^{'}}$ are the normalized stress and strain, respectively. These various parameters are obtained by consulting a series of tables and expressions that depend upon the volume fraction of fibres that is used in the concrete mix.

2.2.4.3 Mansur et al. model

Based on the results of an experimental program, Mansur et al. (1999) proposed a model to characterize the stress-strain relationship of high-strength fibre reinforced concrete, ranging from 70 to 120 MPa. Hooked-end steel fibres in a quantity of 1% to 1.5% were used in the experimental program. The proposed model describes the ascending branch of the curve using Eq. 2-17, where $f_{cu}^{'}$ and $\varepsilon_{cu}^{'}$ are the peak stress and strain of the high-strength concrete. The material parameter β_1 controls the shape of the stress-strain diagram and is computed using Eq. 2-18.

$$f_{cf} = f_{cu}^{'} \left[\frac{\beta_1 \left(\frac{\varepsilon_{cf}}{\varepsilon_{cu}^{'}} \right)}{\beta_1 - 1 + \left(\frac{\varepsilon_{cf}}{\varepsilon_{cu}^{'}} \right)^{\beta_1}} \right] \qquad 2\text{-}17$$

$$\beta_1 = \frac{1}{1 - \frac{f_{cu}^{'}}{\varepsilon_{cu}^{'} E_a}} \qquad 2\text{-}18$$

For the descending branch of the curve, Mansur proposes using Eq. 2-19. In the equation, k_{f1} and k_{f2}, are two parameters that are used to modify the curve to reflect the inclusion of the fibres. These two parameters are defined by Eq. 2-20 and 2-21 and are a function of the peak stress of the concrete, f'_{cu}, the volume fraction of the fibres, v_f, and the aspect ratio of the fibre, L_f / d_f.

$$f = f'_{cu}\left[\frac{k_{f1}\beta_1\left(\frac{\varepsilon_{cf}}{\varepsilon'_{cu}}\right)}{k_{f1}\beta_1 - 1 + \left(\frac{\varepsilon_{cf}}{\varepsilon'_{cu}}\right)^{k_{f2}\beta_1}}\right] \qquad 2\text{-}19$$

$$k_{f1} = \left(\frac{50}{f'_{cu}}\right)^{3.0}\left[1 + 2.5\left(\frac{v_f l_f}{d_f}\right)^{2.5}\right] \qquad 2\text{-}20$$

$$k_{f2} = \left(\frac{50}{f'_{cu}}\right)^{1.3}\left[1 - 0.11\left(\frac{v_f l_f}{d_f}\right)^{-1.1}\right] \qquad 2\text{-}21$$

2.2.5 Toughness of SFRC

The addition of steel fibres to concrete greatly enhances the toughness of the material. Although there have been several standardized methods that have been proposed for determining the toughness of fibre reinforced concretes, there is still a lack of agreement on the method that best quantifies this parameter.

2.2.5.1 ASTM C1018 method

In the ASTM C1018 standard method (ASTM, 1998), a 100 x 100 x 350 mm beam is tested under 4-point bending. Based on the obtained load displacement response several toughness indices are computed. The various indices are obtained by measuring the area under the curve from the point of first cracking to several specified deflections. Furthermore, residual strength values are computed based on these toughness indices.

However there are several concerns with this method including the difficulty in correctly identifying the deflection at first cracking. The fact that the various performance parameters are a function of this deflection makes this very problematic. Furthermore, errors may arise in the deflection values due to twisting and seating of the specimen thereby resulting in some inaccuracies (Banthia and Trottier, 1995). This latter problem can be alleviated by using a "Japanese yoke" setup to measure the net deflection of the specimen.

2.2.5.2 JSCE SF-4 method

The JSCE SF-4 method (JSCE, 1984) uses the same test setup used in the ASTM C1018 method but makes use of a different analysis procedure to quantify the toughness parameter. In this method, the area under the load versus deflection curve up to a deflection of span/150 is calculated and represents the toughness. From this value, the flexural toughness factor (FT) is calculated. The units of the FT-factor are stress and hence the value can be seen to indicate the post cracking residual strength of the material when loaded up to an arbitrary deflection of *L/150* (Banthia and Trottier, 1995).

There are concerns over this method as well, namely the fact that the FT parameter is dependant on the specimen geometry. Furthermore, the chosen deflection of *L/150* is arbitrary (Banthia and Mindess, 2004). Nonetheless this method seems to provide more reliable results when compared to the ASTM C1018 method.

2.2.5.3 ASTM C1399 method

In this method, a standard beam is loaded under a steel plate until cracking (ASTM, 1998b). The steel plate is used in order to prevent the complete failure of the specimen. After cracking, the steel plate is removed and the beam is loaded to obtain a reload versus deflection curve. Thereafter, the residual strength of the beam is determined over a range of deflection values. Figure 2.8 gives a schematic comparison of the analysis procedures involved in the various ASTM and JSCE methods.

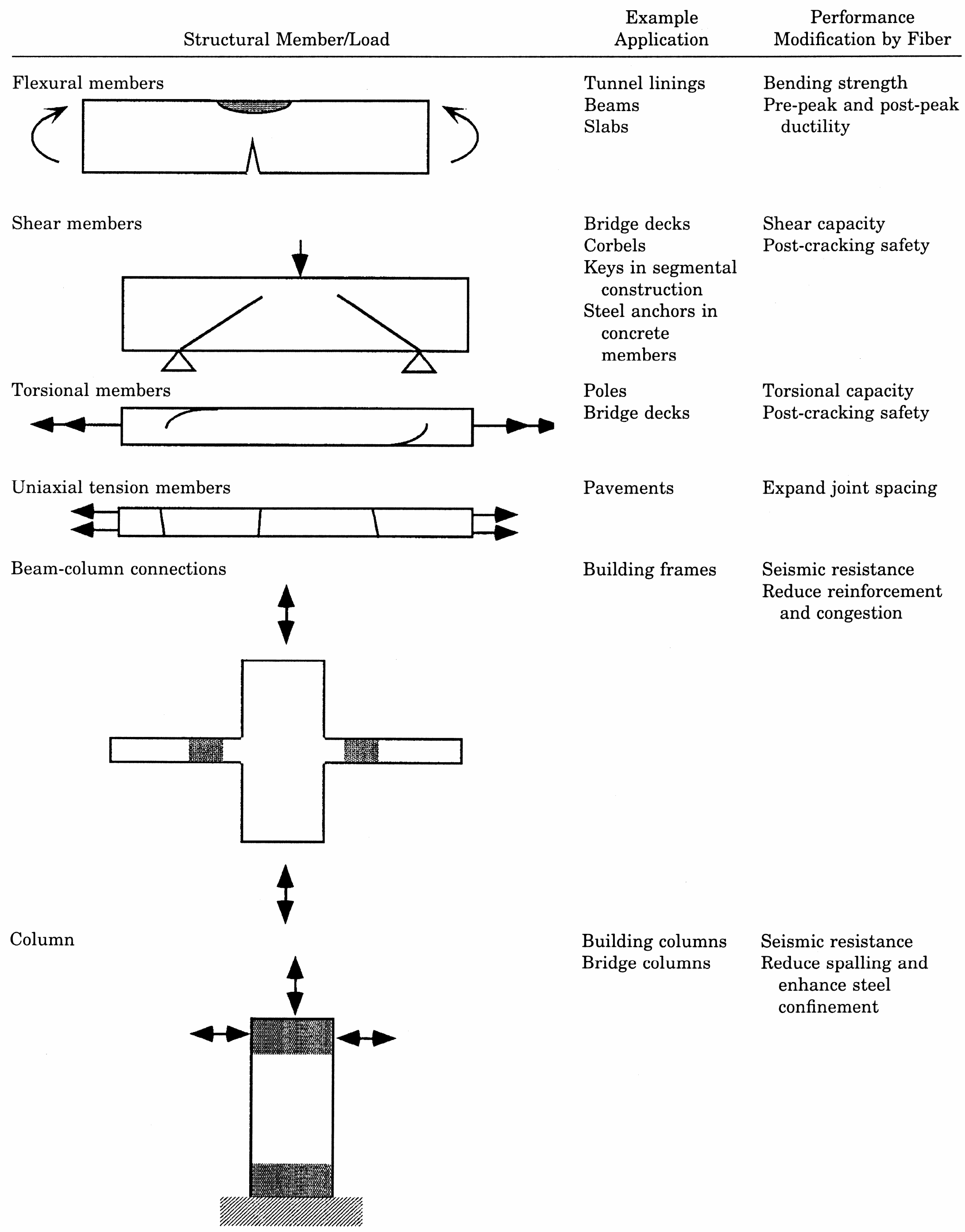

Figure 2.1: Potential structural applications for SFRC

[Adapted from (Li, 2002)]

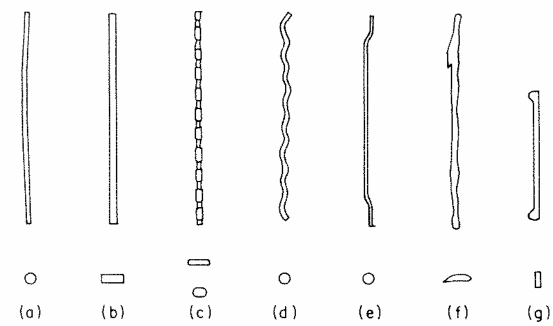

Figure 6.1. Shapes of steel fibres (a) Round, (b) Rectangular, (c) Indented (Duoform, National Standard Patent), (d) Crimped (G. K. N. and Johnson Nephew Ltd.), (e) Hooked ends (Dramix, Z. Bekaerto Ltd. Patent) (f) Melt extract process (Battelle Patent), (g) Enlarged ends (Australian Wire Industries Ltd. Patent)

Figure 2.2: Typical steel fibre geometries

[Adapted from (Johnston, 2001)]

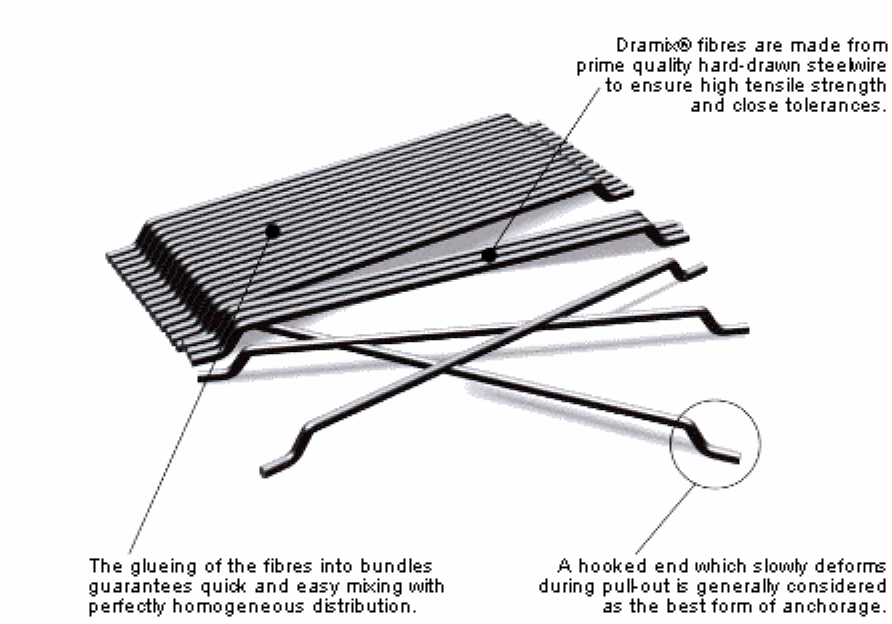

Figure 2.3: Typical hooked-end steel fibre

[Adapted from (CMRI, 2007)]

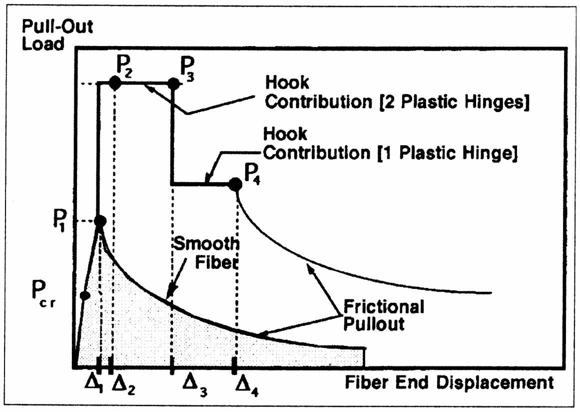

Figure 2.4: Proposed pullout curve for hooked end steel fibres

[Adapted from (Alwan et al., 1991)]

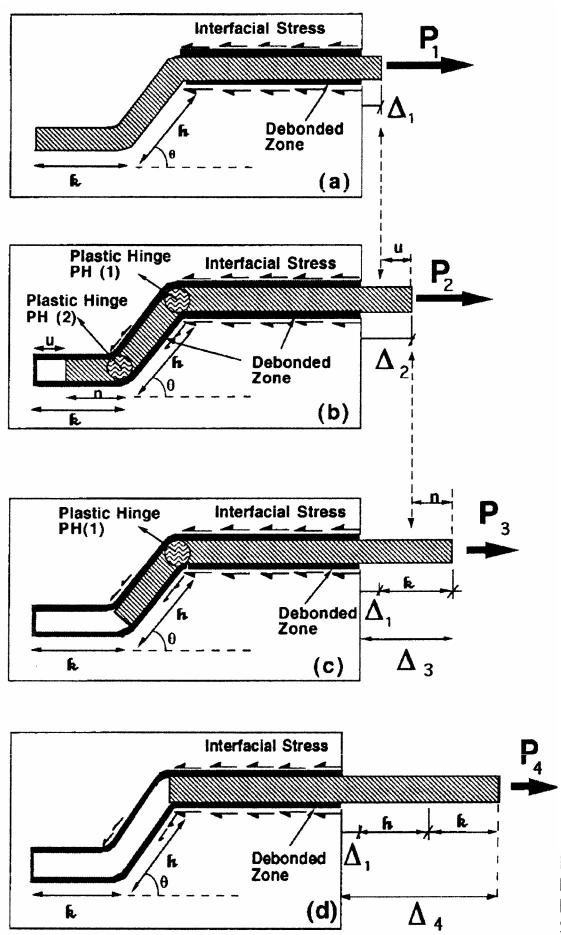

Fig. 11 - a) Hooked steel fiber at onset of complete debonding, b) hooked steel fiber during mechanical interlock with two plastic hinges, c) mechanical interlock with one plastic hinge, d) Hooked Steel fiber at onset of frictional pull-out.

Figure 2.5: Various stages during the pullout of a hooked end steel fibre

[Adapted from (Alwan et al., 1991)]

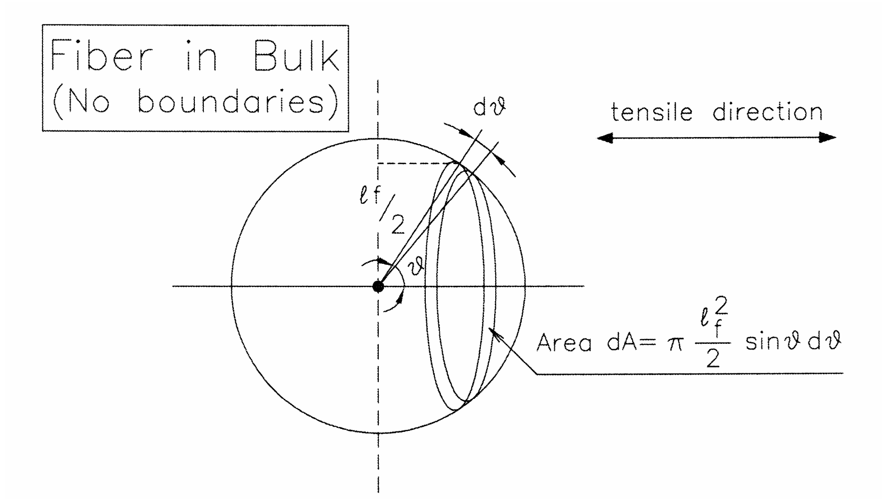

Figure 2.6: Derivation of the orientation factor

[Adapted from (Dupont, 2003)]

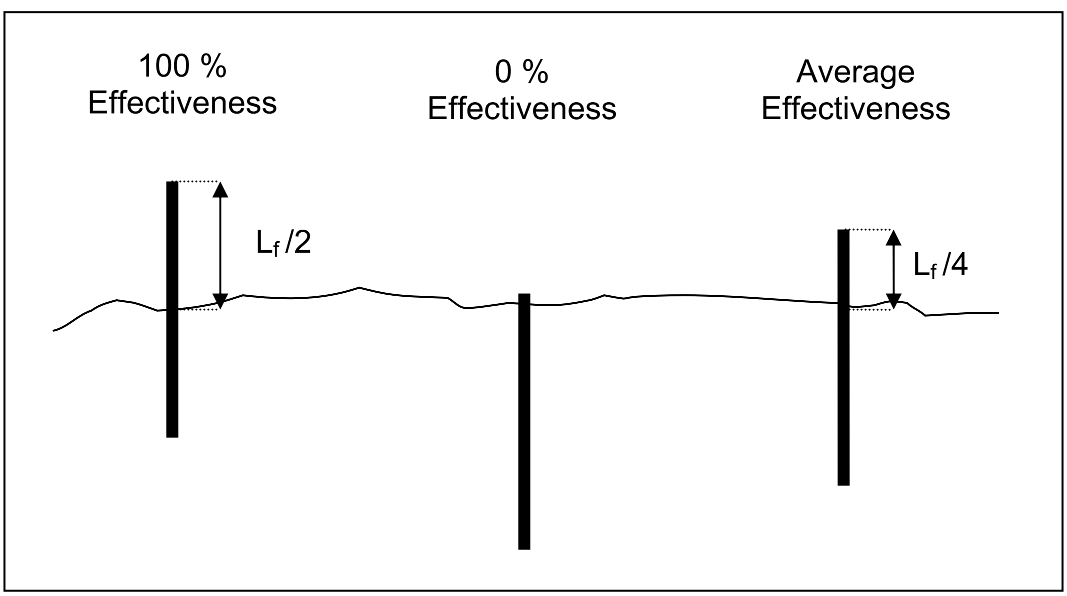

Figure 2.7: Variability in the fibre embedment length

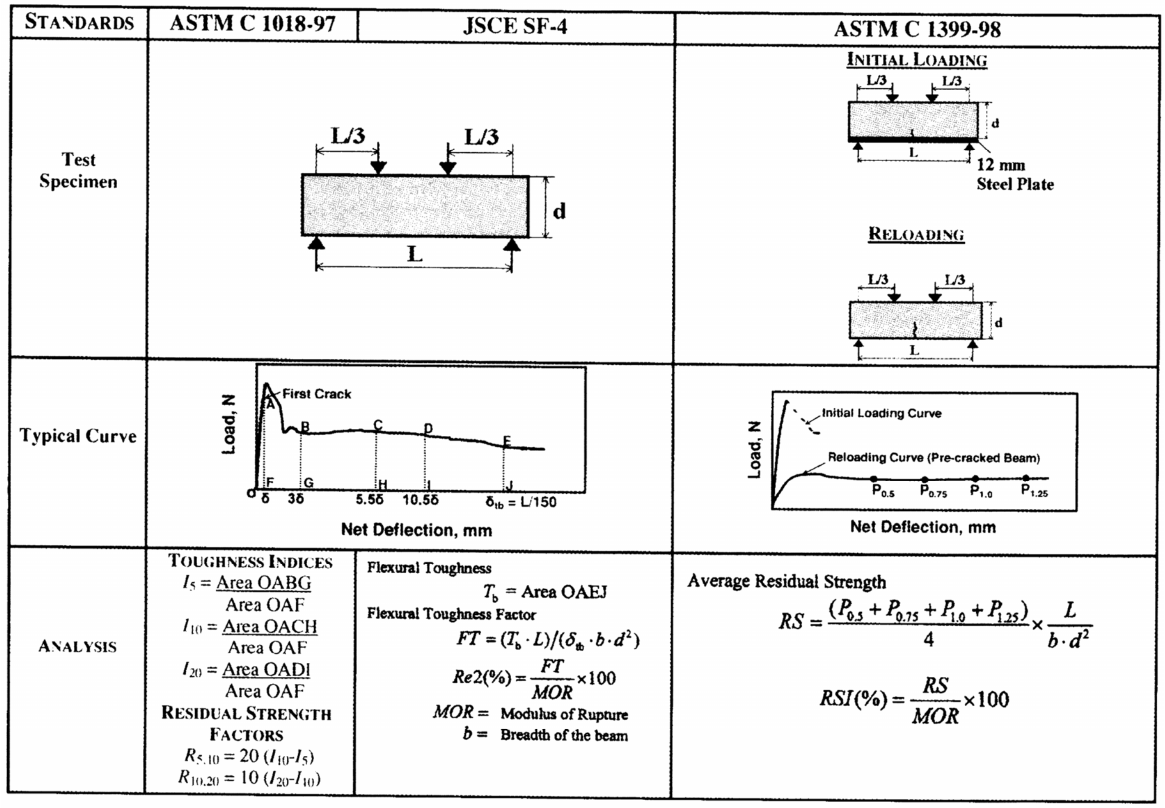

Figure 2.8: Schematic representation of the ASTM and JSCE methods for toughness characterisation

[Adapted from (Banthia and Mindess, 2004)]

2.3 Self-Consolidated Concrete

Although steel fibres improve many of the mechanical properties of concrete, the addition of the randomly oriented fibres may result in reduced workability. Hence, in general, fibre contents less than 1% by volume must be used in order to ensure a workable concrete mix. One innovative solution may lie in the use of a highly flowable self-consolidating concrete (SCC) mix in order to improve workability when fibres are added to the concrete.

This portion of the literature review will begin by defining SCC and its main characteristics (Section 2.3.1). Section 2.3.2 will describe some of the current methods for testing the properties of SCC in the fresh-state. Section 2.3.3 will summarize some of the studies on the use of SCC in combination with steel fibres.

2.3.1 SCC characteristics

SCC is a non-segregating concrete that can flow and fill formwork without any mechanical vibration. This highly flowable concrete was developed in Japan in the1980s as a solution to improve the constructability of reinforced concrete structures (Ozyildirim and Lane, 2003). Since no mechanical vibration is needed when placing this concrete, significant savings in labour costs and construction time can be achieved. Further advantages include noise reduction during construction and a reduction of surface defects leading to a more appealing architectural finish (Gurjar, 2004).

A typical SCC mix is designed by ensuring a proper flowability and viscosity in the fresh state (Ozyildirim and Lane, 2003). The former is normally achieved by using a high range water reducer (HRWR) while the latter is ensured by using a proper selection of fines and aggregates and by using a viscosity modifying admixture (VMA).

2.3.2 SCC in the fresh-state

Several methods can be used to evaluate the various properties of SCC in the fresh state. These tests can be broadly split into two categories: free flow tests and restricted flow tests. These procedures enable an assessment of the filling ability, passing ability, and segregation resistance of the SCC. Among the most common tests for assessing the free deformability of SCC is the slump flow test. Methods that are typically used to assess the restricted deformability include the L-box, V-funnel and Filling-capacity tests.

2.3.2.1 The Slump flow test

In this test, a conventional slump cone is filled with concrete and placed on a flow table (see Fig. 2.9). Thereafter the cone is lifted and the horizontal spread of the concrete is measured. Additionally, the time that is required for the concrete to spread to a diameter of 500 mm is recorded (Gurjar, 2004). Due to the simple nature of this test procedure, it is one of the most common methods used in practice to measure the workability of SCC in the fresh state.

2.3.2.2 The L-box test

The L-box test can be used to evaluate the filling and passing ability of SCC. The apparatus that is used in the test procedure is shown in Fig. 2.10. During the test, the concrete is first placed in the vertical region of the apparatus. Thereafter, a sliding gate is opened to allow the concrete to flow through a series of vertical rebars and into the horizontal portion of the box. As the concrete is allowed to flow, the time required for the SCC to reach points that are 200 and 400 mm down the horizontal portion of the box is recorded. After the SCC ceases to flow, the heights of the concrete at either end of the box are recorded and the ratio of the heights is computed (Koehler and Fowler, 2003).

2.3.2.3 The V-funnel test

This test method is typically used to evaluate the stability and segregation resistance of the SCC. In the test, the concrete is poured into a V-funnel apparatus until it is filled (see Fig. 2.11). The sliding door at the bottom of the funnel is then opened to allow the concrete to flow out. The time that the concrete takes to exit the apparatus is then recorded. In an attempt to measure the segregation resistance of the SCC, the V-funnel is then refilled with concrete. After allowing the concrete to sit in the funnel for approximately 5 minutes, the door is opened and the flow time is recorded (Gurjar, 2004).

2.3.3 Steel fibres in combination with SCC

The use of SCC in combination with steel fibres is an application that may prove to be advantageous. Several investigators have studied the potential benefits and limitations associated with the use of fibres with this type of concrete mix.

2.3.3.1 Khayat and Roussel tests

Khayat and Roussel (Khayat and Roussel, 2000) examined the feasibility of producing an adequately flowable and non-segregating steel fibre reinforced SCC. Sixteen mixtures were produced with various fibre contents and mixture compositions. The characteristics of the various mixtures in the fresh state were measured using a series of tests. A concrete viscometer was used to test the rheological parameters, while the V-funnel and filling capacity tests were used to measure the restricted deformability of the fibre reinforced SCC. Furthermore, the properties of the material were tested using 4 point bending tests. The investigators found that even at fibre contents of 1%, if a proper mix design is used, a cohesive and flowable SCC can be obtained. The investigators also found that a combination of the slump flow and V-funnel tests should be used when assessing the workability of fibre reinforced SCCs.

2.3.3.2 Grunewald and Walveren tests

In their experimental program, Grunewald and Walraven (2001) examined the potential of using SCC with steel fibres. Several test methods that are commonly used for SCC were used to measure the effect of fibres on the fresh-state properties of the steel-fibre reinforced SCC including the slump-flow and V-funnel tests. The results showed that there is a critical fibre content which if surpassed will lead to a stiff SCC mix that has reduced resistance to segregation and a reduced homogeneity. The L-box test showed that a larger free bar spacing must be used when fibres are added to the concrete mix in order to avoid the risk of blocking. Finally, the investigators found that if a proper fibre content and mixture composition is selected, a highly flowable SCC could still be achieved.

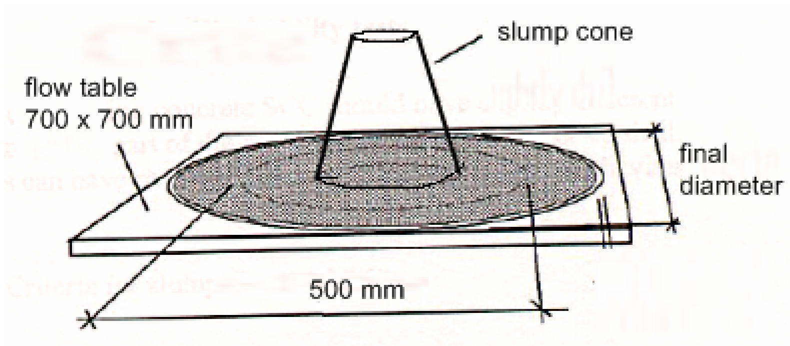

Figure 2.9: Apparatus used in the slump flow test

[Adapted from (Gurjar, 2004)]

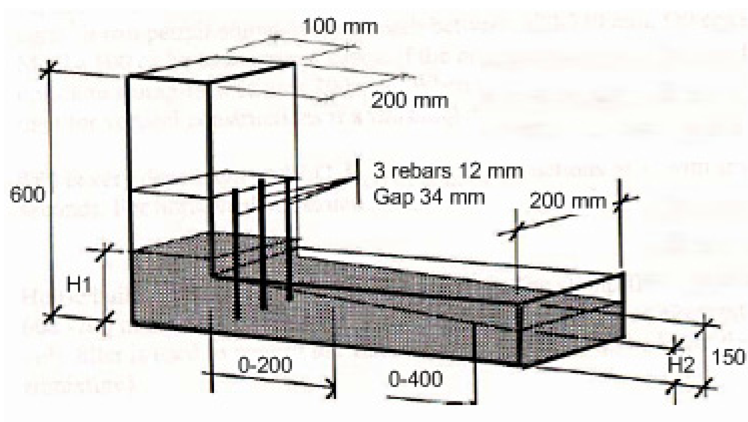

Figure 2.10: Schematic representation of the L-box test method

[Adapted from (Gurjar, 2004)]

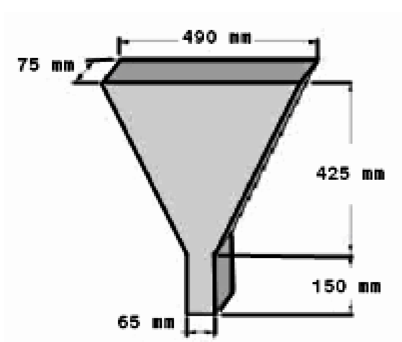

Figure 2.11: Typical V-funnel dimensions

[Adapted from (Gurjar, 2004)]

2.4 The Behaviour of RC Columns and the Benefits of using SFRC

In the earthquake resistant design of reinforced concrete structures the proper detailing of the reinforcement, particularly in the potential plastic hinge regions, is essential in order to ensure ductile performance. In RC columns, this ductility is greatly influenced by the confinement stresses induced by the transverse reinforcement in the column cross-section. The detailing and spacing of the transverse reinforcement plays a major role in confining the concrete core and in preventing longitudinal bar buckling. Tests over the past few decades have shown that suitable arrangements of transverse reinforcement result in two major enhancements:

- an increase in the peak resistance of the column
- an enhanced post-peak ductility

This section of the literature review begins with a description of the available models that can be used to predict the complete stress-strain curve of RC columns (Section 2.4.1). Section 2.4.2 presents a model that can be used to account for the buckling of the longitudinal reinforcement in RC columns. Section 2.4.3 outlines some of the detailing requirements for RC columns in the CSA Standard. Finally, Section 2.4.4 presents some of the past research that focussed on the use of SFRC in columns.

2.4.1 Past models for complete stress-strain behaviour of RC columns

In order to predict the behaviour of columns it is essential to have analytical models that can accurately describe the stress-strain curve of confined and unconfined concrete, particularly with respect to post-peak behaviour. Such models should take into account the various factors that can affect the confinement in the column. Several researchers have tried to develop models that can accurately predict the complete stress-stress curve of RC columns under axial loading based on extensive experimental data.

2.4.1.1 Early work by Richart

Early research by Richart et al. (1928) demonstrated that the strength of concrete is enhanced if the concrete section is confined by an active hydrostatic pressure. Richart derived a simple relationship to show that the maximum confined concrete strength (f'_{cc}), can be approximated with:

$$f'_{cc} = f'_{cu} + k \times f'_{l} \qquad \text{2-22}$$

Where k is equal to 4.1, f'_{l} represents the lateral confining pressure, and where f'_{cu} represents the unconfined concrete strength. Furthermore, Richart et al. (1929) found that concrete that is provided with passive confinement pressure (in the form of spirals) results in a response that is similar to the case in which active fluid pressure is provided.

2.4.1.2 Kent and Park model for confined concrete

Kent and Park (1971) developed a model for concrete that is confined by rectangular transverse reinforcement. This model neglected the increase in strength due to confinement but accounted for the increased ductility that resulted due to the presence of rectangular steel ties. This model was later modified Park et al. (1982) and Scott et al. (1982) to take into consideration the potential strength gains at peak resistance.

2.4.1.3 Sheik and Uzumeri model for effectively confined concrete

Sheikh and Uzumeri (1980, , 1982) suggested that unlike concrete specimens confined by an active fluid pressure which is uniform, concrete specimens that are confined by passive rectangular tie reinforcement are confined by a pressure that is not uniformly applied throughout the volume of the concrete core. They suggested that at high strains, when the cover spalling occurs, part of the core region also becomes ineffective in confining the core concrete. Hence they proposed a model in which the enhanced behaviour of columns confined by rectangular ties is related to an “effectively confined” core area. This area is smaller than the actual core area and is determined using the tie configuration in the section and the tie spacing, based on arching action in the concrete section. The enhancements in strength and ductility are then calculated based on this “effectively confined area”. The remaining region in the core is considered ineffective in confining the core.

2.4.1.4 Mander et al. model for effectively confined concrete

Mander et al. (1988) proposed a model for the complete stress-strain curve of concrete columns confined by circular hoops and rectangular ties, under monotonic and cyclic loading, using an approach similar to that used by Sheik and Uzumeri.

2.4.1.5 Legeron and Paultre model for effectively confined concrete

An earlier model by Cusson and Paultre (1995), was extended by Légeron and Paultre (2003) to predict the complete stress-strain curves of RC columns under monotonic and cyclic loading, for a wide range of concrete strengths, transverse steel tie configurations and yield strengths.

In accordance with the work of Sheikh and Uzumeri and the work of Mander et al., the confinement provided by the ties is assumed to occur in an "effectively confined" core region. The region is calculated using the arching action concept, and is calculated using a confinement effectiveness coefficient, K_e, which is a function of the tie configuration and tie spacing. This arching action is assumed to act in the form of parabolas having initial tangent slopes of *45°* as shown in Fig. 2.12. The coefficient represents the ratio of the smallest effectively confined concrete area, halfway between two layers of transverse ties, to the total concrete core area, and is computed using Eq. 2-23.

$$K_e = \frac{\left(1 - \frac{\sum w_i^2}{6c_x c_y}\right)\left(1 - \frac{s'}{2c_x}\right)\left(1 - \frac{s'}{2c_y}\right)}{\left(1 - \rho_c\right)} \qquad \text{2-23}$$

Where, s' refers to the clear spacing between the transverse reinforcement, and where the quantities c_x and c_y are to the widths of the concrete core parallel to the x and y axis respectively. The parameter $\sum w_i^2$ is the sum of the squares of the clear spacings between adjacent longitudinal bars and ρ_c is the ratio of longitudinal reinforcement in the core section.

Next, using the effectively confined core concept, the "effective" confinement pressure that acts on the core, f'_{le}, is found to be equal to the product of the confinement effectiveness coefficient, K_e, and the nominal lateral pressure provided by the ties, f'_l (Cusson and Paultre, 1995):

$$f'_{le} = K_e \times f'_l = \frac{K_e f_{hcc}}{s}\left(\frac{A_{shy} + A_{shx}}{c_y + c_x}\right) \qquad \text{2-24}$$

In which, A_{shy} and f_{hcc} refer to the total cross-sectional area of transverse reinforcement perpendicular to one direction, and the stress in the transverse steel reinforcement at maximum strength of confined concrete respectively. The quantity s is the centre-to-centre spacing of the ties.

In the case of a square cross-section, the above equation reduces to the following:

$$f'_{le} = K_e \times f'_l = \frac{K_E f_{hcc} A_{sh}}{sc} \qquad \text{2-25}$$

From this value an "effective confinement index at peak strength", I'_E, is calculated using Eq. 2-26 and is defined as the ratio of the effective confinement pressure that acts on the core , f'_{le}, to the unconfined concrete strength, f'_{cu}. It is understood that as this index increases, the amount of confinement in the core increases.

$$I'_E = \frac{f'_{le}}{f'_{cu}} \qquad \text{2-26}$$

Légeron and Paultre, suggest that the stress developed in the transverse reinforcement at peak confined concrete stress is related to the amount of confinement provided to the section. The more a column is confined, the more it is able to effectively use the full yield stress, f_{hy}, of the transverse reinforcement. Légeron and Paultre, developed equations to calculate the stress of transverse steel reinforcement at the peak concrete stress, f'_{hcc} (see Eq. 2-27 to 2-29).

$$\rho_{sey} = \frac{K_e A_{shy}}{sc} \qquad \text{2-27}$$

$$\kappa = \frac{f'_{cu}}{\rho_{sey} E_S \varepsilon'_{co}} \qquad \text{2-28}$$

$$f'_{hcc} = \begin{cases} f_{hy} \longleftarrow \kappa \leq 10 \\ \dfrac{0.25 f'_{cu}}{\rho_{sey}(\kappa - 10)} \geq 0.43 \varepsilon'_{cu} E_S \longleftarrow \kappa > 10 \end{cases} \qquad 2\text{-}29$$

In these equations, ρ_{sey} is the effective sectional ratio of confinement reinforcement in the y direction, κ is a parameter that is used in order to determine if yielding of the transverse reinforcement occurs at the maximum strength of the confined concrete, E_S is the modulus of elasticity of the transverse reinforcement and ε'_{cu} is the peak unconfined concrete strain.

Légeron and Paultre suggest the following empirical equations in order to calculate the peak confined concrete stress, f'_{cc} and peak confined concrete strain, ε'_{cc}:

$$\frac{f'_{cc}}{f'_{cu}} = 1 + 2.4 (I'_E)^{0.7} \qquad 2\text{-}30$$

$$\frac{\varepsilon'_{cc}}{\varepsilon'_{cu}} = 1 + 35 (I'_E)^{1.2} \qquad 2\text{-}31$$

The post-peak strain measured at 50% of maximum confined stress, ε'_{c50c}, defines the post-peak shape of the stress-strain curve, and is defined by the following empirical equation:

$$\frac{\varepsilon'_{c50c}}{\varepsilon'_{c50u}} = 1 + 60 (I_{E50}) \qquad 2\text{-}32$$

Where the post-peak strain measured at 50% of maximum unconfined stress, ε'_{c50u} is taken as being equal to a strain of 0.004, and the effective confinement index I_{E50} at ε'_{c50c} is computed using Eq. 2-33:

$$I_{E50} = \rho_{sey} \frac{f'_{hy}}{f'_{cu}} \qquad 2\text{-}33$$

Based on these formulations, Légeron and Paultre define the complete stress-strain curve of confined concrete under axial loading using 2 points: the peak stress and strain of the confined concrete ($f'_{cc}, \varepsilon'_{cc}$), and the strain of the confined concrete when the axial capacity drops to 50% of the peak value (ε'_{c50c}). A visual presentation of this stress-strain relationship is shown in Fig. 2.13.

The ascending branch of the stress-strain relationship is defined by the relationship in Eq. 2-34 which is based on the work of Popovics (1973), where f_{cc} refers to the stress in the confined concrete corresponding to a chosen strain equal to ε_{cc}. The values, f'_{cc} and ε'_{cc}, refer to the peak confined stress and strain of the concrete. Finally, the constant *k*, is a parameter that controls the slope of the ascending branch of the curve and is computed using Eq. 2-35.

$$f_{cc} = \frac{(f'_{cc})*\left(k \times \dfrac{\varepsilon_{cc}}{\varepsilon'_{cc}}\right)}{k - 1 + (\dfrac{\varepsilon_{cc}}{\varepsilon'_{cc}})^k}, \qquad \varepsilon_{cc} \le \varepsilon'_{cc} \qquad 2\text{-}34$$

$$k = \frac{E_c}{E_c - (\dfrac{f'_{cc}}{\varepsilon'_{cc}})} \qquad 2\text{-}35$$

Légeron and Paultre model the descending post-peak portion of the stress-strain curve with the relationship in Eq. 2-36:

$$f_{cc} = (f'_{cc}) \times exp\left(k_1\left(\varepsilon_{cc} - \varepsilon'_{cc}\right)^{k_2}\right), \ \varepsilon_{cc} > \varepsilon'_{cc} \qquad 2\text{-}36$$

The constants k_1 and k_2 are two parameters that are used to control the curvature of the descending branch of the stress-strain curve and are computed using Eq. 2-37 and 2-38 respectively.

$$k_1 = \frac{ln(0.5)}{\left(\varepsilon_{c50c} - \varepsilon'_{cc}\right)^{k_2}} \qquad 2\text{-}37$$

$$k_2 = 1 + 25\left(I_{E50}\right)^2 \qquad 2\text{-}38$$

In order to evaluate the stress-strain curve of unconfined concrete, these relationships can be used with the exception being that the confined parameters in the equations are replaced by the unconfined parameters ($f'_{cu}, \varepsilon'_{cu}, \varepsilon'_{c50u}$). The parameter k_2 is taken to be equal to 1.5.

2.4.1.6 Other confinement models

There are numerous other analytical models for confined concrete available in the literature. Some of the models that can be used to predict the stress-strain behaviour of confined concrete columns are summarized in Table 2-1 and Fig. 2-14. Sharma (2005) performed a comparative study to evaluate the accuracy of the various models and found that the Légeron and Paultre (2003) model was most efficient in predicting a wide-range of experimental results with the least amount of error.

Table 2-1: Models for confined concrete available in the literature

[Information taken from Sharma and Kaushik (2005)]

(Yong et al., 1988)	- Model of rectilinearly confined columns - Three-part stress-strain relation to predict the constitutive behaviour of confined high-strength concrete
(Bjerkli et al., 1990)	- Model for rectilinear or circular cross-sectional shapes - Three-part stress-strain relation to predict the constitutive behaviour of confined high-strength concrete
(Nagashima et al., 1992)	- Model of rectilinearly confined columns - Two-part stress-strain relation to predict the constitutive behaviour of confined high-strength concrete
(Muguruma et al., 1993)	- Model of rectilinearly confined columns - Three-part stress-strain relation to predict the constitutive behaviour of confined high-strength concrete
(Li et al., 1994)	- Model for rectilinear or circular cross-sectional shapes - Three-part stress-strain relation to predict the constitutive behaviour of confined high-strength concrete
(Cusson and Paultre, 1995)	- Model for rectilinearly confined columns - Two-part stress-strain relation to predict the constitutive behaviour of confined high-strength concrete
(Razvi and Saatcioglu, 1999)	- Model for rectilinear or circular cross-sectional shapes - Two-part stress-strain relation to predict the constitutive behaviour of confined high-strength concrete
(Legeron and Paultre, 2003)	- Model for rectilinear or circular cross-sectional shapes - Stress-strain relationship was calibrated based on a large number of tests

2.4.2 Code requirements for column confinement

In order to ensure the proper performance of RC columns during seismic events, modern design codes have emphasized the importance of ductile detailing. The detailing and spacing of the transverse reinforcement are some of the key parameters that affect the level of confinement in the column and the stability of the longitudinal rebars.

In the equivalent static force procedure of the National Building Code of Canada (NRCC, 2005), the minimum lateral earthquake force is given by Eq. 2-39:

$$V = \frac{S(T_a)M_v I_E W}{R_d R_o} \geq \frac{S(2.0)M_v I_{Eo} W}{R_d R_o} \qquad \text{2-39}$$

Where $S(T_a)$ represents the design spectral response acceleration, M_v is a factor that accounts for higher mode effects on base shear, I_{Eo} is the earthquake importance factor, T_a is the fundamental period of the building and W represents the dead load on the building (including snow and partition load effects). The parameter R_o is the overstrength-related force modification factor, while R_d is the ductility-related force modification factor that reflects the capability of a structure to dissipate energy through inelastic deformations (Mitchell and Paultre, 2006).

The 2004 CSA Standard (CSA, 2004) gives different requirements for the detailing and spacing of the transverse reinforcement based on the type of Seismic Force Resisting System (SFRS) and the corresponding R_d and R_o values. Table 11-1 of the CAC Concrete Design Handbook gives a summary of the design and detailing provisions in the CSA Standard for different types of RC structural systems with corresponding R_d and R_o values (Mitchell and Paultre, 2006).

Clause 21.8 of the CSA Standard gives the requirements for RC columns designed to meet R_d = 1.5, which corresponds to “conventional construction”. For columns, the tie spacing is governed by Clause 7, which requires that the spacing should not exceed the smallest of:

- 16 times the diameter of the smallest longitudinal bar;
- 48 times the tie diameter;
- The least dimension of the compression member; and
- 300 mm in compression members containing bundled bars.

Moderately ductile columns (R_d = 2.5) must meet the requirements in Clause 21.7. Clause 21.7.2.2.3 requires that the tie reinforcement should not exceed the smallest of:

- 8 times the diameter of the smallest longitudinal bar;
- 24 times the tie diameter; and
- Half the least dimension of the compression member

Furthermore, for rectangular columns, the tie spacing can also be controlled by the total transverse reinforcement in the effective area. Clause 21.7.2.2.5(b) requires that the total effective area in each of the principal directions of the cross-section, within the spacing s of the rectangular hoop reinforcement, not be less than the larger amounts required by Equations 21-16 and 21-17 of the CSA Standard.

Equation 21-16 of the CSA standard is given below:

$$A_{sh} = 0.15 k_n k_p \frac{A_g}{A_{ch}} \frac{f_c'}{f_{yh}} s h_c \qquad \text{2-40}$$

Equation 21-17 of the CSA standard is as follows:

$$A_{sh} = 0.09 \frac{f_c'}{f_{yh}} s h_c \qquad \text{2-41}$$

Where A_{sh} is the total transverse steel area within the spacing s, h_c is the cross-sectional dimension of the column core and where f_c' is the specified compressive strength of the concrete and f_{yh} is the specified yield strength of the transverse reinforcement. The parameter A_g is the gross cross-sectional area of the section and A_{ch} is the cross-sectional area of the column core. The factors k_n and k_p are computed using Eq. 2-42 and 2-43.

$$k_n = \frac{n_l}{n_l - 2} \qquad \text{2-42}$$

$$k_p = \frac{P_f}{P_o} \qquad \text{2-43}$$

Where n_l is the total number of longitudinal bars in a cross-section that are laterally supported by the corner of hoops or seismic crossties and where P_f is the maximum factored axial load for earthquake loading cases and P_o is the nominal axial resistance of the column at zero eccentricity.

Finally, ductile moment resisting frame members subjected to flexure and significant axial load (R_d = 4.0) need to meet the requirements of Clause 21.4. The tie reinforcement of ductile columns must meet the requirements in Clauses 21.4.4.2 and 21.4.4.3. For rectangular columns, Clause 21.4.4.2 requires that the tie spacing shall minimally meet the requirements of Equations 21-5 and 21-6 of the CSA Standard.

Equation 21-5 of the CSA standard is given below:

$$A_{sh} = 0.2 k_n k_p \frac{A_g}{A_{ch}} \frac{f_c^{'}}{f_{yh}} s h_c \qquad \text{2-44}$$

Equation 21-6 of the CSA standard is as follows:

$$A_{sh} = 0.09 \frac{f_c^{'}}{f_{yh}} s h_c \qquad \text{2-45}$$

The various parameters in the equations have been previously defined. Furthermore, Clause 21.4.4.3 requires that the transverse reinforcement shall be spaced at distances not exceeding the smallest of the following:

- One-quarter of the minimum member dimension;
- Six times the diameter of the smallest longitudinal bars; or
- s_x as defined by Eq. 2-46:

$$s_x = 100 + \left(\frac{350 - h_x}{3} \right) \qquad \text{2-46}$$

Where h_x is the maximum horizontal centre-to-centre spacing between longitudinal bars on all faces of the column that are laterally supported by seismic hoops or crosstie legs.

2.4.3 Model for the buckling of longitudinal reinforcing bars

Several researchers have examined the buckling behaviour of longitudinal reinforcing bars under compressive loading. One such study was performed by Bae et al. (2005) in which a simple analytical model for the inelastic buckling behaviour of reinforcing bars under compressive loading was proposed. In the extensive experimental program, more than 160 reinforcing bar specimens were tested under monotonic compressive loading. The experiments examined the effect of material properties and geometric properties (such as unsupported length-to-bar diameter ratio (L/d_b) and eccentricity-to-bar diameter ratio (e/d_b) on the behaviour of the longitudinal bars when subjected to compressive loading.

Bae et al. found the inelastic buckling behaviour of longitudinal reinforcing bars is very sensitive to the L/d_b parameter. To demonstrate this finding, the authors presented Fig. 2.15 which shows the stress-strain curve of a group of bars with the same bar diameter but with differing L/d_b ratios. It can be seen that, as the L/d_b ratio increases, the ductility and load-carrying capacity decrease due to the effect of buckling. It was also shown that as the L/d_b ratio increases, at a given axial strain, greater transverse displacements are observed in the reinforcing bar.

Based on the conclusions of their research program, the authors proposed a model to predict the complete stress strain curve of reinforcing bars under compression taking into account the effect of buckling. The authors, based their model on the assumption that the average axial strain (when buckling effects are included) is a summation of the axial strain due to axial displacement (i.e. due to axial stress), and an additional component of axial strain that is due to the transverse displacement that occurs (see Eq. 2-47):

$$\varepsilon_{avg} = \varepsilon_s + \varepsilon_{tra} \qquad \text{2-47}$$

Where ε_{avg}, ε_s and ε_{tra} refer to the average axial strain, the axial strain due to axial stress and the axial strain due to transverse displacement, respectively.

The axial strain due to axial displacement, ε_s, can be estimated from the known material tensile stress–strain curve, of the reinforcement.

The axial strain induced by transverse displacement, ε_{tra}, is dependant on the geometric conditions. In accordance with the experimental results, as the L/d_b ratio increases the axial displacement due to transverse displacement is more pronounced and starts to govern the buckling behaviour. This strain is computed by first calculating the transverse displacement during buckling, Δ_{tra}, (as a function of the axial stress, f_s) and then using Δ_{tra} to compute ε_{tra}.

Based on the experimental results, the authors suggested an empirical model to compute Δ_{tra} as a function of f_s. The model assumes that bar buckling begins when the yield stress is reached. The step by step procedure used in the model is as follows:

Step 1: Before the axial stress, f_s, reaches the yield stress, f_y, the linear elastic response is used.

Step 2: After the stress reaches f_y, the bar begins to buckle. After assuming a value for Δ_{trans}, the corresponding axial stress is computed using Eq. 2-48 to 2-51.

Equations 2-48 and 2-49 are used when $\frac{\Delta_{tra}}{L} \leq 0.04$:

$$\frac{f_s}{f_y} = 1 + \left(\frac{f^*{}_s}{f_y} - 1\right) \times \sqrt{1 - \left(\frac{\Delta_{tra}}{\Delta^*{}_{tra}} - 1\right)^2} \qquad \text{for } \frac{f^*{}_s}{f_y} > 1 \qquad \text{2-48}$$

$$\frac{f_s}{f_y} = \left(\frac{f^*{}_s}{f_y} - 1\right) \times \left(\frac{\Delta_{tra}}{\Delta^*{}_{tra}}\right) + 1 \qquad \text{for } \frac{f^*{}_s}{f_y} \leq 1 \qquad \text{2-49}$$

Equations 2-50 and 2-51 are used when $\frac{\Delta_{tra}}{L} > 0.04$:

$$\frac{f_s}{f_y} = \frac{f^*{}_s}{f_y} + A_a\left(\frac{\Delta_{tra} - \Delta^*{}_{tra}}{L}\right) \qquad \text{for } \frac{f_s}{f_y} \geq \frac{2}{3} \times \frac{f^*{}_s}{f_y} \qquad \text{2-50}$$

$$\frac{f_s}{f_y} = \frac{2}{3} \times \frac{f^*{}_s}{f_y} + \frac{A_a}{2}\left(\frac{\Delta_{tra} - \Delta^*{}_{tra}}{L}\right) > 0.2 \qquad \text{for } \frac{f_s}{f_y} < \frac{2}{3} \times \frac{f^*{}_s}{f_y} \qquad \text{2-51}$$

Where d_b is the nominal bar diameter and L is the unsupported length of the bar. The constant Δ^*_{tra} is taken as being equal to $0.04 \times L$. The value A_a is the initial slope of the descending branch of the curve and is computed using Eq. 2-52. The value f_s^* is computed using Eq. 2-53.

$$A = 4 \times \left(\frac{f_u}{f_y} - 1 \right)^2 - 5 \qquad \text{2-52}$$

$$f_s^* = f_y \times \left[-0.45 \times \left(\frac{f_u}{f_y} \right)^{2.5} \times ln \left(\frac{L/d_b}{4} \right) + \frac{f_u}{f_y} \right] \leq f_u \qquad \text{2-53}$$

Based on these equations the complete f_s - Δ_{trans} curve can be computed (see Fig. 2.16).

Step 3: Next, the axial strain, ε_s, due to axial stress, f_s, is computed using Eq. 2-54, which is a strain hardening law proposed by Mander et al. (1984):

$$f_s = f_u + (f_y - f_u) \times \left(\frac{\varepsilon_u - \varepsilon_s}{\varepsilon_u - \varepsilon_{sh}} \right)^p \qquad \text{2-54}$$

Where f_u is the ultimate stress taken from the tensile stress-strain curve of the bar and where ε_{sh} and ε_u are the strains corresponding to the commencement of strain hardening and the ultimate stress, f_u. The constant P is computed using Eq. 2-55.

$$P = E_{sh} \times \left(\frac{\varepsilon_u - \varepsilon_{sh}}{f_u - f_y} \right) \qquad \text{2-55}$$

Where E_{sh} represents the initial slope of the hardening curve.

Step 4: Next, the axial strain that results from the transverse displacement, ε_{tra}, is computed using Eq. 2-56.

$$\varepsilon_{tra} = max\begin{cases} \left(\dfrac{0.035 \times cos\,\theta_a + \theta_a}{cos\,\theta - 0.035 \times \theta}\right) \times \dfrac{\Delta_{tra}}{d_b} \\ \dfrac{1}{\left(cos\,\theta_a - 0.07 \times \theta_a\right)} \times \left(0.07 \times cos\,\theta_a + \theta_a\right) \times \left(\dfrac{\Delta_{tra}}{d_b} - 0.035\right) \end{cases} \quad 2\text{-}56$$

Where the parameter θ_a is computed using Eq. 2-57.

$$\theta_a = \frac{6.9}{\left(L/d_b\right)^2} - 0.05 \quad 2\text{-}57$$

Step 5: The total average strain, ε_{avg}, can then be computed using Eq. 2-47.

Step 6: Finally the transverse displacement Δ_{trans} is incremented and Steps 2-5 are repeated until the complete f_s - ε_{avg} curve is obtained.

2.4.4 Use of SFRC in columns

Several researchers have investigated the potential of using steel fibres in order to improve the compressive stress-strain behaviour of columns. A summary of some of these experiments is presented in the next sections.

2.4.4.1 Ganesan and Murthy tests

Ganesan and Murthy (1990) tested 8 reinforced concrete columns with various levels of confinement reinforcement. Out of these eight columns, four were additionally reinforced with steel fibres (1.5 % by volume). The columns were then subjected to monotonic axial compression until failure. The researchers found that the addition of fibres delayed cover spalling in the columns. Furthermore, a more diffused cracking pattern was observed in the SFRC specimens. In addition, a comparison of the load-strain curves showed that the addition of fibres resulted in an increase in the ultimate strength of the columns. Moreover, the fibres improved the post-peak resistance of the specimens.

2.4.4.2 Massicotte et al. tests

Massicotte et al. (1998) tested 18 short columns under axial loading in order to investigate the potential benefits associated with the use of SFRC. The variables considered were the amount of fibres in the concrete mix (0%, 0.5% and 1% fibres by volume of concrete) and the amount of transverse reinforcement in the columns. In addition the authors examine the influence of the addition of fibres on cover spalling and core confinement. The results showed that the addition of fibres improved the strength and post-peak ductility of the columns. The fibres also improved the performance of both the core and cover regions.

2.4.4.3 Foster and Attard tests

Foster and Attard (2001) tested 21 columns cast with fibre reinforced concrete under concentric and eccentric compression loads. The concrete strengths ranged from 67 to 88 MPa. Fibres were added to the concrete at a weight fraction of 2%. The results of the study showed that by adding steel fibres to the concrete mix sudden cover spalling can be effectively prevented. Furthermore, the columns showed a superior performance when compared to specimens cast without fibres in terms of post-peak ductility.

Foster (2001) also reported an empirical equation that can be used in order to compute the confining pressure, f_f, that is provided by the fibres in SFRC columns (see Eq. 2-58).

$$f_f = \frac{3}{8} \times \frac{l_f}{d_f} v_f \times \left[0.6\left(f'_c\right)^{2/3}\right] \qquad \text{2-58}$$

Where v_f represents the volume fraction of fibres in the concrete mix and where the parameter $0.6\left(f'_c\right)^{2/3}$ is an empirical factor that is used to estimate the bond-shear strength of the matrix. Finally, the factor 3/8 is a parameter that accounts for the random orientation of the fibres.

2.4.4.4 Campione's model

Campione (2002) developed an empirical model to express the stress–strain relationships of fibre reinforced concrete in compression for both normal and high-strength concrete columns that are constructed with conventional transverse steel reinforcement. Campione also developed analytical expressions for determining the ultimate load corresponding to the complete formation of the concrete failure plane in fibre reinforced concrete columns.

2.4.4.5 Dhakhal's model

Based on results from SFRC compressive cylinder and tension pullout tests, Dhakhal (2006) developed a model that can be used to obtain empirical cyclic path-dependant material models for SFRC. Furthermore, the author examined the influence of bar buckling on cover spalling in SFRC and presented an equation that can be used to estimate the compressive strain corresponding to cover spalling in SFRC columns. The various aspects were then encoded in a finite element based fibre model that can be used to perform cyclic analyses of SFRC columns.

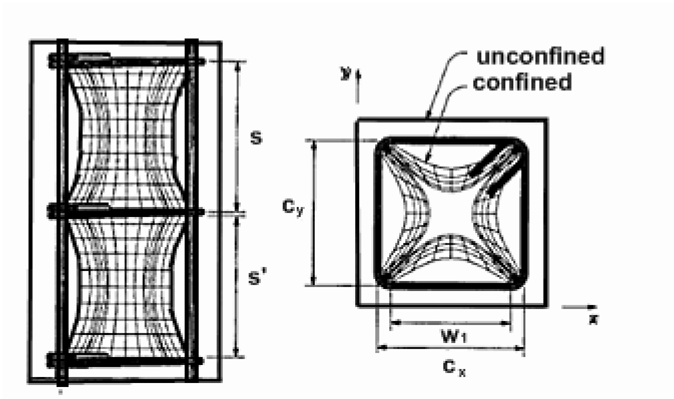

Figure 2.12: Arching action in RC columns

[Adapted from (Cusson and Paultre, 1995)]

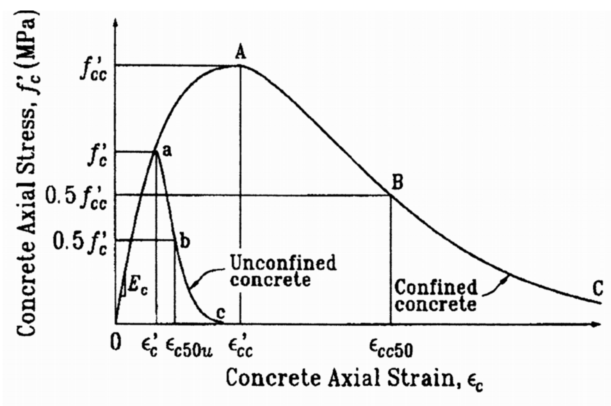

Figure 2.13: Stress-strain relationships for confined and unconfined concrete.

[Adapted from (Legeron and Paultre, 2003)]

Models	Expression for ascending Branch	Expression for descending branch
Yong *et al.*	$\frac{f_c}{f_{cc}} = \frac{A(\varepsilon_c/\varepsilon_{cc}) + B(\varepsilon_c/\varepsilon_{cc})^2}{1 + C(\varepsilon_c/\varepsilon_{cc}) + D(\varepsilon_c/\varepsilon_{cc})}$ where $A = \frac{E_c}{E_{cc}}$, $B = [1{\cdot}82(A-1) - 1]$ $C = A - 2$, $D = B + 1$	Same as the expression of model's ascending branch, but with different values of the two constants: A, B; $A = [(\varepsilon_{2i} - \varepsilon_i/\varepsilon_{cc}][\varepsilon_{2i}E_i/(f_{cc} - f_i)] - [4\varepsilon_i E_{2i}/(f_{cc} - f_{2i})]$ $B = (\varepsilon_i = \varepsilon_{2i})[E_i/(f_{cc} - f_i)] - [4E_{2i}/(f_{cc} - f_{2i})]$
Bjerkli *et al.*	Same as Yong *et al.* model but $B = 0$, $D = 1$	$f_c = f_{cc} - \beta(\varepsilon_c - {}_{cc}) \geqslant f_{ss}$ $\beta = \frac{0{\cdot}15 f_{cc}}{\varepsilon_{c85c} - \varepsilon_{cc}}$ f_{ss} = sustaining branch stress as defined in the model.
Nagashima *et al.*	$f_c = f_{cc}\left[\frac{k(\varepsilon_c/\varepsilon_{cc})}{k - 1 + (\varepsilon_c/\varepsilon_{cc})^k}\right]$ where $k = \frac{E_c}{E_c - E_{cc}}$	Same as above in Bjerkli *et al.* model but, $\beta = \frac{0{\cdot}5 f_{cc}}{\varepsilon_{c50c} - \varepsilon_{cc}}$ $f_{ss} = 0{\cdot}3 f_{cc}$
Muguruma *et al.*	For $0 \geqslant \varepsilon_c \geqslant \varepsilon_{c0}$ $f_c = E_c\varepsilon_c + \frac{(f_{co} - E_c\varepsilon_{co})}{\varepsilon_{co}^2}\varepsilon_c^2$ For $\varepsilon_{co} \geqslant \varepsilon_c \geqslant \varepsilon_{cc}$ $f_c = f_{cc} - \frac{(f_{cc} - f_{co})}{(\varepsilon_{cc} - \varepsilon_{co})^2}(\varepsilon_c - \varepsilon_{cc})$	Same as in Bjerkli *et al.* model but $\beta = \frac{f_u - f_{cc}}{\varepsilon_u - \varepsilon_{cc}}$ f_{ss} = not defined.
Li *et al.*	Same as Muguruma *et al.* model but with different values of parameters.	$\beta = \alpha\frac{f_{cc}}{\varepsilon_{cc}}$ $f_{ss} = 0{\cdot}4 f_{cc}$
Cusson and Paultre	Same as Nagashima *et al.* model with but with different values of parameters.	$f_c = f_{cc}\exp\left[k_1(\varepsilon_c - \varepsilon_{cc})^{k_2}\right]$, where k_1, k_2 are constants.
Razvi and Saatcioglu	Same as Nagashima *et al.* model but with different values of parameters.	$\beta = \frac{0{\cdot}15 f_{cc}}{\varepsilon_{c85c} - \varepsilon_{cc}}$ f_{ss} = not defined.
Legeron and Paultre	Same as Nagashima *et al.* model but, different values of parameters.	Same as the Cusson and Paultre model but, with different values of parameters.

Figure 2.14: Expressions used in the prediction models available in the literature [Adapted from (Sharma et al., 2005)]

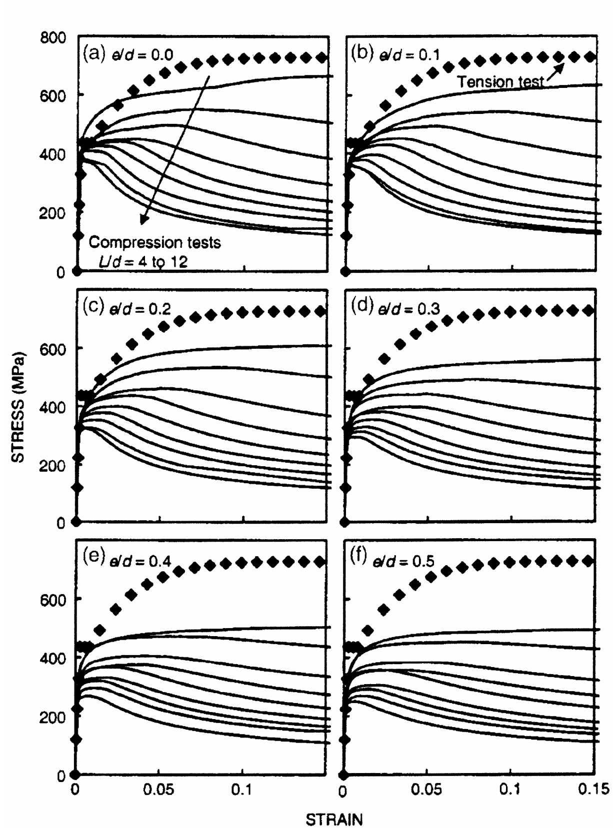

Figure 2.15: Effect of L/d ratio on compressive stress-strain curve of rebars

[Adapted from (Bae et al., 2005)]

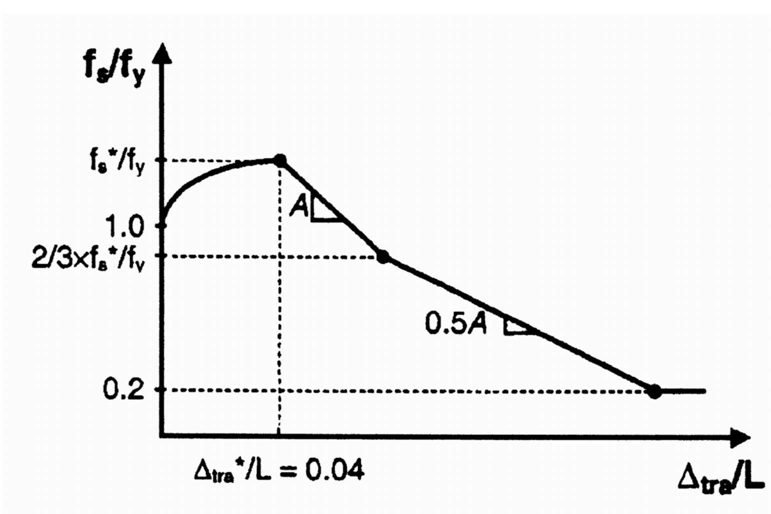

Figure 2.16: Schematic representation of bar buckling model

[Adapted from (Bae et al., 2005)]

2.5 The Behaviour of RC Beams and the Benefits of using SFRC in Beams

Over the past century there has been a considerable amount of research focusing on trying to gain a better understanding of the shear behaviour of reinforced concrete beams. Although much progress has been made, the shear behaviour of beams remains a very complex problem that is not completely understood.

In the mid 1950s the collapse and shear failure of large beams in two US Air-force warehouses shed light on the relative inaccuracy of the shear design equations of the time. It also demonstrated in dramatic fashion the importance of understanding the shear problem when designing RC structural members (Collins and Mitchell, 1997).

Nearly 50 years later although there has been great advancement in our knowledge of the concept of the shear strength in RC members, it still remains imperative to study and provide new solutions to the shear problem in RC beams.

In addition, over the past 2 decades there has been a great interest in studying the potential of using SFRC to improve the shear resistance of beams.

This portion of the literature review will start with a brief examination of the various factors that influence the shear behaviour in RC beams (Section 2.5.1). Section 2.5.2 presents a summary of the most common models for the shear behaviour of RC members. Section 2.5.3 presents the current CSA Standard methods for shear design. Finally Section 2.5.4 presents an overview of the current body of research pertaining to the shear behaviour of SFRC beams and describes some of the equations that have been proposed in the literature.

2.5.1 Factors affecting the shear resistance of RC beams

The shear transfer in a RC member is the sum of several mechanisms: shear stresses in the uncracked concrete, aggregate interlock (or interface shear), dowel action of the longitudinal reinforcement, arching action and residual tensile stresses that are transmitted across the cracks.

Furthermore, unless an adequate amount of web reinforcement is provided, the shear stresses in beams will result in diagonal cracks that may lead to a brittle and premature failure of the structural member.

In addition, there are several parameters that can influence the shear resistance of RC beams. Amongst these one can mention: the shear span-to-depth ratio (a/d), the depth of the member (or size effect), axial load, amount of longitudinal reinforcement, concrete compressive strength, loading conditions, cross-sectional shape, distribution of longitudinal reinforcement.

Over the past few decades, many models have been proposed in the literature for the prediction of the shear resistance of RC members constructed without transverse steel reinforcement. These models range from simple empirical formulations to nonlinear finite element methods.

2.5.2 Models for the shear behaviour of RC beams

2.5.2.1 Kani "comb-tooth" model

Kani (1964) developed a rational model to explain the behaviour of RC beams that are cracked in flexure and subjected to shear stresses (see Fig. 2.17). The "tooth-comb" model considered the concrete between adjacent flexural cracks as being analogous to the "teeth" in a "comb" (with the uncracked concrete representing the backbone of the comb), and postulated that the diagonal cracking in the beam results from the bending of these concrete "teeth" (Collins and Mitchell, 1997). Each concrete "tooth" was idealized as a cantilever that was fixed in the compression zone of the beam, with the "tooth" being loaded by horizontal forces (ΔT) that are produced by the bond in the longitudinal reinforcement. Diagonal cracking is assumed to take place when the bending moment in the "tooth" increases such that the tooth breaks off.

The work presented by Kani was important in that it showed that slender beams that do not contain appropriate amounts of web reinforcement may fail in a brittle manner after the formation of the diagonal cracks. In contrast, beams that have a low a/d ratio can generally sustain further load after the formation of the diagonal cracks (Collins and Mitchell, 1997).

2.5.2.2 Truss Models

Early researchers such as Mörsch (1905) explained the shear stresses in RC beams using the "truss" analogy, where the vertical stirrups in the beam act as vertical tension members of the truss, while the diagonal compressive stresses in the concrete are idealized as the diagonal members of the truss. The longitudinal reinforcement and the flexural compression zone of the beam are represented by the bottom and top cords of the truss respectively.

This idealization neglected the tensile stresses in the concrete and assumed that diagonal compression stresses would be inclined at $45°$ after cracking. Mörsch recognized that the choice of a $45°$ slope was conservative but chose this value citing the difficulty in determining this angle.

Later it was determined that the inaccuracy of the $45°$ truss model was due to the neglect of the tensile stresses in the concrete and the choice of the slope of $45°$.

2.5.2.3 Variable angle truss models

The truss model can be made more accurate by modifying the Mörsch model so as to include a more realistic value for the slope of the diagonal compressive stresses. Figure 2.18 illustrates the equilibrium conditions of a variable-angle truss idealization. From the free-body-diagram there are only 3 equilibrium equations with 4 unknowns (the principal compressive stress, the tensile force in the longitudinal reinforcement, the stress in the stirrups and the inclination of the principal compressive stresses). Hence prior to solving the equilibrium equations, the inclination of the diagonal compressive struts must be known (Collins and Mitchell, 1997).

2.5.2.4 Compression Field Theory

Mitchell and Collins (1974) proposed the Compression Field theory (CFT) in order to solve the equilibrium equations in the variable angle truss model. Wagner (1929) had previously studied the compatibility relationships between deformations in order to investigate the tension fields that develop in a thin-webbed metal girder subjected to shear. Applying Wagner's methodology to reinforced concrete, Mitchell and Collins developed the CFT by assuming that the concrete carries no tension after cracking with the shear being carried by a field of diagonal compression. Using Mohr's circle of strains the compatibility conditions, relationships can be found between the various strains in the system (longitudinal strain of web, transverse strain, principal compressive strain). Furthermore, the angle of inclination of the diagonal compression field could be defined as a function of these strains. In addition, in the CFT, the constitutive relationships linking the strains and the stresses in the various materials were defined (for the steel reinforcement and the diagonally cracked concrete).

With the equilibrium equations, the compatibility equations and the constitutive stress-strain relationships of the materials the various unknowns in the system could now be solved (see Fig. 2.19). Not only does the theory allow one to predict the strength of RC members subjected to shear, it allows for the prediction of the complete load-deformation response (Collins and Mitchell, 1997).

However, the CFT neglected the contribution of the tensile stresses in the cracked concrete and hence can lead to conservative estimates of the shear strength of RC members.

2.5.2.5 Modified Compression Field Theory

Based on the CFT model developed by Mitchell and Collins, Vecchio and Collins (1986) developed the Modified Compression Field Theory (MCFT) which now included the contribution of the tensile stresses in the cracked concrete.

Vecchio and Collins performed tests on reinforced concrete panels subjected to pure shear and based upon the results of these tests recommended an average stress-strain relationship for cracked concrete in tension. Furthermore the previous material relationships for the cracked concrete in compression and the steel reinforcement defined in the CFT were implemented in the MCFT.

Based on equilibrium equations (between average stresses in the concrete and steel reinforcement), compatibility relationships (between average strains in the concrete and steel reinforcement), constitutive material stress-strain relationships (cracked concrete in compression, cracked concrete in tension, steel reinforcement) and relationships for load transmission at cracks, the MCFT can be used in the analysis of RC members subjected to shear. Figure 2.20 presents a summary of the various aspects of the MCFT. Further information on the MCFT, and how it can be used in the analysis of RC members subjected to combined shear, axial load and moment can be found in the work of Collins and Mitchell (1997).

The development of computer programs such as RESPONSE 2000 (Bentz, 2000) have made it practical to use the MCFT to evaluate the shear capacity and complete load-deformation response of RC beams subjected to combined shear and flexure.

2.5.3 CSA 2004 shear design provisions

2.5.3.1 Overview of the CSA shear design provisions

Prior to the mid 1980s the Canadian shear design provisions were based on empirically derived relationships. The 1984 version of the Canadian provisions introduced a "general" design method based on the Compression Field Theory (CFT).

The 1994 CSA shear design provisions introduced a new general design method that was based upon the Modified Compression Field theory (Collins et al., 1996). To use the general design method the engineer needed to check several tables to come up with values for the two main variables in the derivation of the shear resistance of the RC member, namely θ (the angle of inclination of the diagonal compressive stresses to the longitudinal axis of the member) and β (a factor that accounts for the ability of the concrete to transmit tensile stresses between the cracks). This made the general design method more complex than the simplified method, limiting its practical use (Bentz and Collins, 2006).

In the shear design provisions of the 2004 CSA Standard, simplified analytical relationships based upon the MCFT were developed and incorporated which resulted in a simple design procedure. As a result of this simplification, the simplified design method now became a special case of the general design method rather than a method based on the ACI provisions (Bentz and Collins, 2006).

The 2004 CSA Standard requires that members that are subjected to shear be designed so that the factored shear resistance, V_r, meets the requirement in Eq. 2-59:

$$V_r \geq V_f \qquad \text{2-59}$$

Where V_f is the factored shear applied to the RC member.

For traditional reinforced concrete beams, V_r is computed using Eq. 2-60, where V_c represents the concrete contribution to shear and V_s is the transverse steel contribution to shear.

$$V_r = V_c + V_s \qquad \text{2-60}$$

The shear contributions V_c and V_s are computed using Eq. 2-61 and 2-62 respectively.

$$V_c = \phi_c \lambda \beta \sqrt{f'_c} b_w d_v \qquad \text{2-61}$$

$$V_s = \frac{\phi_s A_v f_{yh} d_v \cot\theta}{s} \qquad \text{2-62}$$

Where $b_w d_v$ is the shear area represented by the web width multiplied by the shear depth of the beam. The parameter λ is a factor that takes into account the use of light-weight concrete. The factors ϕ_c and ϕ_s are the material reduction factors for concrete and steel, respectively. In determining V_s, the parameters A_v, f_{yh} and s are the cross-section area, yield stress and spacing of the transverse steel reinforcement.

The quantities β and θ are the main parameters that need to be determined to compute the shear resistance of the RC member.

2.5.3.2 Determination of the factor β and the angle θ

The main way shear forces are assumed to be carried in concrete members without transverse reinforcement is by aggregate interlock. The two main factors that will limit this resistance mechanism are the size effect and the strain effect (a function of the average strain perpendicular to the crack). Hence, based on the MCFT, these two aspects are incorporated in the computation of β (Bentz and Collins, 2006).

Equation 2-63 is used to compute β, where the second term incorporates the size effect factor where s_{ze} is the effective crack spacing in the member (which is a function of the depth of the member and the aggregate size). The parameter ε_x is the longitudinal strain at mid-depth of the member.

$$\beta = \frac{0.40}{\left(1+1500\varepsilon_x\right)} \cdot \frac{1300}{\left(1000+s_{ze}\right)} \qquad \text{2-63}$$

Members that contain a minimum amount of transverse reinforcement should fail by yielding of the stirrups and eventual crushing of the concrete in the web. The CSA method for computing the angle of inclination of diagonal compressive stresses ensures that the RC member reaches the required shear resistance so as to ensure the yielding of the stirrups while also ensuring that the concrete does not crush before the desired shear stress is reached (Bentz and Collins, 2006). Eq. 2-64 is used to compute the angle θ as a function of ε_x.

$$\theta = 29^\circ + 7000\varepsilon_x \qquad \text{2-64}$$

The average longitudinal strain at mid-depth of the member, ε_x, is computed based on the simple free-body diagram presented in Fig. 2.21 and for members subjected to moment and shear reduces to Eq. 2-65. Where, V_f and M_f represent the applied shear load and moment at the critical section of the RC member. The components E_s and A_s represent the modulus and cross-sectional area of the longitudinal reinforcement.

$$\varepsilon_x = \frac{\left(\frac{M_f}{d_v}\right) + V_f}{2 \times E_s \times A_s} \qquad \text{2-65}$$

2.5.3.3 Simplified and General design methods

In the general design method of the 2004 CSA Standard, Eq. 2-65 is used to compute ε_x based on known values of V_f and M_f. Thereafter Eq. 2-63 and 2-64 are used to compute the factor β and the angle θ which are in turn used to compute the factored shear resistance V_r in Eq. 2-60. Hence, the general design method implements the MCFT using a simplified non-iterative procedure.

As was mentioned earlier, the simplified design method is a special case of the general design method. The relationships in the simplified method were derived based on the assumption that the longitudinal strain at mid-depth of the member, ε_x, is equal to 0.85×10^{-3} (Collins et al., 2006). Substituting this strain into the Eq. 2-64 produces an angle θ of 35°. Using a strain of 0.85×10^{-3} in Eq. 2-63 yields a constant value for β in the case of members containing stirrups ($\beta = 0.18$). For members constructed without stirrups β includes a size effect factor as shown in Eq. 2-66 (Bentz and Collins, 2006).

$$\beta = \frac{230}{1000 + d_v} \qquad \text{2-66}$$

Furthermore, in using these expressions, it is assumed that that the steel reinforcement does not exceed 400 MPa and that the specified concrete strength is no more than 60 MPa.

2.5.4 Analytical models for the shear resistance of SFRC beams

Over the past two decades there have been several experimental programs focusing on the use of SFRC in reinforced concrete beams. Most of these experiments demonstrated the advantages that can be gained when steel fibres are used to improve the shear resistance of shear deficient beams. Despite the large body of research, to this date, most international design codes do not contain any guidance for engineers for the design of structural elements constructed with SFRC. As a result, several authors have made attempts at developing models for the prediction of the shear behaviour SFRC beams.

The majority of these methods involve the use of empirical equations to compute the improved shear resistance of RC beams when fibres are added to the concrete matrix. Many of these equations were developed using a limited series of experimental results that do not cover a wide-range of fibre, concrete and beam dimensional parameters. As a result, in most cases the relationships do not produce accurate estimates of the shear resistance of SFRC beams (Minelli, 2005).

Minelli (2005) performed a review of the analytical methods for SFRC beams that have been proposed in the literature and found that most of the empirical methods could be divided into two categories.

The first category considers the fibres to directly influence the shear capacity of the concrete (as determined from tests such as the modulus of rupture test or the splitting test) and hence does not divide the contributions of the concrete and the fibres into separate terms. Examples of such models are those presented by Kwak et al. (2002), Li et al. (1992) and Sharma (1986).

The second category of relationships considers the steel fibres as providing a shear resistance that is in excess of the concrete shear resistance (much in the same way that stirrups can be used to increase the resistance of plain concrete beams). This second category of relationships takes into account the fibre contribution to shear resistance using a so-called “fibre factor” which is a function of the fibre aspect ratio, fibre volume percentage and an empirical fibre bond factor that is a function of the type of fibre that is used and the matrix properties. Examples of this second category are the models presented by Ashour et al. (1992), Narayanan and Darwish (1987), and Mansur et al. (1986) among others.

Table 2-2 presents a summary of some of the relationships that have been proposed in the literature for predicting the shear resistance of SFRC beams. The common feature of most of the relationships is that they are empirical in the way they compute the concrete contribution as well as the fibre contribution. The table briefly lists the main equations in each of the models, further details regarding the various relationships can be found by consulting the listed references.

Table 2-2: Some of the models for predicting the resistance of SFRC beams

(Kwak et al., 2002)	
- f_{spfc} refers to the split cylinder strength - The factor e is a function of the a/d ratio	$\upsilon_u = 3.7 e f_{spfc}^{2/3}\left(\rho \frac{d}{a}\right)^{1/3} + 0.8\left(0.41\tau \frac{L_f V_f d_f}{D_f}\right)$
(Khuntia et al., 1999)	
- The factor α is a function of the a/d ratio	$\upsilon_u = \left(0.167\alpha + 0.25 \frac{L_f V_f d_f}{D_f}\right)\sqrt{f_c'}$
(Imam et al., 1995)	
- Ψ is a size effect factor - The factor ω is a function of the fibre properties	$\upsilon_u = 0.6\Psi\sqrt[3]{\omega}\left[\left(f_c'\right)^{0.44} + 275\sqrt{\frac{\omega}{\left(a/d\right)^5}}\right]$
(Cucchiara et al., 2004)	
- The factor χ is a function of the concrete strength and the a/d ratio	$\upsilon_c = 0.83\xi\sqrt[3]{\rho}\cdot\chi + \frac{1.67\sqrt{f_c'}}{\chi}\rho_w f_{yw}$
(Mansur et al., 1986)	
- Applicable for normal strength concrete	$\upsilon_u = \left(0.16\sqrt{f_c'} + 17.2\frac{\rho V d}{M}\right) + 0.41\left(\tau V_f \frac{l_f}{d_f}\right)$
(Sharma, 1986)	
- k is a function of the test that is used do determine the tensile resistance of the concrete.	$\upsilon_u = k f_t'\left(\frac{d}{a}\right)^{0.25}$
(Narayanan and Darwish, 1987)	
- f_{spfc} refers to the split cylinder strength - The factor e is a function of the a/d ratio	$\upsilon_u = e\left(0.24 f_{spfc}' + 80\rho\frac{d}{a}\right) + 0.41\left(\tau\frac{L_f V_f d_f}{D_f}\right)$
(Ashour et al., 1992)	
- Applicable for high strength concrete	$\upsilon_u = \left(0.7\sqrt{f_c'} + 7\frac{L_f V_f d_f}{D_f}\right)\frac{d}{a} + 17.2\rho\frac{d}{a}$
(Li et al., 1992)	
- f_{sp} refers to the split cylinder strength - A different expression is used for a/d < 2.5	$\upsilon_{frc} = 1.25 + 4.7\left[\left(f_f f_{sp}\right)^{\frac{3}{4}}\left(\rho\frac{d}{a}\right)^{\frac{1}{3}} d^{-\frac{1}{3}}\right]$
(Cassanova, 1996)	
- $\overline{\sigma_p}(w)$ refers to the residual post-cracking strength of SFRC at a crack width w	$V = 0.9bd\cdot\overline{\sigma_p}(w) + V_s$

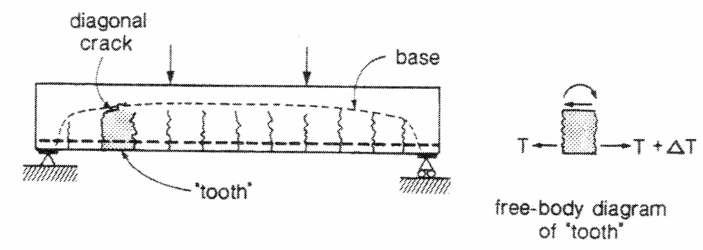

Figure 2.17: Schematization of Kani's tooth comb model

[Adapted from (Collins and Mitchell, 1997)]

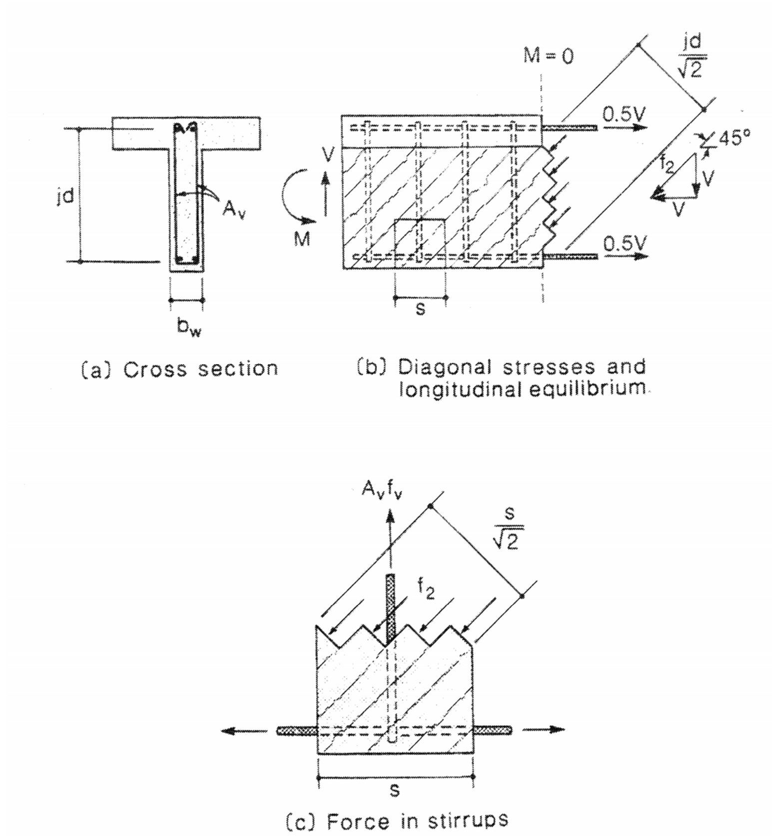

Figure 2.18: The equilibrium conditions of a variable-angle truss idealization

[Adapted from (Collins and Mitchell, 1997)]

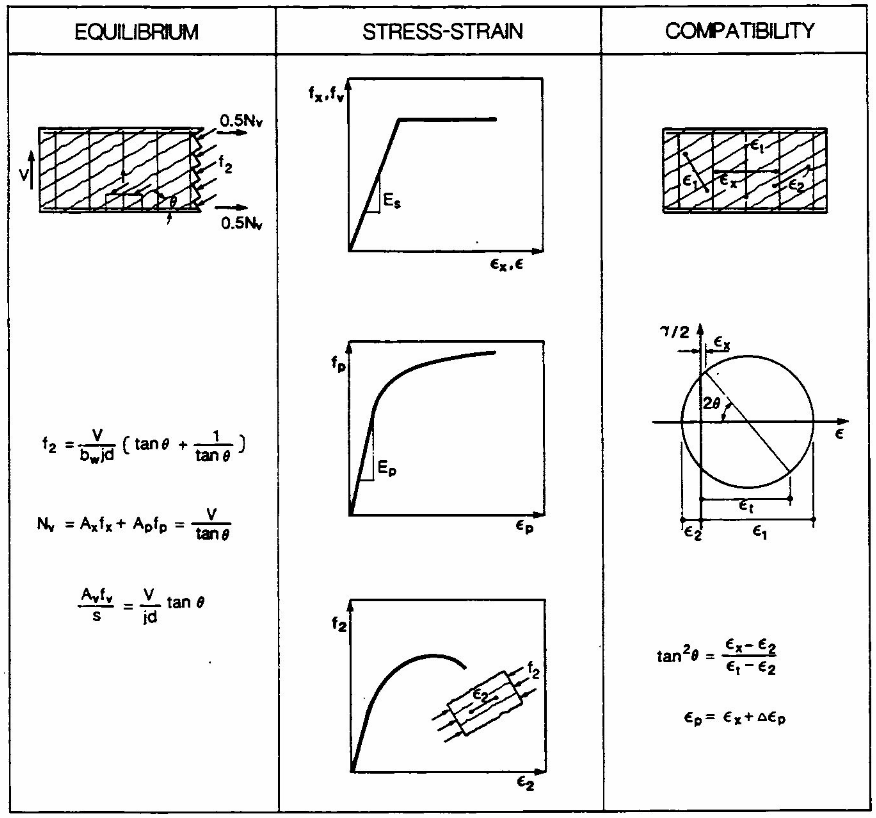

Figure 2.19: Summary of the various aspects of the CFT

[Adapted from (Collins and Mitchell, 1997)]

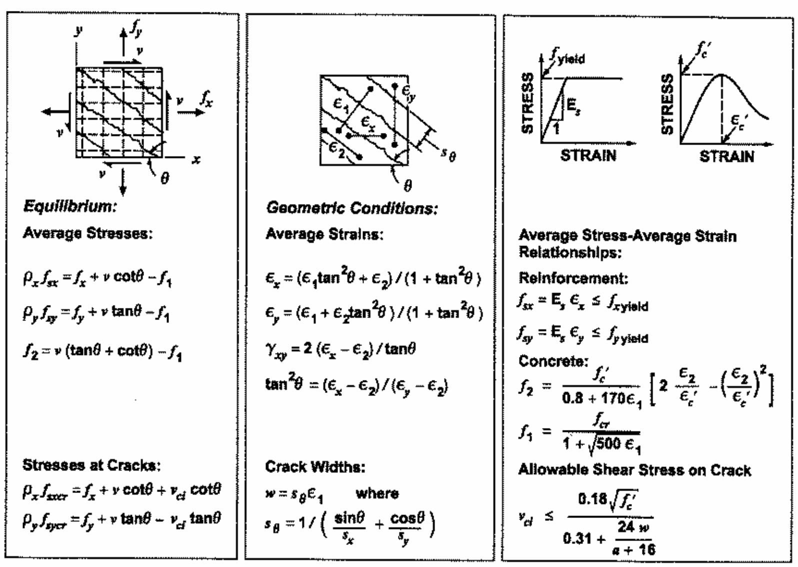

Figure 2.20: Summary of the various aspects of the MCFT

[Adapted from (Minelli, 2005)]

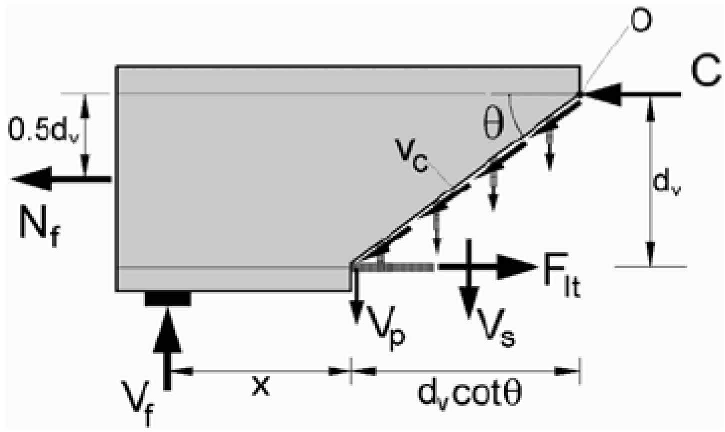

Figure 2.21: Basic shear resistance mechanisms assumed in the CSA 2004 code
[Adapted from (Bentz and Collins, 2006)]

Chapter 3 Experimental Program on Steel Fibre Reinforced Concrete Columns Subjected to Pure Axial loading

3.1 Objectives

The main objective of this phase of the research program was to investigate the performance and ductility enhancements that can be gained from the use of steel fibre reinforced concrete (SFRC) in Reinforced Concrete (RC) columns. An additional objective was to examine if the provision of fibres would permit a reduction of confinement reinforcement. The test program examined the influence of fibres on confinement, cover spalling and bar buckling in RC columns.

3.2 Description of Test Specimens

An experimental program was conducted in order to investigate the effect of fibre reinforced concrete on the response of members subjected to pure axial loading. Several full-scale RC columns, with various ratios of confinement reinforcement and with various fibre contents, were tested. The columns had an overall height of 1200 mm and were 300 x 300 mm in cross-section with a 30 mm clear cover. In addition, sections containing identical reinforcing cages, but with no concrete cover were constructed. In order to place the reinforcing cages in the formwork the specimens with "no cover" had a cover of 5 mm. This enabled the study of the influence of cover spalling on the performance.

The longitudinal reinforcement consisted of 8–15M reinforcing bars (diameter, d_b, of 16 mm and a cross-sectional area, A_s, of 200 mm^2), resulting in a vertical steel reinforcement ratio of 1.8%. The transverse reinforcement was provided by 10M hoops, with seismic hooks (d_b = 11.3 mm and A_s = 100 mm^2). The confinement details were selected using the provisions of the 2004 CSA A23.3-04 Standard (CSA, 2004). In all cases, the chosen hoop spacing for the various specimens was extended over the full height of the column. A summary of the specimens that were included in the test program is given below:

- **A-series:** The A-Series specimens were detailed in accordance with the basic confinement provisions of the CSA Standard, for columns having a ductility-related force modification factor, R_d, of 1.5.
- **B-series:** The B-Series specimens were detailed in accordance with the confinement provisions for moderately ductile columns of the CSA Standard (R_d = 2.5).
- **C-series:** The C-Series Specimens were detailed in accordance with the confinement provisions for ductile columns of the CSA Standard (R_d = 4.0).
- **D-series:** The D-Series Specimens were detailed with a level of transverse reinforcement that is intermediate between R_d = 2.5 and 4.0 of the CSA Standard.

The particulars regarding the cross-section and confinement properties for the various specimens are detailed further in Sections 3.3 to 3.6.

3.3 Transverse Reinforcement for the A-series Specimens

The A-series specimens were detailed in accordance with the confinement provisions in Clause 7 of the 2004 CSA Standard, for columns having a ductility-related force modification factor, R_d of 1.5 (conventional construction). The confinement details are shown in Table 3-1 and Fig. 3.1(a) and (b).

The transverse reinforcement was provided by 10M hoops, with seismic hooks, having straight bar extensions of $6d_b$ for anchorage in the confined core of the specimen. The spacing, s, of the 10M hoops was governed by the bar buckling requirements of Clause 7.6.5.2, resulting in a required spacing of 240 mm ($16d_b$).

Specimen A0 contained SCC concrete without any fibres. Specimens A1, A1.5 and A2 contained SCC concrete with steel fibres at a quantity of 1%, 1.5% and 2% by volume respectively. Specimens A0nc, A1nc and A1.5nc contained SCC concrete with steel fibres in a quantity of 0%, 1% and 1.5% by volume, respectively, in a cross-section that had a 5 mm cover.

Table 3-1: Design details for the A-series specimens

Column Specimen	Cross Section (mm)	Cover (mm)	f'_c (MPa)	% Fibres	Design	Tie Spacing	Actual Tie Spacing
A0	300 x 300	30	50	0 %	As per requirement of $\mathbf{R_d=1.5}$ of CSA	*Clause 7.6.5.2* [240 mm] - $16d_b$ [240 mm] - $48d_t$ [480 mm] - least dim [300 mm]	240 mm
A1				1.0%			
A1.5				1.5%			
A2				2.0%			
A0nc	250 x 250	5		0.0%			
A1nc				1.0%			
A1.5nc				1.5%			

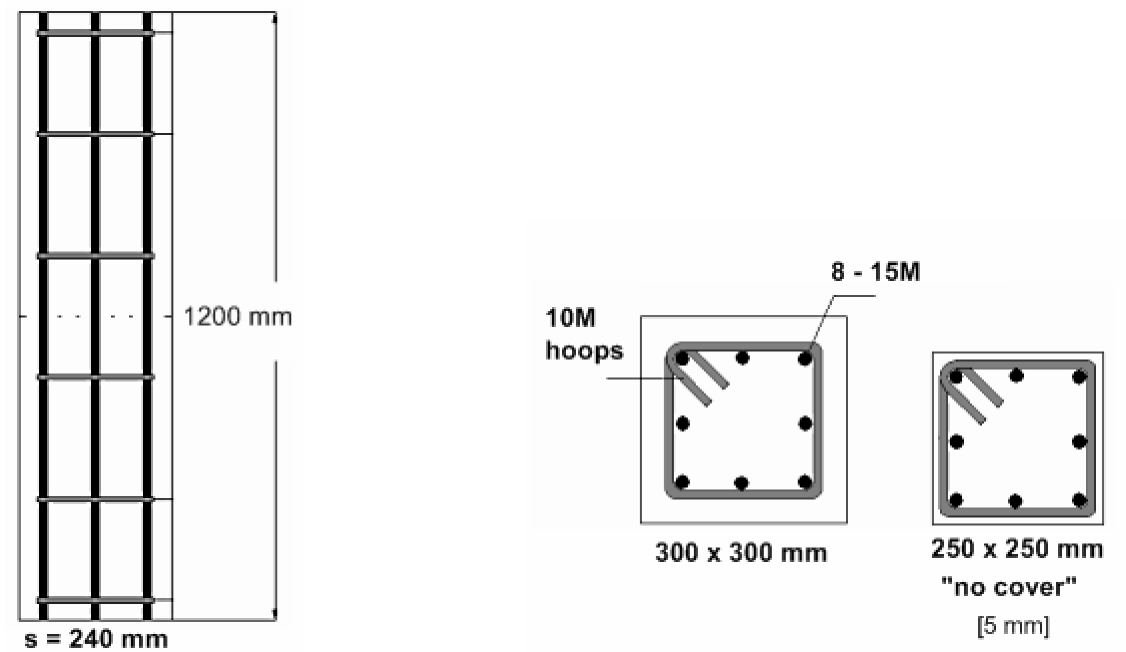

(a) Reinforcement details (b) Cross-sectional properties

Figure 3.1: Reinforcement and cross-sectional properties of the A-series specimens

3.4 Transverse Reinforcement for the B-series Specimens

The B-Series specimens were detailed in accordance with the confinement provisions in Clause 21.7 of the CSA Standard, for columns having a ductility-related force modification factor, R_d of 2.5 (moderately ductile columns). The confinement details are shown in Table 3-2 and Fig. 3.2(a) and (b).

The spacing, s, of the 10M hoops was governed by the bar buckling requirements of Clause 21.7.2.2.3, resulting in a required spacing of 120 mm ($8d_b$). Specimen B0 was constructed without any fibres. Specimens B1, B1.5 and B2 contained SCC concrete with steel fibres having 1%, 1.5% and 2% by volume respectively.

Specimens B0nc, B1nc and B1.5nc were constructed with a 5 mm cover and contained steel fibres in a quantity of 0%, 1% and 1.5% by volume, respectively.

Table 3-2: Design details for the B-series specimens

Column Specimen	Cross Section (mm)	Cover (mm)	f'_c (MPa)	% Fibres	Design	Tie Spacing	Actual Tie Spacing
B0	300 x 300	30	50	0 %	As per requirement of $\mathbf{R_d}$ **=2.5** of CSA	*Clause 21.7.2.2.3* [120 mm] - $8d_b$ [120 mm] - $24d_t$ [240 mm] - ½ dim [150 mm]	120 mm
B1				1.0%			
B1.5				1.5%			
B2				2.0%			
B0nc	250 x 250	5		0.0%			
B1nc				1.0%			
B1.5nc				1.5%			

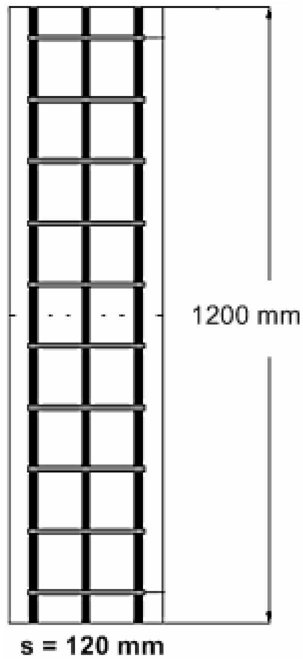

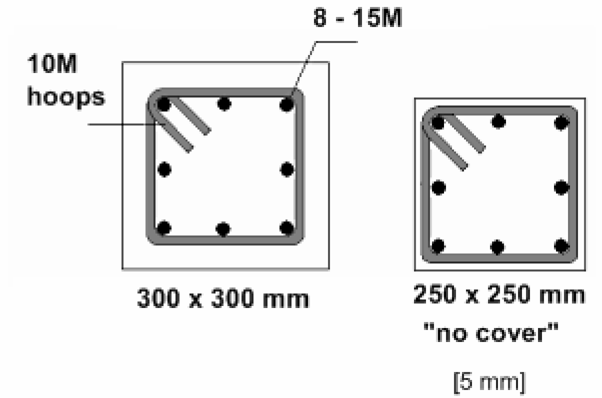

(a) Reinforcement details (b) Cross-sectional properties

Figure 3.2: Reinforcement and cross-sectional properties of the B-series specimens

3.5 Transverse Reinforcement for the C-series Specimens

The C-series specimens were detailed in accordance with the stringent confinement provisions for ductile columns of Clause 21.4 in the CSA Standard (R_d = 4.0). The confinement details are shown in Table 3-3 and Fig. 3.3(a) and (b).

Square and diamond shaped 10M hoops with seismic hooks were provided to ensure support of each longitudinal bar, resulting in an effective area of confinement reinforcement of 341 mm^2 in each principal direction. Clause 21.4.4.3 of the CSA standard is intended to provide a minimum degree of confinement of the core and also to provide lateral support for the longitudinal rebars. Clause 21.4.4.2 of the CSA standard takes into account the effects of axial loading, reinforcement arrangement, member dimensions, cross-sectional area of transverse reinforcement and material properties of the concrete and the transverse steel. These provisions resulted in a minimum hoop spacing, s, of 67 mm (a spacing of 65 mm was chosen).

Specimen C0 contained SCC concrete without any fibres. Specimens C1 and C1.5 contained SCC concrete with steel fibres having 1% and 1.5% by volume, respectively. Specimen C0nc was constructed without fibres in a cross-section that had a 5 mm cover.

Table 3-3: Design details for the C-series specimens

<table>
<tr><th>Column Specimen</th><th>Cross Section (mm)</th><th>Cover (mm)</th><th>f'_c (MPa)</th><th>% Fibres</th><th>Design</th><th>Tie Spacing</th><th>Actual Tie Spacing</th></tr>
<tr><td>C0</td><td rowspan="3">300 x 300</td><td rowspan="3">30</td><td rowspan="4">50</td><td>0%</td><td rowspan="4">As per requirement of $\mathbf{R_d}$ =4.0 of CSA</td><td rowspan="4">Clause 21.4.4.2(b)
[67 mm]
if Pf = 80% Pr_{max}

Clause 21.4.4.3
[75 mm]
- ¼ dim. [75 mm]
- S_x [149 mm]
- $6d_b$ [90 mm]</td><td rowspan="4">65 mm</td></tr>
<tr><td>C1</td><td>1%</td></tr>
<tr><td>C1.5</td><td>1.5%</td></tr>
<tr><td>C0nc</td><td>250 x 250</td><td>5</td><td>0%</td></tr>
</table>

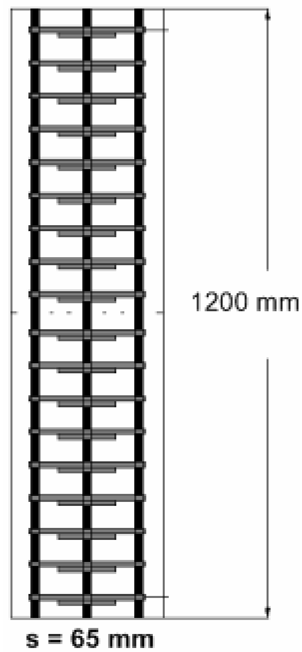

(a) Reinforcement details

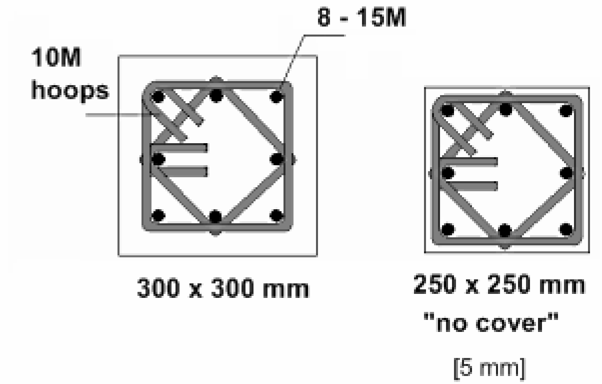

(b) Cross-sectional properties

Figure 3.3: Reinforcement and cross-sectional properties of the C-series specimens

3.6 Transverse Reinforcement for the D-series Specimens

The D-Series Specimens were detailed with a level of transverse reinforcement that is intermediate between R_d = 2.5 and 4.0 of the CSA Standard. The confinement details are shown in Table 3-4 and Fig. 3.4(a) and (b).

The transverse reinforcement was provided by 10M hoops at a spacing of 80 mm. Specimen D0 contained SCC concrete without any fibres. Specimen D1.5 contained SCC concrete with steel fibres in a quantity of 1.5% by volume. Both specimens were constructed with a 30 mm cover.

Table 3-4: Design details for the D-series specimens

Column Specimen	Cross Section (mm)	Cover (mm)	f'_c (MPa)	% Fibres	Design	Tie Spacing	Actual Tie Spacing
D0	300 x 300	30	50	0 %	Between **R_d =2.5** and **4.0**	R_d =*2.5* [120 mm]	80 mm
D1.5	300 x 300	30	50	1.5%		R_d =*4.0* [40 mm]	

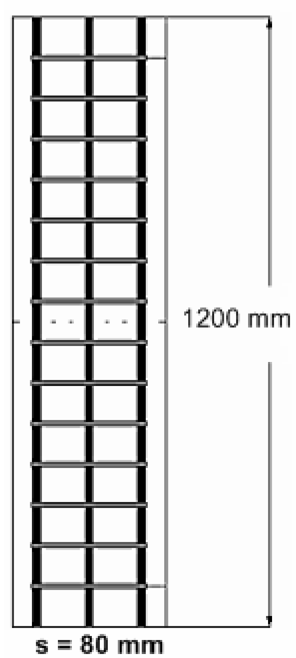

(a) Reinforcement details

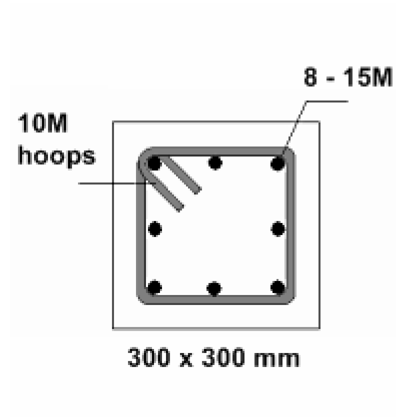

(b) Cross-sectional properties

Figure 3.4: Reinforcement and cross-sectional properties of the D-series specimens

3.7 Material Properties

3.7.1 Reinforcing steel

The properties of the reinforcing steel are summarized in Table 3-5. In order to ensure consistency, all the specimens were constructed using weldable grade steel reinforcement. Tension tests were performed on three random specimens for each bar size. The typical stress strain relationship of the 10M and 15M reinforcing bars are shown in Fig. 3.5. Table 3-6 lists the reinforcement that was used in each specimen. The longitudinal reinforcement had average yield strengths, f_y, of 515 MPa and 478 MPa, while the transverse reinforcement had an average yield strength of 409 MPa.

Table 3-5: Reinforcing steel properties

Bar description	f_y (MPa) [std. dev.]	ε_{sh} (mm/mm) [std. dev.]	f_u (MPa) [std. dev.]	ε_u (mm/mm) [std. dev.]
10M	409 [4.0]	0.0095 [0.0005]	640 [1.0]	0.1743 [0.0012]
15M-a	515 [2.1]	0.0194 [0.0003]	625 [1.1]	0.1650 [0.0127]
15M-b	478 [12.8]	0.0207 [0.0013]	589 [12.2]	0.1679 [0.0061]

Table 3-6: Listing of reinforcing steel found in each specimen

Specimens	Reinforcement material properties	
	Transverse reinforcement	Longitudinal reinforcement
A0, A1, A1.5, A2, B0, B1, B1.5, B2, C0, C1, C1.5 D0, D1.5	10M	15M-a
A0nc, A1nc, A1.5nc, B0nc, B1nc, B1.5nc, C0nc	10M	15M-b

3.7.2 Steel fibres

Hooked end steel fibres, were used to attain 1% (76.8 kg/m^3), 1.5% (115.2 kg/m^3), and 2% fibre reinforcement (153.6 kg/m^3) by volume of concrete.

The fibres, which are manufactured by Bekaert Steel Wire Corporation under the Dramix ZP-305 brand, are made from cold-drawn steel wire and are deformed with hooked ends. Table 3-7, presents the properties of a fibre. The fibres had an aspect-ratio (l/d) of 55. The tensile strength of the fibre was 1100 N/mm^2. Figure 3.6 shows the typical Dramix ZP-305 fibre dimensions.

Table 3-7: Steel fibre properties

Fibre type	Length l_f (mm)	Diameter d_f (mm)	Aspect ratio $\frac{l_f}{d_f}$ (mm/mm)	Tensile strength f_{fy} (MPa)
Dramix ZP-305	30	0.55	55	1100

3.7.3 SCC concrete mix composition

The concrete used in the various specimens consisted of a pre-packaged, self-consolidating concrete mix with a specified strength of 50 MPa. Table 3-8 lists the various SCC properties as specified by the manufacturer (the mix was produced by KING Packaged Materials Company under the KING MS Self-Consolidating Concrete brand). The mix contained a maximum aggregate size of 10 mm with a sand-to-aggregate ratio of approximately 0.45 and a water-cement ratio of approximately 0.42. Furthermore, the SCC product contained an air-entraining admixture, a superplasticizer and a VMA. These components are all incorporated into the blend in the form of dry powder.

The concrete for all the column specimens was produced at McGill University's Jamieson Structures Laboratory. Two series of casts were used to produce the 20 reinforced concrete columns. Cast-A included the columns containing the plain SCC mix as well as the columns cast with 1.5% and 2% by volume fibre contents. Cast-B was used for the second series of columns that included the specimens that had a fibre content of 1% and included the "no cover" companion column specimens. Table 3-9 lists the columns that were cast in each series.

The concrete was cast in batches, with each batch consisting of five pre-packaged bags of the SCC material. The pre-packaged blend was mixed with water in a quantity of 3.15 L/kg. Subsequently, the blend was mixed for a period of three minutes after which the fibres were slowly added. After six minutes of mixing, the concrete was placed into the formwork.

Table 3-8: Concrete mix proportions

Characteristics	Content	
HSF Cement	kg/m^3	500
Mass Density		2300
Coarse Aggregate		765
Fine aggregate		915
Ratio Fine/Total Aggregates	---	0.45
Water-cement ratio		0.42
Air Content	%	7

Table 3-9: Listing of columns found in the two cast-series

Cast	Column specimens
Cast-A	A0, A1.5, A2, B0, B1.5, B2, C0, C1.5
Cast-B	A1, A0nc, A1nc, A1.5nc, B1, B0nc, B1nc, B1.5nc, C1, C0nc D0, D1.5

3.7.4 Workability of the steel fibre-reinforced SCC

In order to assess the workability of the steel fibre reinforced SCC, several established test methods were used to assess the effect of the fibres on the flow characteristics of the concrete. The slump flow test was chosen to assess the free deformability of the concrete, while the L-box and V-funnel tests where chosen to investigate the restricted deformability.

Due to time constraints, only the slump flow test was used during the actual casting of the columns. Subsequent to the first cast and using the same materials and production procedure, the various mixes that were used in the experimental program were tested using the L-box and V-funnel tests

Table 3-10 summarizes the average results from the test program. The results from the slump flow test and the V-funnel test demonstrate that the addition of fibres reduces the workability of the SCC. The 1.5% fibre concrete seems to be an upper limit for a semi-workable mix. In addition, the V-funnel was not successful with the 2% fibre quantity. This suggests that this quantity of fibres would cause great problems in workability. Also it is noted that the standard L-box test was not successful when fibres were added to the concrete mix suggesting that this test method should be modified such that the clear spacing between the bars exceeds the fibre length for fibre reinforced SCC.

These results were in conformity with observations made during the actual casting of the columns. It was found that the 1% mix was very workable and required little or no vibration. The 1.5% mix required slight vibration but was still workable. On the other hand, the 2% mix was not very workable and required significant vibration during placement in all columns. It was observed that a certain amount of segregation had taken place at this high fibre content.

Table 3-10: Average results from the workability tests

Fibre volume (%)	Slump flow test		V-funnel test	L-box test
	Slump (mm)	Slump diameter (mm)	Time (sec)	Time (sec)
0.0	290	690	2.7	3.0
1.0	270	585	3.9	unsuccessful
1.5	250	500	11.9	unsuccessful
2.0	210	360	unsuccessful	unsuccessful

3.7.5 Material properties of the SCC and steel fibre reinforced SCC

A series of lab cured cylinders and flexural beams were prepared and tested to determine the hardened concrete material properties. The compressive strength, f'_{co}, and compressive stress strain relationships were determined by testing cylinders that had a diameter of 100 mm and a height of 200 mm. The modulus of rupture, f_r was determined from flexural beams that had dimensions of 100 x 100 x 400 mm. Table 3-11 summarizes the experimental results.

Table 3-11: Hardened Concrete properties

Series	f'_{co} (MPa) [std. dev.]	ε'_{co} (mm/mm) [std. dev.]	f_r (MPa) [std. dev.]
0.0% Cast-A	49.5 [2.67]	0.0022 [0.0001]	8.5 [0.17]
1.5% Cast-A	47.6 [2.53]	0.0023 [0.0001]	10.2 [0.38]
2.0% Cast-A	45.9 [2.23]	0.0020 [0.0001]	8.8 [0.67]
0.0% Cast-B	43.8 [2.54]	0.0022 [0.0001]	7.7 [0.34]
1.0% Cast-B	42.6 (1.37)	0.0022 [0.0001]	8.0 [0.54]
1.5% Cast-B	42.4 [1.55]	0.0023 [0.0001]	8.5 [0.62]

It is noted that the concrete in Cast-B had a lower compressive cylinder strength than that in Cast-A, due to a change in the manufacturing process.

Figure 3.6(a) shows typical compressive stress-strain relationships of the concrete with and without steel fibres for the various specimens produced during Cast-A. As can be seen, the addition of steel fibres has not significantly improved the maximum compressive strength of the concrete. However, the more substantial effect is observed in the descending branch of the stress-strain curve, as the addition of fibres has significantly improved the toughness of the compressive stress-strain response. Similar results were obtained for the concrete produced in Cast-B (see Fig. 3.6(b)).

The flexural beams were tested using the JSCE SF-4 method of FRC toughness characterization (JSCE, 1984). In this test method, which uses the same setup as the ASTM C-1018 standard test method (ASTM, 1998), the beam is subjected to four-point bending and the load-displacement curve is recorded. An arrangement with two transducers attached to a rectangular "yoke" system that surrounds the specimen was used in order to measure the actual mid-span deflection. This test allowed for an evaluation of the improvement in toughness due to the presence of fibre reinforcement.

Figures 3.7(a) and (b) show typical load deflection responses obtained from the modulus of rupture tests for specimens produced during Cast-A and Cast-B respectively. As expected, the plain concrete specimens have no ductility with a brittle failure occurring when the first crack forms. However, the addition of steel fibres has transformed the brittle response of the plain concrete specimen into a ductile and controlled failure response as seen in the descending branch of the load-deflection curves. The improved post-peak resistance resulted from the ability of the fibres to bridge the cracks. It can be seen that the specimen with 2% fibre content shows a lower resistance than that of the specimen containing 1.5% fibres, which could be linked to the observed segregation problems associated with this higher fibre content.

In the JSCE SF-4 method, the flexural toughness is quantified using a factor called the flexural toughness factor (FT). The first step involves computing the area under the load versus deflection curve up to a deflection of span/150 (this value represents the toughness). Thereafter, the factor FT is calculated using Eq. 3-1:

$$FT = \frac{Area_{OABC} \times L}{\left(L/150 \right) \times b \times h^2} \qquad 3\text{-}1$$

Where $Area_{OABC}$ is the area under the load-deflection curve up to a deflection of L/150 (see Fig. 3.9). The quantity L represents the span of the beam as measured from the centre of the beam supports (300 mm in the standard test method). The values b and h represent the width and height of the beam (both 100 mm in the standard test method).

The units of the FT-factor are stress and hence the value can be seen to indicate the post cracking residual strength of the material when loaded up to an arbitrary deflection of *L/150* (Banthia and Mindess, 2004). Table 3-12 presents the calculated FT values.

Table 3-12: FT-factors for the various concretes

Series	JSCE SF4 method	
	Area OABC	FT factor
0.0% - Cast-A	---	---
1.5% - Cast-A	49	7.3
2.0% - Cast-A	46.1	6.9
0.0% - Cast-B	----	---
1.0% - Cast-B	33.4	5.0
1.5% - Cast-B	40.9	6.1

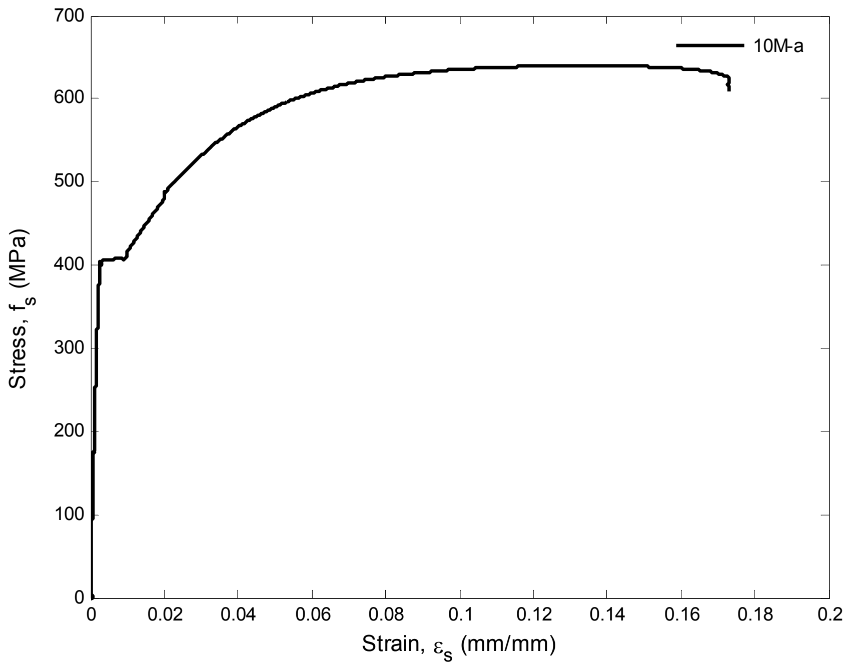

(a) Typical stress-strain curve for the 10M reinforcing bars

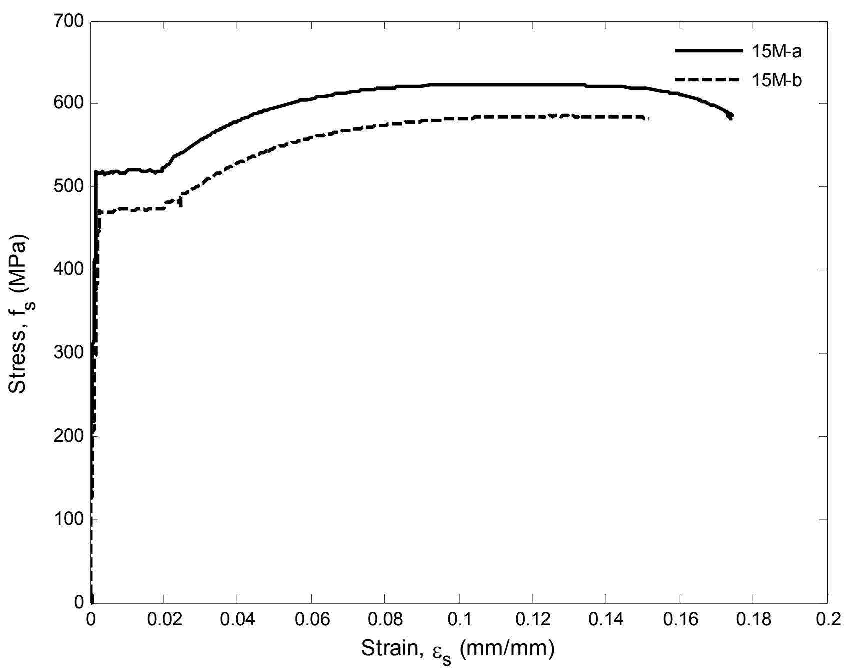

(b) Typical stress-strain curves for the 15M reinforcing bars

Figure 3.5: Stress-strain responses for the transverse and longitudinal reinforcing bars

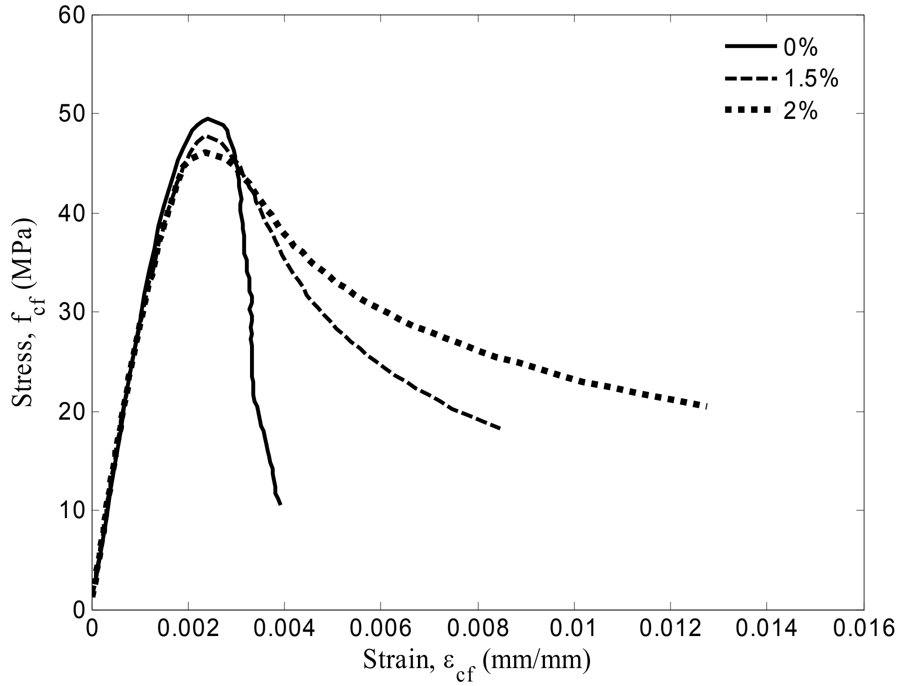

(a) Typical stress-strain curves for the various concrete mixes used in Cast-A

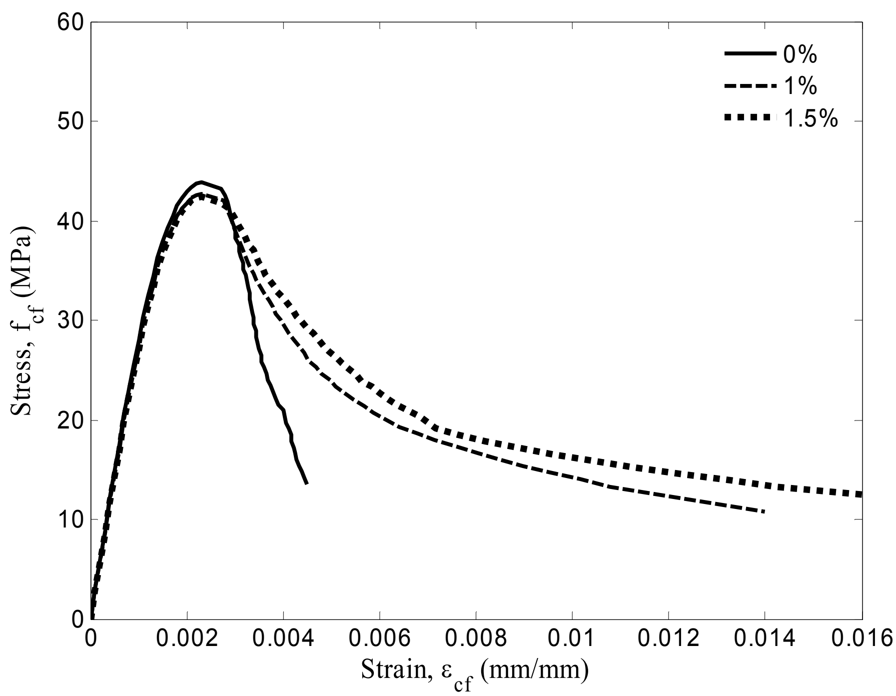

(b) Typical stress-strain curves for the various concrete mixes used in Cast-B

Figure 3.6: Typical concrete compressive stress-strain responses

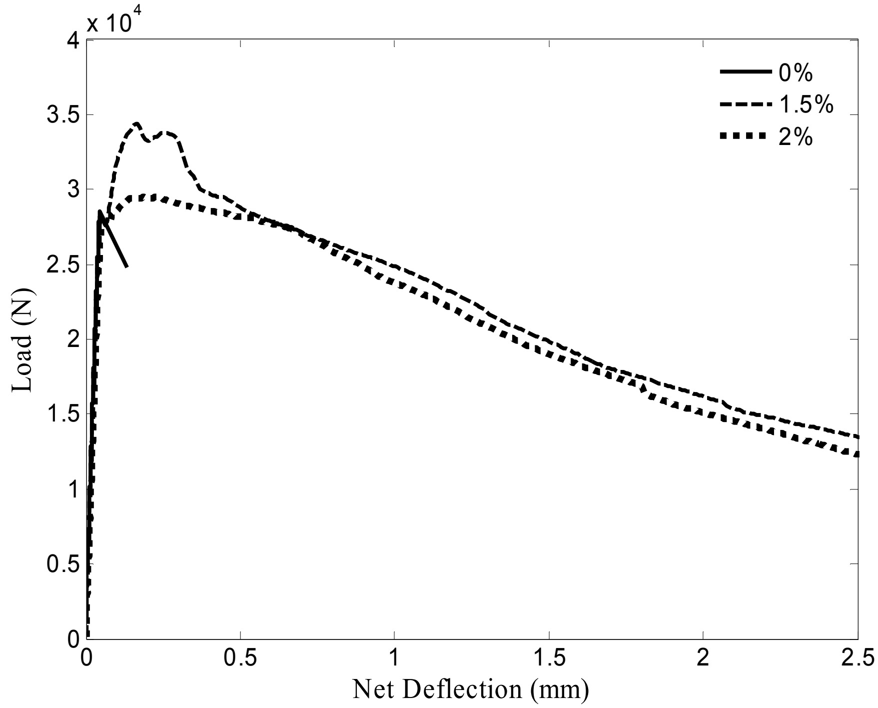

(a) Typical load-deflection curves for the various concrete mixes used in Cast-A

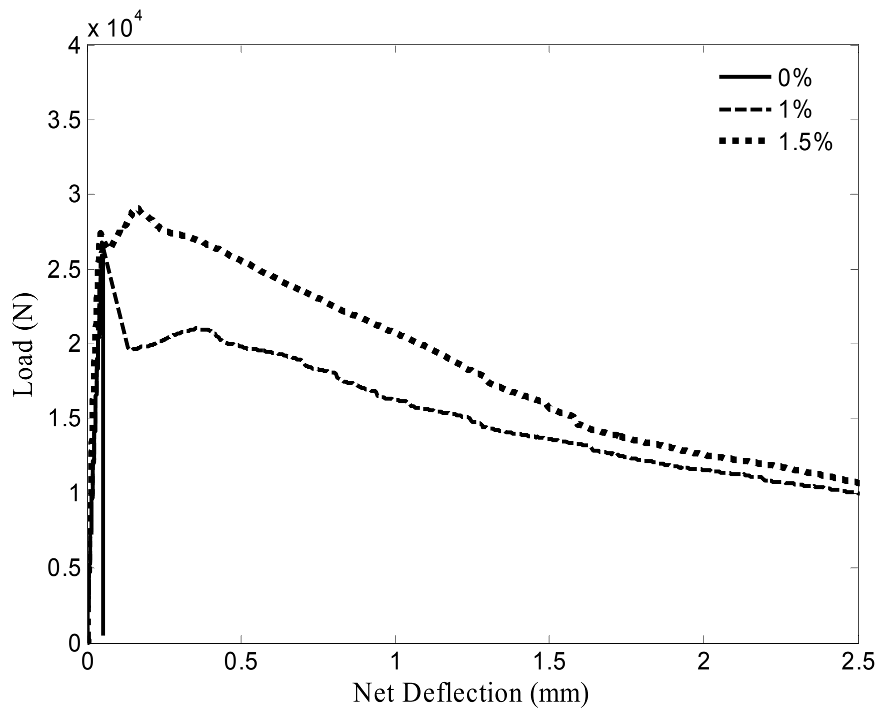

(b) Typical load-deflection curves for the various concrete mixes used in Cast-B

Figure 3.7: Typical flexural beam load-deflection curves

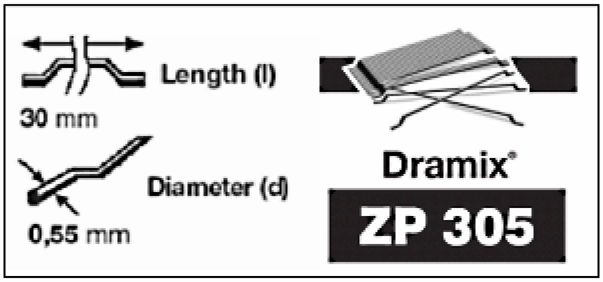

Figure 3.8: Typical ZP-305 fibre dimensions

[Adapted from(Bekaert, 2007)]

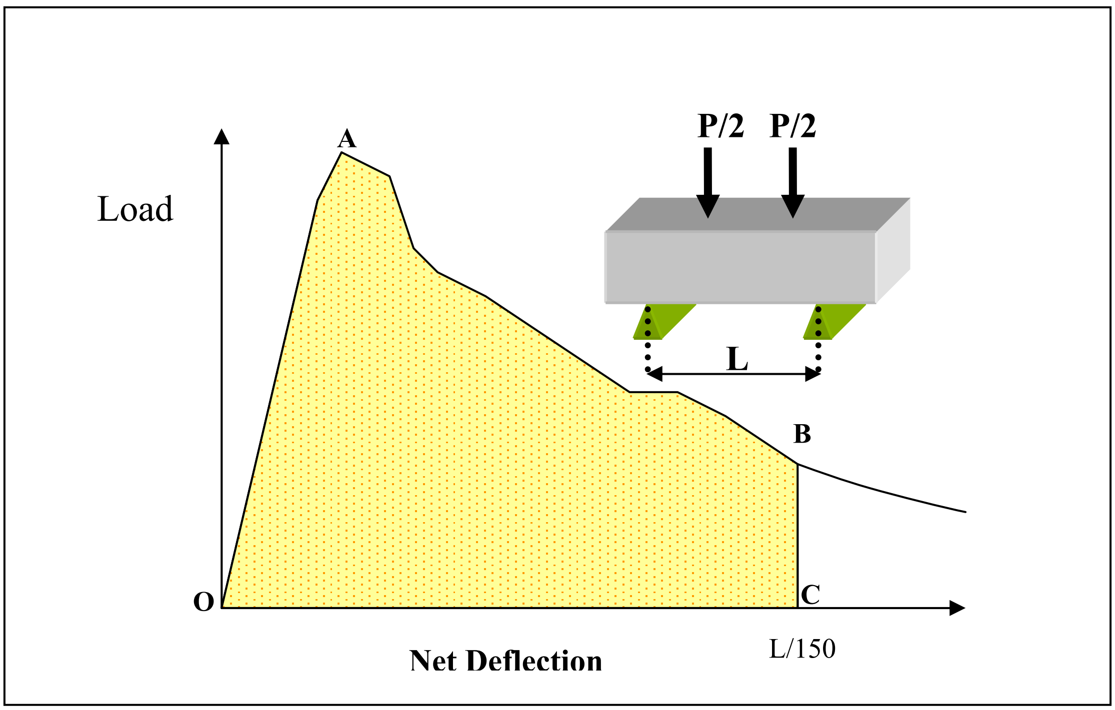

Figure 3.9: JSCE SF-4 method of FRC toughness characterization

3.8 Testing

3.8.1 Test setup

Figure 3.10 shows some of the typical columns before they were cast in the formwork. During the construction of the columns it was noted that the A-series specimens were relatively easy to construct. In contrast, the C-series specimens required significantly more effort and time to complete due to the more congested reinforcement detailing found in this series of columns.

After casting the concrete, the specimens were moist cured using wet burlap and plastic sheets for a period of five days after which the formwork was stripped. For the first series of experiments (Cast-A), the first specimen was tested at an age of 38 days while the last specimen was tested at an age of 48 days. For the second series of tests (Cast-B), the first and last specimens were tested at an age of 32 days and 44 days respectively.

All the specimens were tested under pure axial loading using the 11,400 KN capacity MTS testing machine in the Jamieson Structures Laboratory in the Department of Civil Engineering and Applied Mechanics at McGill University. The specimens were placed vertically on top of a steel plate. Special attention was taken to ensure that the specimens were aligned vertically under the compression head of the loading machine to eliminate loading eccentricities. A thin layer of capping compound was used to cap the end plates at the top and bottom of each specimen to ensure an adequate bearing surface at the column ends. Steel collars were placed at the top and bottom of each specimen in order to provide additional confinement in these regions. Figure 3.11 shows a typical specimen prior to testing.

3.8.2 Loading procedure

All 20 specimens were tested in the same manner. A loading rate of 2.5 kN per second was used up to a load of 3000 kN. Subsequent to this load stage, the loading rate was switched to “displacement control” at a rate of 0.002 mm per second. The tests then continued until the resistance of the given specimen dropped to 35% of the peak axial load or when the axial displacement reached a value of 30 mm. Throughout the tests observations regarding crack patterns and failure mechanisms were made.

3.8.3 Instrumentation

During each test, the behaviour of each column specimen was monitored continually using electronic instrumentation. All electronic readings were recorded during the tests through the use of a computerized data acquisition system. Electrical resistance strain gauges were glued to the reinforcing bars to measure strains in the steel, while linear voltage differential transducers (LVDTs) were utilized to measure external displacements.

3.8.3.1 Load measurements

The internal load cell of the MTS testing machine was used to measure the axial loads that were applied to the column specimens.

3.8.3.2 Displacement measurements

A total of four linear voltage differential transducers (LVDTs) were utilized to measure the axial deformations of each specimen under applied load. The LVDTs were placed vertically at the corners of the East and West faces of each column over a central height of 970 mm to measure the shortening of the four corners of each specimen. The placement of these LVDTs can be seen in Fig. 3.12. Special care was taken to ensure that the cover spalling would not interfere with the readings.

3.8.3.3 Strain measurements

Electrical resistance strain gauges were utilized to measure the strains in the steel reinforcement. The strain gauges, which had a 5 mm gauge length, were glued to the reinforcing steel and provided measurements of local strains in the steel reinforcement as the specimens were loaded. The location for the placement of the strain gauges is shown in Fig. 3.13 to 3.16. Each instrumented longitudinal bar had a pair of strain gauges at its mid-height in an attempt to capture the onset of bar buckling. The instrumented hoops were located directly above the mid-height of the specimens.

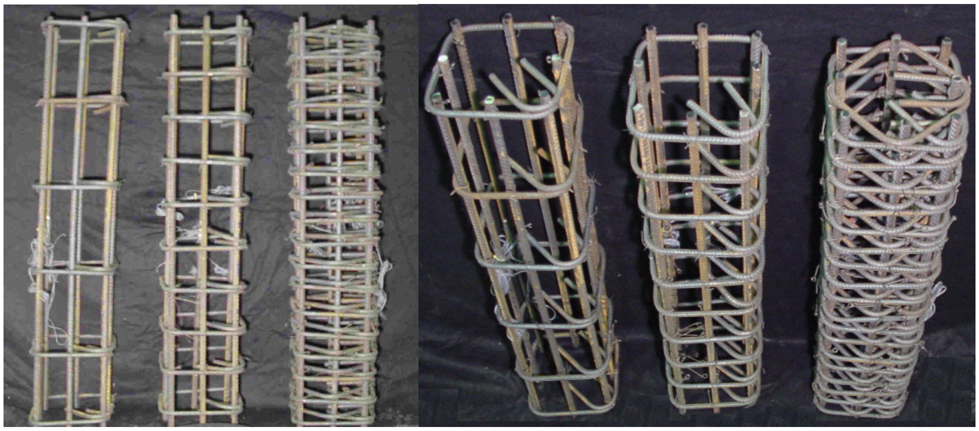

Figure 3.10: Typical reinforcing cages before casting

Figure 3.11: Axially loaded specimen prior to testing

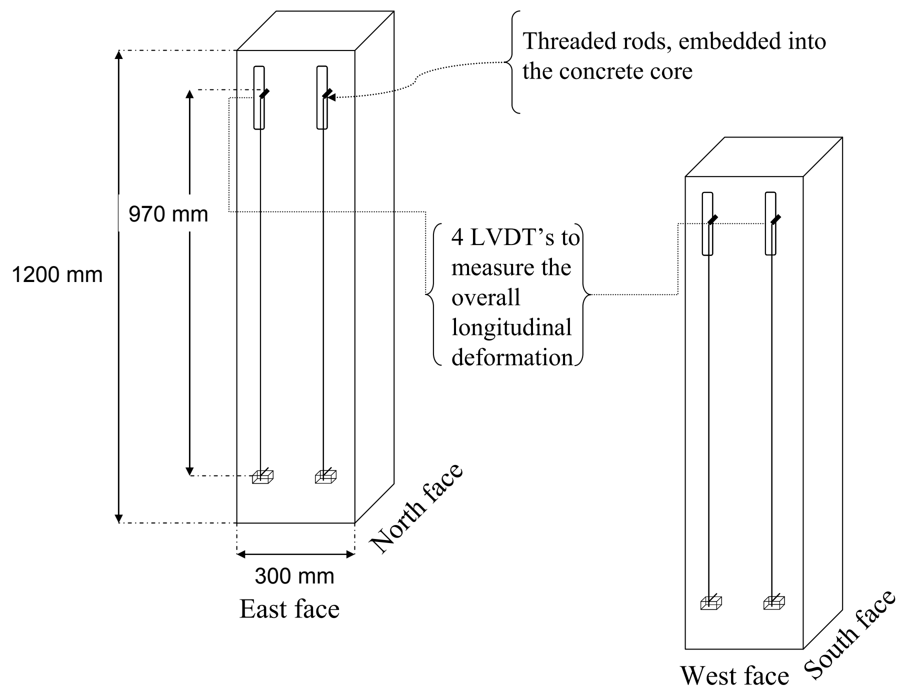

(a) Specimens constructed with cover.

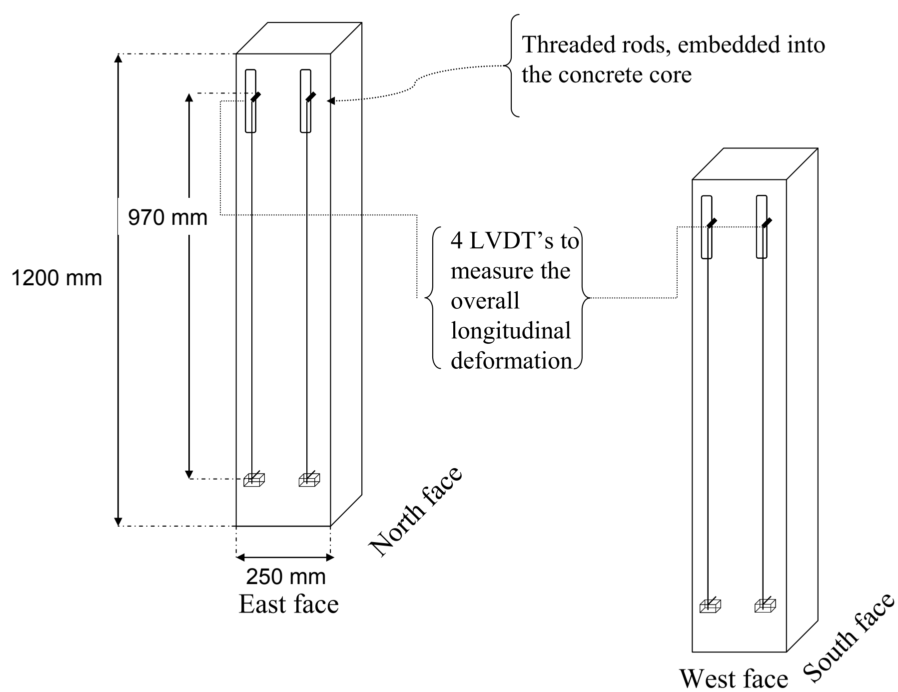

(b) Specimens constructed without cover.

Figure 3.12: Location of LVDTS on the west and east faces of the columns

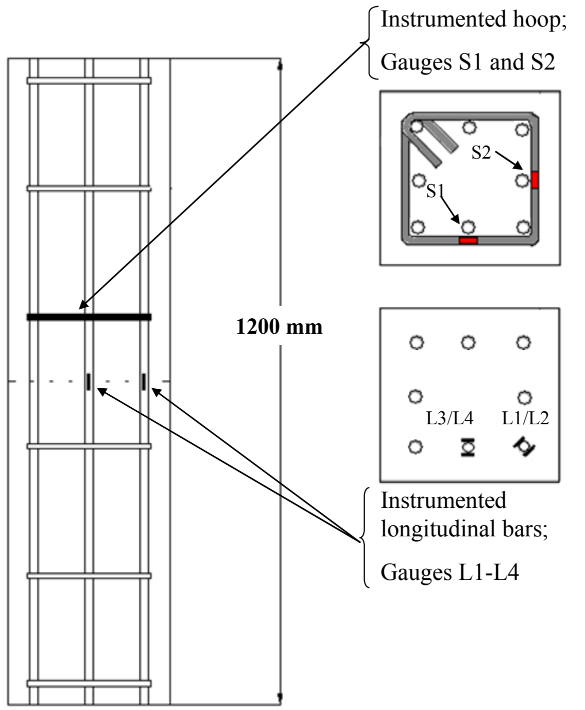

Figure 3.13: Location of electrical resistance strain gauges for A-series specimens

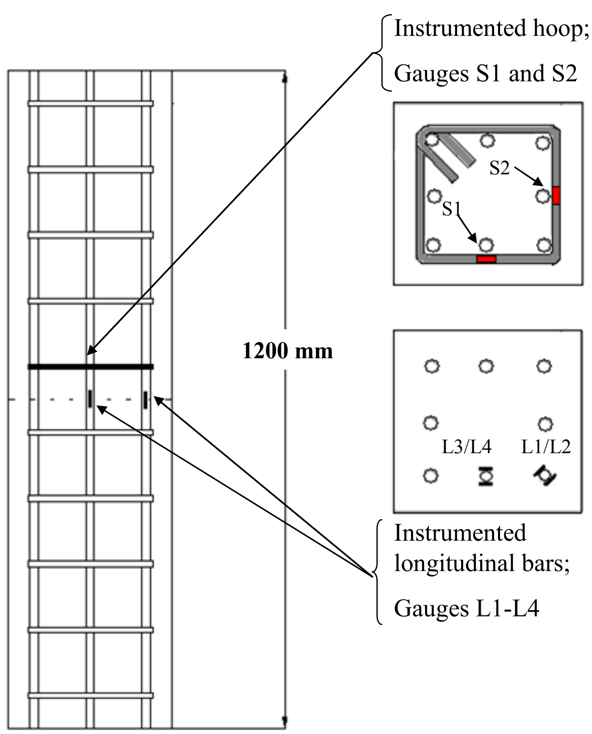

Figure 3.14: Location of electrical resistance strain gauges for B-series specimens

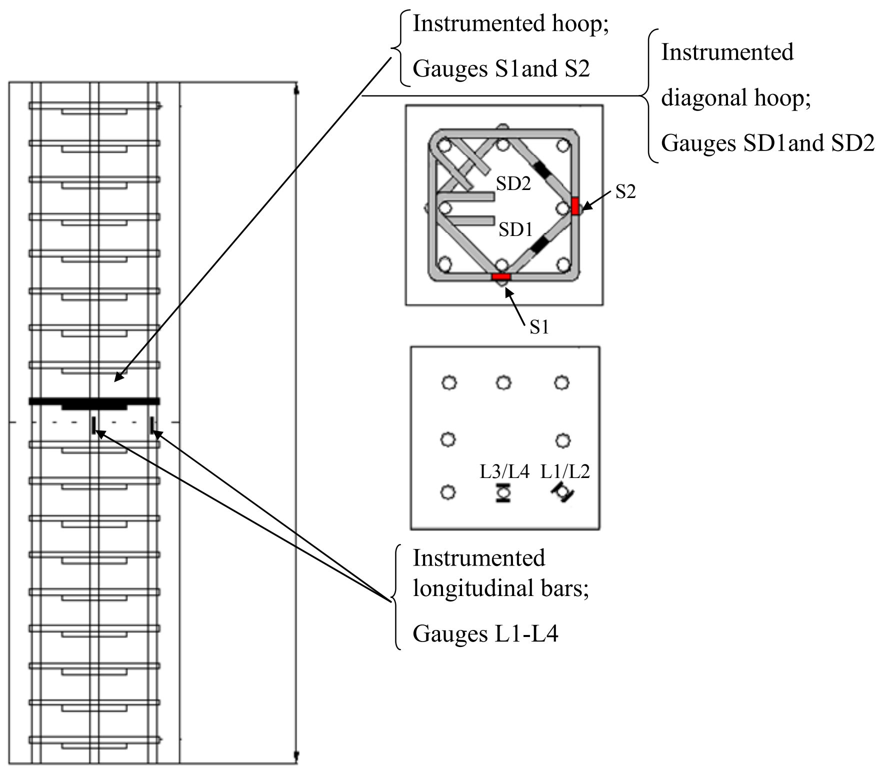

Figure 3.15: Location of electrical resistance strain gauges for C-series specimens

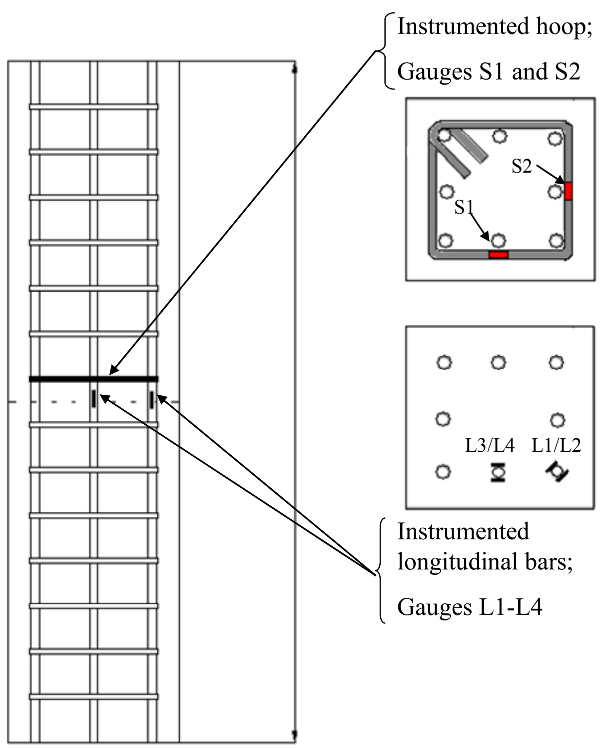

Figure 3.16: Location of electrical resistance strain gauges for D-series specimens

Chapter 4 Presentation of the Experimental Results for the Column Specimens

4.1 Chapter Overview

In this chapter the responses of the 20 column specimens are presented. Section 4.2 presents the experimental results associated with the 13 columns that were constructed with 30 mm cover. Section.4.3 presents the results for the 7 companion columns that were constructed with 5 mm cover.

Each column analysis will begin with a presentation of the experimental load-strain response, where the load corresponds to the axial load applied to the cross-section and where the strain corresponds to the average of the deformations measured by the four LVDTs in the central 970 mm region of each specimen.

In addition, the normalized load-strain response will be presented for each specimen, where the normalized load, P_n, is computed using the relationship in Eq. 4-1:

$$P_n = \frac{P_c}{0.85 \times f'_{co} \times (A_{net})} \qquad \text{4-1}$$

In this equation, P_c represents the axial load carried by the concrete (calculated by removing the load carried by the longitudinal reinforcement from the total axial load). The quantities f'_{co} and A_{net} represent the concrete compressive strength and the net concrete area in each column (where A_{net} is computed by subtracting the longitudinal steel area from the cross-sectional area of the specimen).

Furthermore, each column analysis will present the measured strains in the longitudinal and transverse steel reinforcement.

4.2 Observed Behaviour of Specimens with 30 mm cover

4.2.1 Response of Specimen A0

Specimen A0 was detailed in accordance with the confinement provisions of Clause 7 of the 2004 CSA Standard, for columns having a ductility-related force modification factor, R_d of 1.5. The spacing of the transverse reinforcement was 240 mm and this column contained no fibres.

The load-strain response of Specimen A0 is given in Fig. 4.1(a). A peak load carrying capacity of 4510 kN was reached in this specimen. Immediately after the peak load, the response showed a very sudden and steep drop in load carrying capacity. In brief, due to the large spacing between the ties, this column showed a poor post-peak response. The concrete contribution versus strain is shown in Fig. 4.1(a) and the normalised concrete load contribution is shown in Fig. 4.1(b). Figure 4.2 details the observed behaviour for Specimen A0.

Strains measured on the vertical reinforcing bars by the electrical strain gauges are shown in Fig. 4.1(c). The plots of the recorded strains versus the applied loading of gauges L1 and L2 show that the yield strain was reached in these gauges near the peak capacity of the column. The plots also show a large jump in compressive strains at this load stage before a sudden drop in load carrying capacity. The gauges that were placed on the mid-side longitudinal reinforcing bar show that yielding was not reached on this bar. Although the corner bars yielded they did not reach very large strains due to the large spacing of the hoops. The mid-side bars had very little lateral support compared to the corner bars and hence did not achieve yielding.

Figure 4.1(d) shows the measured strains in the instrumented hoop near the mid-height of the column. Both gauges S1 and S2 show that the hoop at this location did not reach yield before the failure of the column. This result can be linked to the large hoop spacing and the resulting poor confinement.

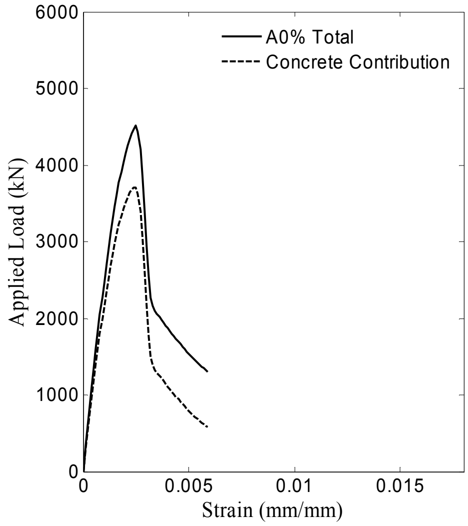

(a) Total applied load, P_{total}, versus strain and concrete load contribution, P_c, versus strain

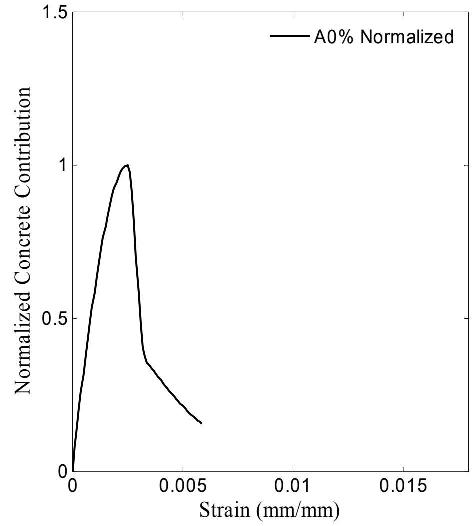

(b) Normalized concrete contribution, $\frac{P_c}{P_{co}}$, versus strain

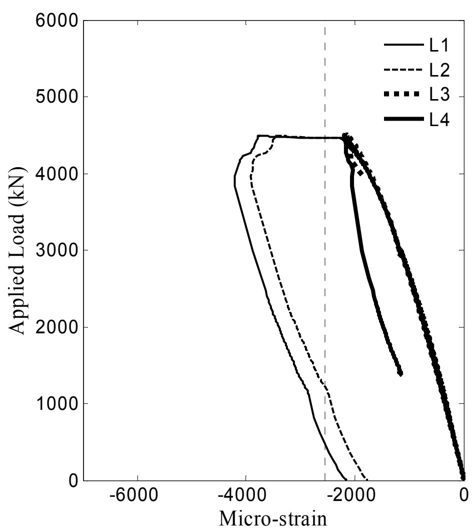

(c) Measured strains in longitudinal reinforcement

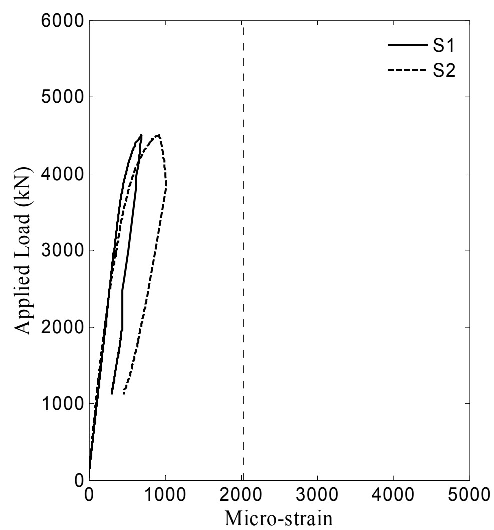

(d) Measured strains in transverse reinforcement

Figure 4.1: Experimental results for Specimen A0

<table>
<tr>
<td rowspan="2"></td>
<td>(a)</td>
<td rowspan="2"></td>
<td>(b)</td>
</tr>
<tr>
<td>- Just prior to the peak resistance some splitting cracks had initiated at the lower south-east and north-east corners of the column as well as at the location of the right-side longitudinal bar on the North face.</td>
<td>- As the peak load carrying capacity was reached the cracking began to extend upwards from the bottom corners to the mid-height of the column.</td>
</tr>
<tr>
<td rowspan="2"></td>
<td>(c)</td>
<td rowspan="2"></td>
<td>(d)</td>
</tr>
<tr>
<td>- With further loading crushing was observed at the mid-height of the column on the North face.

- Spalling of the concrete cover and buckling of the longitudinal reinforcing bars were observed, and occurred in a very sudden manner.</td>
<td>- The vertical bars displayed a buckling length approximately equal to the spacing between the transverse reinforcement.</td>
</tr>
</table>

Figure 4.2: Major events for Specimen A0

4.2.2 Response of Specimen A1

Specimen A1, was detailed with the same amount of transverse reinforcement contained in Specimen A0, and hence met the requirements of R_d of 1.5 of the CSA standard, with a tie spacing of 240 mm. However, this column contained steel fibres in the quantity of 1% by volume of concrete.

The load-strain response of Specimen A1 is shown in Fig. 4.3(a). A peak load carrying capacity of 4471 kN was reached in this specimen. As the column was loaded beyond its peak resistance, its load carrying capacity began to drop. However, this drop in post-peak capacity was not sudden. Rather as further strain was applied the load carrying capacity decreased in a controlled and stable manner, demonstrating that the column had some post-peak ductility. The concrete contribution versus strain is shown in Fig. 4.3(a) and the normalised concrete load contribution with respect to strain is shown in Fig. 4.3(b). Figure 4.4 details the observed behaviour for Specimen A1.

The strain gauges on the vertical bars were placed in the same locations as for Specimen A0, the plots of the recorded strains versus the applied loading are shown in Fig. 4.3(c). The plots of all the gauges placed on the longitudinal reinforcement demonstrate that the yield strain was reached in the corner and mid-side bars. The plots also show that much larger compressive strains were reached in the longitudinal reinforcement of this column before the drop in load carrying capacity, when compared to Specimen A0.

Figure 4.3(d) shows the measured strains in the instrumented hoop near the mid-height of the column. Both gauges S1 and S2 show that the yield strain was just reached in the transverse hoop before the drop in load carrying capacity. The presence of fibres has enhanced the confinement in the column and the transverse reinforcement yielded.

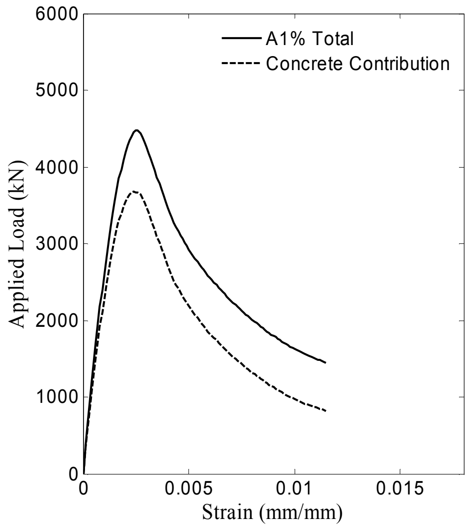

(a) Total applied load, P_{total}, versus strain and concrete load contribution, P_c, versus strain

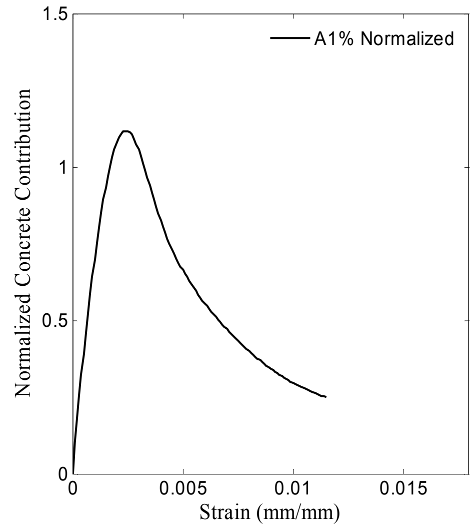

(b) Normalized concrete contribution, $\frac{P_c}{P_{co}}$, versus strain

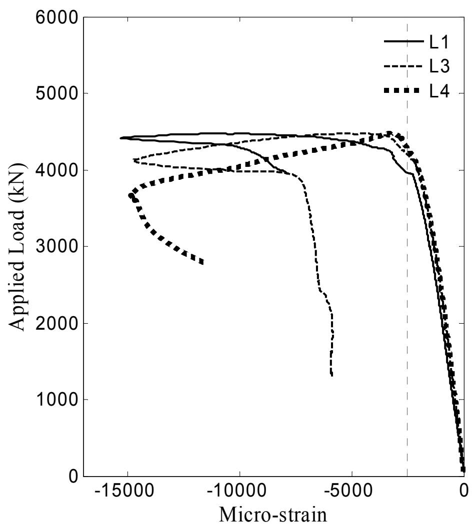

(c) Measured strains in longitudinal reinforcement

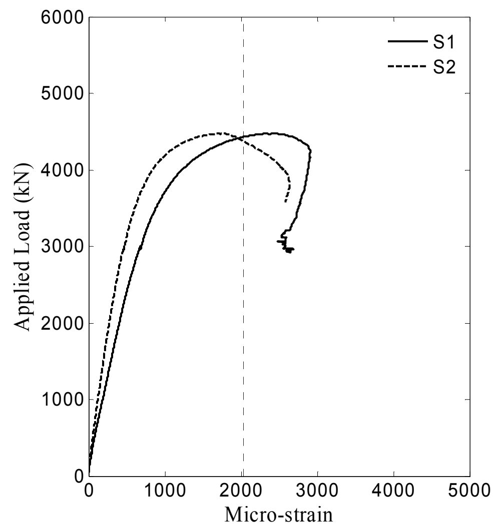

(d) Measured strains in transverse reinforcement

Figure 4.3: Experimental results for Specimen A1

	(a) - Just prior to the peak resistance some splitting cracks and some horizontal cracking patterns had initiated at the mid-height of the column.		(b) - As the peak load carrying capacity was reached signs of crushing had initiated at the mid-height of the column (on the North and East faces), and began to extend horizontally.
	(c) - As the loading continued, crushing and cover spalling continued to take place. - Furthermore, extensive splitting cracks began to develop at the locations of the longitudinal reinforcing bars on the East and West faces of the column.		(d) - As loading continued large pieces of cover began to become detached from the core region of the column.
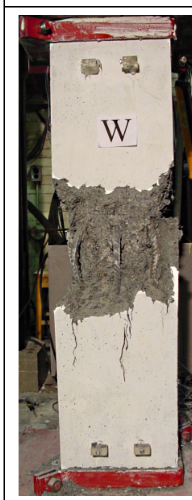	(e) - At the end of the experiment it was noted that the vertical bars displayed a buckling length approximately equal to the spacing between the transverse reinforcement		(f) - Picture showing the buckled reinforcing bars.

Figure 4.4: Major events for Specimen A1

4.2.3 Response of Specimen A1.5

Specimen A1.5 was detailed with the same amount of transverse reinforcement as Specimen A0. Therefore the spacing of the transverse reinforcement was 240 mm. The difference was that this column contained steel fibres in the quantity of 1.5% by volume of concrete.

The load-strain response of Specimen A1.5 is given in Figure 4.5(a). A peak load carrying capacity of 5783 kN was reached in this column. As the specimen was loaded beyond its peak resistance, its load carrying capacity began to drop. However, similar to was observed in Specimen A1, this drop in capacity, although occurring at a steady rate, was controlled. This behaviour, demonstrates that the inclusion of fibres in this specimen has allowed the column to develop a new level of post-peak ductility. The concrete contribution versus strain is shown in Fig. 4.5(a) and the normalised concrete load contribution with respect to strain is shown in Fig. 4.5(b). Figure 4.6 details the observed behaviour for Specimen A1.5.

The plots of the measured strains in the longitudinal reinforcement are shown in Fig. 4.5(c). The plots demonstrate that the yield strain was reached in all of the gauges near the peak capacity of the column. The gauges L1 and L2 showed some signs of buckling with the gauge on the inner side of the bar showing larger compressive strains than the gauge on the outer side of the bar.

Figure 4.5(d) shows the measured strains in the instrumented hoop near the mid-height of the column. Both gauges S1 and S2 show that the yield strain was reached in the transverse hoop. It is noted that large tensile strains were measured as the column experienced the gradual decrease in load carrying capacity. These results demonstrate that the steel fibres were able to improve the confinement and the integrity of this column, which led to higher strains in the transverse reinforcement and an improved response.

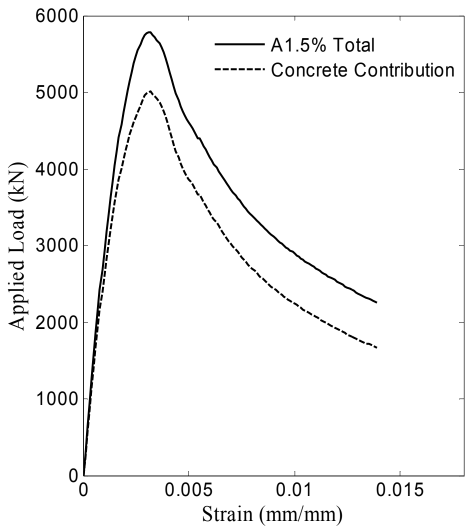

(a) Total applied load, P_{total}, versus strain and concrete load contribution, P_c, versus strain

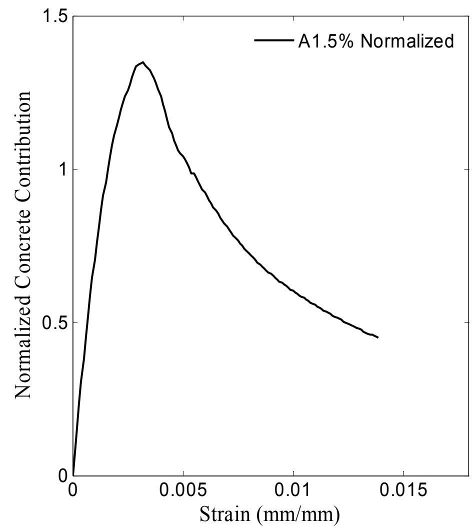

(b) Normalized concrete contribution, $\frac{P_c}{P_{co}}$, versus strain

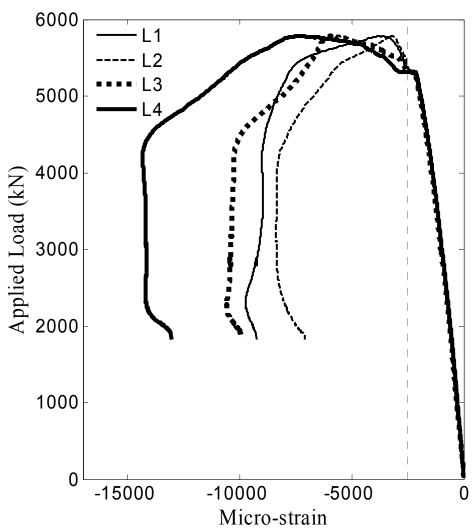

(c) Measured strains in longitudinal reinforcement

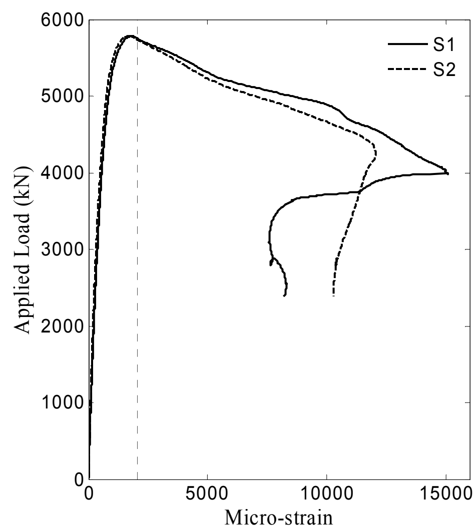

(d) Measured strains in transverse reinforcement

Figure 4.5: Experimental results for Specimen A1.5

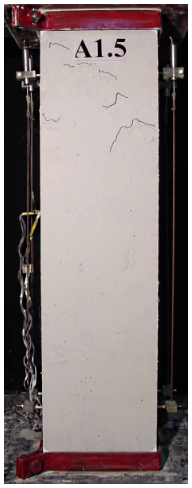	(a) - Just prior to the peak resistance a longitudinal splitting crack was observed near the top of the column.	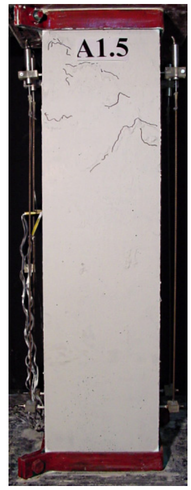	(b) - When the peak load was reached some splitting cracks initiated at the top third of the North face of the column.
	(c) - As the column was loaded beyond its peak capacity this cracking pattern began to extend both horizontally and vertically and signs of crushing began to become visible.	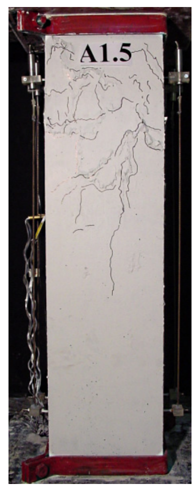	(d) - As loading continued this cracking behaviour continued to extend downwards towards the mid-height of the column. - The cracks were developing in all directions, showing that crushing and cover spalling of the column was occurring at a controlled and stable rate.
	(e) - Eventually, some pieces of cover began to become detached from the core concrete region of the column.		(f) - It was noted that the vertical bars displayed a buckling length approximately equal to the spacing between the transverse reinforcement.

Figure 4.6: Major events for Specimen A1.5

4.2.4 Response of Specimen A2

Specimen A2 was detailed with the same amount of transverse reinforcement used in all of the A-series columns (spacing of 240 mm) but contained steel fibres in the quantity of 2% by volume of concrete.

The load-strain response of Specimen A2 is given in Fig. 4.7(a). A peak load carrying capacity of 5610 kN was reached in this column. In accordance with what was observed in Specimens A1 and A1.5, the post-peak response of the column showed a controlled and steady decline in capacity with increasing strain demonstrating that this column has developed a certain level of post-peak ductility that was not present in the column that was cast without fibres. The concrete contribution versus strain is shown in Fig. 4.7(a) and the normalised concrete load contribution with respect to strain is shown in Fig. 4.7(b). Figure 4.8 details the observed behaviour for Specimen A2.

The plots of the measured strains for the gauges that were placed on the vertical bars show that that the yield strain was reached in all the gauges with the development of very large compressive strains (see Fig. 4.7(c)).

Figure 4.7(d) shows the measured strains in the instrumented hoop near the mid-height of the column. Both gauges S1 and S2 show that the yield strain was reached in the transverse hoop. It is noted that large tensile strains were measured as the column experienced the gradual decrease in load carrying capacity.

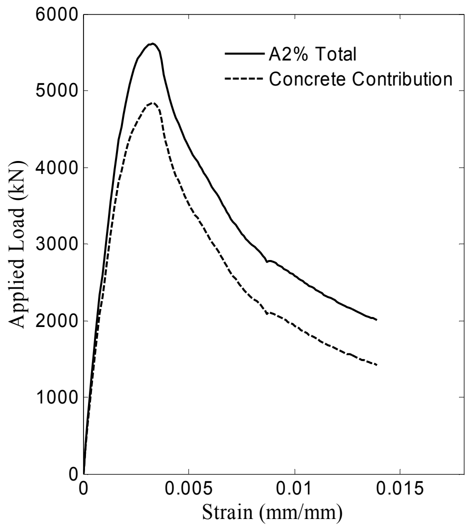

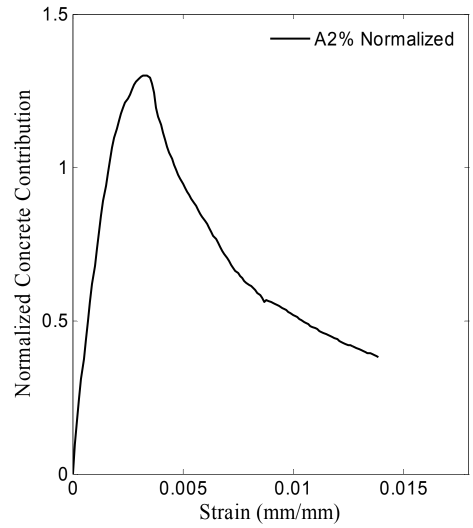

(a) Total applied load, P_{total}, versus strain and concrete load contribution, P_c, versus strain

(b) Normalized concrete contribution, $\frac{P_c}{P_{co}}$, versus strain

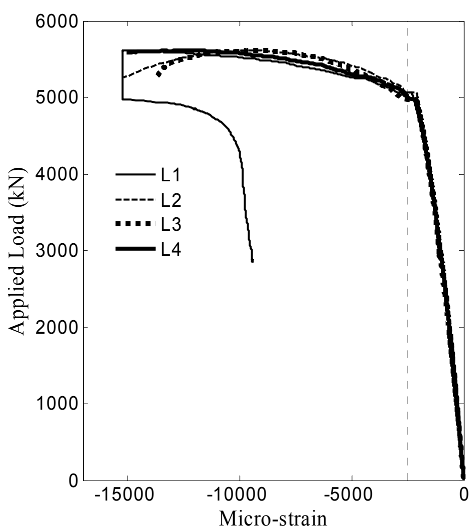

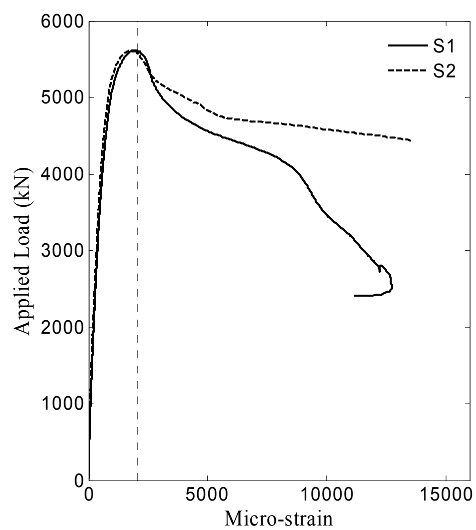

(c) Measured strains in longitudinal reinforcement

(d) Measured strains in transverse reinforcement

Figure 4.7: Experimental results for Specimen A2

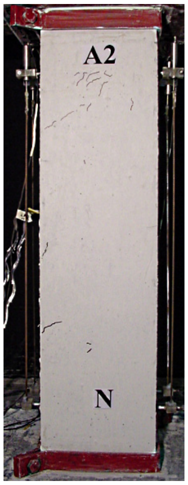	(a) - Just prior to the peak resistance some splitting cracks had initiated in the upper region of the North face of the column.		(b) - With further loading, these cracks began to extend at an angle of approximately 45° towards the mid-height of the column.
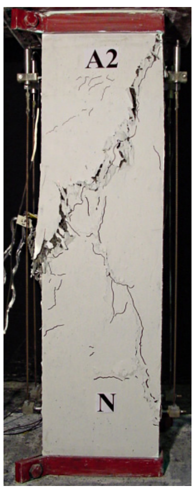	(c) - The observed cracking patterns indicated that crushing and cover spalling of the column were taking place, but that these mechanisms were occurring at a stable rate.		(d) - In addition, some vertical splitting cracks were observed indicating that bar buckling was taking place.
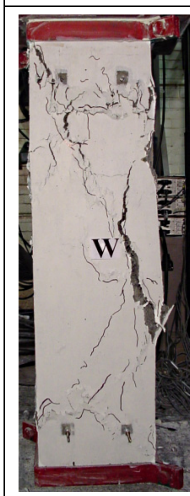	(e) - As loading continued, some large pieces of cover began to become detached from the core region of the column.		(f) - At the end of the experiment, it was noted that the vertical bars displayed a buckling length approximately equal to the spacing between the transverse reinforcement.

Figure 4.8: Major events for Specimen A2

4.2.5 Response of Specimen B0

Specimen B0 was detailed in accordance with the confinement provisions for moderately ductile columns in the CSA Standard (R_d = 2.5) resulting in a hoop spacing, s, of 120 mm. This column contained no fibres

The load-strain response of Specimen B0 is given in Fig. 4.9(a). A peak load carrying capacity of 4762 kN was reached in this column. Immediately after the peak load, the response showed a very abrupt drop in load carrying capacity due to sudden cover spalling. After this rapid drop, the ascending branch of the load response curve began to stabilise and the decrease in the load carrying capacity was somewhat controlled. Due to the intermediate spacing between the ties, the column had some limited post-peak ductility. The concrete contribution versus strain is shown in Fig. 4.9(a) and the normalised concrete load contribution with respect to strain is shown in Fig. 4.9(b). Figure 4.10 details the observed behaviour for Specimen B0.

Strains measured on the vertical reinforcing bars by the electrical strain gauges for Specimen B0 are shown in Fig. 4.9(c). The plots show that the yield strain was attained in all gauges near the peak capacity of the column. The plots also show a large jump in compressive strains for gauges L1 and L2 before the sudden drop in capacity.

Figure 4.9(d) shows the measured strains in the instrumented hoop near the mid-height of the column. Both gauges S1 and S2 show that the hoop strain at this location did not reach yield before the failure of the column.

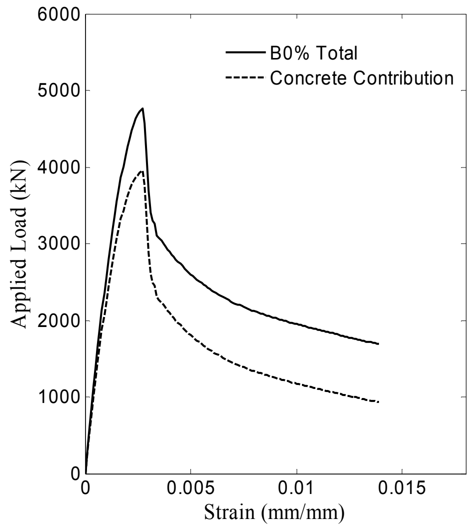

(a) Total applied load, P_{total}, versus strain and concrete load contribution, P_c, versus strain

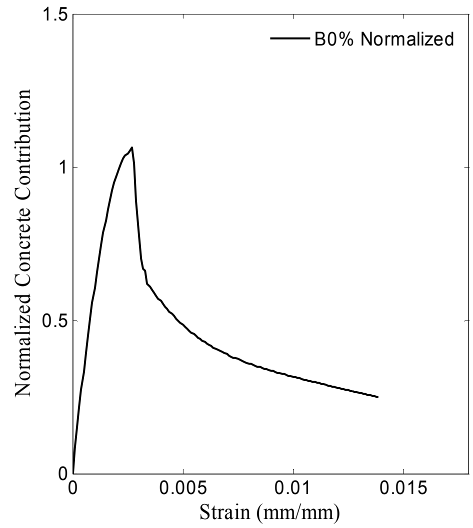

(b) Normalized concrete contribution, $\frac{P_c}{P_{co}}$, versus strain

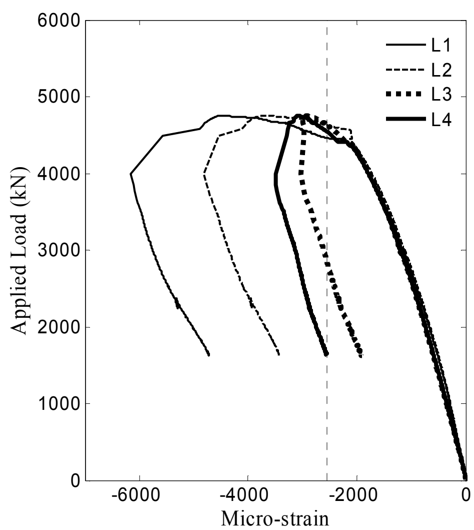

(c) Measured strains in longitudinal reinforcement

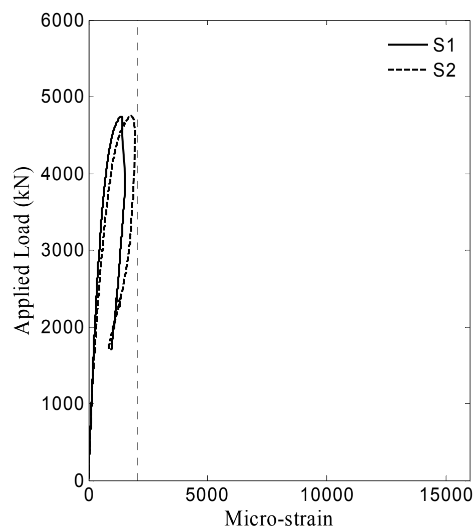

(d) Measured strains in transverse reinforcement

Figure 4.9: Experimental results for Specimen B0

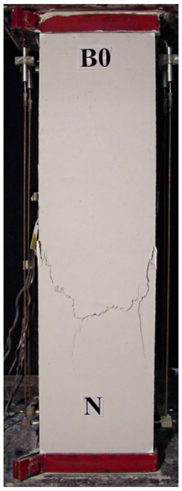	(a) - The first indications of distress were observed just prior to the peak resistance of the column. - At this load level some splitting cracks had initiated and signs of crushing were visible just below the mid-height region of the column		(b) - As the column was loaded beyond its peak load carrying capacity, crushing was observed in this region.
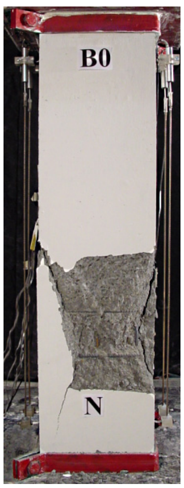	(c) - Furthermore splitting cracks were observed and spalling of the concrete cover occurred in a very sudden manner.		(d) - In addition, the vertical reinforcing bars began to buckle.
	(e) - The vertical bars displayed a buckling length approximately equal to the spacing between the transverse reinforcement.		(f) - Specimen B0 at the end of testing.

Figure 4.10: Major events for Specimen B0

4.2.6 Response of Specimen B1

Specimen B1 was detailed with the same amount of transverse reinforcement contained in Specimen B0, and hence met the requirements of R_d of 2.5 of the CSA standard, with a tie spacing of 120 mm. However, this column contained steel fibres in the quantity of 1% by volume of concrete.

The load-strain response of Specimen B1 is shown in Fig. 4.11(a). The column was able to reach a peak load carrying capacity of 4461 kN. In terms of post-peak response, the column showed a controlled drop in capacity which was in contrast to the sudden decline in resistance seen in the specimen that was cast without fibres. This behaviour demonstrated that the column had some post-peak ductility. The concrete contribution versus strain is shown in Fig. 4.11(a) and the normalised concrete load contribution with respect to strain is shown in Fig. 4.11(b). Figure 4.12 details the observed behaviour for Specimen B1.

The plots of the recorded strains versus the applied loading are shown in Fig. 4.11(c). The plots for of all of the gauges demonstrate that the yield strain was reached near the peak capacity of the column. The plots show that somewhat larger compressive strains were atteigned in the longitudinal reinforcement of this column when compared to the strains observed in column B0.

Figure 4.11(d) shows the measured strains in the instrumented hoop near the mid-height of the column. Both gauges S1 and S2 show that the yield strain was reached in the transverse hoop. The addition of fibres has increased the level of confinement in this column, resulting in the higher tensile strains in the transverse reinforcement.

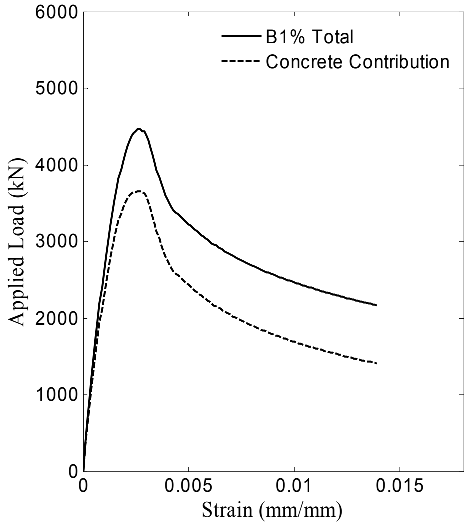

(a) Total applied load, P_{total}, versus strain and concrete load contribution, P_c, versus strain

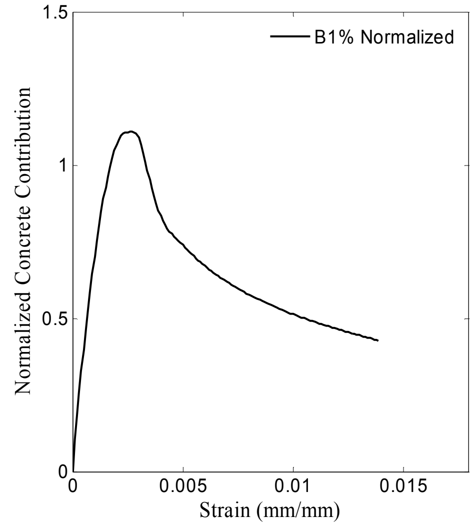

(b) Normalized concrete contribution, $\dfrac{P_c}{P_{co}}$, versus strain

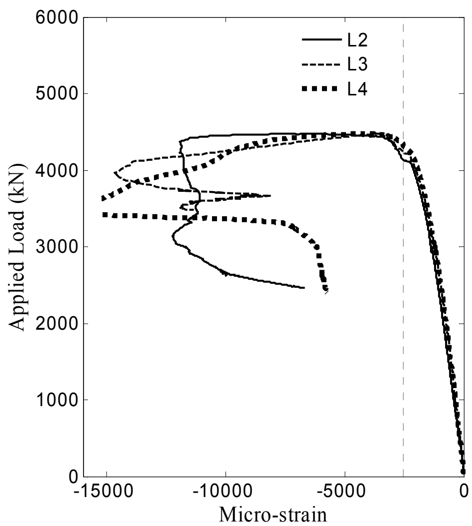

(c) Measured strains in longitudinal reinforcement

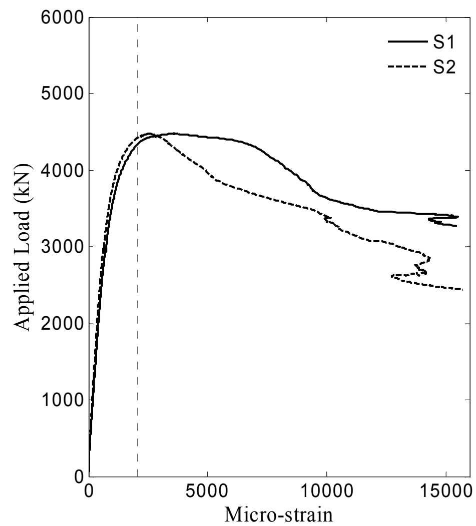

(d) Measured strains in transverse reinforcement

Figure 4.11: Experimental results for Specimen B1

(a)

- The first signs of distress were observed just prior to the column's peak carrying capacity. At this load level some diagonal splitting cracks had initiated at the mid-height on the North face of the column.

(b)

- When the peak load carrying capacity was reached, these cracks began to extend with a diffused cracking pattern.

(c)

- Crushing was also visible on the West and East faces of the column.

(d)

- However the cover spalling mechanism was very gradual and controlled, with only surface concrete becoming detached from the column during the early stages of the post-peak loading.

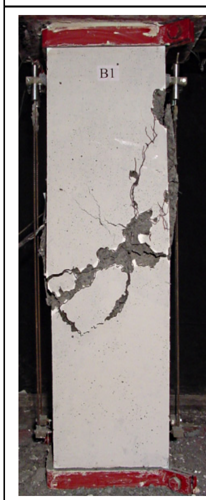

(e)

- As loading continued, cover spalling continued to develop, with larger pieces of cover becoming detached from the core region of the column.

- It was also apparent that bar buckling was occurring with the longitudinal bars pushing against large pieces of cover concrete.

(f)

- Specimen B1 at the end of testing.

- It was noted that the vertical bars displayed a buckling length approximately equal to the spacing between the transverse reinforcement.

Figure 4.12: Major events for Specimen B1

4.2.7 Response of Specimen B1.5

Just like Specimens B0 and B1, the transverse reinforcement in specimen B1.5 was detailed in conformity with the requirements of R_d of 2.5 of the CSA standard, resulting in a spacing of 120 mm. However, this column contained steel fibres in the quantity of 1.5% by volume of concrete.

The load-strain response of Specimen B1.5 is given in Fig. 4.13(a). A peak load carrying capacity of 5891 kN was reached in this column. As strain was applied beyond the peak resistance, the load carrying capacity of the column decreased in a controlled and stable manner. The concrete contribution versus strain is shown in Fig. 4.13(a) and the normalised concrete load contribution with respect to strain is shown in Fig. 4.13(b). Figure 4.14 details the observed behaviour for Specimen B1.5.

The measured strains in the gauges show that very large compressive strains were reached in the longitudinal reinforcement of this column before the drop in load carrying capacity (see Fig. 4.13(c)). Gauges L1 and L2 showed some signs of buckling with the inner gauge showing a larger jump in compressive strain when compared to the outer gauge. The same observation is made when comparing gauges L3 and L4.

Figure 4.13(d) shows the measured strains in the instrumented hoop near the mid-height of the column. Both gauges S1 and S2 show that the yield strain was attained in the transverse hoop.

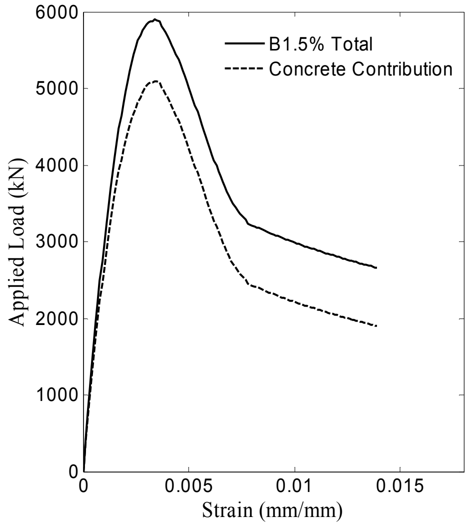

(a) Total applied load, P_{total}, versus strain and concrete load contribution, P_c, versus strain

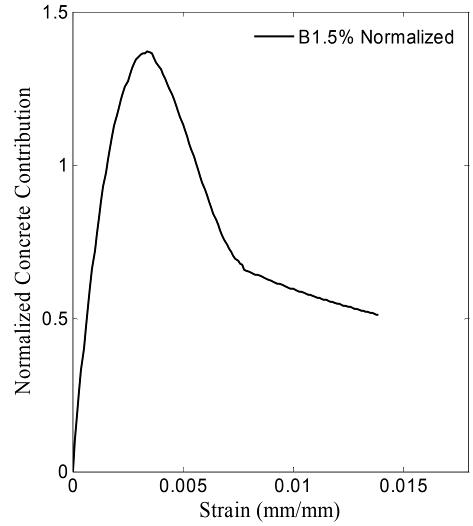

(b) Normalized concrete contribution, $\frac{P_c}{P_{co}}$, versus strain

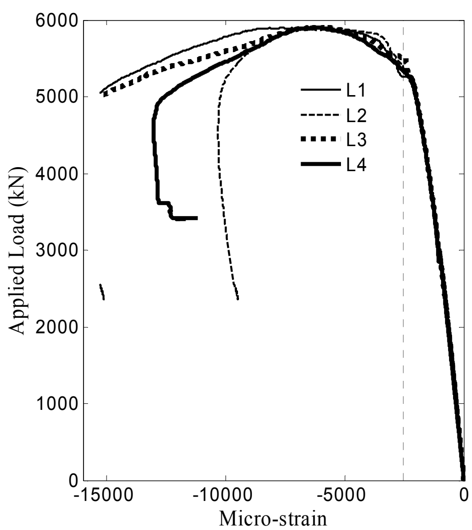

(c) Measured strains in longitudinal reinforcement

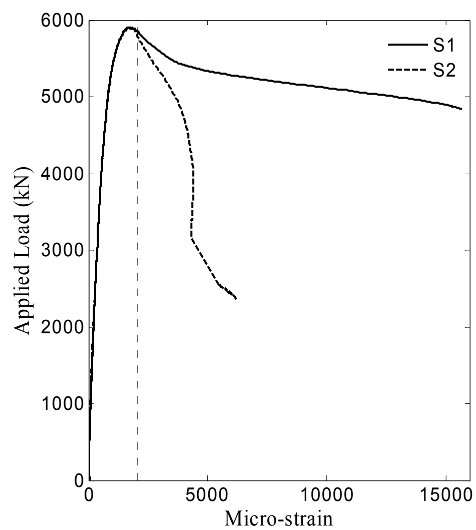

(d) Measured strains in transverse reinforcement

Figure 4.13: Experimental results for Specimen B1.5

<table>
<tr>
<td>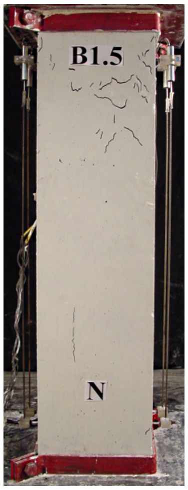</td>
<td>(a)
- No indications of distress were apparent until the peak axial capacity of the column was reached.
- At this load level some diagonal splitting cracks had initiated in the lower and upper regions of the column.</td>
<td></td>
<td>(b)
- As the column was loaded beyond its peak capacity, these cracks began to extend in all directions in the upper region of the column with a diffused cracking pattern</td>
</tr>
<tr>
<td></td>
<td>(c)
- In addition, several splitting cracks began to extend downwards towards the mid-height of the column</td>
<td></td>
<td>(d)
- The cover spalling and crushing mechanisms were gradual and controlled.</td>
</tr>
<tr>
<td></td>
<td>(e)
- As loading continued, larger pieces of cover began to become slightly detached from the core region of the specimen.
- It was also apparent that bar buckling was occurring with the longitudinal bars pushing against large pieces of cover concrete.</td>
<td></td>
<td>(f)
- Specimen B15 at the end of testing
- It was noted that the vertical bars displayed a buckling length approximately equal to the spacing between the transverse reinforcement.</td>
</tr>
</table>

Figure 4.14: Major events for Specimen B1.5

4.2.8 Response of Specimen B2

In accordance with the detailing of the other B-series specimens, the spacing of the transverse reinforcement in Specimen B2 was 120 mm. In addition, this column contained steel fibres in the quantity of 2 % by volume of concrete.

The load-strain response of Specimen B2 is given Fig. 4.15(a). The behaviour of this specimen is in conformity with was observed in the other fibre reinforced specimens in the B-series with the column showing a somewhat ductile post-peak response after reaching its peak capacity of 5336 kN. The concrete contribution versus strain is shown in Fig. 4.15(a) and the normalised concrete load contribution with respect to strain is shown in Fig. 4.15(b). Figure 4.16 details the observed behaviour for Specimen B2.

The plots for the strain gauges on the vertical bars are shown in Fig. 4.15(c). The plots show that very large compressive strains were reached in all of the gauges.

Figure 4.15(d) shows the measured strains in the instrumented hoop near the mid-height of the column. It is noted that large tensile strains were measured in both gauges S1 and S2, pointing to the beneficial influence of the fibres.

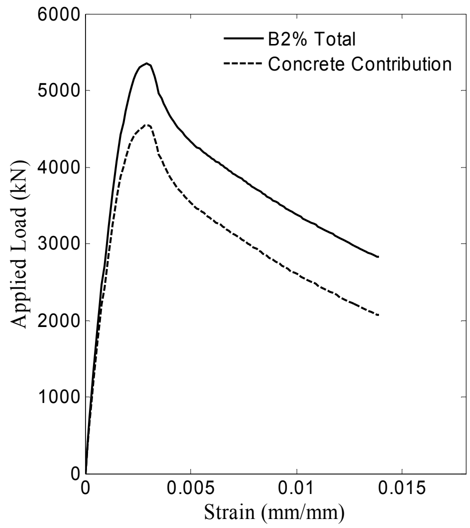

(a) Total applied load, P_{total}, versus strain and concrete load contribution, P_c, versus strain

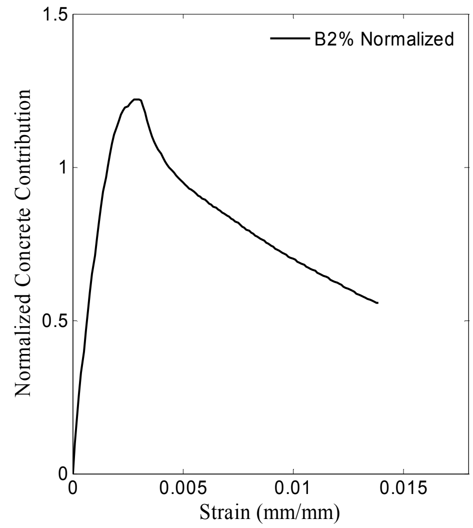

(b) Normalized concrete contribution, $\frac{P_c}{P_{co}}$, versus strain

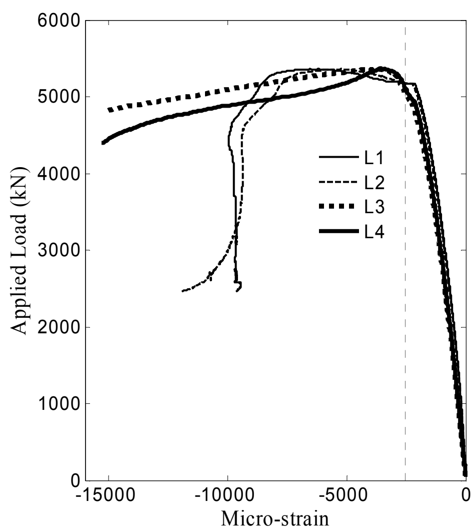

(c) Measured strains in longitudinal reinforcement

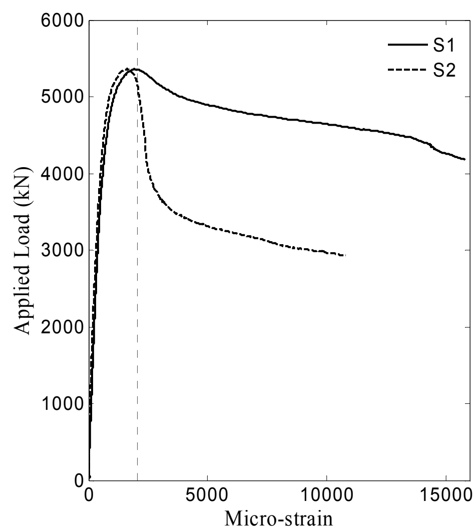

(d) Measured strains in transverse reinforcement

Figure 4.15: Experimental results for Specimen B2

	(a) - The first signs of damage were observed near the peak capacity of the column. - At this load level, several vertical splitting cracks had initiated in the upper region of the column.		(b) - As the column was loaded beyond its peak capacity these cracks began to extend horizontally and diagonally in the upper region of the column with a diffused cracking pattern.
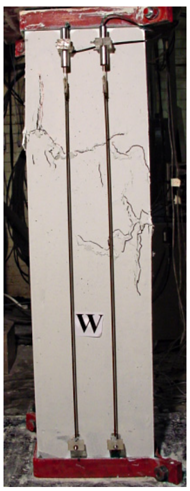	(c) - Splitting cracks were also observed at the mid-height of the west face of the column.		(d) - Observed cracking patterns indicated that crushing and cover spalling of the column were occurring at a stable rate.
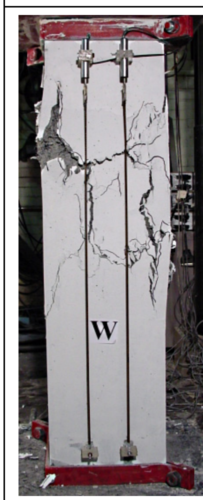	(e) - It was also apparent that bar buckling was occurring with the longitudinal bars pushing against large pieces of cover concrete		(f) - Specimen B2 at the end of testing. - It was noted that the vertical bars displayed a buckling length approximately equal to the spacing between the transverse reinforcement.

Figure 4.16: Major events for Specimen B2

4.2.9 Response of Specimen C0

The more stringent confinement provisions in the CSA Standard for ductile columns (Rd = 4.0) were used to detail specimen C0. For this column, square and diamond shaped 10M hoops were used and the design provisions resulted in a hoop spacing, s, of 65 mm. This column contained no fibres.

The load-strain response of Specimen C0 is shown in Fig. 4.17(a). A peak resistance of 5044 kN was reached in this column. Immediately after the peak load, the response showed a slight but sudden drop in load (with the capacity dropping to about 80% of the peak load). After this abrupt drop, the descending branch of the load response curve stabilised with the column maintaining its load carrying capacity even at very large deformations. Due to the close spacing between the ties and the improved detailing of the transverse reinforcement in the column cross-section, Specimen C0 displayed an exceptionally well controlled post-peak response with the only drop in capacity occurring during cover spalling. The concrete contribution versus strain is shown in Fig. 4.17(a) and the normalised concrete load contribution with respect to strain is shown in Fig. 4.17(b). Figure 4.18 details the observed behaviour for Specimen C0.

Strains measured on the vertical reinforcing bars by the electrical strain gauges for Specimen C0 are shown in Fig. 4.17(c) and show that the yield strain was reached in all gauges. The plots show that very large compressive strains were reached in the longitudinal reinforcement. These strains are much larger than those observed in Specimens A0 and B0 which contained lower levels of confinement reinforcement.

Figure 4.17(d) shows the measured strains in the instrumented hoop near the mid-height of the column. Both gauges S1 and S2 show that the hoop strain at this location just reached yield before failure. In addition to the gauges that were placed on the mid-height hoop, two additional gauges (S3 and S4) were placed on the diamond shaped hoops. The readings show that the yield strain was reached at this location.

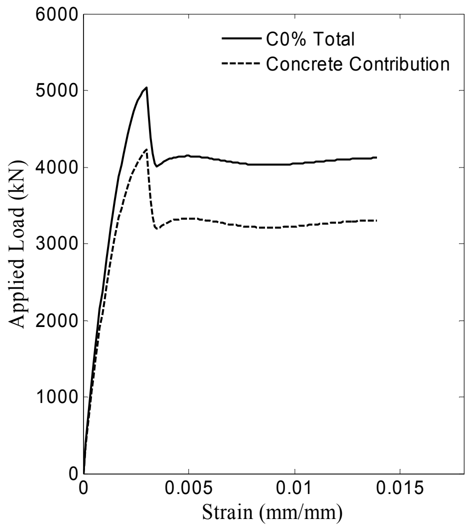

(a) Total applied load, P_{total}, versus strain and concrete load contribution, P_c, versus strain

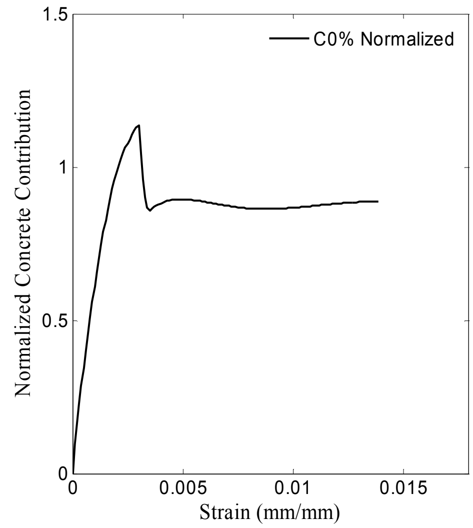

(b) Normalized concrete contribution, $\frac{P_c}{P_{co}}$, versus strain

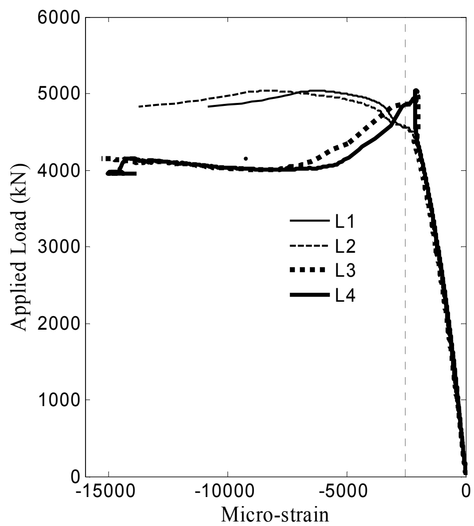

(c) Measured strains in longitudinal reinforcement

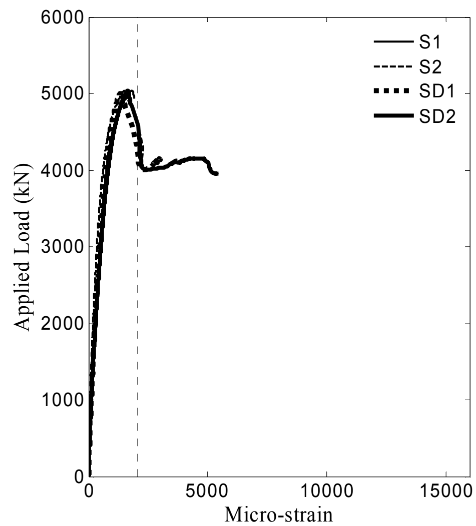

(d) Measured strains in transverse reinforcement

Figure 4.17: Experimental results for Specimen C0

	(a) - Just prior to the peak resistance, some splitting cracks had initiated near the mid-height region of the column		(b) - Soon thereafter, crushing was observed in this region. - Furthermore extensive splitting cracks were seen and spalling of the concrete cover occurred in a very sudden manner over the height of the column.
	(c) - As loading continued, much of the cover began to become detached from the core region of the column		(d) - At a deformation of approximately 29 mm, one of the hoops fractured near the mid-height region.
	(e) - Throughout the test, the hoops ensured that the integrity of the core region of the column was maintained		(f) - Specimen C0 at the end of testing

Figure 4.18: Major events for Specimen C0

4.2.10 Response of Specimen C1

Specimen C1 was detailed with the same amount of transverse reinforcement contained in Specimen C0, and hence met the requirements of R_d of 4.0 of the CSA standard, with a tie spacing of 65 mm. However, this column contained steel fibres at a quantity of 1% by volume of concrete.

The load-strain response of Specimen C1 is shown in Fig. 4.19(a). This specimen was able to reach a peak load carrying capacity of 4650 kN. As loading was applied beyond the peak capacity of the specimen, the load began to drop in a controlled manner. After this controlled decrease in resistance, the capacity of the column stabilised at 92% of the peak value with the column maintaining it's the load carrying capacity even at very large deformations. Due to the close spacing between the ties and the improved detailing of the transverse reinforcement in the column cross-section, as well as the presence of steel fibres in the concrete mix, the column displayed an outstanding post-peak response. The concrete contribution versus strain is shown in Fig. 4.19(a) and the normalised concrete load contribution with respect to strain is shown in Fig. 4.19(b). Figure 4.20 details the observed behaviour for Specimen C1.

The strain gauges on the vertical bars and transverse hoops were placed in the same locations as for Specimen C0; the plots of the recorded strains versus the applied loading for the longitudinal bars are shown in Fig. 4.19(c). The plots show that very large compressive strains were reached in all of the gauges.

Figure 4.19(d) shows the measured strains in the instrumented hoop near the mid-height of the column. It is noted that very large tensile strains were measured in gauges S1 and S2. The same observation is made for the gauges that were placed on the diamond shaped hoop.

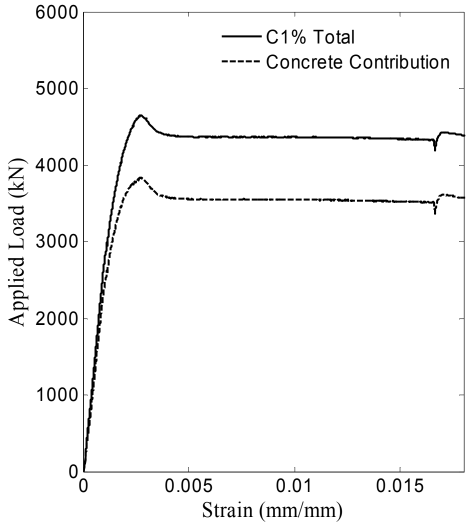

(a) Total applied load, P_{total}, versus strain and concrete load contribution, P_c, versus strain

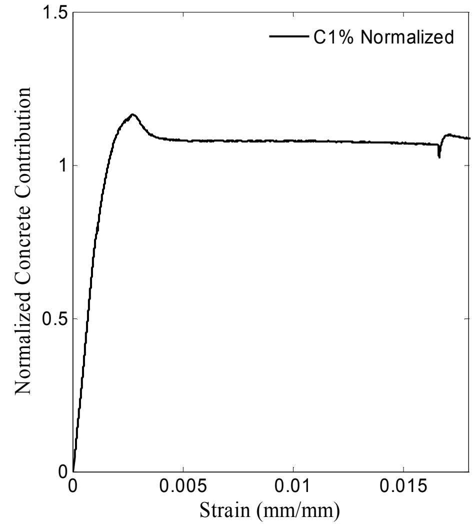

(b) Normalized concrete contribution, $\frac{P_c}{P_{co}}$, versus strain

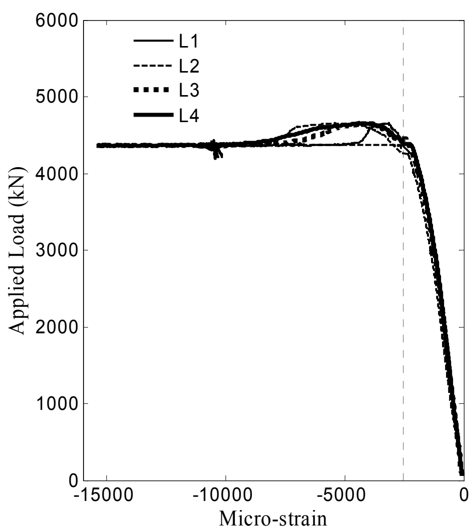

(c) Measured strains in longitudinal reinforcement

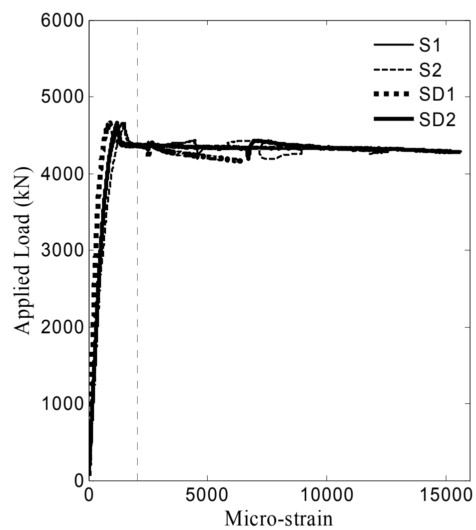

(d) Measured strains in transverse reinforcement

Figure 4.19: Experimental results for Specimen C1

	(a) - No indications of distress were apparent before the peak capacity was reached. - At that time, some diagonal splitting cracks had initiated at the upper region of the column		(b) - As further loading was applied, crushing and signs of cover spalling began to become visible with slight spalling of some of the surface concrete around the crack patterns that had formed in the upper region of the column.
	(c) - With further loading, new splitting cracks developed extending downwards towards the mid-height of the column.		(d) - The cover spalling and crushing mechanisms were very gradual and controlled.
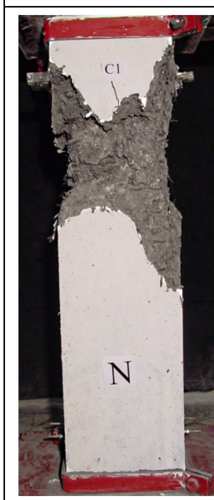	(e) - As cover spalling continued to occur, larger pieces of cover began to become detached from the column. - However it was observed that even at very large deformations the integrity of the core concrete region was maintained with little or no buckling of the reinforcement.		(f) - Specimen C1 at the end of testing

Figure 4.20: Major events for Specimen C1

4.2.11 Response of Specimen C1.5

Specimen C1.5 was detailed with the same amount of transverse reinforcement that was present in the other C-series specimens (s = 65 mm). This column contained steel fibres in a quantity of 1.5 % by volume of concrete.

The load-strain response of Specimen C1.5 is given in Fig. 4.21(a). In accordance to what observed in Specimen C1, this column displayed an extremely well controlled post-peak response after reaching its peak capacity of 6210 kN. Initially, the load dropped in a controlled manner to reach 90% of the columns' maximum resistance. As further strain was applied, the descending branch of the load response curve stabilised with the column maintaining its load carrying capacity even at very large deformations. Once again, this exceptional response could be attributed to the high amount of transverse reinforcement in this column and the added benefit that resulted from the presence of steel fibres in the concrete mix. The concrete contribution versus strain is shown in Fig. 4.21(a) and the normalised concrete load contribution with respect to strain is shown in Fig. 4.21(b). Figure 4.22 details the observed behaviour for Specimen C1.5.

The strain gauges on the vertical bars and transverse hoops were placed in the same locations as for Specimen C0. Similar to the previous observations, the plots for of all of the gauges show that large compressive strains were reached in the bars (see Fig. 4.21(c)).

Figure 4.21(d) shows the measured strains in the instrumented hoop near the mid-height of the column. Once again, large tensile strains were measured in all of the gauges that were placed on the transverse hoops.

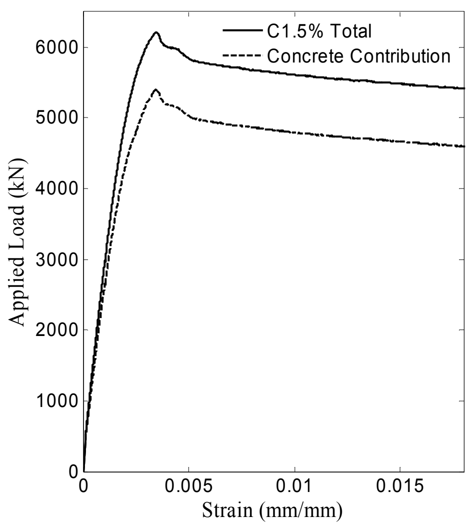

(a) Total applied load, P_{total}, versus strain and concrete load contribution, P_c, versus strain

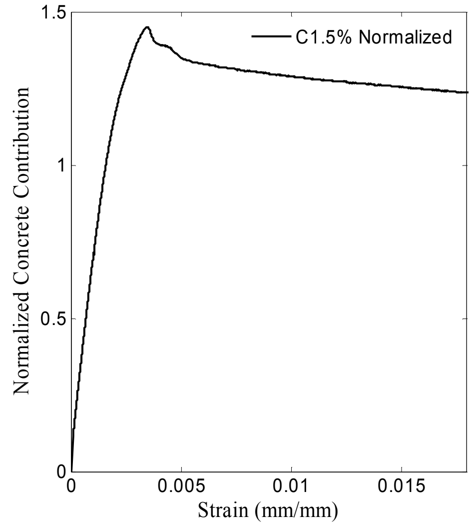

(b) Normalized concrete contribution, $\frac{P_c}{P_{co}}$, versus strain

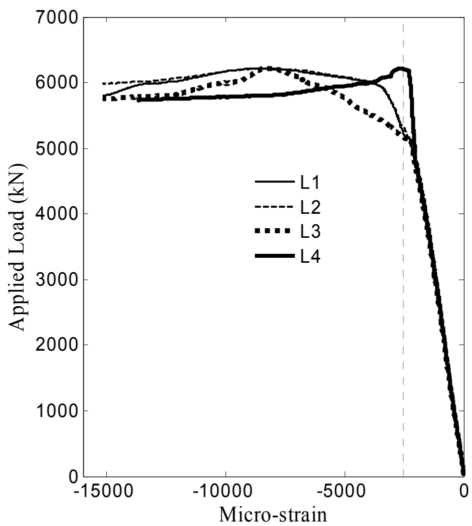

(c) Measured strains in longitudinal reinforcement

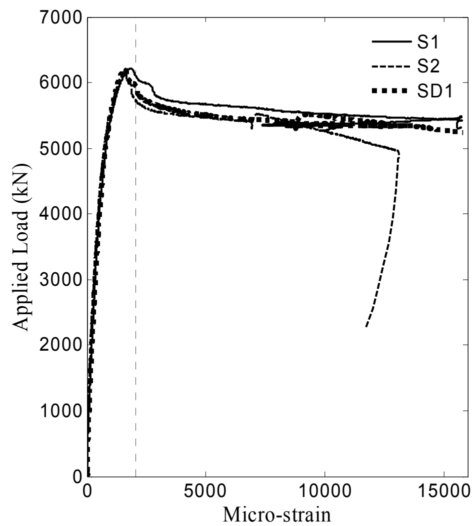

(d) Measured strains in transverse reinforcement

Figure 4.21: Experimental results for Specimen C1.5

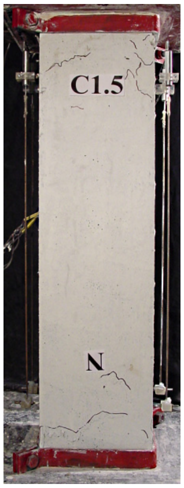	(a) - The first evidence of distress was apparent near the peak capacity of the column with the development of some longitudinal splitting cracks near the top of the column.		(b) - Soon thereafter, splitting cracks were also visible. - As the load carrying capacity of the column began to drop, these cracks began to extend in all directions in the upper region of the column
	(c) - As the loading continued, crushing and signs of cover spalling began to be visible with slight spalling of some of the surface concrete.		(d) - The cover spalling and crushing mechanisms were very gradual and controlled.
	(e) - Even at very large deformations the integrity of the core concrete region was maintained with little or no buckling of the reinforcement	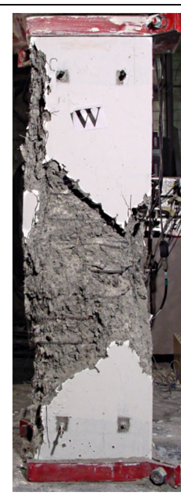	(f) - Specimen C1.5 at the end of testing

Figure 4.22: Major events for Specimen C1.5

4.2.12 Response of Specimen D0

Specimen D0 was detailed with a level of transverse reinforcement that is intermediate between R_d = 2.5 and 4.0 of the CSA Standard, resulting in a hoop spacing of 80 mm. This column contained no fibres.

As shown in Fig. 4.23(a), Specimen D0 reached a peak capacity of 4526 kN. Immediately after the peak load, the response of the specimen showed a sudden drop in capacity (with the resistance dropping to about 75% of the peak load). After this sudden drop the ascending branch of the load response curve began to stabilise and the decrease in the load carrying capacity was somewhat controlled. Due to the intermediate spacing between the ties, the column showed a well controlled post-peak response. The concrete contribution versus strain is shown in Fig. 4.23(a) and the normalised concrete load contribution with respect to strain is shown in Fig. 4.23(b). Figure 4.24 details the observed behaviour for Specimen D0.

Strains measured on the vertical reinforcing bars by the electrical strain gauges for Specimen D0 are shown in Fig. 4.23(c). The plots show that the yield strain was reached in all gauges near the peak capacity of the column. The plots also show that very large compressive strains were reached in the longitudinal reinforcement of this column

Figure 4.23(d) shows the measured strains in the instrumented hoop near the mid-height of the column. Gauge S1 shows that the hoop strain at this location just reached yield before the failure of the gauge. It should be noted that gauge S2 did not function during the experiment.

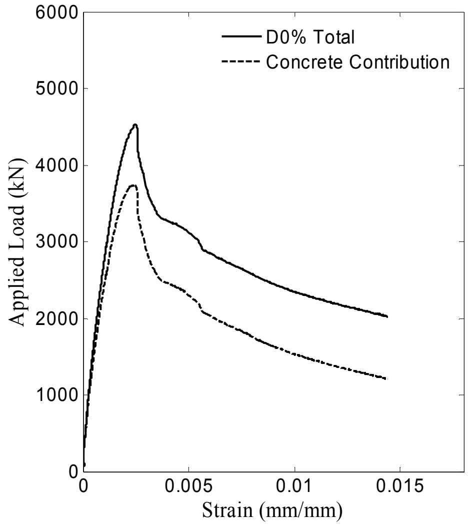

(a) Total applied load, P_{total}, versus strain and concrete load contribution, P_c, versus strain

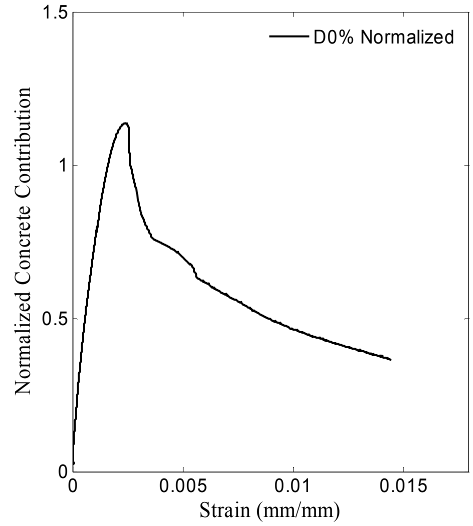

(b) Normalized concrete contribution, $\dfrac{P_c}{P_{co}}$, versus strain

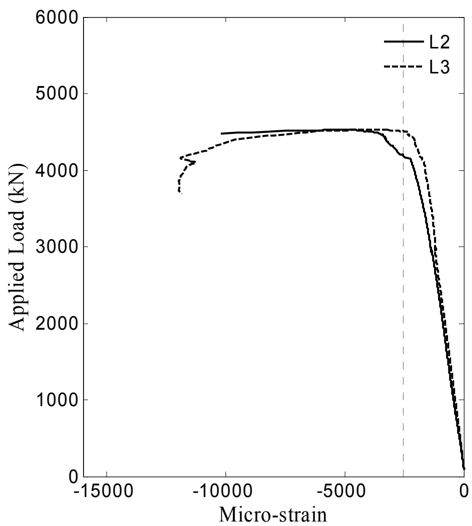

(c) Measured strains in longitudinal reinforcement

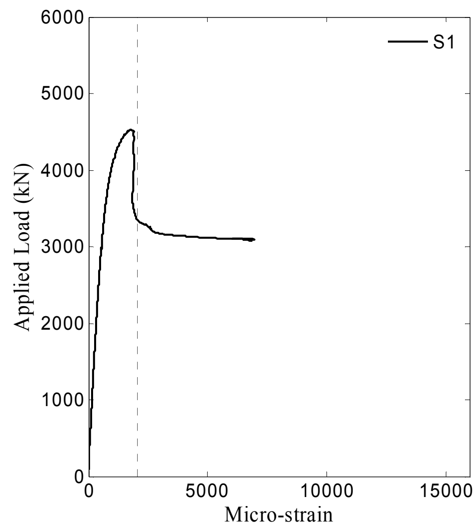

(d) Measured strains in transverse reinforcement

Figure 4.23: Experimental results for Specimen D0

(a)

- The first indications of distress were observed just prior to the peak capacity of the column.
- At this load level some splitting cracks had initiated at the mid-height region of the column.

(b)

- As the specimen was loaded beyond its peak capacity, crushing was observed at the mid-height of the column.

(c)

- Furthermore, extensive splitting cracks were observed at the locations of the longitudinal bars and spalling of the concrete cover began to occur in a sudden manner.

(d)

- In addition, it was apparent that the longitudinal reinforcing bars were buckling, with the bars in the failure region having a buckling length approximately equal to the spacing between the transverse reinforcement.

(e)

- Specimen D0 after sudden cover spalling

(f)

- Specimen D0 at the end of testing

Figure 4.24: Major events for Specimen D0

4.2.13 Response of Specimen D1.5

Just like Specimen D0, specimen D1.5 was detailed with a level of transverse reinforcement that was intermediate between R_d = 2.5 and 4.0 (s = 80 mm). However, this column contained steel fibres in a quantity of 1.5% by volume of concrete.

The load-strain response of specimen D1.5 is given in Fig. 4.25(a). A peak load carrying capacity of 5215 kN was reached in this specimen. As loading was applied beyond the peak capacity of the column, the load carrying capacity of the specimen began to drop. However, in contrast to what was observed in specimen D0, this drop in capacity was not sudden. Rather, the load carrying capacity decreased in a gradual manner, demonstrating that the column had some improved post-peak ductility. The concrete contribution versus strain is shown in Fig. 4.25(a) and the normalised concrete load contribution with respect to strain is shown in Fig. 4.25(b). Figure 4.26 details the observed behaviour for Specimen D1.5.

The strain gauges on the vertical bars and transverse hoops were placed in the same locations as for Specimen D0; the plots of the recorded strains versus the applied load are shown in Fig. 4.25(c) and show that very large compressive strains were reached in the longitudinal reinforcement of this column.

Figure 4.25(d) shows the measured strains in the instrumented hoop near the mid-height of the column. Both gauges S1 and S2 show that the yield strain was reached in the transverse hoop.

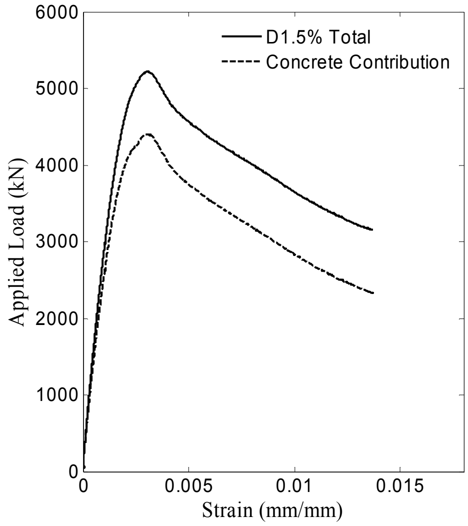

(a) Total applied load, P_{total}, versus strain and concrete load contribution, P_c, versus strain

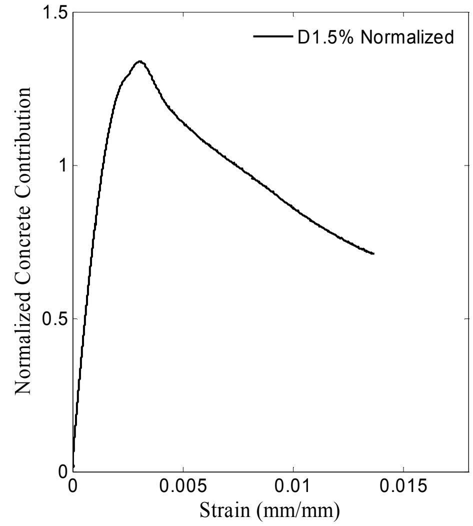

(b) Normalized concrete contribution, $\frac{P_c}{P_{co}}$, versus strain

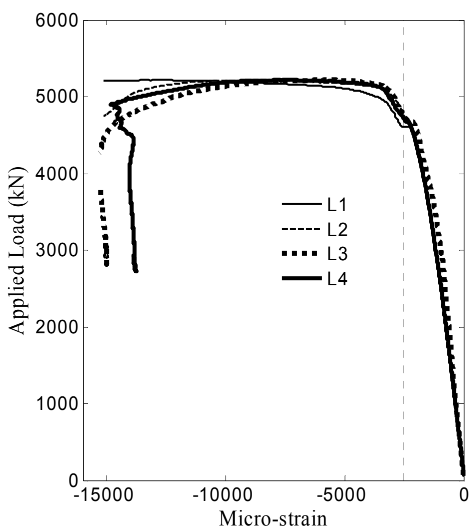

(c) Measured strains in longitudinal reinforcement

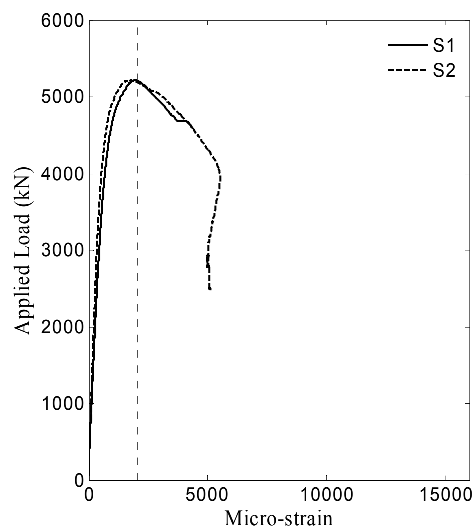

(d) Measured strains in transverse reinforcement

Figure 4.25: Experimental results for Specimen D1.5

	(a) - Just prior to the peak resistance, some diagonal and longitudinal splitting cracks had initiated at the mid-height of the column.		(b) - As further loading was applied, these cracks began to extend in all directions with a diffused cracking pattern.
	(c): - In addition, splitting cracks were observed near the mid-height of the column. - This and other observed cracking patterns indicated that crushing and cover spalling were occurring at a stable rate.		(d) - As the loading continued, crushing and cover spalling continued to develop, with spalling of some of the surface concrete around the crack patterns. - Gradually, these mechanisms began to extend throughout the height of the column
	(e) - Progressively, larger pieces of cover began to become detached from the core region of the column - Some of vertical bars displayed a buckling length approximately equal to the spacing between the transverse reinforcement.		(f) - Specimen D15 at the end of testing.

Figure 4.26: Major events for Specimen D1.5

4.3 Presentation of Results for Specimens Constructed without Cover

This section presents the results of the 7 companion specimens that were constructed without cover. For brevity, the strain gauge data associated with these columns will not be presented as the behaviour was similar to what was discussed in the full-cover specimens.

4.3.1 Response of Specimen A0nc

Specimen A0nc was detailed in accordance with requirements of R_d of 1.5 of the CSA Standard. The spacing of the transverse reinforcement was 240 mm. This column contained no fibres. Hence, the details of this column were identical to those of Specimen A0 with the exception being that this specimen was constructed without cover.

The load-strain response of Specimen A0nc is given in Fig. 4.27(a). A peak resistance of 3253 kN was attained in this column. Immediately after the peak load, the response of the specimen showed an abrupt decline in load carrying capacity. Due to the large spacing between the ties, the column showed a poor post-peak response. The normalised concrete load contribution with respect to strain is shown in Fig. 4.27(b). Figure 4.28 details the observed behaviour for Specimen A0nc.

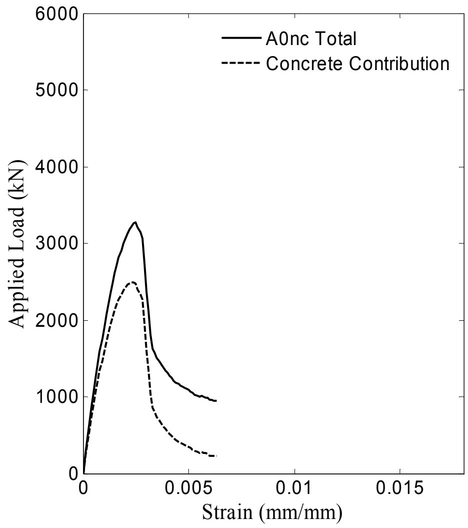

(a) Total applied load, P_{total}, versus strain and concrete load contribution, P_c, versus strain

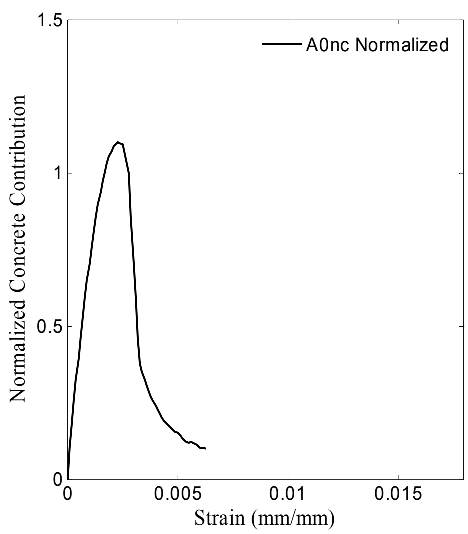

(b) Normalized concrete contribution, $\dfrac{P_c}{P_{co}}$, versus strain

Figure 4.27: Experimental results for Specimen A0nc

	(a) - Just prior to the peak resistance some horizontal splitting cracks had initiated at the locations of transverse reinforcement at the mid-height of the column.	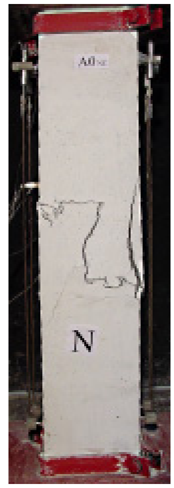	(b) - As the load carrying capacity began to drop, a longitudinal splitting crack began to form at the location of the mid-side longitudinal bar on the North face.
	(c) - Furthermore, spalling of the minimum concrete cover was occurring at the corners of the column.		(d) - In addition, the concrete in the ineffective core region began to crush and disintegrate.
	(e) - It was also apparent that buckling of the vertical bars was taking place. - The cracking mechanisms and the buckling of the vertical reinforcing bars occurred in a very sudden manner.		(f) - Specimen A0nc at the end of the testing procedure

Figure 4.28: Major events for Specimen A0nc

4.3.2 Response of Specimen A1nc

Specimen A1nc was detailed with the same amount of transverse reinforcement found in Specimen A0nc (s = 240 mm). However, this column contained steel fibres in the quantity of 1% by volume of concrete. Therefore, the details of this column were identical to those of Specimen A1 with the exception being that this specimen was constructed without cover.

As is seen in Fig. 4.29(a), a peak load carrying capacity of 3420 kN was reached in this column. As the column was loaded beyond its peak resistance, the load carrying capacity began to drop. However, the post-peak response was improved, with the descending branch of the load strain curve showing a sustained yet gradual decrease in load carrying capacity. The normalised concrete load contribution with respect to strain is shown in Fig. 4.29(b). Figure 4.30 details the observed behaviour for Specimen A1nc.

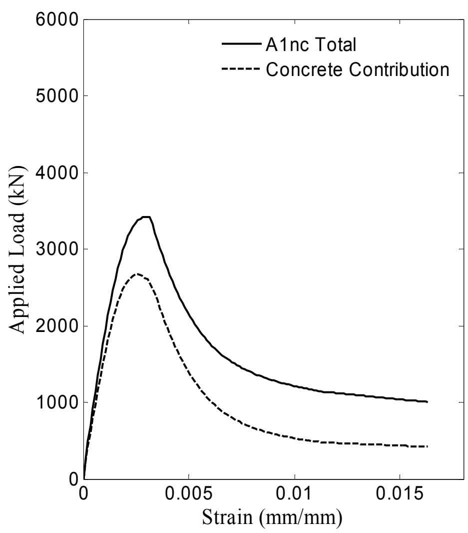

(a) Total applied load, P_{total}, versus strain and concrete load contribution, P_c, versus strain

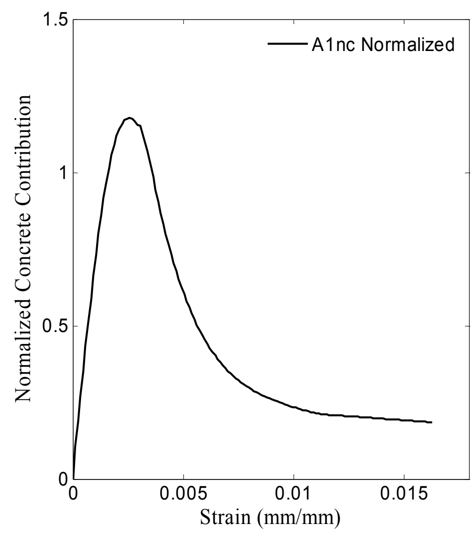

(b) Normalized concrete contribution, $\frac{P_c}{P_{co}}$, versus strain.

Figure 4.29: Experimental results for Specimen A1nc

<table>
<tr><td rowspan="2">
</td><td>(a)</td><td rowspan="2">
</td><td>(b)</td></tr>
<tr><td>- Just prior to the peak resistance, a splitting crack had initiated at the mid-height of the column at the location of the transverse reinforcement.</td><td>- When the peak load was reached, a diagonal splitting crack formed and began to extend vertically from the mid-height towards the upper region of the column.</td></tr>
<tr><td rowspan="2">
</td><td>(c)</td><td rowspan="2">
</td><td>(d)</td></tr>
<tr><td>- As the loading continued, crushing continued to occur.

- Furthermore, extensive splitting cracks began to develop and branch out of the initial splitting crack.</td><td>- In addition, it was also apparent that buckling of the longitudinal reinforcing bars was taking place.</td></tr>
<tr><td rowspan="2">
</td><td>(e)</td><td rowspan="2">
</td><td>(f)</td></tr>
<tr><td>- Nonetheless, the cracking mechanisms and the crushing of the ineffective core region occurred in a gradual yet sustained manner.</td><td>- Specimen A1nc at the end of the testing procedure</td></tr>
</table>

Figure 4.30: Major events for Specimen A1nc

4.3.3 Response of Specimen A1.5nc

The details of this column were identical to those of Specimen A1.5 (s = 240 mm, v_f = 1.5%) with the exception being that this specimen was constructed without cover.

The load-strain response of Specimen A1.5nc is given in Fig. 4.31(a). Similar to what was observed in specimen A1nc, the column displayed a somewhat controlled post-peak response beyond its peak capacity of 3763 kN, demonstrating that the column had some post-peak ductility. The normalised concrete load contribution with respect to strain is shown in Fig. 4.31(b). Figure 4.32 details the observed behaviour for Specimen A1.5nc.

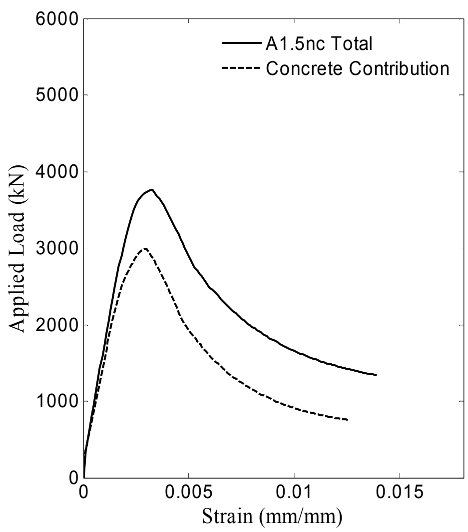

(a) Total applied load, P_{total}, versus strain and concrete load contribution, P_c, versus strain

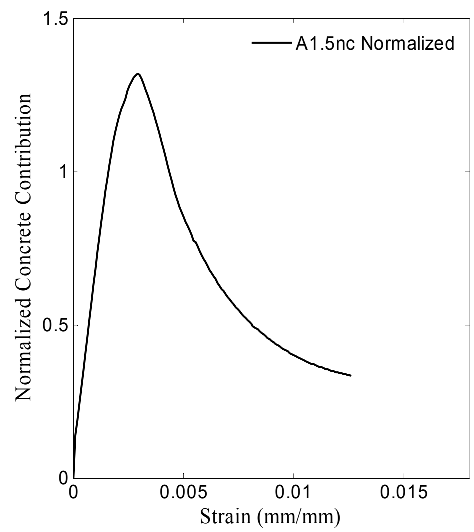

(b) Normalized concrete contribution, $\frac{P_c}{P_{co}}$, versus strain.

Figure 4.31: Experimental results for Specimen A1.5nc

	(a) - The first signs of distress occurred just prior to the peak capacity of the specimen, with some early signs of crushing appearing in the upper region of the column near the location of the transverse reinforcement.		(b) - When the peak load was reached, the crushing continued with the formation of longitudinal splitting cracks extending downwards towards the mid-height of the column.
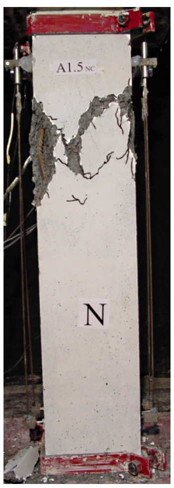	(c) - As the loading continued, crushing continued to occur with spalling of the surface concrete at the location of the longitudinal reinforcement.		(d) - However this behaviour was gradual with integrity being maintained in much of the core concrete region.
	(e) - At the termination of the experiment it was noted that the vertical bars displayed a buckling length approximately equal to the spacing between the transverse reinforcement.		(f) - Specimen A1.5nc at the end of the testing procedure

Figure 4.32: Major events for Specimen A1.5nc

4.3.4 Response of Specimen B0nc

Specimen B0nc was detailed in accordance with requirements of R_d of 2.5 of the CSA Standard. The spacing of the transverse reinforcement was 120 mm and this column contained no fibres. Hence, the details of this column were identical to those of Specimen B0 with the exception being that this specimen was constructed without cover.

The load-strain response of Specimen B0nc is given in Fig. 4.33(a). A peak resistance of 3319 kN was reached in this column. As loading continued the load carrying capacity of the column began to drop. Due to the intermediate spacing between the ties, the column showed an improved post-peak response. The normalised concrete load contribution with respect to strain is shown in Fig. 4.33(b). Figure 4.34 details the observed behaviour for Specimen B0nc.

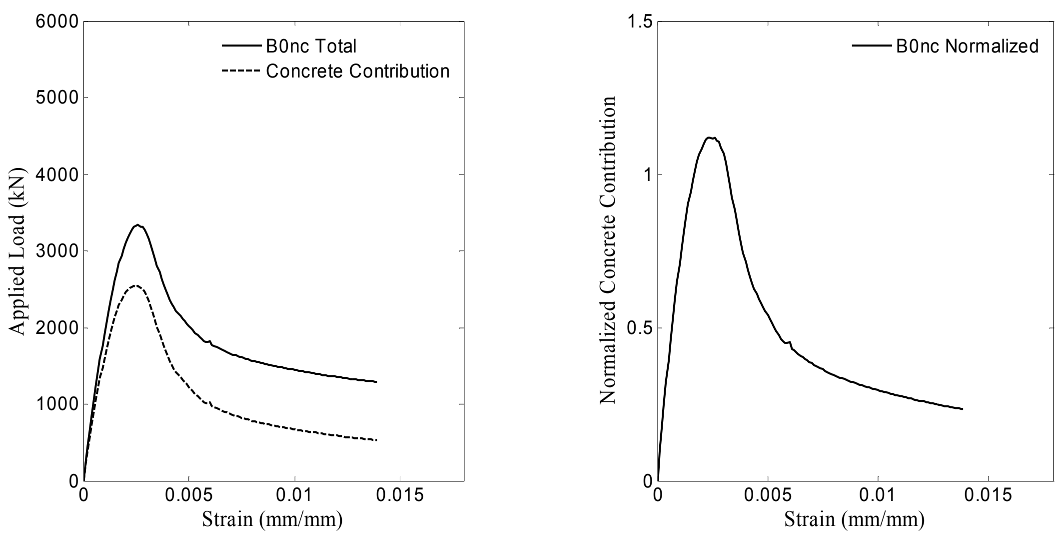

(a) Total applied load, P_{total}, versus strain and concrete load contribution, P_c, versus strain

(b) Normalized concrete contribution, $\frac{P_c}{P_{co}}$, versus strain.

Figure 4.33: Experimental results for Specimen B0nc

	(a) - Just prior to the peak resistance a longitudinal splitting crack formed near the mid-height of the column.		(b) - When the peak load was reached, some horizontal splitting cracks initiated at the locations of transverse reinforcement at the mid-height of the column
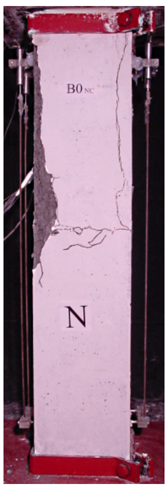	(c) - As loading increased, a splitting crack formed at the location of the corner longitudinal bars.		(d) - As further loading was applied, spalling of the minimum concrete cover began to occur at the locations of the transverse reinforcement and at the corners of the column. - In addition, the concrete in the ineffective core region between the transverse reinforcement began to crush and disintegrate.
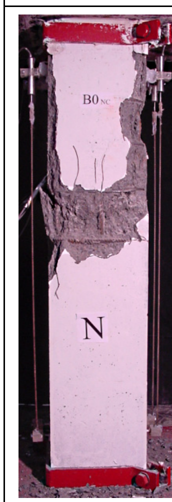	(e) - It was also apparent that buckling of the longitudinal bars was taking place. - The cracking mechanisms and the buckling of the vertical reinforcing bars occurred in a sudden manner.		(f) - Specimen B0nc at the end of the testing procedure

Figure 4.34: Major events for specimen B0nc

4.3.5 Response of Specimen B1nc

Specimen B1nc was detailed with the same amount of transverse reinforcement found in the other B-series specimens (s = 120 mm). In addition, this column contained steel fibres in the quantity of 1% by volume of concrete. Therefore, the details of this column were identical to those of Specimen B1 with the exception being that this specimen was constructed without cover.

The load-strain response of Specimen B1nc is given in Fig. 4.35(a). A peak load carrying capacity of 3437 kN was reached in this column. The descending branch of the load strain curve shows that the inclusion of fibres in this column resulted in some improvements in terms of post-peak ductility. The normalised concrete load contribution with respect to strain is shown in Fig. 4.35(b). Figure 4.36 details the observed behaviour for Specimen B1nc.

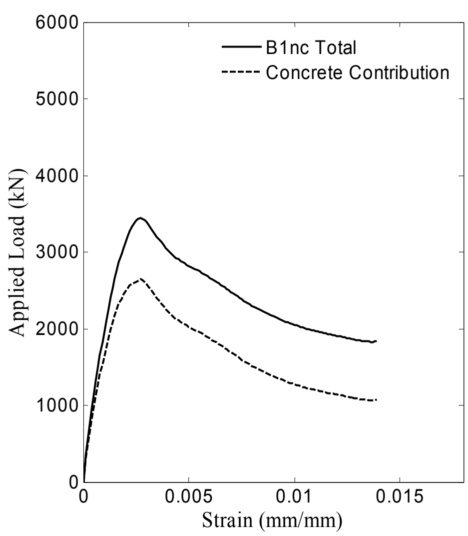

(a) Total applied load, P_{total}, versus strain and concrete load contribution, P_c, versus strain

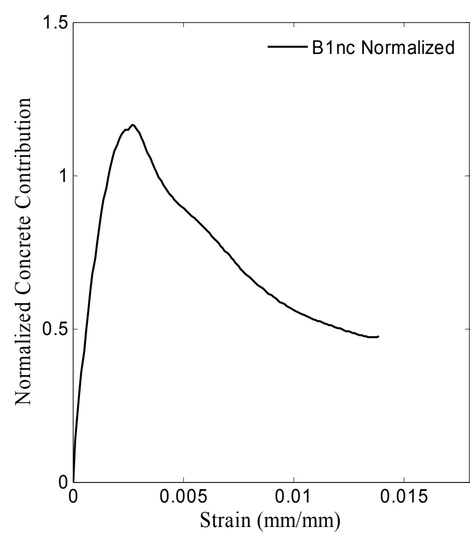

(b) Normalized concrete contribution, $\frac{P_c}{P_{co}}$, versus strain.

Figure 4.35: Experimental results for Specimen B1nc

<table>
<tr>
<td rowspan="2">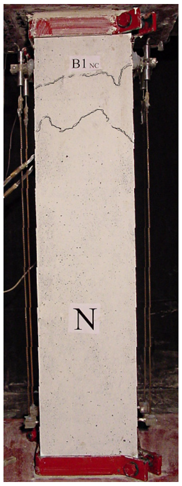
</td>
<td>(a)</td>
<td rowspan="2">
</td>
<td>(b)</td>
</tr>
<tr>
<td>- Just prior to the peak resistance splitting cracks had initiated in the upper region of the column at the location of the transverse reinforcement</td>
<td>- As the load carrying capacity began to drop, another splitting crack formed at the subsequent tie location. In addition, crushing began to occur</td>
</tr>
<tr>
<td rowspan="2">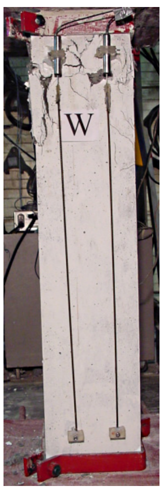
</td>
<td>(c)</td>
<td rowspan="2">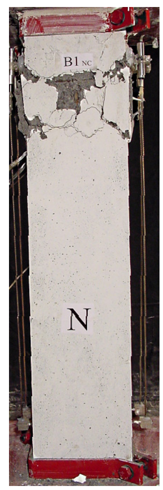
</td>
<td>(d)</td>
</tr>
<tr>
<td>- It was also apparent that buckling or the longitudinal bars was taking place due to the development of longitudinal splitting cracks in between the tie locations.</td>
<td>- The cracking mechanisms and the crushing of the ineffective core region occurred in a gradual yet sustained manner.</td>
</tr>
<tr>
<td rowspan="2">
</td>
<td>(e)</td>
<td rowspan="2">
</td>
<td>(f)</td>
</tr>
<tr>
<td>- As further loading was applied, spalling of the minimum concrete cover began to occur in between the tie locations.</td>
<td>- Specimen B1nc at the end of the testing procedure</td>
</tr>
</table>

Figure 4.36: Major events for Specimen B1nc

4.3.6 Response of Specimen B1.5nc

The details of this column were identical to those of Specimen B1.5 (s = 120 mm, v_f = 1.5%) with the exception being that this specimen was constructed without cover.

As shown in Fig. 4.37(a), the load-strain response of Specimen B1.5nc was well-controlled beyond its peak capacity of 3840 kN. The normalised concrete load contribution with respect to strain is shown in Fig. 4.37(b). Figure 4.38 details the observed behaviour for Specimen B1.5nc.

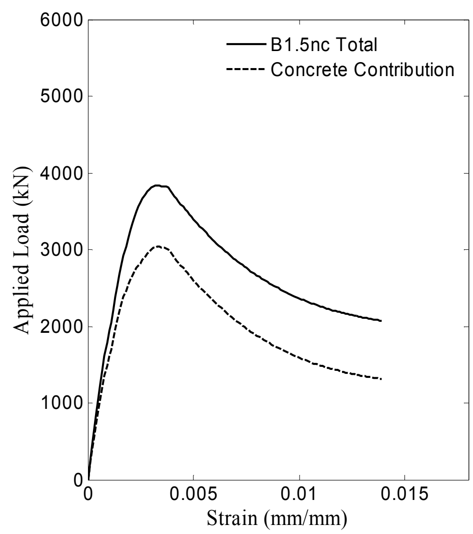

(a) Total applied load, P_{total}, versus strain and concrete load contribution, P_c, versus strain

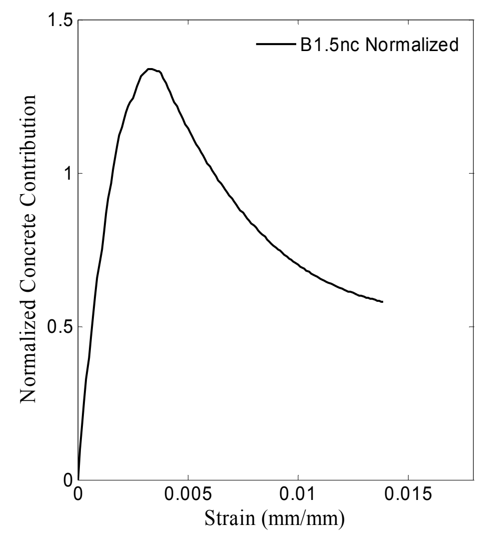

(b) Normalized concrete contribution, $\frac{P_c}{P_{co}}$, versus strain.

Figure 4.37: Experimental results for Specimen B1.5nc

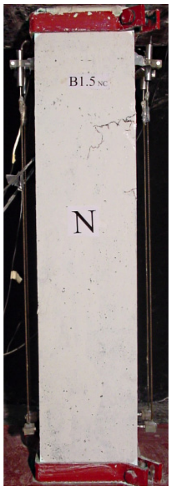	(a) - The first sign of distress occurred near the peak capacity of the column, with the development of a splitting crack in the upper region of the specimen at the location of the transverse reinforcement.		(b) - Furthermore some longitudinal splitting cracks began to form on the west face of the column.
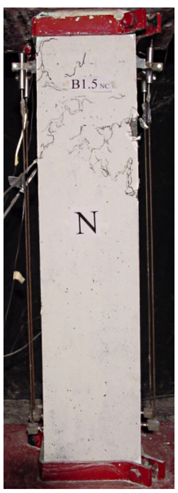	(c) - As the load carrying capacity began to drop, the crushing continued with the formation of a diffused crack pattern.		(d) - As the loading continued, spalling of the surface concrete at the location of the longitudinal reinforcement and at the location of the transverse reinforcement was observed.
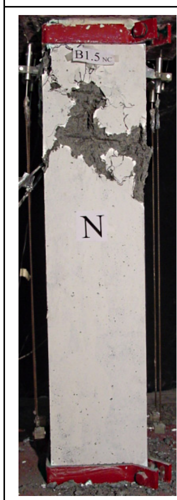	(e) - Furthermore, it was apparent that the buckling of the longitudinal bars was taking place. - Nevertheless, the cracking mechanisms and the crushing of the ineffective core region occurred in a gradual yet sustained manner.		(f) - The appearance of specimen B1.5nc at the end of the testing procedure

Figure 4.38: Major events for Specimen B1.5nc

4.3.7 Response of Specimen C0nc

Specimen C0nc was detailed in accordance with the confinement provisions of R_d = 4.0 of the CSA Standard resulting in a hoop spacing of 65 mm. In addition, this column contained no fibres. Therefore, the details of this column were identical to those of Specimen C0 with the exception being that this specimen was constructed without cover.

The load-strain response of Specimen C0nc is given in Fig. 4.39(a). A peak resistance of 3814 kN was reached in this column. After reaching the peak load, the load response curve stabilised with the column maintaining its maximum load even at very large deformations. Due to the close spacing between the ties this column displayed an excellent response. One can also note that no drop in capacity is observed due to the fact that no cover was provided in this specimen. The normalised concrete load contribution with respect to strain is shown in Fig. 4.39(b). Figure 4.40 details the observed behaviour for Specimen C0nc.

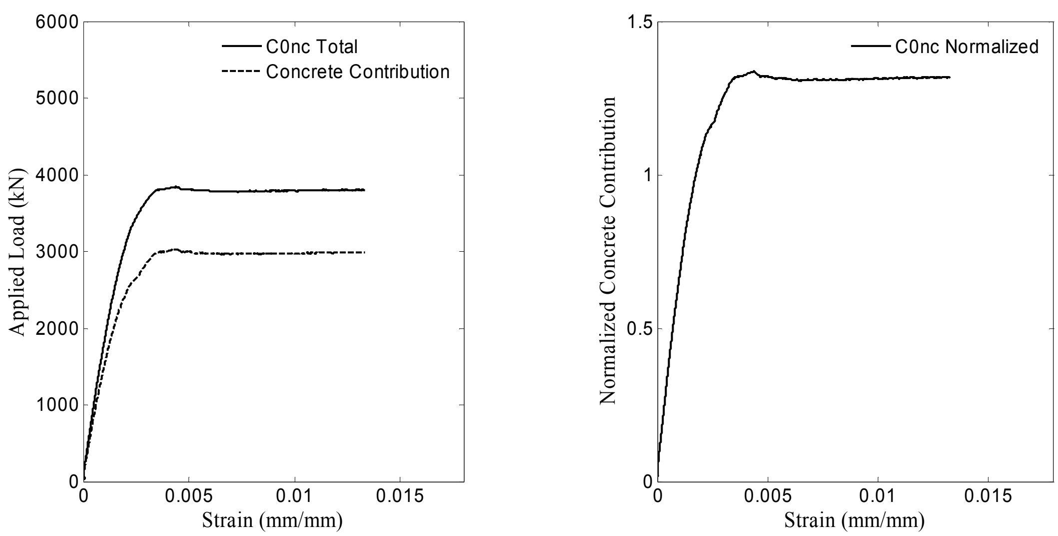

(a) Total applied load, P_{total}, versus strain and concrete load contribution, P_c, versus strain

(b) Normalized concrete contribution, $\frac{P_c}{P_{co}}$, versus strain.

Figure 4.39: Experimental results for Specimen C0nc

	(a) - Just prior to the peak resistance some splitting cracks had initiated at the location of the transverse reinforcement near the mid-height of the column.		(b) - In addition, extensive transverse splitting cracks began to form at the other tie locations throughout the column height.
	(c) - As further load was applied the minimum cover concrete across the column height began to spall.		(d) - The observed cracking and spalling patterns occurred at very sudden rate.
	(e) - It was observed that at even very large deformations the integrity of the core concrete region was maintained with little or no buckling of the reinforcement.		(f) - Specimen C0nc at the end of the testing procedure

Figure 4.40: Major events for Specimen C0nc

Chapter 5 Comparison of Responses of Column Specimens

5.1 Chapter Overview

This chapter compares the responses of the column specimens with the aim of developing a better understanding of the benefits associated with the use of steel fibres in RC columns.

Section 5.2 examines the influence of transverse reinforcement and the influence of fibres in improving the maximum load resistance of RC columns.

Section 5.3, compares the behaviour of the columns in each series to determine the influence of transverse reinforcement and the presence of fibres on the load carrying capacities and post-peak resistances.

Section 5.4, examines the ability of fibres in partially replacing conventional confinement reinforcement.

Sections 5.5 and 5.6 examine the effect of fibres on the core confinement and cover spalling.

5.2 Summary of Peak loads

Table 5-1 summarises the peak loads, P_{total}, that were reached by the various columns that were tested in the experimental program. Furthermore, the peak concrete contribution, P_c, and normalised concrete contribution, P_n (see Eq. 4-1), of each column is presented.

In general two observations can be made. Firstly, there is the direct correlation between the level of confinement reinforcement and the increase in peak capacity in the specimens constructed without fibres. Specimen A0 had very little confinement due to the large spacing in the transverse reinforcement and therefore, its peak normalized load is about equal to one. On the other end of the spectrum is Specimen C0, which was designed with the stringent requirements for ductile columns. As is expected, this specimen had the greatest improvement in peak resistance. Secondly, one can see the beneficial influence of the fibres in increasing peak axial capacity as is demonstrated in the normalised results of all 4 specimen configurations.

Table 5-1: Peak load carrying capacities of the various columns

Specimen	Peak Load P_{total} (kN)	Peak Concrete Contribution P_c (kN)	Normalised Concrete Contribution P_n
Specimens constructed with full-cover			
A0	***4510***	***3701***	***0.977***
A1	4471	3671	1.118
A15	5783	5008	1.347
B0	***4762***	***3957***	***1.064***
B1	4461	3655	1.110
B15	5891	5095	1.370
C0	***5044***	***4288***	***1.137***
C1	4650	3827	1.166
C15	6209	5394	1.447
D0	***4526***	***3743***	***1.136***
D15	5215	4391	1.334
Specimens constructed without cover			
A0nc	***3253***	***2489***	***1.090***
A1nc	3420	2670	1.170
A15nc	3763	2986	1.318
B0nc	***3319***	***2531***	***1.117***
B1nc	3437	2631	1.165
B15nc	3839	3034	1.339
C0nc	***3814***	***2992***	***1.323***

5.3 Comparative Analysis of Each Test Series

5.3.1 Specimens A0, B0, C0

Specimens A0 (R_d of 1.5, s = 240 mm), B0 (R_d of 2.5, s = 120 mm) and C0 (R_d of 4.0, s = 65 mm) were detailed with a wide range of confinement provisions for different levels of ductility in the CSA Standard. Furthermore, these four columns contained no fibres. Hence, a comparison of the results of these columns allows for an investigation into the effect of confinement in the form of transverse reinforcement on the response of columns in compression. A comparison of the load versus average axial strain responses for the three columns is shown in Fig. 5.1(a).

Specimen A0 had very little confinement due to the large spacing of the transverse reinforcement and therefore this column showed a sudden loss in load carrying capacity after the peak resistance was reached. Due to the intermediate spacing between the ties in Specimen B0, this column showed an improved post-peak response when compared to Specimen A0. As expected, Specimen C0, which contained the largest amount of confinement reinforcement, exhibited the most ductile behaviour. Due to the close spacing between the ties and the improved detailing of the transverse reinforcement in the cross-section, this column displayed an exceptionally well controlled response. These results clearly show that an increase in column confinement, in the form of well detailed and closely spaced transverse reinforcement, results in a more ductile and controlled post-peak behaviour.

5.3.2 A-series Specimens

The A-series specimens were detailed in accordance with the basic confinement provisions of the CSA Standard (R_d = 1.5) resulting in a tie spacing, s, of 240 mm. The various columns contained a varying amount of fibre reinforcement, and therefore a comparison of the results allows for an investigation into the performance and ductility enhancements that can be gained from the use of steel-fibre reinforced concrete. A comparison of the normalized concrete stress-strain responses for the four columns is shown in Fig. 5.1(b).

Specimen A1.5 was detailed with the same amount of transverse reinforcement contained in Specimen A0. However, this column contained steel fibres in the quantity of 1.5% by volume of concrete. As seen in Fig. 5.1(b), a significant increase in the peak load was observed for this fibre-reinforced specimen. In addition, this column showed a greatly improved post-peak response. This performance enhancement can be attributed to the role of the fibres in improving the confinement of the column and the influence of the fibres in delaying cover spalling. Similar conclusions can be made upon examining the response of Specimen A1 which had a fibre content of 1%.

It is also noted that the response of Specimen A2, which contained 2% fibres by volume, was not better than the response of the specimen constructed with a fibre content of 1.5% (as seen in Fig. 5.1(b)). This reduced fibre efficiency may have been the result of segregation during the needed vibration for this column and due to "clumping" of the fibres.

5.3.3 B-series Specimens

All the columns in this series had an intermediate amount of confinement reinforcement (R_d of 2.5; s = 120 mm). The various columns contained varying amounts of fibre reinforcement ranging from 0% to 2% fibres by volume. A comparison of the normalized concrete stress-strain responses for the four columns is shown in Fig. 5.1(c).

The tests conducted on the B-series specimens once again demonstrate that the addition of fibres greatly improves the performance of the columns when compared to the specimen without fibres. An increase in peak resistance was observed in the fibre reinforced specimens (see Specimens B1 and B1.5).Furthermore, the columns containing fibres demonstrated improved post-peak ductility, with the ability to maintain a higher post-peak load capacity with increasing strain when compared to Specimen B0. Once again, these enhancements in performance could be attributed to the influence of the fibres in improving the confinement of the column sections and the ability of the fibres to delay cover spalling.

Finally it is also noted that the response of Specimen B2, which had a fibre content of 2% had a lower peak load compared to specimen containing 1.5% fibres. This result again points to the possible reduction in fibre efficiency at this higher fibre content.

5.3.4 C-series Specimens

Specimens C0, C1, and C1.5 were detailed in accordance with the more stringent confinement provisions of the CSA Standard (R_d of 4.0, s = 65 mm). The various columns contained a varying amount of fibre reinforcement ranging from 0% to 1.5%.

A comparison of the normalized concrete stress-strain responses for the three columns is shown in Fig. 5.1(d). In terms of peak load capacity, an increase in the peak resistance was observed in Specimen C1.5. This improvement was not as significant in Specimen C1.

In terms, of post-peak behaviour, Specimen C0, had an exceptionally well controlled response with the only drop in capacity occurring during cover spalling. This can be attributed to the close spacing between the ties and the improved detailing of the transverse reinforcement in the column cross-section. The columns containing fibres displayed remarkably well-controlled post-peak behaviour. The observed enhancements in performance could be attributed to the influence of the fibres in delaying and minimizing the effects of cover spalling.

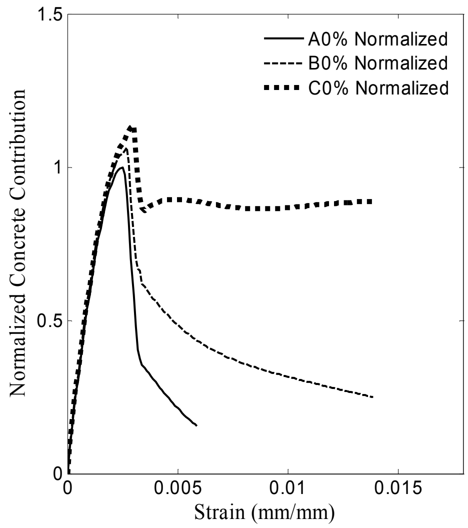

(a) Specimens A0, B0, C0

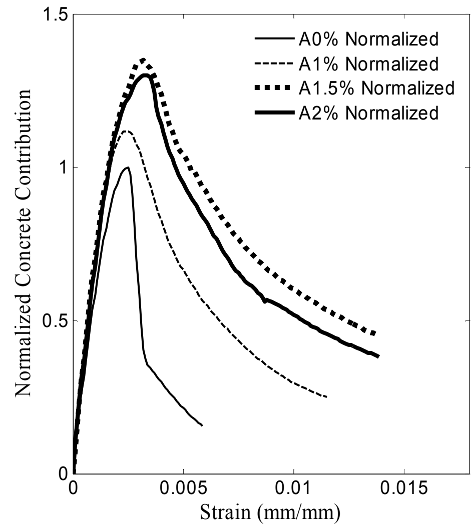

(b) A-series Specimens

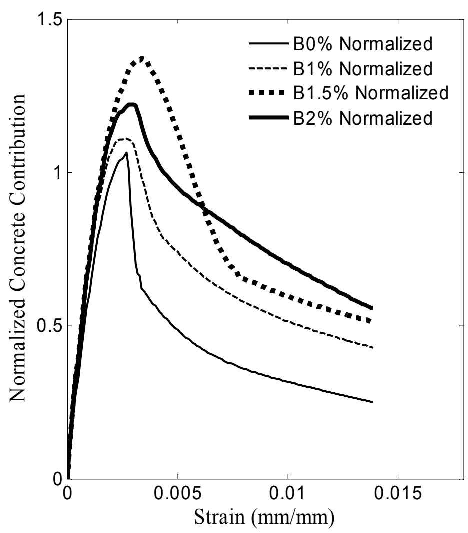

(c) B-series Specimens

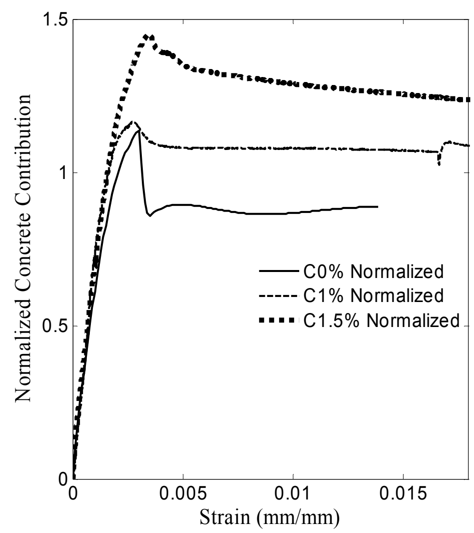

(d) C-series Specimens

Figure 5.1: Comparison of the Normalised load- strain responses for the specimens in the various series

5.4 The Ability of Fibres to Partially Substitute for the Transverse Reinforcement

5.4.1 Specimens A1.5, A1 vs. Specimen B0

A comparison of the experimental results of Specimens A1.5 and B0 is shown in Fig. 5.2(a). It is noted that Specimen B0 had a two-fold increase in the amount of transverse reinforcement when compared to the A-series columns. This response comparison demonstrates that the addition of steel fibres in a column with minimum confinement reinforcement results in a column that has a level of performance that surpasses that of Specimen B0. In addition, Specimen A1, which contained 1% fibres by volume showed a response that matched that of Specimen B0.

5.4.2 Specimens A1.5, A1 vs. Specimen D0

A comparison of the experimental results of Specimens A1.5 and D0 is shown in Fig. 5.2(b). Specimen D0 had a three-fold increase in the amount of transverse reinforcement when compared to Specimen A1.5. The response of Specimen A1.5 shows that this column was able to dissipate an amount of energy that was comparable to that of the specimen containing three times the amount of transverse reinforcement.

5.4.3 Specimens B1.5, B1 vs. Specimen D0

A comparison of the experimental results of Specimens B1.5 and D0 (Fig. 5.2(c)) demonstrates that the addition of fibres to a column detailed in accordance with the provisions of Rd = 2.5 (s =120 mm) results in a column that has an enhanced performance when compared to a column that has no fibres but contains 1.5 times the amount of transverse reinforcement. Specimen B1, which contained 1% fibres by volume, also showed a response that was improved when compared to that of Specimen D0.

5.4.4 Specimen D1.5 vs. Specimen C0

A comparison of the experimental results of Specimen D1.5 and C0 is shown in Fig. 5.2(d). Specimen D1.5 had a tie spacing of 80 mm. This column was able to maintain a higher load capacity than that of Specimen C0 (R_d = 4.0) up-to a strain of 0.01 (after which its capacity dropped below that of Specimen C0 which continued to maintain its strength even at very high strains).

5.4.5 Summary

In brief, these results demonstrate that the addition of an adequate quantity of fibres can substitute for some of the transverse reinforcement in RC columns. This reduction in traditional confinement reinforcement can potentially result in savings in combined material and labour costs during construction.

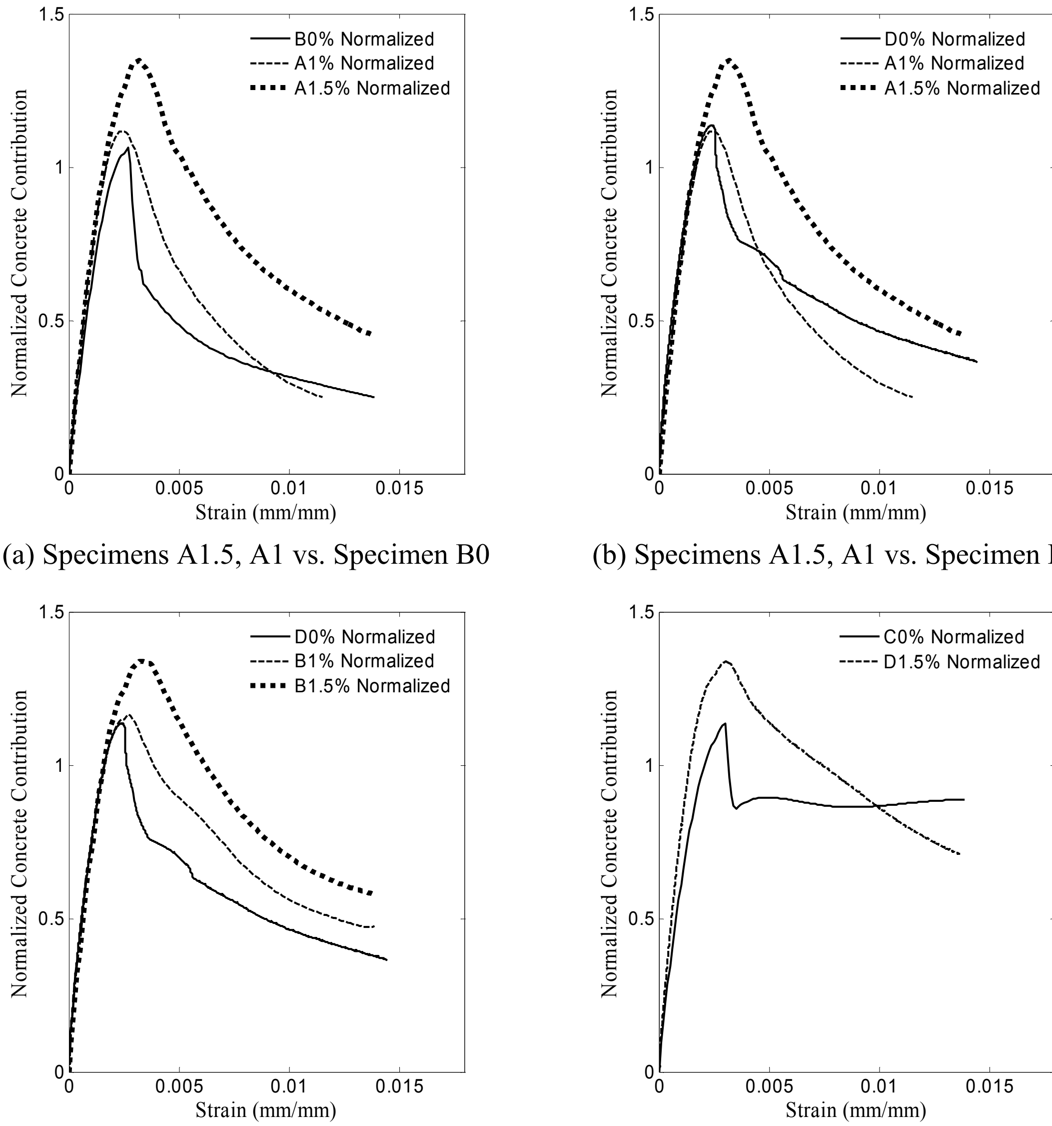

(a) Specimens A1.5, A1 vs. Specimen B0

(b) Specimens A1.5, A1 vs. Specimen D0

(c) Specimens B1.5, B1 vs. Specimen D0

(d) Specimen D1.5 vs. Specimen C0

Figure 5.2: Normalised load- strain responses showing the ability of fibres to substitute for some of the transverse reinforcement in RC columns

5.5 Influence of Fibres on Core Confinement

The results from the specimens constructed without cover demonstrate that fibres can improve the confinement of the concrete within the core region of columns. Figure 5.3 shows a comparison of the results for the columns in the A-nc and B-nc series. In general, one can see that the influence of the fibres is seen in two aspects. Firstly, there is the improvement in peak load capacity and peak strain. This influence is more pronounced for the columns containing 1.5% volume of fibres, and is less dramatic for the columns with 1% fibres by volume. Secondly, and more importantly, there is the influence on the post-peak response. Both the specimens containing 1.5% and 1% fibres by volume demonstrated a significantly improved post-peak behaviour when compared to the specimens without fibres, indicating the ability of the fibres to enhance the confinement properties within the core area of these columns.

These results demonstrate that the influence of the fibres is not only to delay cover spalling but also to improve the overall confinement of the core.

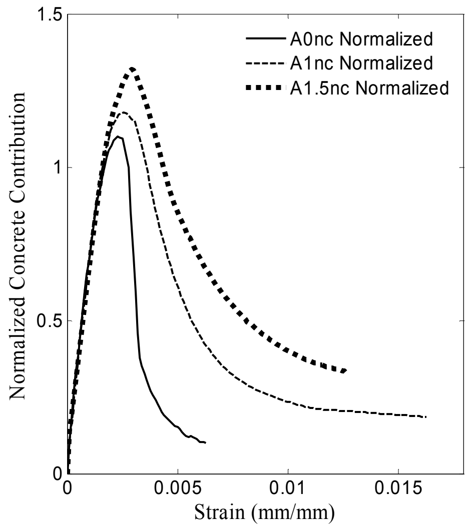

(a) Specimens A0nc, A1nc and A1.5nc

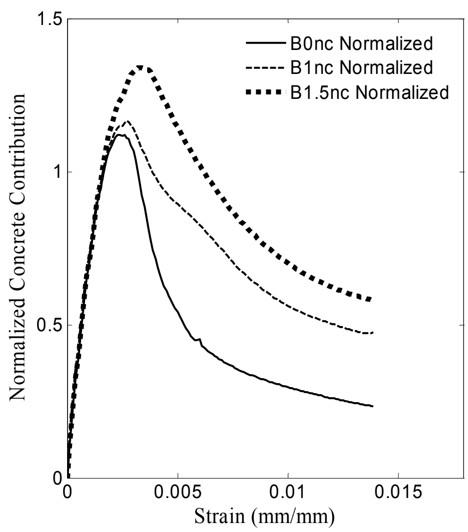

(b) Specimens B0nc, B1nc and B1.5nc

Figure 5.3: Influence of the fibres on the response of the specimens constructed without cover

5.6 Influence of Fibres on Cover Spalling and Bar Buckling

The specimens containing steel fibre reinforcement demonstrated an ability to significantly delay cover spalling from the core concrete section. In all of the SFRC specimens that were tested, the cover remained intact well beyond the peak load. In fact it was observed that the mechanism of sudden cover spalling was all but eliminated. This is due to the ability of the fibres to limit the progression of cracks in the concrete, thereby resulting in greater material integrity at large strains. However, observations made during testing demonstrated that although the cover did not spall, the longitudinal bars buckled and hence pushed against large pieces of SFRC that were still carrying load but were partially detached from the core. This "detachment" was observed to occur more rapidly in the specimens with a larger spacing of transverse reinforcement (such as the A–series specimens), pointing to the possible influence of buckling in this "detachment" process.

The normalized cover contribution, $\frac{P_{c,cover}}{P_{co}}$, was computed by subtracting the core load-strain response of the "nc"-specimens (without cover) from the corresponding specimens with cover using Eq. 5-1:

$$\left(\frac{P_{c,\mathrm{cov}er}}{P_{co}}\right)=\frac{P_c - P_{c,nc}}{0.85\times f'_c\times A_{net}} \qquad \text{5-1}$$

Where $P_{c,nc}$ represents the load carried in the specimen constructed without cover and P_c represents the load carried in the companion specimen that had cover. The quantity A_{net} represents the net cross-sectional area of the full-cover specimen (i.e., 300 x 300 mm).

The normalized cover responses for the various specimens are shown in Fig. 5.4 and 5.5. It can be seen that after the addition of fibres, the cover carries significant load and partially participates in the confinement of the core.

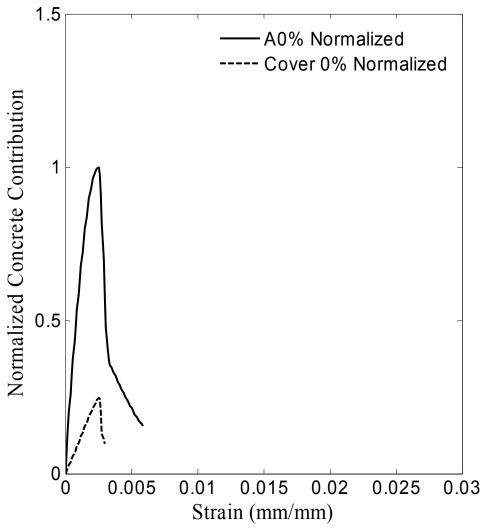

(a) Cover contribution in Specimen A0

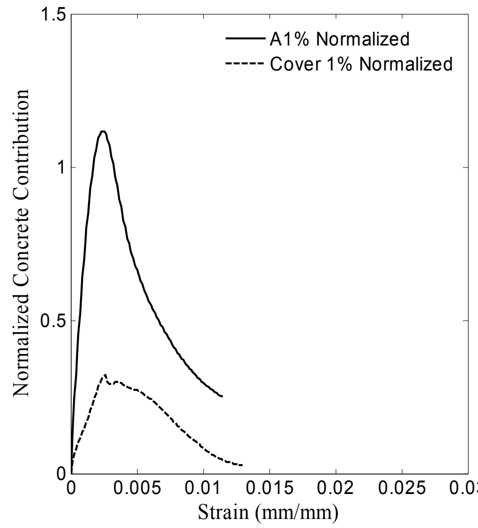

(b) Cover contribution in Specimen A1

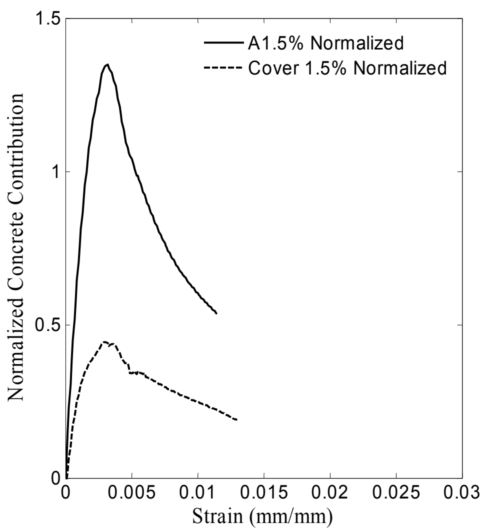

(c) Cover contribution in Specimen A1.5

Figure 5.4: Normalised cover contribution for the A-series specimens

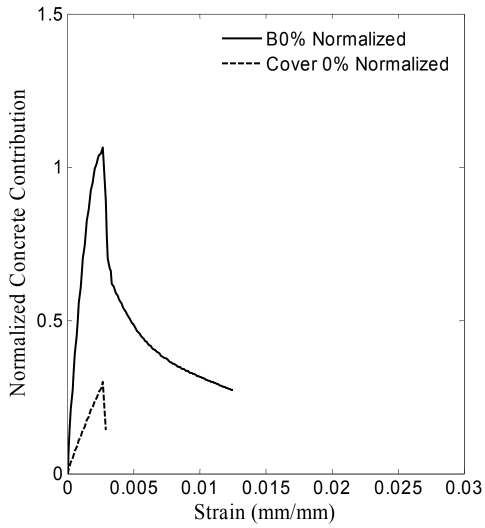

(a) Cover contribution in Specimen B0

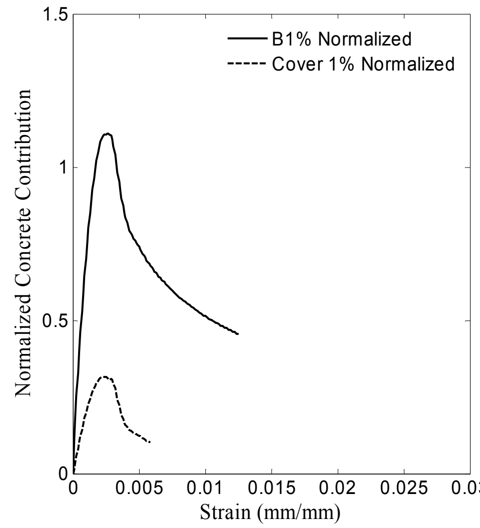

(b) Cover contribution in Specimen B1

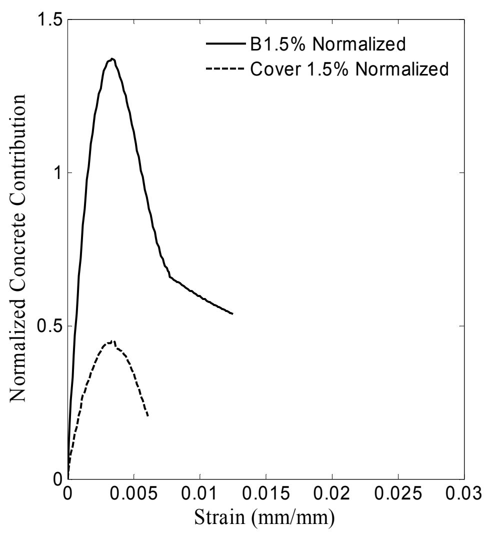

(c) Cover contribution in Specimen B1.5

Figure 5.5: Normalised cover contribution for the B-series specimens

Chapter 6 Modelling the Influence of Fibres in Columns Containing SFRC

6.1 Chapter Overview

In this chapter a model for the prediction of the response of RC and SFRC columns is presented. Section 6.2 presents a method for the prediction of the response of traditional RC columns based on several available models in the literature. In Section 6.3 a model is presented for the material response of SFRC in compression. In Section 6.4 the model presented for traditional RC columns is modified so as to account for the beneficial influence of steel fibres.

6.2 Response Predictions of RC Columns

As was detailed in the literature review portion of this thesis, there are numerous models available in the literature that can accurately predict the complete stress-stress curve of reinforced concrete columns under axial loading. For the purpose of this study, the model presented by Légeron and Paultre (2003) for the behaviour of confined and unconfined concrete will be implemented. In addition, the model presented by Bae et al. (2005) is used in order to take into account the buckling of the longitudinal reinforcement. The various aspects of the prediction models are detailed further in Sections 6.2.1 to 6.2.3. The results of the application of the model are presented in Section 6.2.4.

6.2.1 Confined concrete

Sheik and Uzumeri (1980), suggested that concrete specimens that are confined by passive rectangular tie reinforcement are confined by a pressure that is not uniformly applied throughout the volume of the concrete core. Rather, they suggested that at high strains, when cover spalling occurs, part of the core region also becomes ineffective in confining the core concrete. Hence they proposed a model, in which the enhanced behaviour of rectangular columns confined by rectangular ties is related to an "effectively confined" core area. This area is smaller than the actual core area and is determined using the tie configuration in the section and the tie spacing, based on arching action in the concrete section. The enhancements in strength and ductility are then calculated based on this "effectively confined area". The remaining region in the core is considered ineffective in confining the core. Park et al. (1982) developed a model which accounted for the confinement effects. The model presented by Légeron and Paultre (2003) builds upon this concept to predict the complete stress-strain curves of reinforced concrete columns under axial loading for a wide range of concrete strengths, transverse steel tie configurations and yield strengths. In accordance with the work of previous authors, the confinement provided by the ties is assumed to occur in an "effectively confined" core region. The region is calculated using the arching action concept, and is computed using a confinement effectiveness coefficient, K_e , which is a function of the tie configuration and tie spacing. The coefficient represents the ratio of the smallest effectively confined concrete area, halfway between two layers of transverse ties, to the total concrete core area.

For the purpose of this study, the relationships suggested by Légeron and Paultre in Eq. 2-23 to 2-38 will be used in order to compute the stress-strain contribution of the confined concrete in the core region of the columns. The details regarding the model parameters can be found in Section 2.4.1.5 of the literature review.

6.2.2 Unconfined concrete

In order to evaluate the stress-strain curve of unconfined concrete (which will be used for the cover region of the columns), the relationships in Eq. 2-34 to 2-38 are used, with the exception that the confined parameters are replaced by the unconfined parameters ($f'_{cu}, \varepsilon'_{cu}, \varepsilon'_{c50u}$).

However the model is modified slightly for the cover region so as to take into account the effect of sudden cover spalling. Thus, the following restrictions apply:

- At an unconfined concrete strain of 0.003, the stress suddenly drops to a value equal to 40% of the peak concrete stress.
- At a strain of 0.004, the stress reaches 0.

- For the strain values that are intermediate between 0.003 and 0.004, a straight-line segment is used to reduce the stress in the concrete.

A schematic representation of the modified and original models is shown in Fig. 6.1.

6.2.3 Buckling of the longitudinal bars

The model described by Bae et al. (2005) is used in order to take into account the buckling of the longitudinal reinforcement. The details of the model can be found in Section 2.4.3 of the literature review.

This model was used to estimate the effect of tie-spacing on the behaviour of the stress-strain and buckling behaviour of longitudinal reinforcement in the columns that were tested in the experimental program. The results of this analysis are shown in Fig. 6.2. Recall that in the present study tie-spacings of 240 mm (A-series typical), 120 mm (B-series typical) and 65 mm (C-series typical) were used. For the applicable strain ranges, it can be seen that buckling has little or no influence on reducing the load-carrying capacity of the bars with a tie-spacing of 65 mm. However, there is a certain instability observed in the case of the bars with a tie-spacing of 240 mm.

6.2.4 Application of the models to predict the response of the tested columns

Using the aforementioned models, the complete load-strain responses of the columns that were constructed without fibres were computed. The results for columns A0, B0 and C0 are shown in Fig. 6.3. One can see that there is excellent agreement between the results that were obtained experimentally and those computed using the analytical models.

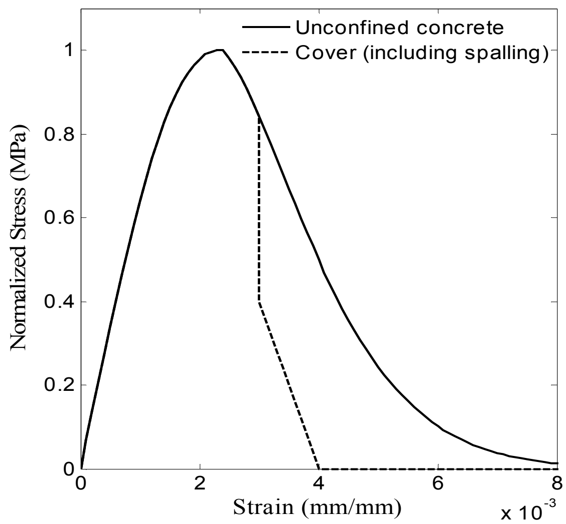

Figure 6.1: Typical stress-strain curve for unconfined concrete and the modified curve that takes into account cover spalling

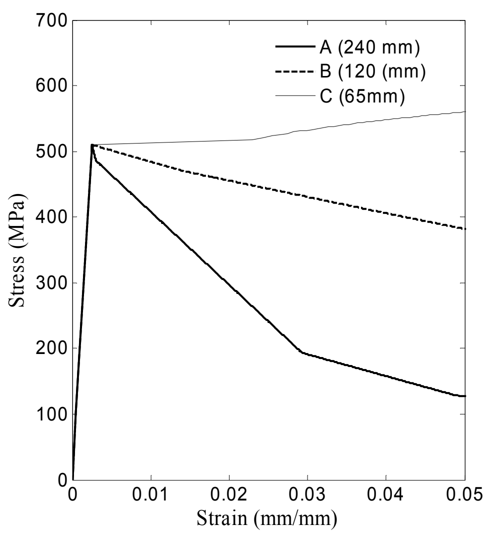

Figure 6.2: Stress-strain curves of the longitudinal reinforcing bars taking into account the effects of buckling

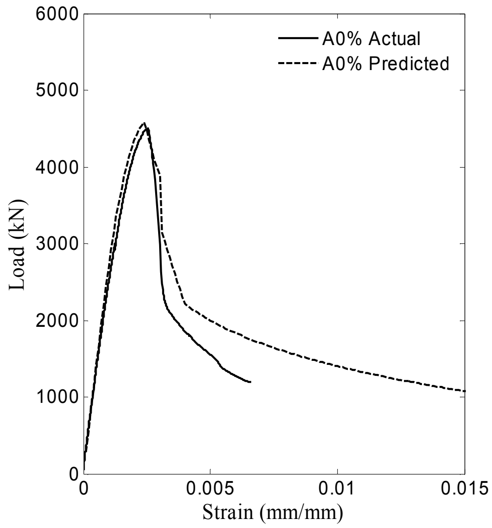

(a) Column A0%

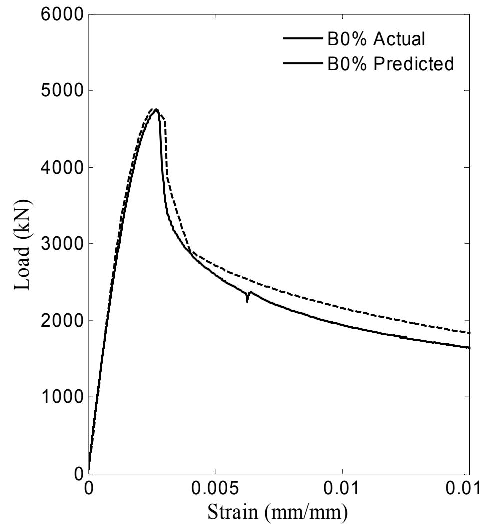

(b) Column B0%

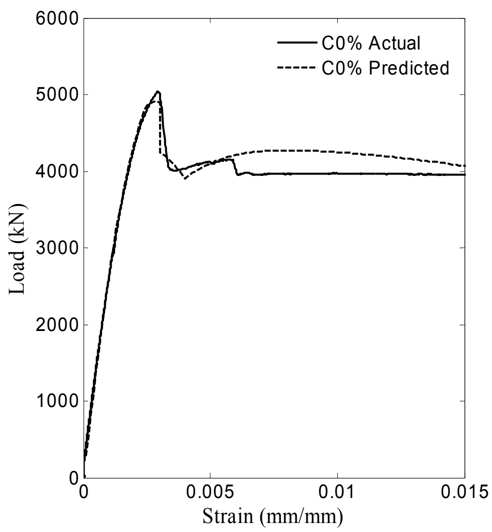

(c) Column C0%

Figure 6.3: Actual and predicted load-strain curves for the various columns

6.3 Model for the Material Stress-Strain Curve of SFRC

In order to model the beneficial effects of using steel fibres in RC columns, it is essential to develop a model for the material stress-strain curve of SFRC in compression.

In order to capture the compressive response of SFRC, a model is derived based on the experimental results from the cylinder tests.

Upon examining the results from the cylinder specimens, it was found that the effect of fibres was not seen in the ascending branch of the stress-strain curve. Thus, the previously described model for the compressive response of unconfined concrete is used until the point of peak strain. Consequently, the relationships defined in Eq. 2-34 and 2-35 are used for this purpose.

In order to model the influence of the fibres in the descending portion of the stress-strain curve, the model proposed by Mansur et al. (1999) for high-strength SFRC is modified herein. Mansur et al. suggested using Eq. 6-1 to model this post-peak effect for SFRC.

$$f_{cf} = f_c' \left[\frac{k_{f1}\beta_1 \left(\frac{\varepsilon_{cf}}{\varepsilon_{cu}'} \right)}{k_{f1}\beta_1 - 1 + \left(\frac{\varepsilon_{cf}}{\varepsilon_{cu}'} \right)^{k_{f2}\beta_1}} \right] \quad \varepsilon_{cf} \geq \varepsilon'_{cu} \qquad 6\text{-}1$$

The factors k_{f1} and k_{f2} are calculated using Eq. 6-2 and 6-3 and are based on the work of Mansur et al. In order to use this relationship, the required constants were derived based on the results from this experimental program and are presented in Table 6-1.

$$k_{f1} = \left(\frac{C_a}{f_c'} \right)^{e_a} \times \left(1 + X_a \times \frac{v_f L_f}{d_f} \right)^{e_{2a}} \qquad 6\text{-}2$$

$$k_{f2} = \left(\frac{C_a}{f_c'} \right)^{e_b} \times \left(1 + X_b \times \frac{v_f L_f}{d_f} \right)^{e_{2b}} \qquad 6\text{-}3$$

Table 6-1: Constants to be used in Eq. 6-2 and 6-3

Constants	For $\varepsilon_{cf} \leq 0.004$	For $\varepsilon_{cf} > 0.004$
C_a	30.2	4.62
e_a	0.49	0.47
X_a	-0.22	-7.8 x 10^{-5}
e_{2a}	24.9	-6.4
e_b	0.52	0.51
X_a	0.11	0.83
e_{2b}	-1.09	-0.34

Figure 6.4(a) shows the resulting stress-strain curves using the model for a concrete with a nominal cylinder compressive strength of 49 MPa. Figures 6.4(b) to 6.4(d) compare the normalized results from the model with those from the actual material stress strain curves. One can see that there is good agreement between the results (note that the experimental curve for v_f = 0.5% is taken from the results of the tensile series experimental program which is presented in Chapter 7).

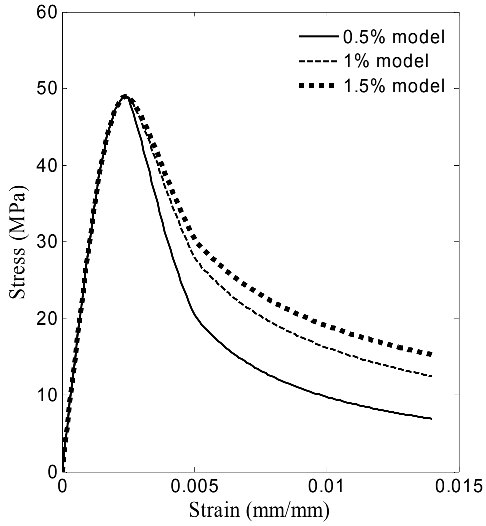

(a) Stress-strain curves computed using the SFRC model

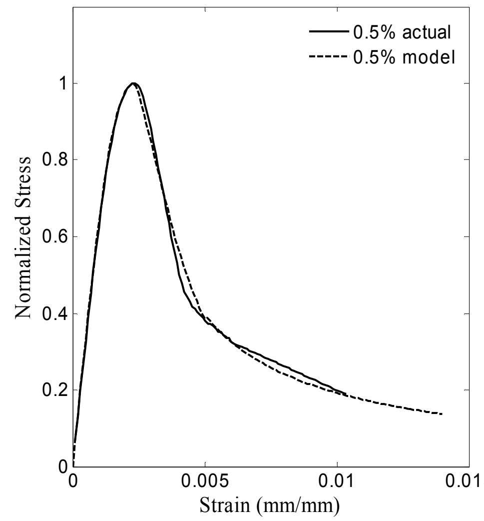

(d) Normalised stress-strain curves from the model and experiments for $v_f = 0.5\%$

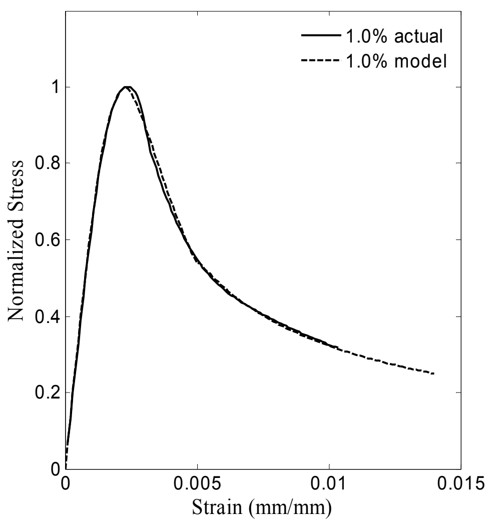

(c) Normalised stress-strain curves from the model and experiments for $v_f = 1.0\%$

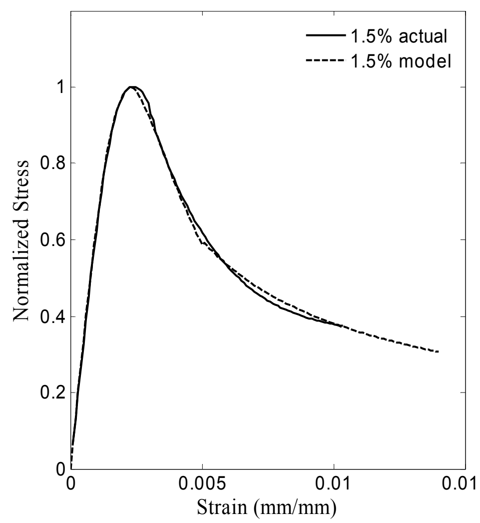

(d) Normalised stress-strain curves from the model and experiments for $v_f = 1.5\%$

Figure 6.4: Cylinder stress-strain curves computed using the SFRC material model

6.4 Response Predictions of SFRC Columns

Based upon observations made during the experimental program it was seen that the addition of fibres greatly enhanced the performance of the columns. This section presents a model to account for the positive influence of the fibres in enhancing the response of RC columns. The model will take the previously described model for the specimens without fibres (as presented in Section 6.2) and will modify this model so as to include the influence of the fibres.

From the results of the experiments it was observed that the positive contribution of the fibres can be described by 2 factors; an increase in peak load carrying capacity and a significant improvement in the post-peak response. These two aspects are taken into account in the present model and are discussed further in Sections 6.4.1 and 6.4.2 to 6.4.4 respectively.

6.4.1 Peak load effect

After examining the behaviour of the RC columns containing steel fibres it is evident that the fibres increased the peak load carrying capacity of the tested specimens when compared to the companion specimens that were constructed without fibres. This finding was in accordance with experimental results that have been presented by several other authors (Massicotte et al., 1998, Ramesh et al., 2003, Ganesan and Ramana Murthy, 1990). However, an increase in peak stress was not seen in the cylinder test stress-strain curves. The result observed in this experimental program may be due to the fact that the cylinders that were tested were relatively small (100 x 200mm) and hence few fibres would have been oriented in the direction perpendicular to the cylinder axis. Hence this effect will be modeled separately using an empirical formula.

It has long been known that the presence of lateral confinement in concrete increases the maximum compressive strength. Early research by Richart et al. (1928) demonstrated that the strength of concrete is enhanced if the concrete section is confined by an active hydrostatic pressure. Furthermore Richart et al. (1929) found that concrete that is provided with passive confinement pressure (in the form of spirals) results in a response that is similar to the case in which active fluid pressure is provided. Richart derived a simple relationship to show that the maximum confined concrete strength (f'_{cc}), can be approximated with:

$$f'_{cc} = f'_{cu} + k \times f'_{l} \qquad 6\text{-}4$$

Where k is equal to 4.1, f'_{l} is the lateral confining pressure, and f'_{cu} is the unconfined concrete strength.

The observed increase in the peak capacity of the full-scale RC columns containing steel fibres can be related to the additional confinement effect that is provided in the concrete due to the inclusion of the fibres. This can be the result of the benefits seen in the concrete core and cover (Campione, 2002).

The effective number of fibres per unit area, N_{fibres}, can be calculated using Eq. 6-5 for fibres randomly oriented in three dimensions (Hannant, 1978, Lee, 1990):

$$N_{fibres} = \frac{v_f}{A_f} \times \alpha \times \eta_l \qquad 6\text{-}5$$

A_f is the cross-sectional area of the fibre. The orientation factor, α, accounts for the random orientation of the fibres. The length factor, η_l, is used to account for the variability in fibre embedment length (η_l= 0.5, if one takes the effective embedment length as $L_f / 4$).

The confining pressure provided by the fibres can be taken as the number of fibres per unit area (N_{fibres}) times the average pullout force per fibre. Using this same approach, Foster (2001) suggested that the confining pressure that is provided by the steel fibres in RC columns can be approximated using Eq. 6-6:

$$f_f = \alpha \times \left(\frac{v_f L_f}{d} \right) \times \left[0.6 \times (f'_{cu})^{2/3} \right] \qquad 6\text{-}6$$

The length, L_f, that is used in the equation is taken as the length of the fibre without the hooks in the case of hooked-end steel fibres, and assumes a constant bond shear strength along the length of the fibre.

Foster, suggested using a value of 3/8 for the orientation factor (see Fig. 6.5). To arrive at this value, Foster took only the fibres that are oriented from $\theta = 30^{o}$ to 90^{o} to the cracking plane as being effective based on data published by Maage (1977) as well as Banthia and Trottier (1995) that suggested that fibres oriented between $\theta = 0^{o}$ and 30^{o} have a reduced pullout efficiency. Numerous other authors have suggested using a value of 0.5 for this quantity (Hannant, 1978, Dupont, 2003) by taking all fibres between 0^{o} and 90^{o} to be effective. Herein a value that is in the range of 3/8 and 0.5 will be used.

Rossi (1998) suggested that there is a certain critical range of fibre quantities which results in the efficiency of the fibres in improving resistance to be most optimal. Figure 6.6 shows a schematic representation of this effect. The quantity P_e represents a volume percentage beyond which the efficiency of the fibres is improved due to a positive group effect contribution.

Figure 6.7 was developed in order to provide a schematic idealization of the influence of fibre volume for uniform tensile stress. The first scenario is the case of low fibre content. If fibres are sufficiently spread apart from each other (see Fig. 6.7(a)), they act independently of one another. Hence due to larger crack widths across the crack, the less favourably inclined fibres can be assumed to be ineffective as they are acting independently of the other fibres and are not able to contribute. This situation would correspond to a fibre volume that is smaller than P_e.

However as the spacing between the fibres is reduced this causes the efficiency of the fibres to increase due to the group effect of the fibres that are interacting with each other. As the fibre volume increases, the crack widths are now better controlled allowing the less well inclined fibres to develop their pullout strength and participate towards the overall fibre contribution in the composite (see Fig. 6.7(b)). Hence as one increases the volume of fibres beyond P_e the efficiency on a per fibre basis should also improve.

However, after a certain volume percentage one reaches the value P_{fm}. After this point, increasing the number of fibres in the matrix is no longer beneficial due to the group effect which is now "negative" and hinders the efficiency of the fibres. This negative effect arises due to clumping and segregation at this fibre volume (see Fig. 6.7(c)).Hence by increasing the fibre content beyond this value, one will only see a slight increase in the resistance of the matrix at best, and even a decrease in the mechanical properties of the matrix in a worst case scenario.

This is in agreement with the results of this experimental program. In examining the behaviour of the columns that contained a fibre content of v_f =1% and v_f =1.5 %, it was found that the fibres were somewhat more efficient in increasing the peak resistance of the columns when a fibre content of 1.5% was used. Furthermore, it was found that after a certain fibre content, the efficiency of the fibres ceased to improve (as is evident from the results of the specimens containing a fibre dosage of v_f = 2%).

This concept will be utilized to modify the equation suggested by Foster. In this present study an effective orientation factor, α_{eff} will be used, where α_{eff} takes into account the improvement in the efficiency due to the positive group effect.

A schematic representation of the variation of α_{eff} is shown in Fig. 6.8. One can see that α_{eff} is taken to be in the range of 3/8 to 0.5. That is, at lower fibre contents, the interaction of the fibres would be minimal hence the factor suggested by Foster of 3/8 can be used, with the fibres that are less well inclined to the cracking plane being neglected. However, as the fibre content is increased to the optimal fibre volume, the efficiency on a per fibre basis should increase due to the increased effectiveness of these inclined fibres which are now contributing to the overall effectiveness of the matrix. For the type of concrete and fibre that is used in this experimental program the value of P_e is chosen to be 1%, whilst the value of P_{fm} is taken to be 1.5%.

Hence, the confining pressure, f_{fib}, that is provided by the fibres is now calculated using Eq. 6-7:

$$f_{fib} = \alpha_{eff} \times \left(\frac{v_f L_f}{d_f} \right) \times \left[0.6 \times \left(f'_c \right)^{2/3} \right] \qquad 6\text{-}7$$

Recalling the equation proposed by Richart, a similar approach can be used to develop a formula that can approximate the expected increase in the peak concrete stress, Δf_{cf}, due to the addition of steel fibres. Equation 6-8 shows this expected increase in compressive strength due to the fibre effect.

$$\Delta f_{cf} = 4.1 \times \left(f_{fib} \right) \qquad 6\text{-}8$$

Hence by using Eq. 6-9 and 6-10 the improved compressive resistance of the unconfined concrete and confined concrete can be calculated and used in the model.

$$f'_{cu\,f} = f'_{cu} + \Delta f_{cf} \qquad 6\text{-}9$$

$$f'_{cc\,f} = f'_{cc} + \Delta f_{cf} \qquad 6\text{-}10$$

6.4.2 Taking into account the post-peak effect

The more important fibre contribution is in the post-peak response of the columns. This effect can be included using the material stress-strain model presented in Section 6.3. Recall that in Section 6.2, for the prediction of the response of non-fibre reinforced RC columns, the contribution of the core to confinement was limited using an “effectively confined core area”. Furthermore, the previous model limited the contribution of the cover due to the sudden cover spalling mechanism. It is postulated that the influence of the fibres in enhancing the post-peak resistance of the columns is due to the contribution of the fibres in these two regions.

6.4.3 Post-peak contribution in the core region

The core area of a column, can be separated into two distinct regions; A_{KE} and A_{ineff} (see Fig. 6.9). In the model for RC columns, the contribution of the core to confinement was limited to the “effectively confined core area” (A_{KE}) which can be computed using

Eq. 6-11. Since this region is well confined, the SFRC model assumes that the contribution of the fibres to post-peak ductility is not seen in this region.

Secondly, there is the area that corresponds to the previously assumed "ineffectively confined core area" (A_{ineff}). For SFRC columns, it is postulated that this area now contributes in confining the core. This area is defined in Eq. 6-12 and is shown schematically in Fig. 6.10.

$$A_{KE} = (K_e) \times A_{core} \tag{6-11}$$

$$A_{ineff} = (1 - K_e) \times A_{core} \tag{6-12}$$

It is assumed that the "plain" concrete contribution in this region is already taken into account indirectly in the model that was presented in Section 6.2. Therefore in order to account for the contribution of the fibres one can simply include the residual stress-strain curve that results from subtracting the compressive response of the SFRC from that of the response of the unconfined concrete. Hence, Eq. 6-13 can be used to compute the positive influence of the fibres in this region.

$$P_{ineff} = (f_{cf} - f_{cu}) \times (A_{ineff}) \tag{6-13}$$

Where f_{cf} refers to the stress in the SFRC at a given strain and is calculated using the model presented in Section 6.3. In Eq. 6-13, f_{cu} refers to the stress in the plain unconfined concrete at the same strain.

6.4.4 Post-peak contribution in the cover region

6.4.4.1 Cover spalling in RC and SFRC columns

In traditionally reinforced RC columns, the cover is assumed to spall away at a very early strain. Furthermore, this spalling is presumed to occur very abruptly. Hence in the model that was presented in Section 6.2, for RC columns it was assumed that the cover spalls away suddenly with a abrupt drop in strength at a strain of 0.003. Furthermore, the cover was assumed to have completely spalled at a strain of 0.004.

Foster et al. (1998) suggested that cover spalling in RC columns is initiated due to the triaxial stress condition that occurs between the confined core, the tie reinforcement and the cover shell which causes cracking to initiate at the core-cover interface. Before the cover concrete can begin to spall away from the core of the column cross-section, fracture must initiate at the interface of the core concrete and the cover shell. As load is increased, expansion due to volumetric growth occurs in the core. This expansion causes the strain in the tie reinforcement to increase, which results in a confining pressure to be applied to the core (see Fig. 6.11). Hence, in providing this confinement to the core, tension stresses are initiated at the core-cover interface, and the inevitable consequence of this triaxial stress state is the cover spalling mechanism (Foster, 2001).

Although cover spalling cannot occur before this crack initiation, several "driving force mechanisms" (or buckling mechanisms) are required to cause the cover shell to buckle. Several mechanisms have been suggested in the literature, including: buckling of the cover shell, dilatation of the longitudinal steel relative to the surrounding concrete and outward bending of the longitudinal steel (Foster, 2001, Paultre et al., 1996). However in all cases, due to the weakness of the concrete in tension after cracking, the spalling mechanism occurs rather suddenly (as was seen in all of the non-fibre reinforced RC columns in this experimental program).

In this research program, it was observed that with the inclusion of fibres, cover spalling was delayed. Rather than occurring suddenly, the cover spalling was transformed into a gradual and controlled mechanism.

The previous assumptions used in the analysis of traditional RC columns are based on the understanding that the cover spalling is initiated when the tensile stress capacity at the core-cover interface is reached. By examining the uniaxial tensile stress-strain curves of plain concrete and SFRC one can see that the fibres have a capability to maintain a residual tensile stress after the peak stress is attained (see Chapter 8).

This can also be understood by examining the fracture energy associated with the two materials. The fracture energy, G_f , is defined as the energy required to form a crack of unit area that can no longer transfer tensile stress. Normal concrete has a fracture energy in the range of 0.1 N/mm, while due to the presence of the bridging action of fibres the fracture energy in SFRC can be in the range of 1-6 N/mm (Dhakal, 2006). For example, for the type of deformed fibre used in this present study (Dramix ZP305), Barros and Figueiras (1999) suggested Eq. 6-14 to calculate the fracture energy.

$$\frac{G_f^{\ Fe}}{G_{fo}^{\ Fe}} = 19.953 + 3.213 w_f \qquad \text{6-14}$$

In the equation, $G_{fo}^{\ Fe}$ represents the fracture energy of plain concrete, $G_f^{\ Fe}$ represents the fracture energy of the SFRC and w_f represents the weight fraction of fibres in the concrete mix. For the range of fibres used in this experimental program, the $G_f^{\ Fe}$ value is in the range of 2.8-3.2 N/mm, a 30 fold increase over the reported value for traditional concrete mixes. Dhakal (2006) has shown that due to this dramatic increase in fracture energy, substantially larger values of spalling strain can be reached in SFRC columns when compared to RC columns.

Hence with SFRC, it can now be assumed that the cover concrete can have some contribution to confinement. Furthermore, it can be assumed that the cover spalling occurs, but is a much more gradual process.

However, what now becomes important is the driving mechanisms that cause cover spalling. As was mentioned earlier one of the possible driving mechanisms for the spalling of the cover is the effect of volumetric expansion of the longitudinal bars on the surrounding concrete. In traditional RC columns, this effect may play a secondary role, but since SFRC can carry tension across the core-cover interface after the initiation of cracking, the amount of buckling that occurs in the reinforcement can have a significant effect on the acceleration of the spalling mechanism. This mechanism in SFRC has also been reported by Dhakal (2006) as a significant driving mechanism in the spalling of SFRC.

This finding correlates well with observations made during this research program; during the experiments it was observed that the bar buckling mechanism was not eliminated by the mere presence of the fibres. Rather, as bar buckling occurred, and with increased strain, the bars pushed against large pieces of SFRC cover that were still attached to the core due to the bridging effect of the fibres. Eventually with sufficient strain, it was observed that due to buckling, the cover would detach from this interface, causing the cover to effectively “spall”.

6.4.4.2 Cover spalling factor for SFRC

Taking the observations made in the previous section into account, the cover contribution can be included in the present model by replacing the stress-strain curve previously assumed for the cover by the material stress-strain curve of SFRC (as presented in Section 6.3). Furthermore, in order to account for cover spalling in the SFRC specimens the following assumptions are made:

- Cover spalling is assumed to initiate at the same strain of 0.003. This is in agreement with observations made during testing as the initial stages of spalling were observed to initiate near the peak capacity of all the SFRC columns tested in the experimental program.
- The cover spalling is assumed to take place gradually and is taken into account with a spalling factor , Ψ .

The load contribution of the fibres in the cover region can therefore be computed using Equation 6-15, where Ψ is a factor that accounts for the delayed cover spalling in SFRC members. A graphical representation of the Ψ -factor is shown Fig. 6.12.

$$P_{cover} = \left(\Psi \times f_{cf}\right) \times \left(A_{cover}\right) \qquad 6\text{-}15$$

With a larger hoop spacing, buckling of the longitudinal reinforcement will be more rapid resulting in a larger transverse displacement. For instance, for the range of hoop spacings used in this test series, Bae’s model has been used to estimate the amount of transverse deformation that is expected in the longitudinal bars due to buckling (Bae et al., 2005). The results of the analysis are shown in Fig. 6.13. One can see that with a large tie spacing of 240 mm, significant transverse deformations are reached at early strains. On the other hand, for a smaller tie spacing of 65 mm, the buckling effect is all but eliminated.

Figure 6.12 contains a parameter ε_{spall} which corresponds to the strain at which effective spalling is complete. Taking the above considerations into account it is understood that for well-confined sections, the ε_{spall} value should be larger (i.e. degradation of the Ψ-factor should be more gradual and stable), while for less confined sections containing a larger hoop spacing, the ε_{spall} value should be smaller and hence result in a more rapid decline of the Ψ-factor.

In the present study, the ε_{spall} strain values are chosen based on approximations regarding observed behaviour during the experiments (see Table 6-2). For the A-series columns which contained a large spacing, the ε_{spall} strain is chosen to be 0.01. Due to the fact that buckling of the bars did not occur in the heavily confined C-series specimens, for these columns the ε_{spall} is taken to be sufficiently large such that the Ψ-factor stabilizes at 50% even at high strains. Figure 6.14(a) shows a Plot of the spalling factors for the various columns in this test series. Figure 6.14(b) shows the resulting SFRC compressive stress-strain curves taking into account the effects of spalling.

Table 6-2: Spalling strains for the various columns

Column Series	Tie spacing s (mm)	Spalling strain ε_{spall} (mm/mm)
A	240	0.010
B	120	0.015
C	65	∞

6.4.5 Predictions of the responses of the SFRC columns

The proposed equations have been used to estimate the peak capacities and responses of the various columns that were tested in the experimental program. The results of this analysis are presented in Table 6-3 and Fig. 6.15 to 6.17. One can see that there is good agreement between the predicted and experimental results for both the peak capacities and the load-strain responses.

Table 6-3: Calculated capacities using the proposed model

Column	Tie spacing s (mm)	Fibre content v_f (%)	Concrete Strength f'_{co} (MPa)	Fibre Confinement Contribution $\Delta f'_{cf}$ (MPa)	Actual Peak capacity P_{exp} (kN)	Calculated Peak capacity P_{calc} (kN)	Experimental/ Calculated $\frac{P_{exp}}{P_{calc}}$
A1	240	1	43.9	5.5	4471	*4592*	***0.97***
A1.5		1.5	49.5	11.9	5783	*5619*	***1.03***
B1	120	1	43.9	5.5	4461	*4823*	***0.93***
B1.5		1.5	49.5	11.9	5891	*5828*	***1.01***
C1	65	1	43.9	5.5	4650	*4991*	***0.93***
C1.5		1.5	49.5	11.9	6209	*5873*	***1.06***

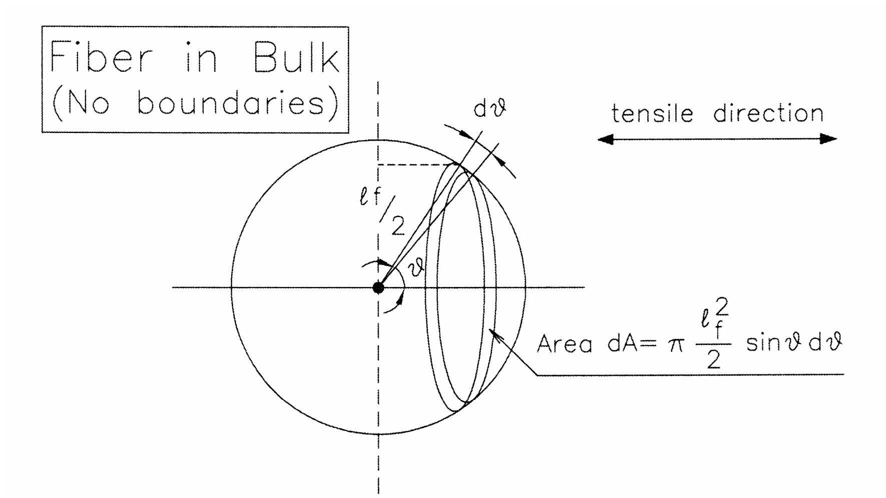

(a) Orientation factor if all possible orientations of the fibre are considered
[adapted from (Dupont, 2003)]

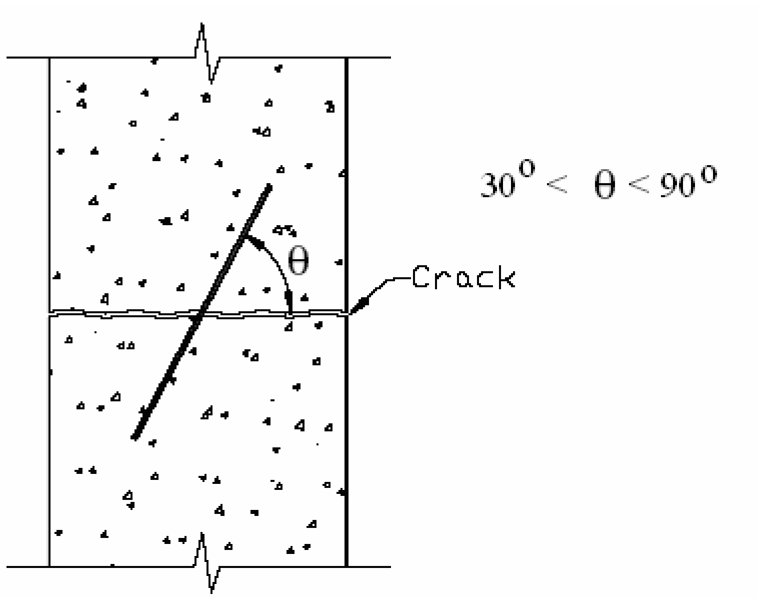

(b) α = 3/8 when the angle of the fibre to the cutting plane, θ, is between 30 and 90 degrees
[adapted from (Foster, 2001)]

Figure 6.5: Various derivations of the orientation factor, α

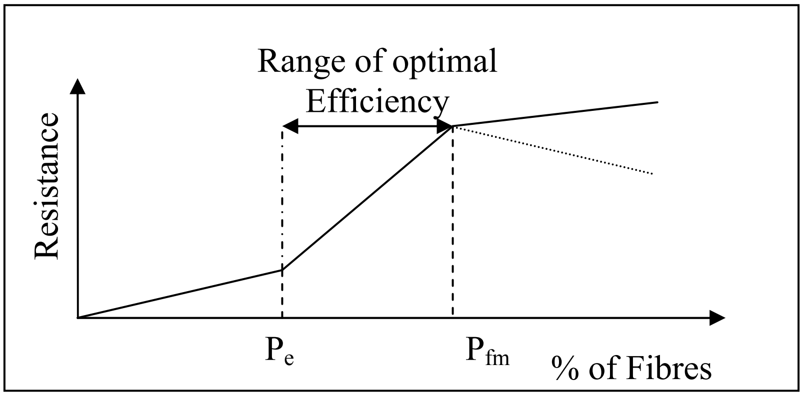

Figure 6.6: Range of optimal fibre efficiency

[Adapted from (Rossi, 1998)]

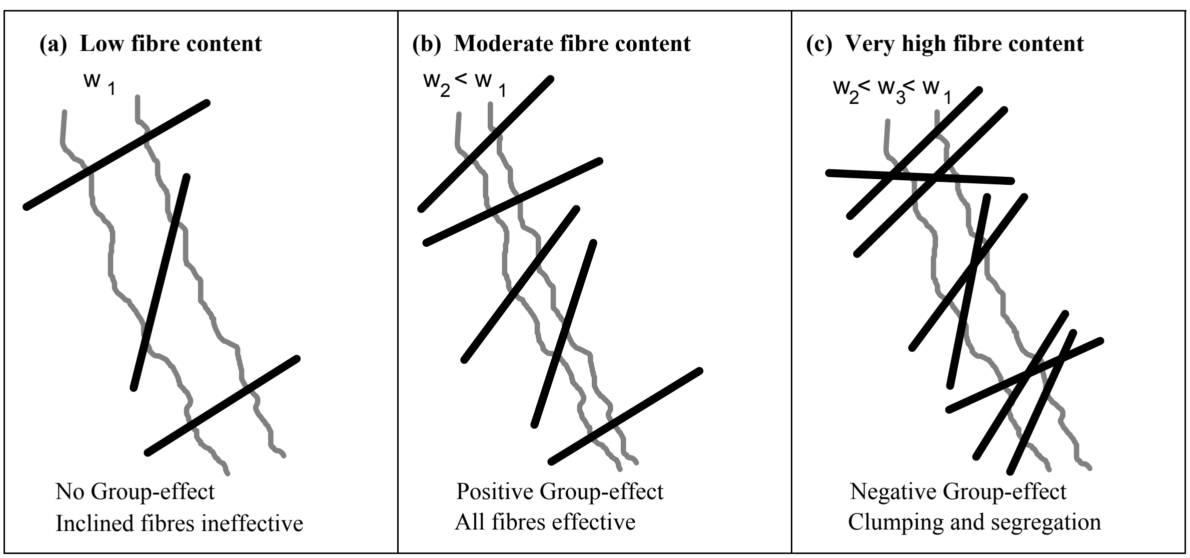

Figure 6.7: Schematic Idealisation of the influence of fibre volume for uniform tensile stress

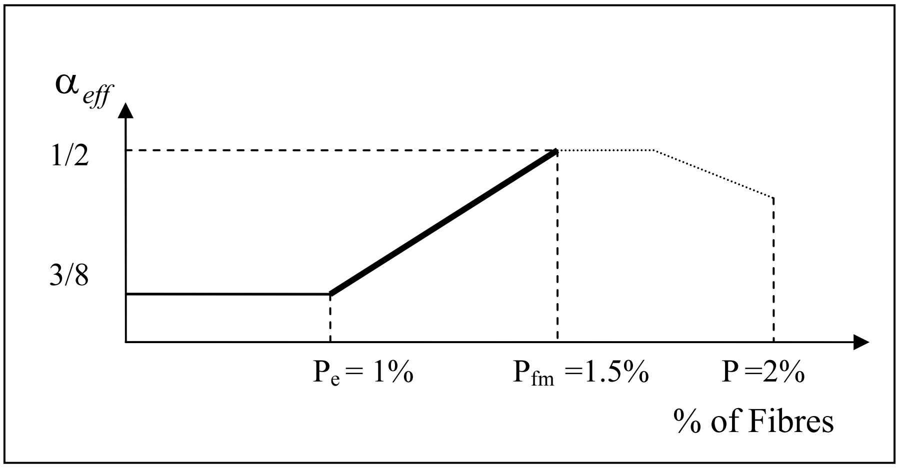

Figure 6.8: Schematic representation of the effective orientation factor, α_{eff}

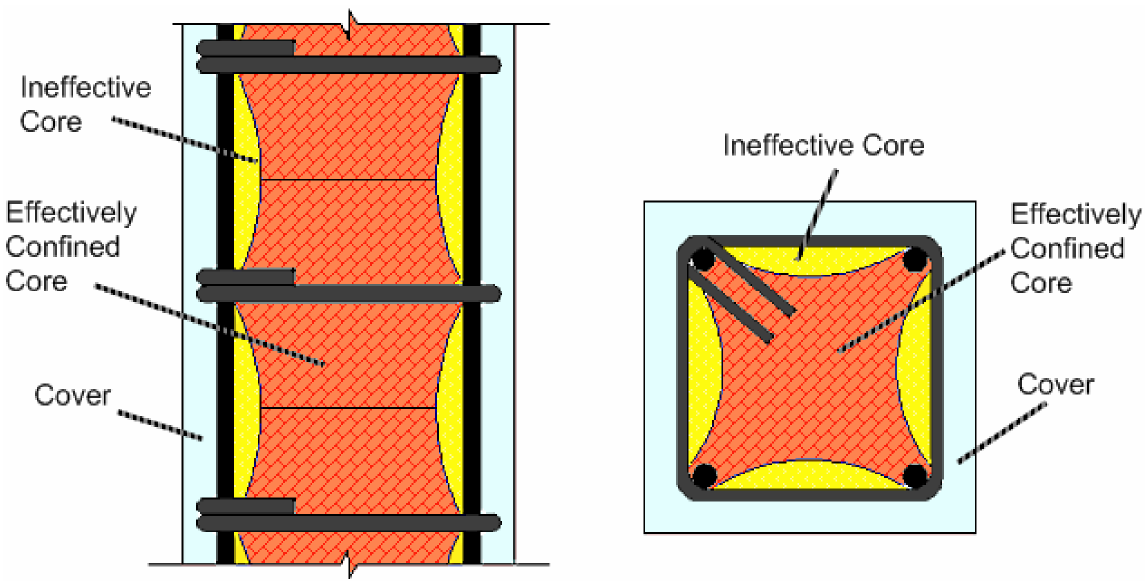

Figure 6.9: Schematization of the various regions affected by the fibres

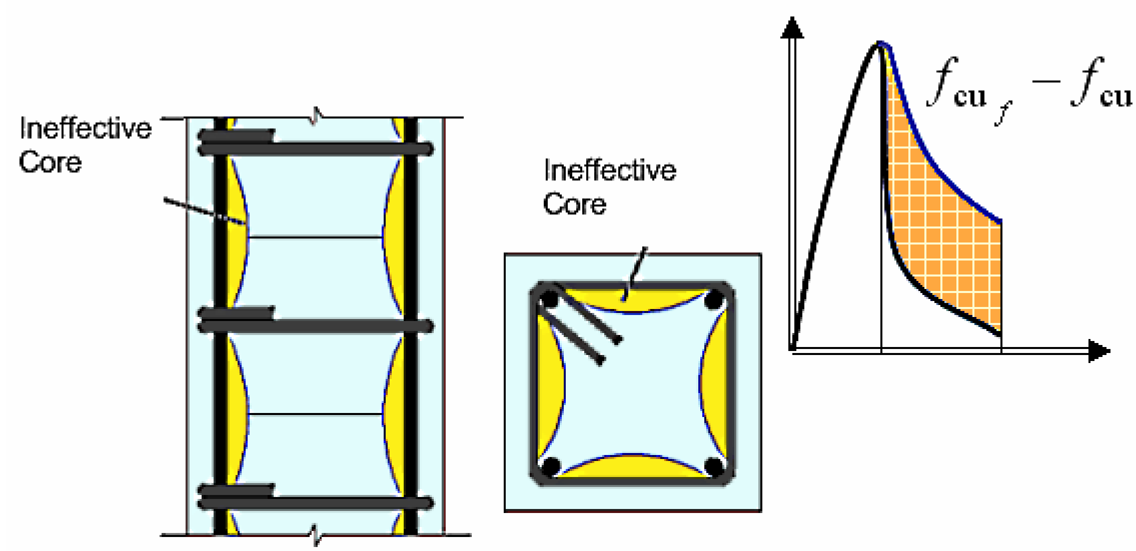

Figure 6.10: Schematization of the ineffectively confined core area, A_{ineff}

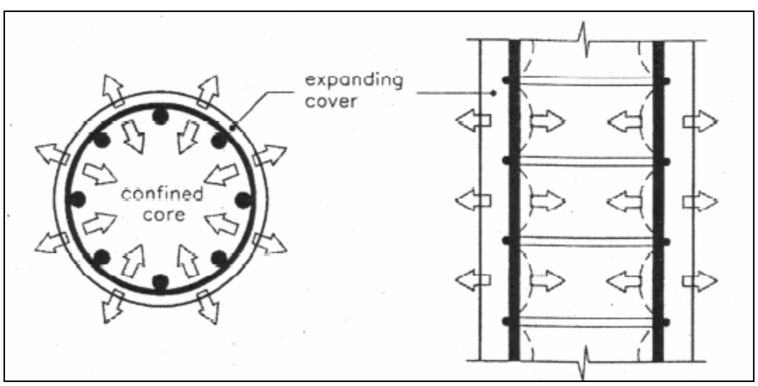

Figure 6.11: Mechanics of cover spalling

[Adapted from Foster (2001)]

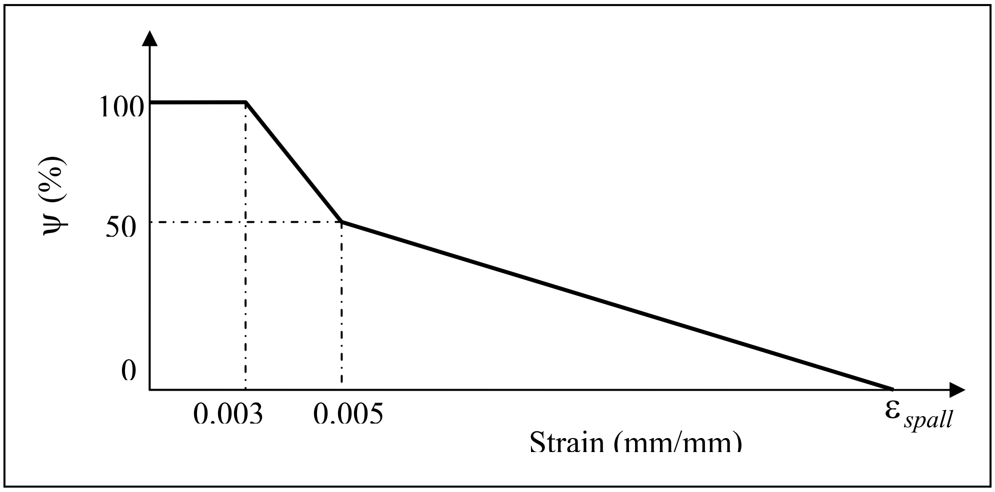

Figure 6.12: Graphical representation of the spalling factor in SFRC

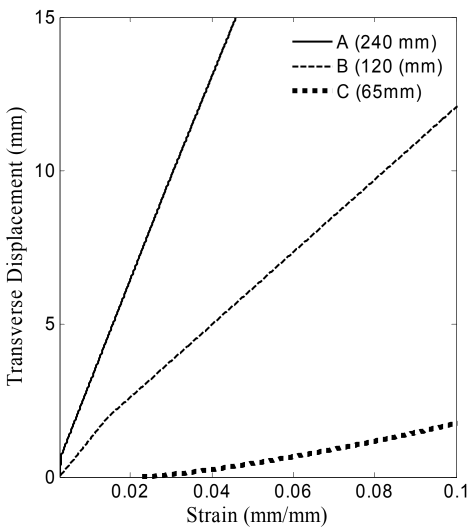

Figure 6.13: Transverse displacement in longitudinal reinforcement for the various column configurations

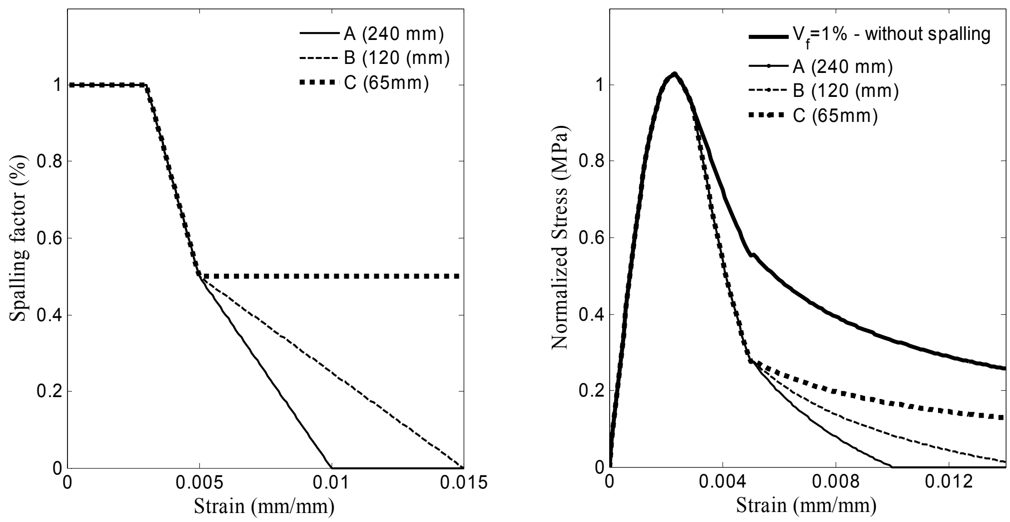

(a) Ψ -factor as a function of strain (b) $f_{cu\,f} \times \Psi$ as a function of strain for $v_f = 1.0\%$

Figure 6.14: SFRC material compressive stress-strain curves taking into account the effects of spalling

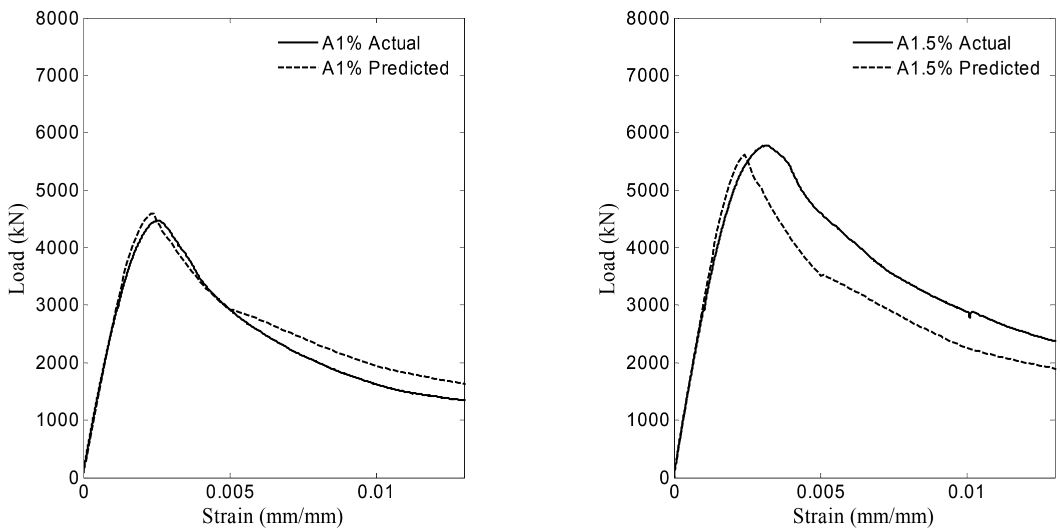

(a) Column A1% (b) Column A15%

Figure 6.15: Actual and predicted load-strain curves for the A-series specimens

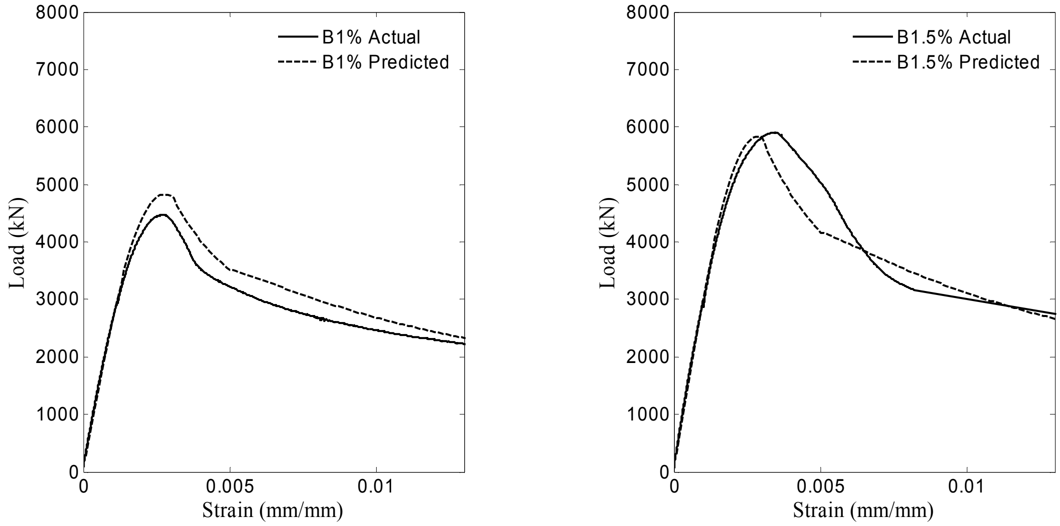

(a) Column B1% (b) Column B15%

Figure 6.16: Actual and predicted load-strain curves for the B-series specimens

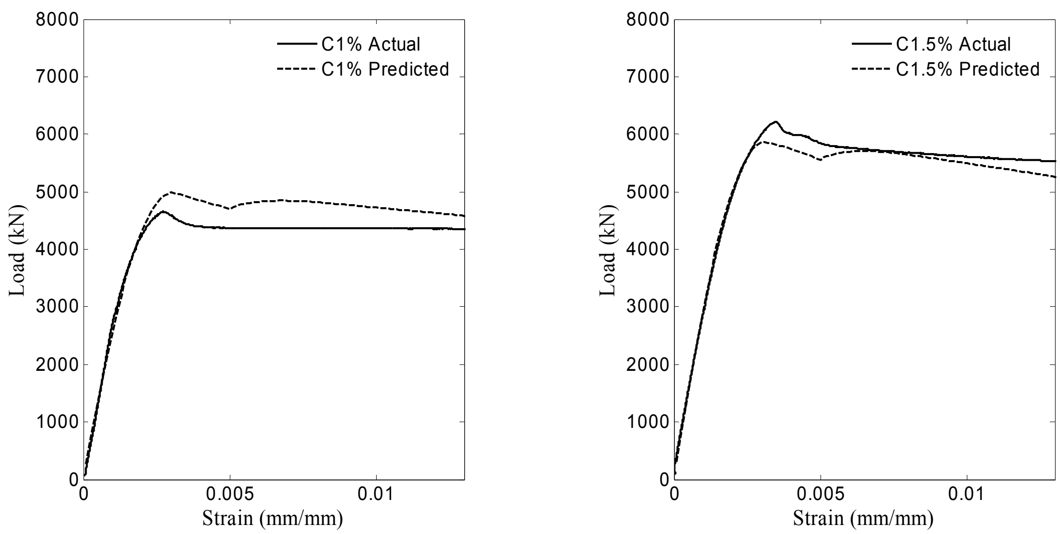

(a) Column C1% (b) Column C15%

Figure 6.17: Actual and predicted load-strain curves for the C-series specimens

6.5 Concluding Remarks

A procedure for predicting the complete load-strain response of SFRC columns was presented. The model takes into account the influence of the fibres in increasing the peak load-carrying capacity of the columns as well as the enhancements in the post-peak response.

An approach was presented in order to predict the expected improvements in the peak resistance taking into account the random orientation of the fibres, the efficiency of the fibres at various fibre contents and the beneficial influence of fibres on confinement.

To include the expected improvements in post-peak behaviour, the model uses an approach where the load-strain response of the plain RC column is adjusted for the presence of fibres based on the expected material stress-strain curve of SFRC. Furthermore, the model includes expressions that take into account the effects of the fibres in delaying cover spalling.

The method provides reasonably accurate predictions for the various specimens that were tested in this experimental program.

Chapter 7 Experimental Program on Steel Fibre Reinforced Concrete Members Subjected to Pure Tension

7.1 Objectives

The main objective of this phase of the research program was to investigate the influence of steel fibres on the structural response of RC tension members. Several researchers have found that the random orientation of the fibres can improve the response of reinforced concrete by influencing cracking and enhancing the post-cracking response of the concrete (Bischoff, 2003, Abrishami and Mitchell, 1997). The test program examined the influence of steel fibres on the control of cracking and on tension stiffening. The experimental approach involved the testing of RC and SFRC specimens subjected to pure tension loading.

7.2 Tension Stiffening

Figure 7.1 shows a typical load-strain response of a RC member subjected to pure tension as well as the response of the reinforcement alone ("bare bar" response). If one was to ignore the tensile stresses in the concrete, then the predicated response would follow the path of line ODE. In other words, the response would be identical to that of the "bare" steel element. In reality, the response follows line OABC, which is somewhat different from the "bare bar" response. This difference is a result of the ability of the concrete to carry tensile stresses.

Figure 7.2(a) shows the manner in which the axial load is shared between the steel reinforcement and the concrete and the influence of cracking on the response of the RC element. Prior to cracking, the tensile loads carried by the concrete, N_c, and the steel, N_s, are uniform along the length of the specimen. The actual member response is therefore initially linear elastic and corresponds to $N_1 = N_s + N_c$ (see Fig. 7.2(b)).

When load N_2 is reached (see Fig. 7.2(b)) the tensile strength of the concrete f_{cr} is attained and the member cracks. After cracking is initiated, N_c and N_s are no longer uniform along the length. At the crack location, the steel reinforcement carries all the tensile forces, while between the cracks the tensile stresses are shared between the steel and the concrete. Hence, once cracking has initiated the concrete is not able to carry tension at the crack locations, but it still able to develop tensile stresses in between the cracks. This variation in tensile stress in between the cracks reduces the average tensile stress in the concrete, and as further cracks develop the stress in the concrete will be further reduced (Collins and Mitchell, 1997).

As shown in Fig. 7.1, the tension carried by the concrete, N_c, stiffens the response. The ability of the concrete to carry these tensile stresses reduces the average member deformation and is what causes the variance between the actual member response and the "bare bar" response. This difference in the responses is known as "tension stiffening".

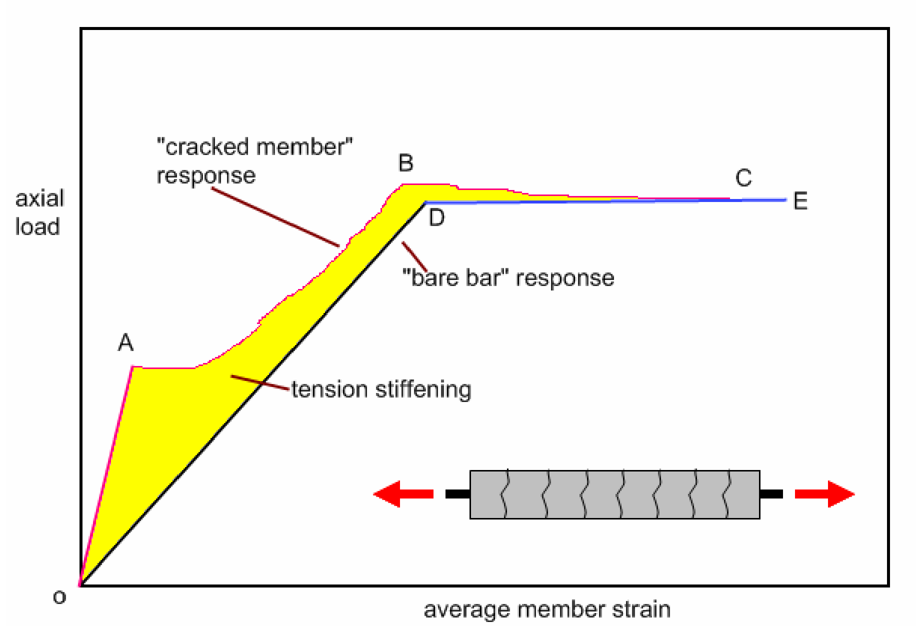

Figure 7.1: Typical Load-strain response for a RC tension member

[Adapted from (Bischoff, 1983)]

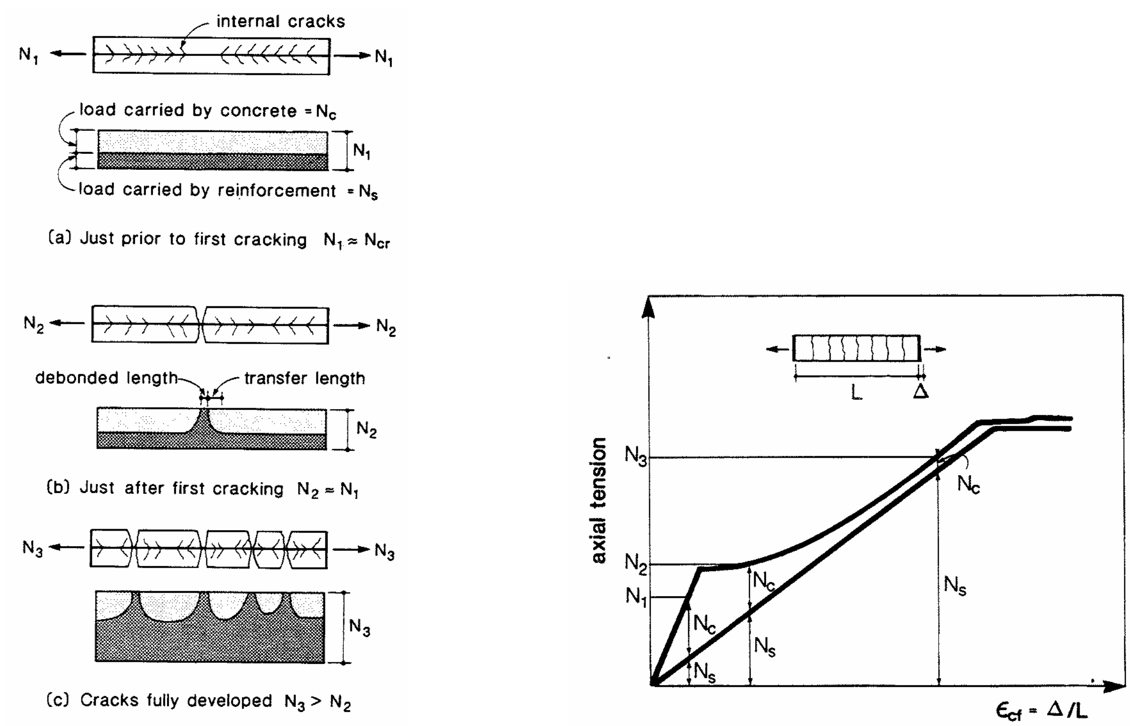

(a) Load sharing between concrete and reinforcement

(b) Influence of tension in concrete on load-deformation response

Figure 7.2: Tension stiffening in RC tension members

[Adapted from (Collins and Mitchell, 1997)]

7.3 Description of Test Specimens

A testing program was conducted to investigate the effect of steel fibre reinforced concrete on the response of members subjected to pure tension loading. Three specimens each containing a single reinforcing bar and varying amounts of steel fibres were tested. In addition a "bare-bar" specimen was tested so as to be able to isolate the contribution of the concrete during the analysis of the results. Figure 7.3 shows the geometry for a typical specimen. The details regarding the fibre content and cross-sectional properties are given in Table 7-1. All the specimens had a length of 1100 mm. The cross-section was composed of a single reinforcing bar in a 100 mm x 100 mm concrete cross-section, resulting in a clear concrete cover of 42.5 mm in each specimen. This resulted in a reinforcement ratio of 2%. The reinforcing bar was extended 125mm outside each end of the concrete section to allow for proper gripping in the testing apparatus.

Table 7-1: Design details for the various tension specimens

Tension Specimen	Cross-Section	Specimen Length	Size of reinforcing bar in section	Specified Concrete Strength	% Fibres
T0%	100mm x 100 mm	1100 mm	15M	40 MPa	0.0%
T0.5%					0.5%
T1%					1.0%

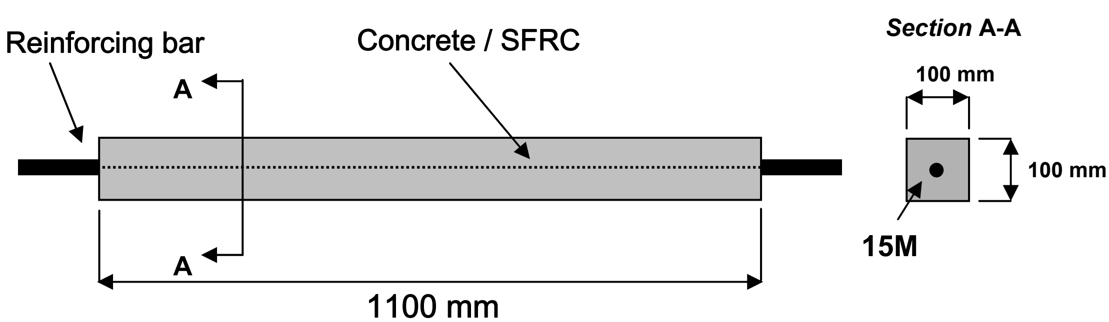

Figure 7.3: Schematic representation of the Tension test specimens

7.4 Material Properties

7.4.1 Reinforcing steel

The properties of the reinforcing steel are summarized in Table 7-2. All the specimens were constructed using weldable grade steel reinforcement with a specified yield strength of 400 MPa. Tension tests were performed on three random specimens for each bar size. The typical stress strain relationship of the15M reinforcing bars (16 mm diameter with A_s = 200 mm^2) is shown in Fig. 7.4.

In addition, one “bare-bar” was tested in the MTS machine under the same loading conditions as the companion concrete-encased specimens so as to obtain an accurate representation of the “bare bar” response.

Table 7-2: Reinforcing steel properties

Bar description	f_y (MPa) [std. dev.]	ε_{sh} (mm/mm) [std. dev.]	f_u (MPa) [std. dev.]	ε_u (mm/mm) [std. dev.]
15M	478 [12.8]	0.0207 [0.0013]	588.6 [12.2]	0.1679 [0.0061]

7.4.2 Steel fibres

In this testing program, hooked end steel fibres were used to attain 0.5% fibre reinforcement (38.4 kg/m^3) and 1% fibre reinforcement (76.8 kg/m^3) by volume of concrete.

The same 30 mm hooked-end steel fibres used in the column tests were used for this phase of the experimental program (Bekaert Dramix ZP-305). The details regarding the properties of the fibre are presented in Table 7-3.

Table 7-3: Steel fibre properties

Fibre type	Length l_f (mm)	Diameter d_f (mm)	Aspect ratio $\frac{l_f}{d_f}$ (mm/mm)	Tensile strength f_{fy} (MPa)
Dramix ZP-305	30	0.55	55	1100

7.4.3 SCC Concrete

The concrete for all the tensile specimens was produced at McGill University's Jamieson Structures Laboratory. The same pre-packaged self-consolidating concrete mix used in the column test-series was selected for this phase of the experimental program (KING MS Self-Consolidating Concrete). The details regarding the SCC mix and the casting procedure can be found by consulting Chapter 3 of this thesis.

A series of lab cured cylinders and flexural beams were prepared and tested to determine the concrete properties of each batch used during the casting of the columns. The compressive strength, f'_{co} , and compressive stress-strain relationships were determined by testing cylinders, having a diameter of 100 mm and a height of 200 mm. The modulus of rupture, f_r, was determined from flexural beams that had dimensions of 100 x 100 x 400 mm. Table 7-4 summarizes the concrete properties.

Figure 7.5(a) shows the typical compressive stress-strain relationships of the concrete with and without steel fibres for the various fibre contents used in the experimental program. Figure 7.5(b) shows the load deflection responses obtained from the modulus of rupture tests. As expected, one can see that the addition of fibres, has significantly improved the toughness of the compressive stress-strain and flexural load-strain responses.

Table 7-4: Concrete properties

Series	f'_{co} (MPa) [std. dev.]	ε'_{co} (mm/mm) [std. dev.]	f_r (MPa) [std. dev.]
0%	40.6 [2.61]	0.002 [0.0001]	6.42 [0.31]
0.5%	39.9 [2.02]	0.002 [0.0002]	6.39 [0.52]
1.0 %	38.6 [1.82]	0.002 [0.0002]	6.21 [0.41]

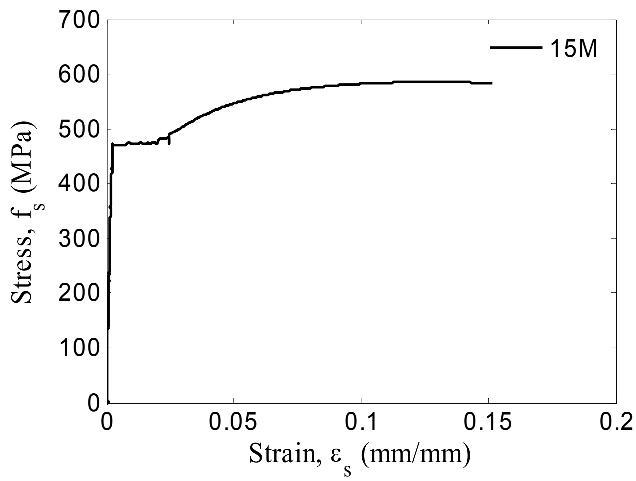

Figure 7.4: Typical Stress-strain responses for 15M reinforcing bars

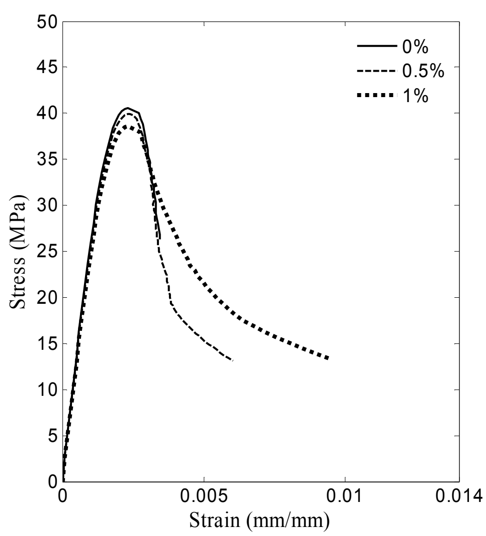

(a) Concrete compressive stress-strain responses

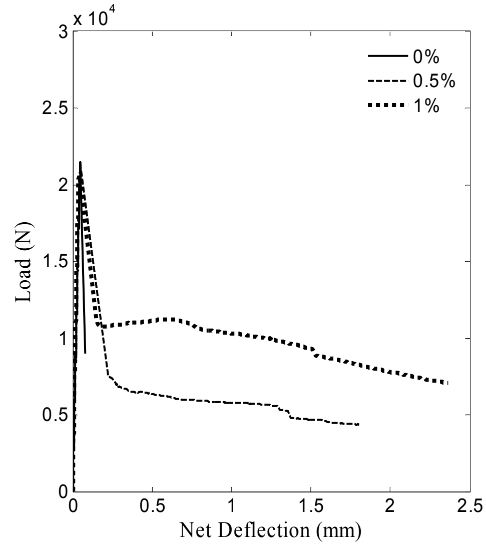

(b) flexural beam load-deflection curves

Figure 7.5: Concrete material properties

7.5 Testing

All the specimens were tested under pure tensile loading using a 11,400 kN capacity MTS testing machine. The load was transferred through a pair of tension grips at the top and bottom of the reinforcing bar. This resulted in tension being transferred from the steel reinforcing bar to the reinforced concrete section. Figure 7.6(a) shows a typical specimen prior to testing

The internal load cell of the universal testing machine was used to measure the axial tensile load that was applied to the various specimens. In addition, two linear voltage differential transducers (LVDTs) were utilized to measure the axial deformations of each member under applied load. The LVDTs were placed along each side of the specimen over a central height of 900 mm to measure the total elongation of the RC member. The LVDTs were clamped to threaded steel rods that were placed into the specimen prior to casting (see Fig. 7.7).

All the specimens were tested in the same manner. A loading rate of 0.001 mm/sec was used up to a load of 70 kN. Subsequent to this load stage, the loading rate was switched to 0.002 mm/sec until yielding of the reinforcing bar was detected. At that point the rate was increased to 0.005 mm/sec for the remainder of the experiment. The tests then continued until the axial displacement of the MTS machine reached a value of 24 mm.

Throughout the tests observations regarding crack patterns and failure mechanisms were made and photographs of the specimens were taken at regular intervals.

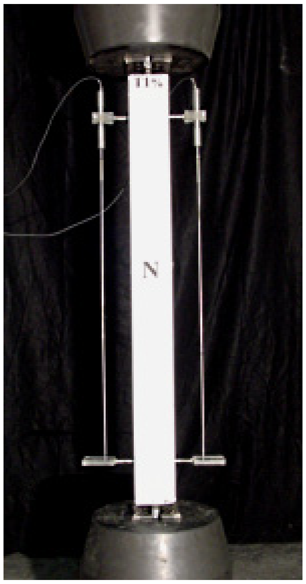

(a) Axially loaded specimen just prior to testing

(b) Specimens in formwork prior to casting

Figure 7.6: Setup used during the testing of the tensile specimens

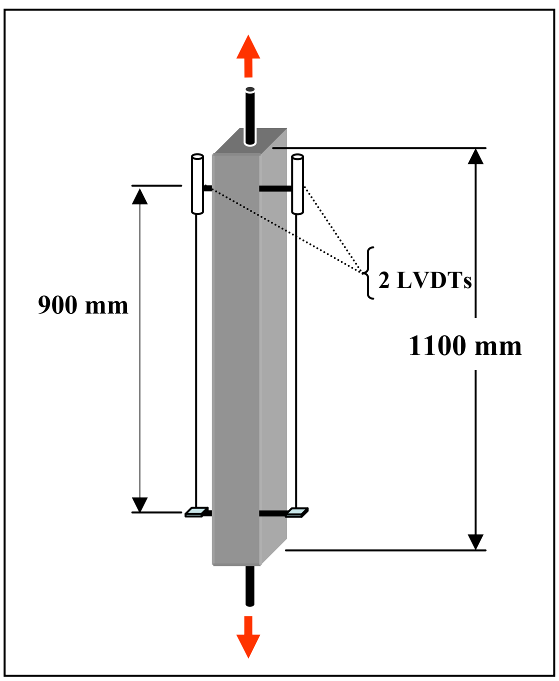

Figure 7.7: Location of LVDTs on the tensile series test specimens

Chapter 8 Presentation of the Experimental Results for the Tension Specimens

8.1 Chapter Overview

In this chapter the behaviour of the tensile specimens is discussed. Section 8.2 outlines the method that was used in order to determine the post-cracking response of the concrete. Section 8.3 presents the results from the tension stiffening tests, the resulting tensile stresses carried by the cracked concrete as well as the fibre contributions to the tensile capacity. Section 8.4 provides observations that were made during testing.

8.2 Accounting for Shrinkage and Evaluating Tension Stiffening

It is well known that concrete can experience a certain amount of shrinkage before testing. Since this will cause an initial shortening of the test specimens, this effect must be included in order to properly calculate the tensile contribution of the concrete (Bischoff, 2003).

Assuming that the strains are uniform over the member cross-section the expected strain in the shortened specimens due to shrinkage can be computed using Eq. 8-1 (Bischoff, 2001, Collins and Mitchell, 1997).

$$\varepsilon_{c,i} = \frac{\varepsilon_{shr}}{1+\eta\rho} \qquad \text{8-1}$$

Where ε_{shr} represents the free shrinkage strain of the concrete (a negative value to represent shortening) and $\varepsilon_{c,i}$ equals the initial member strain for the condition of zero axial load (i.e., $N = 0$). The quantity η represents the modular ratio, which is equal to the ratio between the steel and concrete elastic moduli ($\frac{E_s}{E_c}$). Finally, the value ρ represents the reinforcing steel ratio ($\frac{A_s}{A_c}$).

In order, to account for this expected member shortening, shrinkage measurements were taken on companion specimens having the same cross-sectional area as the specimens tested under tensile loading (namely a cross-section of 100 x 100 mm). The calculated free shrinkage results are summarised in Table 8-1.

Table 8-1: Measured shrinkage values

Fibre volume v_f (%)	Free Shrinkage ε_{shr} (mm/mm)	Initial member strain for zero axial load $\varepsilon_{c,i}$ (mm/mm)
0	- 0.00079	- 0.00068
0.5	- 0.00076	- 0.00066
1	- 0.00076	- 0.00066

In order to isolate the tensile influence of the concrete, the bare bar response needed to be subtracted from the total specimen response. The procedure described by Bischoff (2001) is used for this purpose so as to properly take into account the effect of shrinkage. In the procedure, which is schematically summarised in Fig. 8.1, the original member response origin is shifted to an idealised origin to obtain the shrinkage compensated response. Thereafter the "bare bar" response is subtracted from the "shrinkage compensated" response to obtain the contribution of the concrete.

(*a*) Effect of shrinkage on member response; (*b*) details showing relationship between test response and shrinkage compensated response.

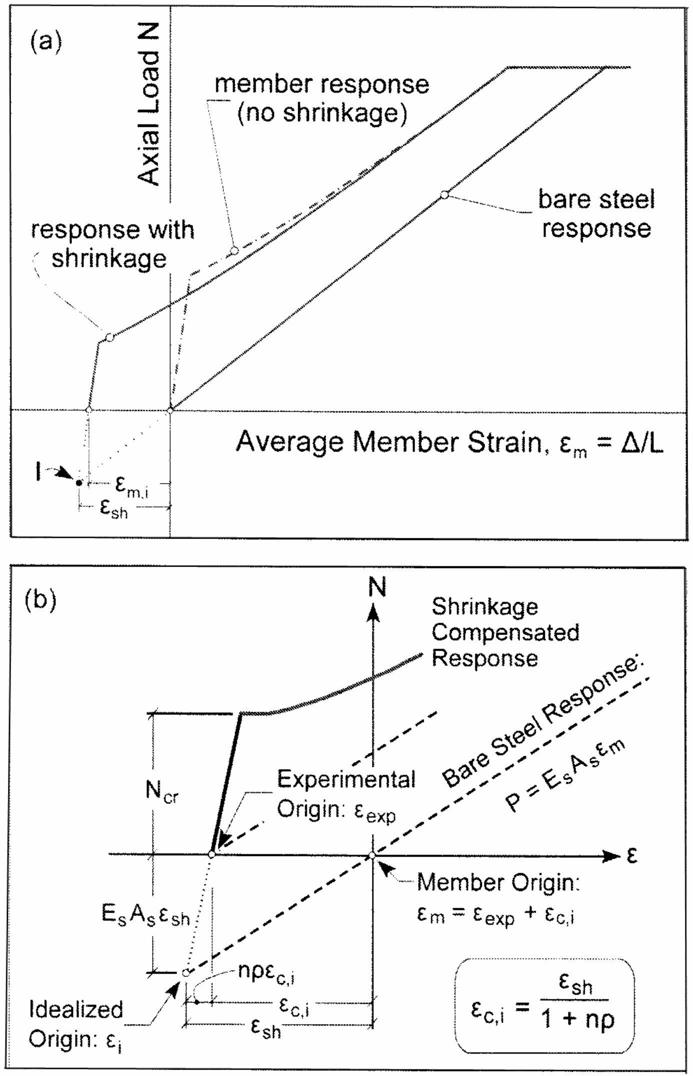

Figure 8.1: Accounting for the shrinkage effects on the member response
[Adapted from (Bischoff, 2001)]

8.3 Presentation of the Results

Figures 8.2(a) to (c), show the measured responses for the various specimens. Note that the member responses have been adjusted using the procedure outlined in Section 8.2 to account for shrinkage.

As can be seen from the results, the addition of fibres in the concrete has resulted in an increased stiffness in the response after cracking. Furthermore, one can see that the cracking is much better controlled when the fibres are added to the matrix. For instance, the response of Specimen T0% (see Fig. 8.2(b)) shows numerous drops in load as a result of sudden crack formation (as seen by the numerous peaks). As can be seen from Fig. 8.2(c) and (d) as the fibre content increases the crack formation has a less pronounced influence on the response.

Using these plots, the tension stiffening contribution in the concrete was computed by subtracting the bare bar response from the adjusted response of each specimen. The result of this analysis is presented in Fig. 8.3(a). One can see that the addition of fibres has not increased the cracking strength of the concrete. This is to be expected for the fibre quantities used in this experimental program. However the significant contribution of the fibres is seen in the post-peak portion of the curve where the SFRC demonstrates an ability to carry significant tensile stress after cracking and at relatively high tensile strains. Whereas traditional RC is only able to carry tension in between the cracks, the fibres have the ability to bridge and transmit tension across the cracks in addition to the tension in between the cracks, resulting in the improved response (Abrishami and Mitchell, 1997, Bischoff, 2003).

The tension stiffening factor, β_t, can be computed using Eq. 8-2:

$$\beta_t = \frac{\sigma_c}{f_{cr}} \tag{8-2}$$

Where the quantity f_{cr} is equivalent to the concrete cracking stress and the value σ_c represents the post-cracking stress in the concrete at a given tensile strain. Fig. 8.3(b) compares the tension stiffening factor as a function of strain for all of the specimens. One can see that the factor β_t is improved due to the positive influence of the steel fibres on the post-cracking resistance.

In order to gain a better understanding of the influence of the fibres in improving the post-peak response of the concrete, the fibre contribution to the tensile response was computed by subtracting the tensile response of the SFRC specimens from that of the tension specimen without fibres. The resulting fibre contributions for fibre contents of 0.5% and 1% are shown in Fig. 8.3(c). The fibre contribution responses have the same general shape as the pullout response of a hooked-end fibre.

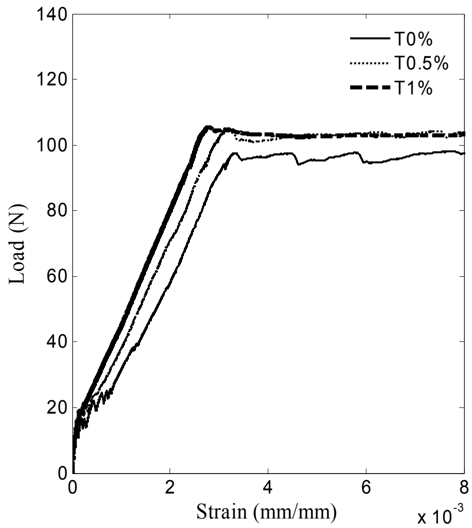

(a) Experimental load-strain curves for the various specimens

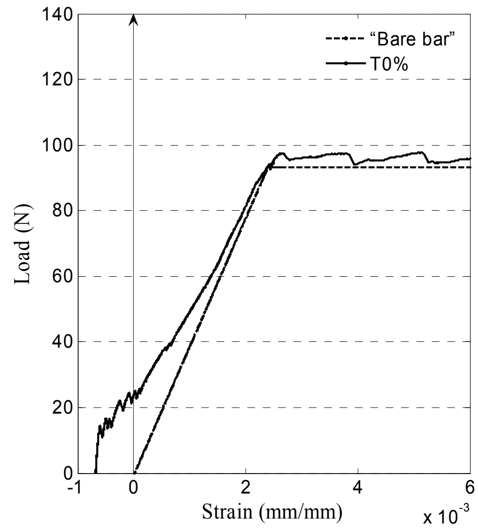

(b) Shrinkage compensated response for Specimen T0%

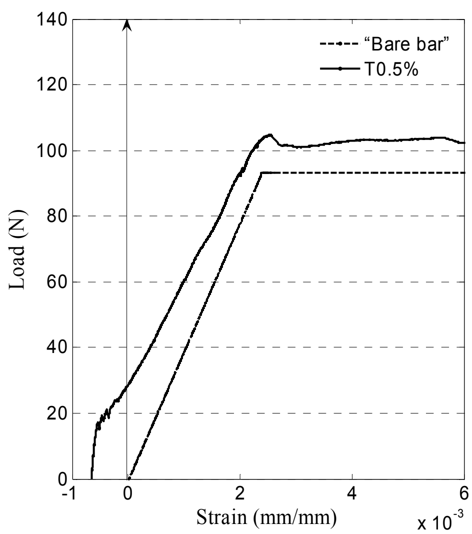

(c) Shrinkage compensated response for Specimen T0.5%

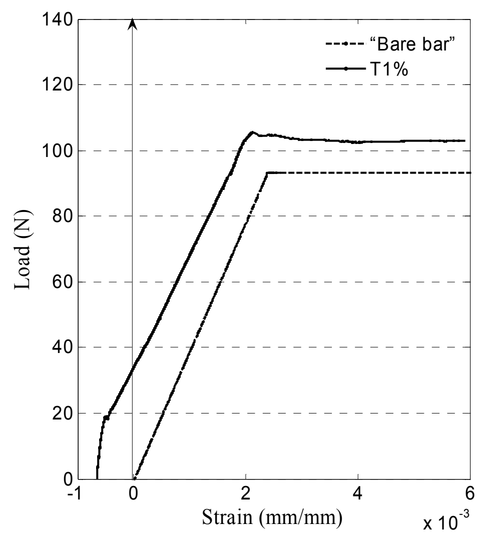

(d) Shrinkage compensated response for Specimen T1%

Figure 8.2: Experimental results for the tension specimens

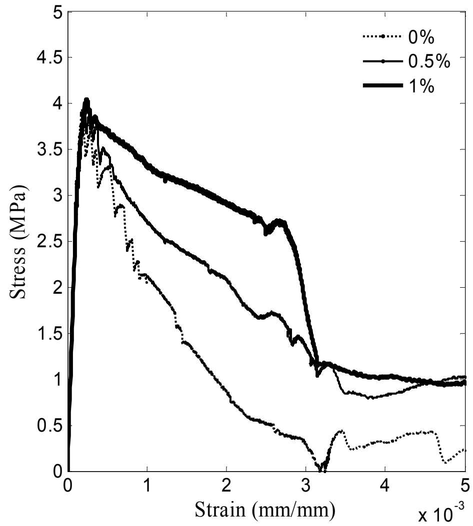

(a) Concrete/SFRC contribution to tensile resistance

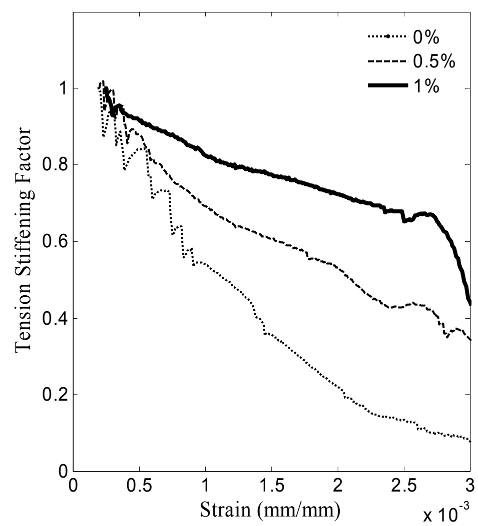

(b) The tension stiffening factor, β_t

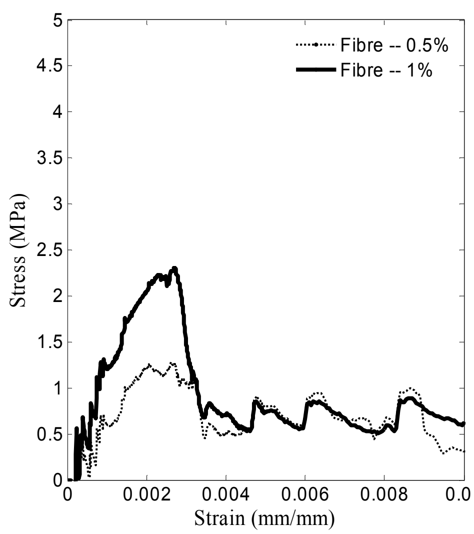

(c) The isolated fibre contributions for fibre contents of 0.5% and 1%

Figure 8.3: Concrete and fibre contributions for the tension specimens

8.4 Observations

Figure 8.4 shows the cracking patterns for the specimens at the end of testing. One can see that the crack spacing was reduced when fibres were added to the concrete mix, with specimen T1% having the smallest average crack spacing (13 cracks, average spacing of 78 mm) and Specimen T0% having the largest crack spacing (9 cracks, average spacing of 110 mm). The crack widths at a given load were reduced in the SFRC specimens when compared to the RC specimen without fibres.

Furthermore, it was observed that a more diffused cracking pattern occurred in the SFRC specimens. For instance Specimen T1% had several "forking" type cracks throughout the specimen length where secondary cracks would branch off from the main cracks.

The cracks in the RC specimen without fibres had similar crack widths. However for the SFRC specimens it was observed that although many cracks formed, after yielding major cracking was concentrated at one crack location where fibre pullout was observed. This can be seen in Fig. 8.5(a) and (b) which show the concentration of the major cracking at one crack location in Specimens T0.5% and T1%. Figure 8.5(c) shows the observed fibre pullout occurring at the major crack location in Specimen T1%.

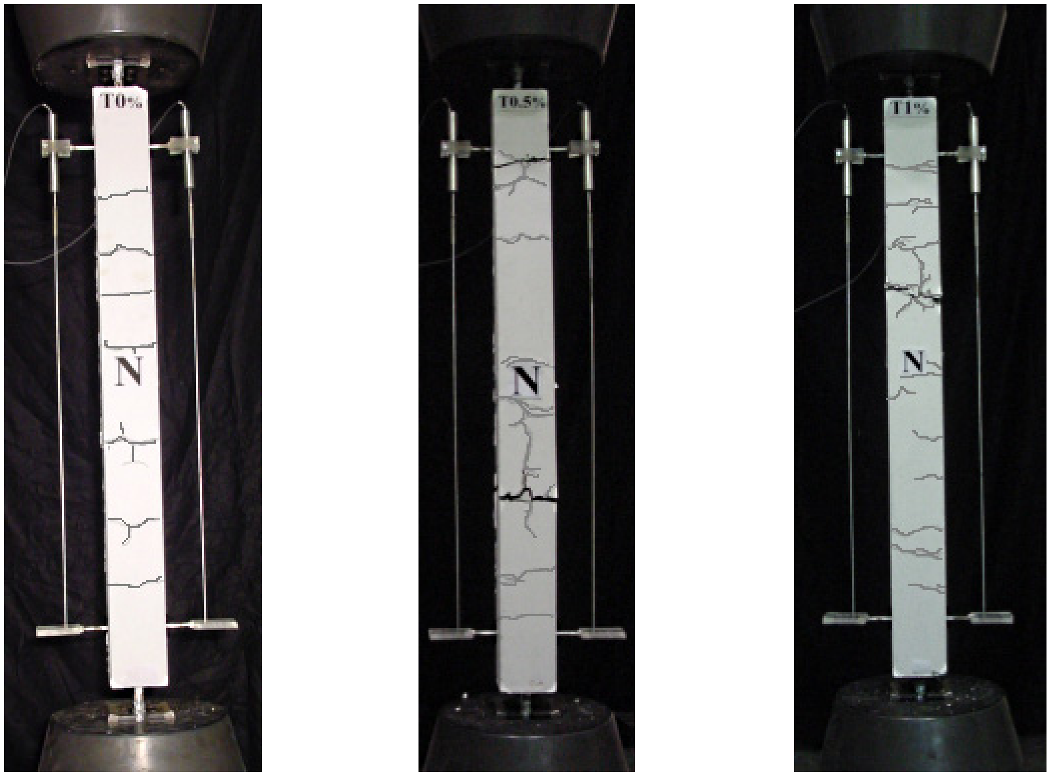

(a) Specimen T0% (b) Specimen T0.5% (c) Specimen T1%

Figure 8.4: Cracking patterns for the various specimens at the end of testing

(a) Specimen T0.5% (b) Specimen T1% (c) Pullout at main crack location

Figure 8.5: Concentration of Fibre pullout at one crack location in SFRC specimens

Chapter 9 Modelling the Influence of Fibres on Tension Stiffening

9.1 Chapter Overview

In this chapter, a model is presented for the prediction of the tension stiffening response in SFRC tension members. Section 9.2 presents a method for the prediction of the response of tension stiffening in traditional RC members based on a model that is available in the literature. Section 9.3 presents a model that can be used to capture the pullout response of hooked-end steel fibres. In Section 9.4, the model presented for traditional RC members is modified so as to account for the beneficial influence of steel fibres. Section 9.5 compares the experimental results to those predicted using the models.

9.2 Model for the Tension Stiffening in Reinforced Concrete

There are several empirical relationships that have been proposed in the literature to predict the tension stiffening in reinforced concrete (CEB-FIP, 1978, Collins and Mitchell, 1991). Recall that the tension stiffening in the concrete can be described using a factor β_t that is equivalent to the normalised post-cracking stress in the concrete ($\frac{\sigma_c}{f_{cr}}$).

Herein the simple model presented by Fields and Bischoff (2004) will be used in order to get an accurate representation of tension stiffening in the concrete. Bischoff (2001) suggests that when shrinkage effects are included in the analysis of the member response, one finds that tension-stiffening factor is a material property that is unaffected by the reinforcing ratio or concrete strength. Using this assumption and based on experimental findings, Fields and Bischoff suggest an exponential relationship to compute the tension stiffening bond factor in reinforced concrete (see Eq. 9-1).

$$\beta_t = e^{-800\left(\varepsilon_{tf} - \varepsilon_{cr}\right)} \qquad 9\text{-}1$$

Note that β_t is a factor that varies between 1 (just prior to cracking) and 0 (when there is a complete loss of bond). The quantity ε_{tf} represents the idealized concrete strain caused by a given stress and accounts for shrinkage. The value ε_{cr} represents the elastic strain in concrete at cracking.

Using this approach the post-cracking strength in the concrete can be computed using Eq. 9-2.

$$\sigma_c = f_{cr} \times \beta_t \qquad \text{for} \quad \varepsilon_{tf} \geq \varepsilon_{cr} \tag{9-2}$$

The quantity σ_c represents the post-cracking stress in the concrete as a function of axial strain ε_{cf} and β_t is computed using Eq. 9-1.

9.3 Model for the Pullout Response of Single Fibres

Most of the models available in the literature for the pullout strength of fibres are based on the assumption that the pullout strength is a function of the bond-shear strength between the fibre and the matrix. Many authors use this approach even in the case of hooked-end steel fibres using a bond-shear strength value that indirectly accounts for the contribution of the hooks to the pullout strength. Although this approach gives a satisfactory prediction of the total pullout strength, it does not adequately describe the various stages in the pullout process.

Several investigators have shown that the end-anchorage properties in steel fibres play a significant role in improving the pullout resistance (Alwan et al., 1991, Chanvillard and Aitcin, 1996). In the case of hooked-end steel fibres, Alwan et al. (1991) showed that the mechanical clamping of the hook plays a significant role in increasing the pull-out load, suggesting that the mechanical contribution of the hook is a function of the cold work needed to straighten the fibre as it is being pulled out from the matrix. Furthermore, Alwan et al. demonstrated that this contribution is approximately independent of matrix type and fibre embedment length.

Alwan et al. proposed that the various stages in the pullout process can be schematically described by Fig. 9.1. At load P_1 the fibre-matrix interface is assumed to be completely debonded. After debonding, a "mechanical clamping" stage follows in which the fibre hook is subjected to cold-work that causes the hook to deform, straighten and pullout from its print (loads P_3 and P_4).

Recall that the values P_3 and P_4 can be computed using Eq. 2-2 to 2-5 that were presented in Section 2.2. In the relationships for P_3 and P_4, the load P_1 represents the load at the onset of complete debonding while P_3 and P_4 represent the first and second pullout load plateaus respectively (see Fig. 9.1). The value $\Delta P'$ represents the mechanical pullout load contribution due to the formation of two plastic hinges, while $\Delta P''$ represents the corresponding value due to the formation of one plastic hinge. The displacement values Δ_3 and Δ_4 that are shown in Fig. 9.1 can be computed using Eq. 2-6 and 2-7 and are a function of the hook geometry (see Section 2.2).

The mechanical pullout contribution of the hook (for the type of steel fibre that was used in the experimental program) was computed using the procedure proposed by Alwan et al. (1991). Using Eq. 2-4 a value of 125 N was computed for $\Delta P'$, while Eq. 2-5 yielded a value of 51 N for $\Delta P''$.

In order to compute the total pullout strength one would have to compute the contribution at debonding (P_1) to the pullout strength. Grunewald (2004) reported that Kutzing (2000) performed a literature review on the average bond shear strength (τ_{bond}) from single fibre pull-out tests (see Table 9-1) for various ranges of concrete matrix strengths.

Table 9-1: Range of bond shear strength values for various concrete matrices
[Adapted from (Grunewald, 2004)]

Matrix Compressive strength class	Compressive strength range f'_{co} (MPa)	Bond shear stress τ_{bond} (MPa)
Normal strength	≤ 50	2.0-3.0
Medium strength	≥ 50 & ≤ 70	3.4-4.5
High strength	> 70	5.0-6.0

In the McGill experiments the matrix strength was near the upper value of the normal strength concrete range. This suggests, the shear bond strength (τ_{bond}) can be estimated as 3 MPa for the SFRC used in this experimental program.

Given this value, the expected pullout load at de-bonding, P_1 (for the straight portion of the fibre), can be calculated using the relationship proposed by Hannant in Section 2.2.2. In the computation one can take the embedment length as being equal to half the length of the straight portion of the fibre neglecting the hook (denoted by $L_{f,straight}$).

The total pullout load can be calculated using Eq. 9-3, by adding P_1 to the expected hook contribution during pullout, $\Delta P'$ (computed using Eq. 2-4). This calculation yields a total pullout strength of approximately 189 N.

$$F_{pullout} = \tau_{bond} \times \pi \times d_f \times \frac{L_{f,straight}}{2} + \Delta P' \qquad 9\text{-}3$$

In order to assess the accuracy of this approach, this value can be compared to some published experimental results from pullout tests performed by Armelin and Banthia (1997). In their test program, Dramix hooked-end steel fibres (similar in geometry to the fibre used in the experimental program performed at McGill) were embedded in a 58 MPa concrete matrix and tested under pullout loading. These authors found that for this type of matrix and fibre, an average pullout force of 173 N is obtained. One can see that the value computed using Eq. 9-3 agrees satisfactorily with the result from the Armelin and Banthia experiments.

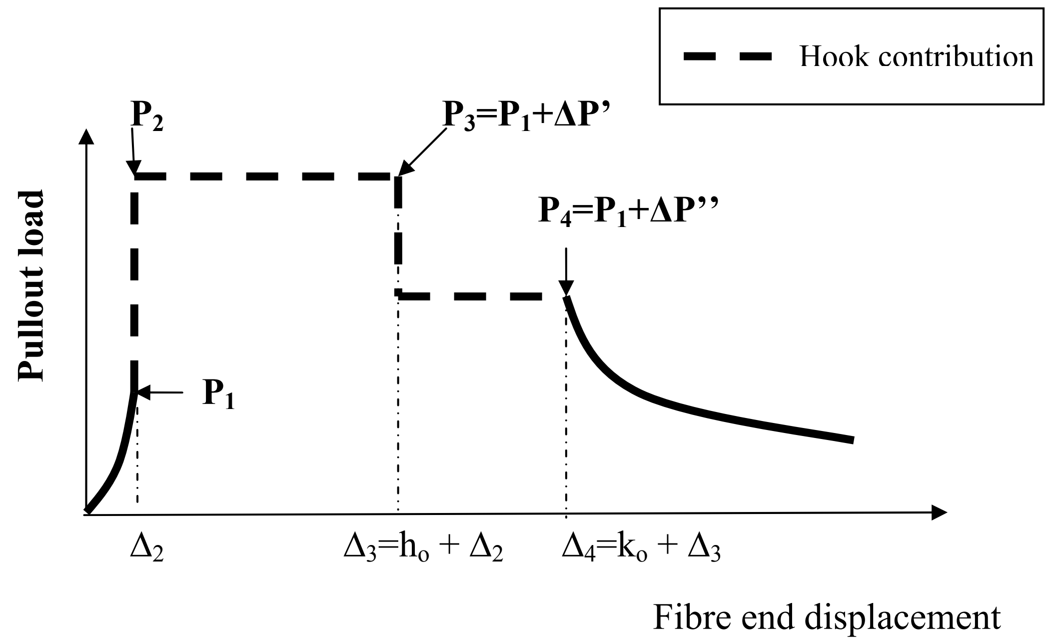

From Section 2.2:

$$P_3 = P_1 + \Delta P' \qquad 2\text{-}2$$

$$P_4 = P_1 + \Delta P'' \qquad 2\text{-}3$$

$$\Delta P' = \frac{\left[\dfrac{f_y \pi r_f^{\,2}}{3\cos\theta}\right]\left[1 + \dfrac{\mu\cos\beta}{(1-\mu\cos\beta)}\right]}{[1-\mu\cos\beta]} \qquad 2\text{-}4$$

$$\Delta P'' = \frac{\left[\dfrac{f_y \pi r_f^{\,2}}{6\cos\theta}\right]}{[1-\mu\cos\beta]} \qquad 2\text{-}5$$

Figure 9.1: Pullout curve for hooked end steel fibres according to Alwan et al. (1991)

9.4 Model for the Tension Stiffening in SFRC

Based on the assumptions presented in Section 9.3 a model that can predict the tensile response of SFRC was developed. The model parameters were derived based on the expected pullout behaviour of hooked-end steel fibres.

The proposed "pullout contribution curve" that is used to define a pullout factor "Ω" is described in Fig. 9.2. The curve has been derived based on the expected maximum pullout load of a single fibre, $F_{pullout}$ (computed using Eq. 9-3), and by using Eq. 2-4 and 2-5 to compute $\Delta P'$ and $\Delta P''$ to account for the pullout contribution provided by the hooked portion of the fibre. The various "Ω" values that describe the shape of the curve can be computed using the relationships in Eq. 9-4 to 9-7.

The displacement value Δ_1 is based on the assumption that de-bonding commences when the peak tensile strength of the plain concrete is reached. This assumption is made based on the observation that no gain in peak tensile capacity was seen in the SFRC specimens. Hence Δ_1 corresponds to Δ_{cr}, where Δ_{cr} is the displacement in the tension specimen corresponding to the elastic cracking strain of the concrete, ε_{cr}.

The value Δ_2 corresponds to the phase at which complete de-bonding has occurred (for the type of fibre used in this study this value is estimated as being equal to 0.2 mm). The displacements Δ_3 and Δ_4 can be computed using Eq. 2-6 and 2-7 and are a function of the hook geometry (based on the geometry of the fibre used in this study the quantities k and h are taken as being equal to 1.5 mm).

$$\Omega_m = \left(\frac{F_{pullout}}{F_{pullout}}\right) = 1.0 \qquad 9\text{-}4$$

$$\Omega_1 = \left(\frac{F_{pullout} - \Delta P'}{F_{pullout}}\right) \qquad 9\text{-}5$$

$$\Omega_3 = \left(\Omega_1 + \frac{\Delta P''}{F_{pullout}}\right) \qquad 9\text{-}6$$

$$\Omega_4 = \left(\frac{0.4 \times F_{pullout}}{F_{pullout}} \right) \qquad 9\text{-}7$$

The effective number of fibres per unit area, N_{fibres}, for fibres randomly oriented in three dimensions can be calculated using Eq. 6-5 which was presented in Section 6.4.1.

The contribution of the fibres to the post-cracking resistance, σ_{fib}, as a function of axial strain can be can be computed using Eq. 9-8.

$$\sigma_{fib} = N_{fibres} \times \Omega \times F_{pullout} \qquad 9\text{-}8$$

The fibre contribution can be added to the tensile contribution of the plain concrete to obtain the expected response of the SFRC as given in Eq. 9-19. Note that the concrete response σ_c is approximated using the model presented in Section 9.2

$$\sigma_{sfrc} = \sigma_c + \sigma_{fib} \qquad 9\text{-}9$$

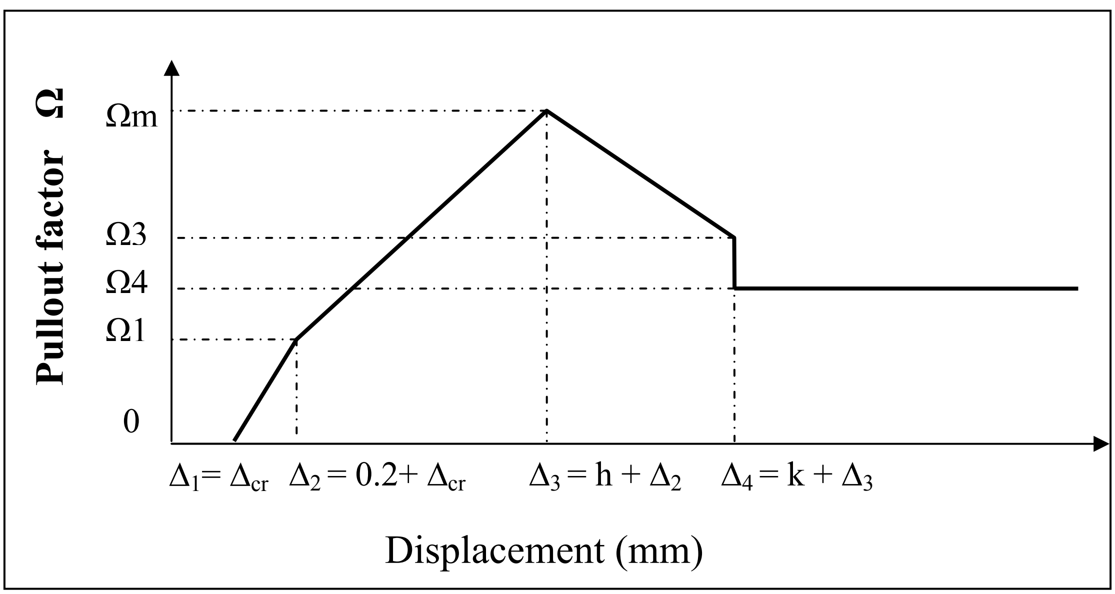

Figure 9.2: Schematic representation of the idealised pullout curve showing the pullout factor, Ω, as a function of displacement

9.5 Predictions of the Tensile Responses using the Analytical Models

Figure 9.3 shows the tensile response of the plain concrete specimen. The predicted response was computed using the Fields and Bischoff model presented in Section 9.2. One can see that there is good agreement between the actual and estimated results.

Figure 9.4 shows the isolated fibre contributions to tensile stress. The predicted response for each fibre content was computed using Eq. 9-8. One can see that estimated responses agree well with the actual responses for both fibre contents.

Finally, Fig. 9.5 shows that the post-cracking response of the SFRC, as computed using Eq. 9-9, satisfactorily predicts the actual tension stiffening response of the SFRC for both fibre contents.

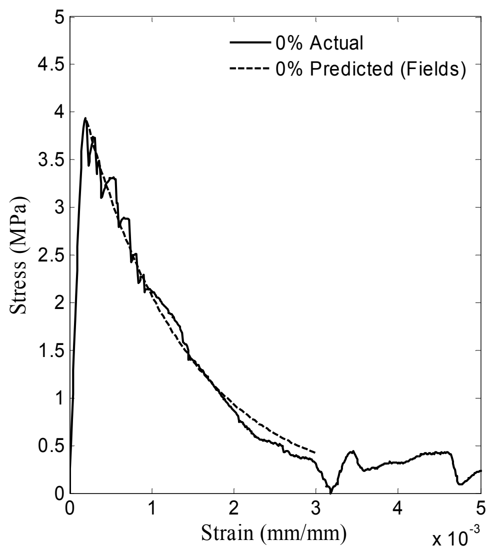

Figure 9.3: Actual and predicted tension stiffening responses for the plain concrete specimen

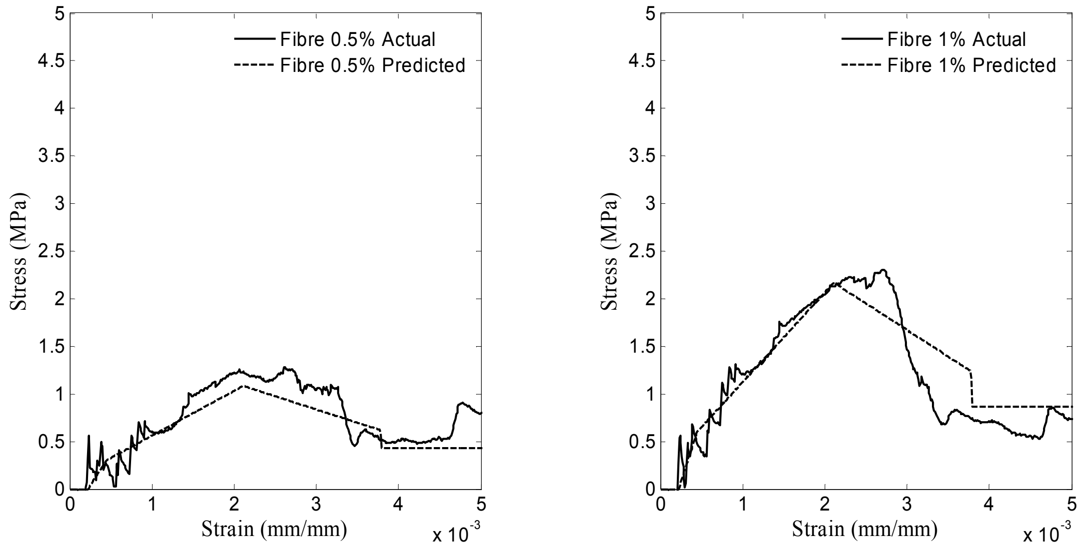

(a) Predicted fibre contribution: $v_f = 0.5\%$ (b) Predicted fibre contribution: $v_f = 1\%$

Figure 9.4: Actual and predicted fibre contributions

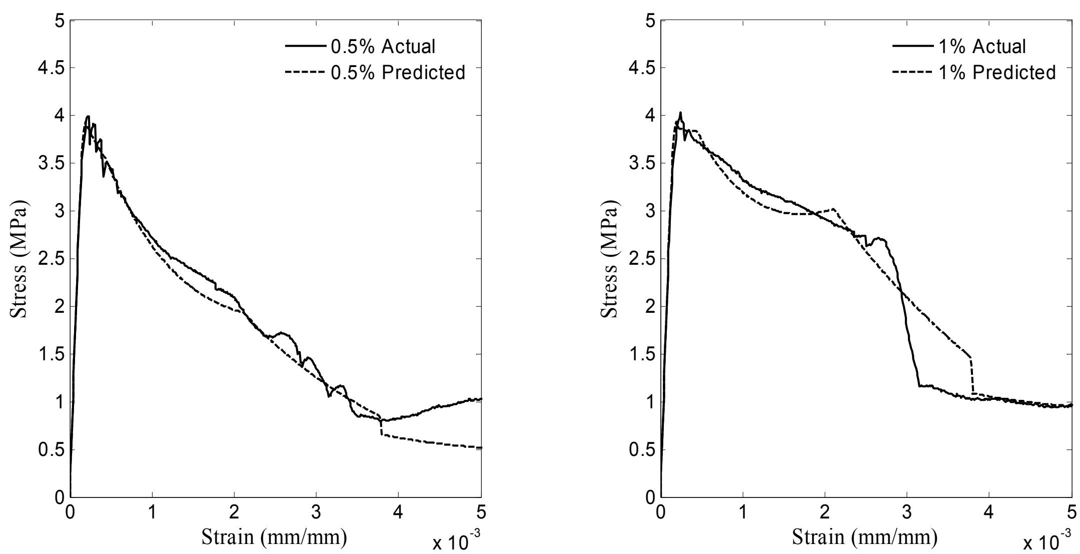

(a) Predicted tension stiffening: $v_f = 0.5\%$ (b) Predicted tension stiffening: $v_f = 1\%$

Figure 9.5: Actual and predicted tension stiffening responses of SFRC

9.6 Concluding Remarks

A procedure for predicting the influence of fibres on the tension stiffening response of concrete was presented. This method uses an approach where the tension stiffening response of concrete is adjusted for the presence of fibres based on the expected pullout behaviour of the hooked-end steel fibres. The method provides reasonably accurate predictions for the various specimens that were tested in this experimental program.

Chapter 10 Experimental Program on the Effect of Steel Fibre Reinforced Concrete on the Shear Resistance of Beams

10.1 Objectives

The objective of this phase of the research program was to investigate the influence of steel fibres on the structural response of RC beam elements (shear resistance, crack control and flexural response). An additional objective was to examine if the addition of fibres can substitute for the traditional shear reinforcement in RC beams.

10.2 Description of Test Specimens

The experimental program involved the testing of three specimens containing varying amounts of steel fibres. Figure 10.1 shows the geometry for a typical specimen. The details regarding the fibre content and cross-sectional properties are given in Table 10-1. All of the beams were 150 mm wide, 250 mm deep and had a span of 2 m. Two 15M reinforcing bars were provided in each beam, resulting in a reinforcement ratio of 1.07%. In addition a 40 mm clear cover was provided in each specimen. Specimen B0.0% contained no fibres while Specimens B0.5% and B1.0% were constructed with concrete containing steel fibres in a quantity of 0.5% and 1% by volume, respectively. All the specimens were constructed without web reinforcement in order to examine the influence of the fibres in improving the response.

Table 10-1: Design details for the various beam specimens

Beam specimen	Cross-Section	Specimen Length	Flexural reinforcement	a/d ratio	Transverse reinforcement	% Fibres
B0.0%	150 mm x 250 mm	2000 mm	2 - 15M	2.97	N/A	0.0%
B0.5%						0.5%
B1.0%						1.0%

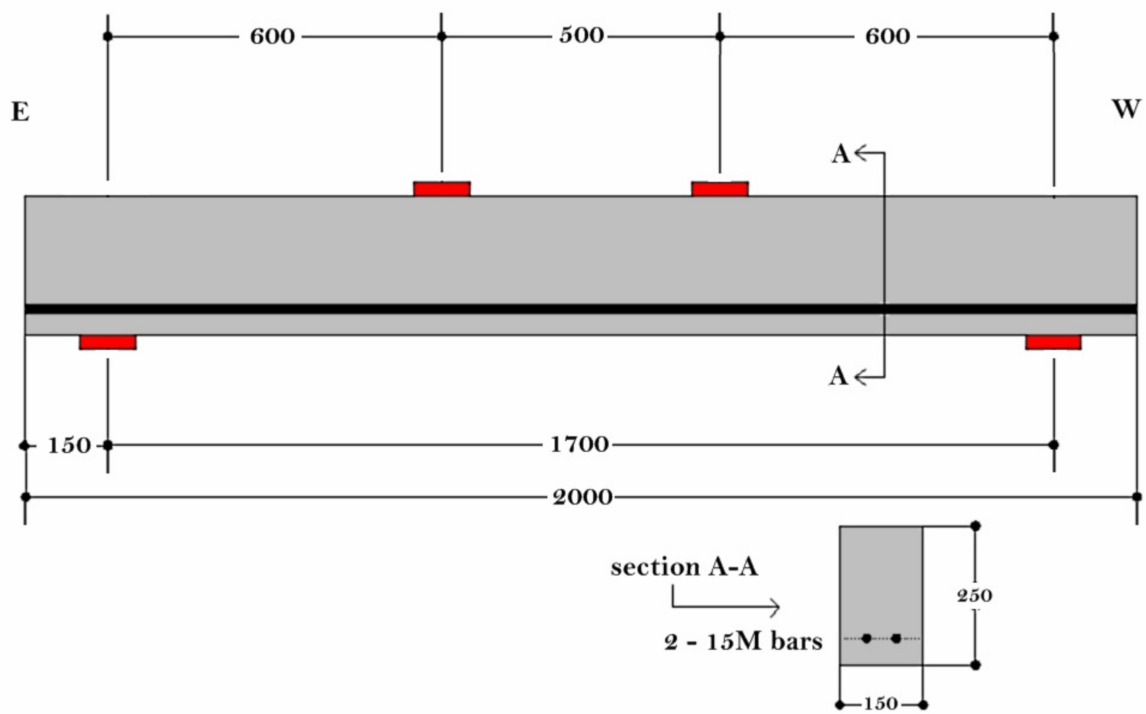

Figure 10.1: Beam test specimens

10.3 Material Properties

10.3.1 Reinforcing steel

The properties of the reinforcing steel are summarized in Table 10-2. The longitudinal reinforcement in all of the specimens had a specified yield strength of 400 MPa. Tension tests were performed on three random specimens for each bar size. The typical stress strain relationship of the15M reinforcing bars (d_b = 16 mm, A_s = 200 mm^2) is shown in Fig. 10.2.

Table 10-2: Reinforcing steel properties

Bar description	f_y (MPa) [std. dev.]	ε_{sh} (mm/mm) [std. dev.]	f_u (MPa) [std. dev.]	ε_u (mm/mm) [std. dev.]
15M	478 [12.8]	0.0207 [0.0013]	588.6 [12.2]	0.1679 [0.0061]

10.3.2 Steel fibres

In this testing program, hooked end steel fibres that were 30 mm in length (Bekaert Dramix ZP-305), were used to attain 0.5% fibre reinforcement (38.4 kg/m3) and 1% fibre reinforcement (76.8 kg/m3) by volume of concrete. The details regarding the properties of the fibre are presented in Table 10-3.

Table 10-3: Steel fibre properties

Fibre type	Length l_f (mm)	Diameter d_f (mm)	Aspect ratio $\frac{l_f}{d_f}$ (mm/mm)	Tensile strength f_{fy} (MPa)
Dramix ZP-305	30	0.55	55	1100

10.3.3 Concrete

The specimens were cast using three batches of normal-strength concrete having varying fibre contents. The first batch contained no fibres while a fibre content of 0.5% and 1% was used for batches 2 and 3 respectively. All the concrete used to construct the specimens was provided by a local ready-mix plant. Table 10-4 summarizes the composition of these concretes. It is noted that batches 1 through 3 were exact in composition except for the amount of fibres and the quantity of superplasticizer in each mix. A series of lab cured cylinders and flexural beams were prepared and tested to determine the concrete properties of each batch used during the casting of the beams.

Table 10-5 summarizes the various concrete properties. The concrete compressive strengths were obtained by testing standard cylinders, having a diameter of 150 mm and a height of 300 mm. At the time of testing the plain concrete mix had a compressive strength, f'_{co}, of 23.6 MPa while the concrete mixes containing 0.5% fibres and 1% fibres by volume had strengths of 21.3 MPa and 19.6 MPa respectively.

The average splitting tensile strengths, f_{sp}, ranged in between 2.3 and 2.2 MPa for the three batches. The splitting tests were carried out on standard cylinders 150 mm in diameter and 300 mm in length. The average moduli of rupture values, f_r, were obtained by testing beams that were 100 mm by 100 mm by 400 mm in size that were subjected to third point loading over a span of 300 mm

Figure 10.3(a) shows the compressive stress-strain responses for the various concretes. Figure 10.3(b) shows the load deflection responses obtained from the modulus of rupture tests. As expected, one can see that the addition of fibres, has significantly improved both concrete properties.

Table 10-4: Composition of the concretes used in the various specimens

Characteristics	Quantity	Batch 1 (0 % fibres)	Batch 2 (0.5 % fibres)	Batch 3 (1.0 % fibres)
cement (Type 10)	kg/m^3	290	290	290
coarse aggregates (20mm)		350	350	350
coarse aggregates (14mm)		525	525	525
fine aggregates (sand)		980	980	980
water		175	175	175
steel fibre content		0 (0%)	40 (0.5%)	80 (1%)
water reducing agent	ml/100 kg	250	250	250
superplasticizer	ml/m^3	2000	1000	1500
slump	mm	250	160	150
air content	%	5.5	8.0	11
Density	kg/m^3	2312	2311	2309

Table 10-5: Concrete properties

Series	f'_{co} (MPa) [std. dev.]	f_{sp} (MPa) [std. dev.]	f_r (MPa) [std. dev.]
Batch 1 - 0%	23.6 [0.68]	2.28 [0.13]	4.32 [0.02]
Batch 2 - 0.5%	21.3 [1.26]	2.20 [0.21]	3.62 [0.13]
Batch 3 - 1.0 %	19.6 [0.35]	2.30 [0.30]	4.04 [0.14]

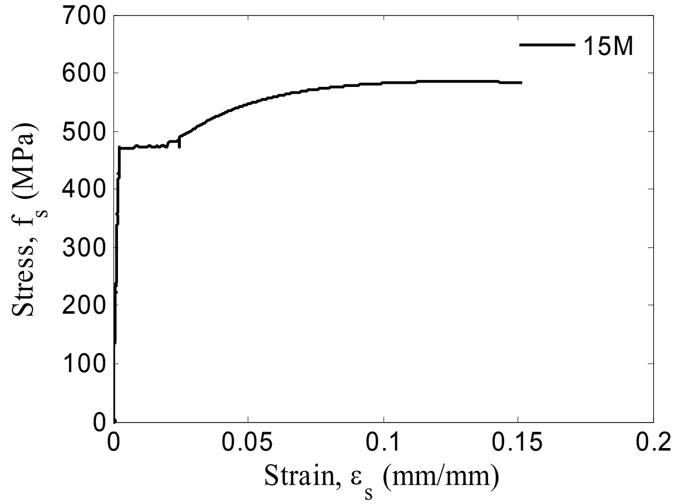

Figure 10.2: Stress-strain responses for 15M reinforcing bars

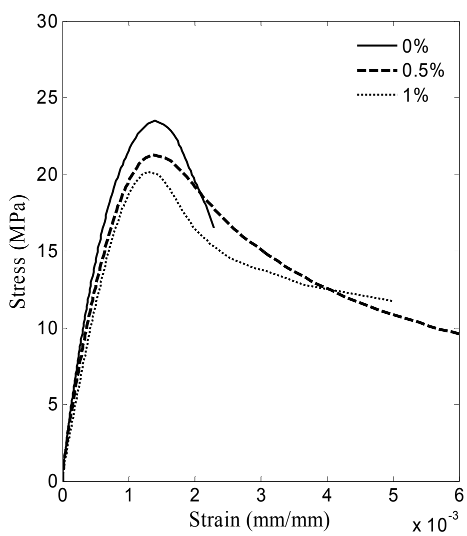

(a) Compressive stress-strain curves

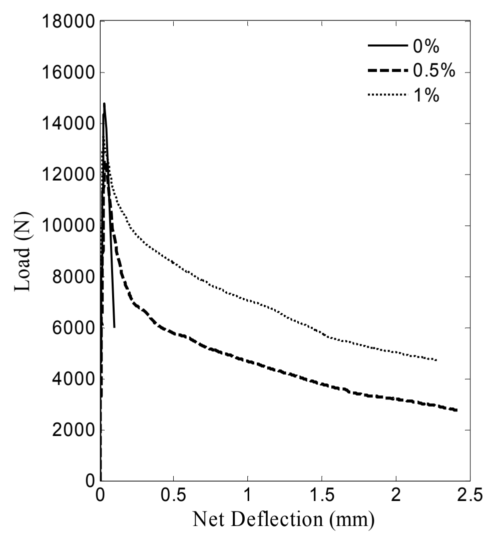

(b) Flexural beam load-deflection curves

Figure 10.3: Typical results from the concrete material tests

10.4 Testing

All the beams were simply supported over a length of 1700 mm and were subjected to four point loading with a shear span of 600 mm (resulting in a shear span-to-depth ratio, a/d, of approximately 3) and had a constant moment region of 500 mm. The load transfer and support details are shown in Fig. 10.6. The loads were applied to the specimens using the 11,400 kN capacity MTS testing machine in the Jamieson Structures Laboratory in the Department of Civil Engineering and Applied Mechanics at McGill University. Figure 10.5 shows a typical specimen prior to testing

The internal load cell of the universal testing machine was used to measure the axial load that was applied to the various specimens. In addition, several linear voltage differential transducers (LVDTs) were utilized to measure the concrete strains and vertical displacements at various locations in the beams. Figure 10.8 shows the localization of the transducers. Three LVDTS were placed in a rosette pattern in each shear span in order to intercept the diagonal cracks that were expected to form. In addition, vertical LVDTs were placed at midspan, below the loading points and at the two supports.

Electrical resistance strain gauges were glued to one reinforcing bar in each specimen in order to measure the tensile strains in the longitudinal rebar. As shown in Fig. 10.7, the gauges were located at midspan, at the point-load locations and at the support points.

All the specimens were tested in the same manner. A loading rate of 1 kN/min was used up to a load of 26 kN. Subsequent to this load stage, the loading was switched to "deflection control" at a rate of 0.075 mm/min until the failure of the specimen was detected or the resistance of the specimen dropped to 85% of the peak value. The first load stage L1 was set at 16 kN and subsequent to this load, the load stages were set at 4 kN intervals until the end of testing. Throughout the experiments, observations regarding crack widths and failure mechanisms were made.

Figure 10.4: Specimen and formwork prior to casting

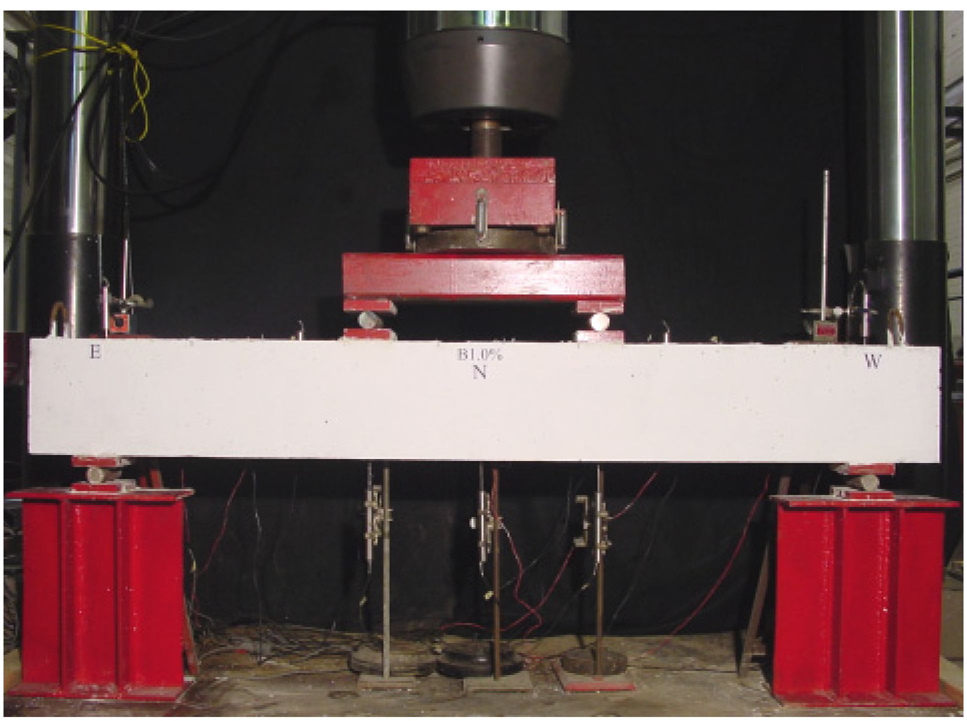

Figure 10.5: Beam specimen just prior to testing

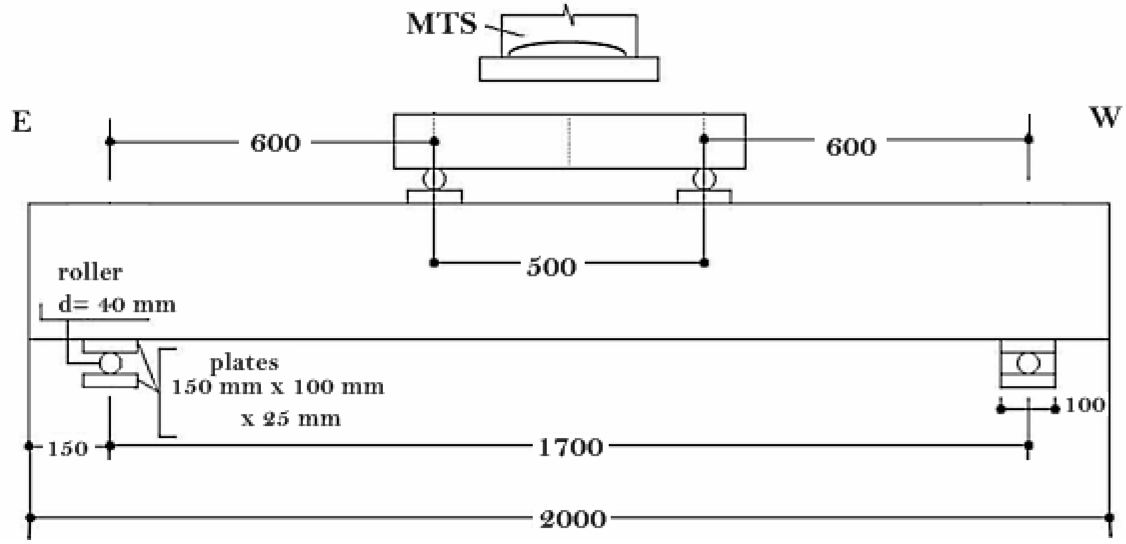

Figure 10.6: Load transfer and support details

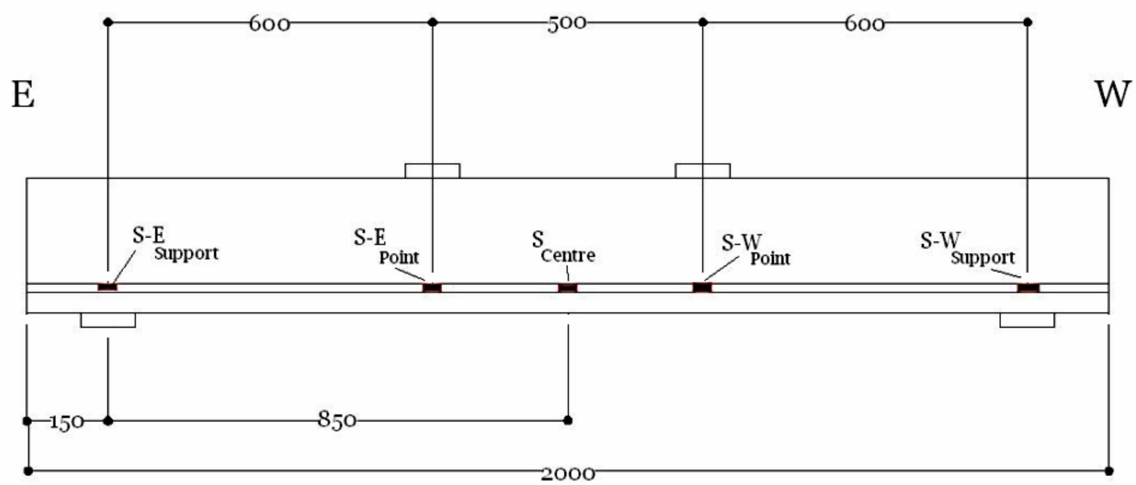

Figure 10.7: Locations of the strain gauges in a typical specimen

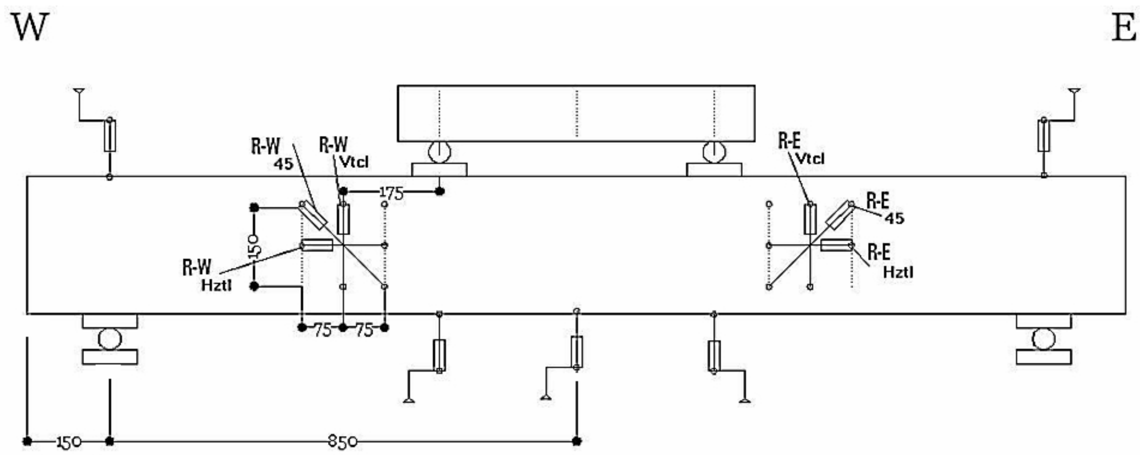

Figure 10.8: Locations of the LVDTs

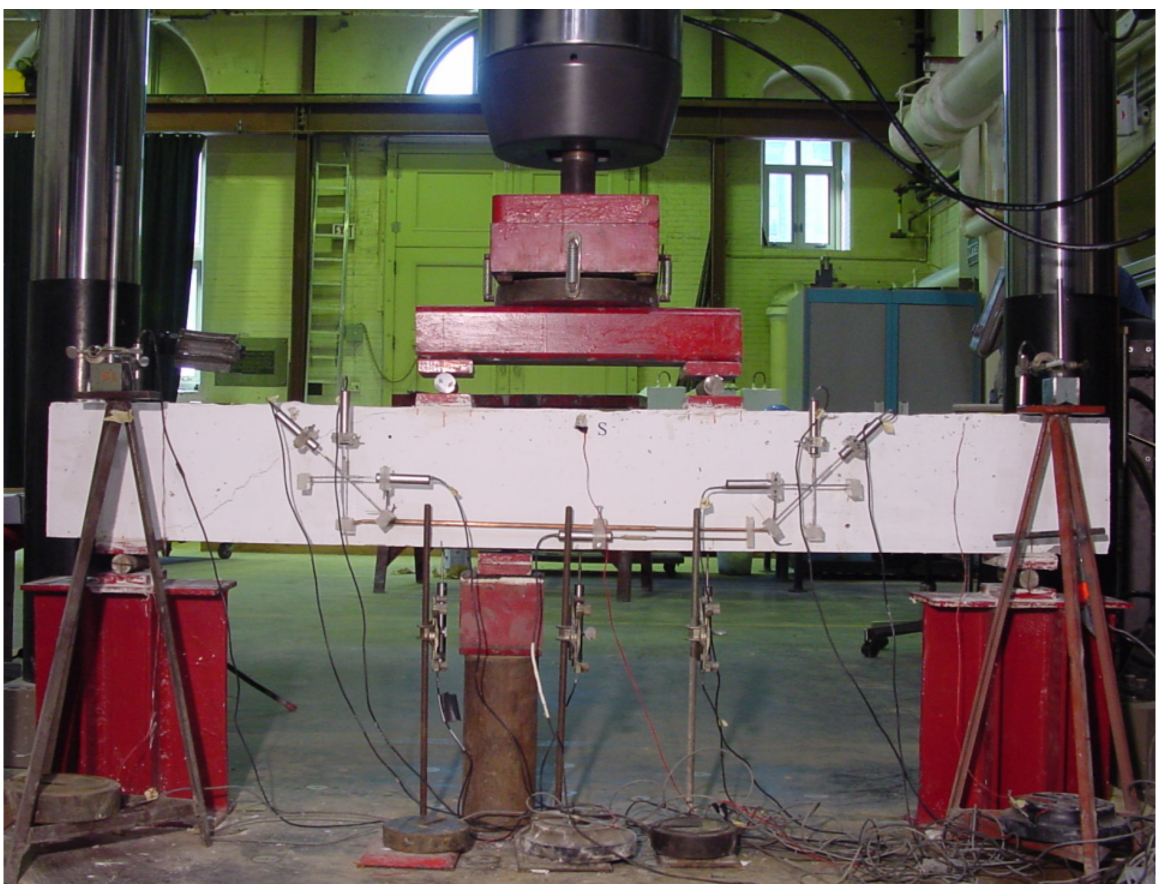

Figure 10.9: Picture of specimen showing the LVDTs and the rosette arrangements

Chapter 11 Experimental Results for the Beam Specimens

11.1 Chapter Overview

In this chapter the behaviour of the three beam specimens is discussed. Section 11.2 presents the experimental results. Section 11.3 compares the results from the various specimens and discusses the main advantages that result from the use of steel fibres in RC beams.

11.2 Experimental Results

The load-deflection responses for the three beams as well as the measured strains in the concrete and steel reinforcement are presented in this section.

11.2.1 Specimen B0.0%

Specimen B0.0% was constructed without web reinforcement and contained no fibres. A loading rate of 1 kN/min was applied to the specimen until the load reached 24 kN (corresponding to a shear load, V, of 12 kN). At that stage, loading was switched to deflection control at a rate of 0.075 mm/min until failure of the specimen.

Figure 11.1 summarizes the major events that occurred during the testing of this beam. The first hairline cracks occurred at an applied load of approximately 8 kN (V = 4 kN). The first flexural-shear cracks began to form on the East shear-span of the beam at a load of approximately 30 kN (V = 15 kN). Soon thereafter, further flexural cracks appeared on the West side of the beam (at V= 23 kN). At a load of approximately, 73 kN (V = 36.5 kN) a sudden shear crack formed on the West side of the beam resulting in a brittle shear failure with a sudden loss in load carrying capacity.

Figure 11.2 (a) shows a plot of the shear load that was applied to the specimen versus the corresponding mid-span deflection. The failure occurred at shear load of 36.5 kN with a corresponding mid-span deflection of approximately 4.9 mm. As was expected, due to the fact that no shear reinforcement was present in this RC beam specimen, the specimen showed a brittle shear response well before the flexural capacity could be reached.

Figure 11.2 (b) shows the measured strains in the longitudinal steel reinforcement. Due to the fact that the specimen showed a brittle shear response, failure occurred well before yielding of the longitudinal reinforcement could be attained. For example, the measured strain in the longitudinal reinforcement at mid-span only reached a maximum tensile strain of 1519 με.

The strains in the concrete were measured by means of two rosettes that were strategically placed at the locations of expected shear cracking. The measured strains in the East side and West side rosettes are shown in Fig. 11.2(c) and 11.2(d) respectively. A comparison of the strain measurements clearly shows that the failure occurred on the West side of the beam as evident by the large jump in strains in the LVDT that was placed at 45^{o} at this location. This LVDT showed a maximum concrete strain of 6380 με. The fact that the companion LVDT on the East side of the beam only showed a maximum strain of 1800 με demonstrates that the failure occurred in a sudden and brittle manner (since it was observed that both LVDTs were registering similar strain values just prior to failure).

The maximum crack width just prior to the brittle shear failure was 0.05 mm for the main flexural-shear crack in the West shear span, while the largest flexural crack reached a maximum value of 0.2 mm at midspan. The shear crack after failure was 0.6 mm.

Load stage	V (kN)	Mid-span Δ (mm)	
L2	4	0.23	- First hairline cracks appear in the constant moment region

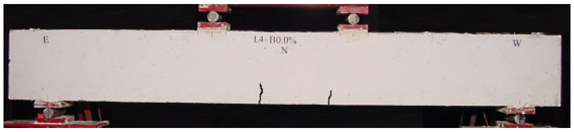

Load stage	V (kN)	Mid-span Δ (mm)	
L8	15	1.52	- First crack appears outside the constant moment region

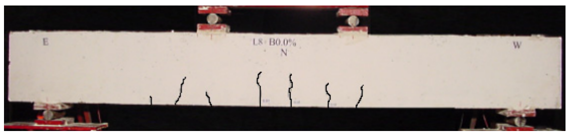

Load stage	V (kN)	Mid-span Δ (mm)	
L12	23	2.66	- Flexural-shear crack beginning to form on the E-side of the beam

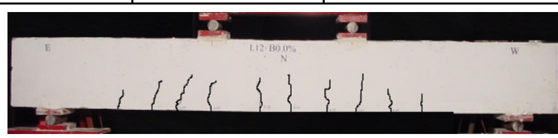

Load stage	V (kN)	Mid-span Δ (mm)	
L15	29	3.55	- Flexural-shear crack beginning to form on the W-side of the beam

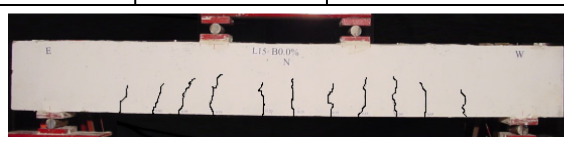

Load stage	V (kN)	Mid-span Δ (mm)	
L19	36.5	4.90	- Sudden formation of shear crack on the W side of the beam, - Peak capacity reached

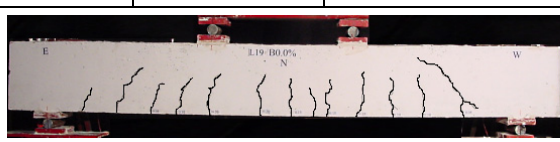

Load stage	V (kN)	Mid-span Δ (mm)	
failure	36.5	4.90	- Specimen fails (brittle shear failure)

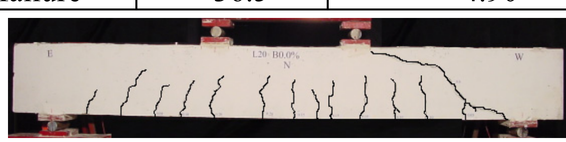

Figure 11.1: Major events for specimen B0.0%

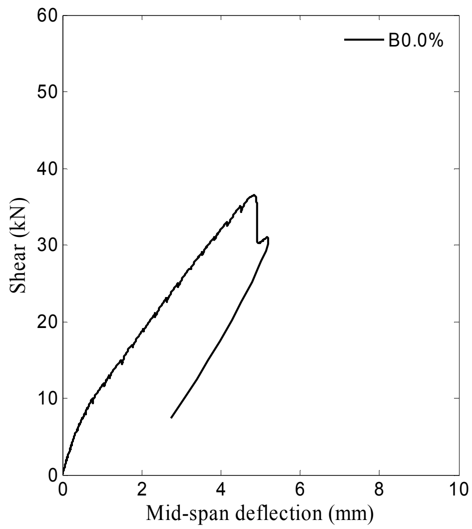

(a) Shear-load versus mid-span deflection

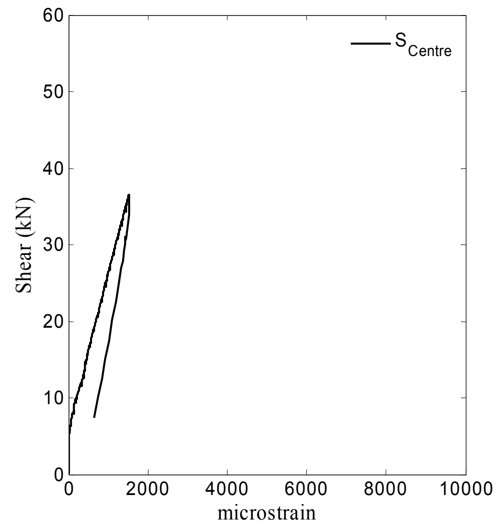

(b) Tensile strains in the longitudinal reinforcement

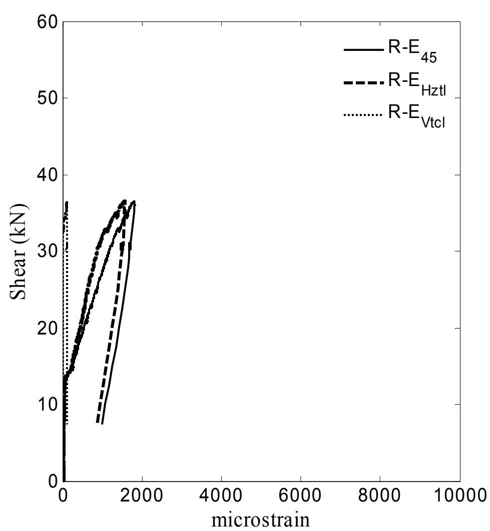

(c) Strains in the East-side Rosette LVDTs

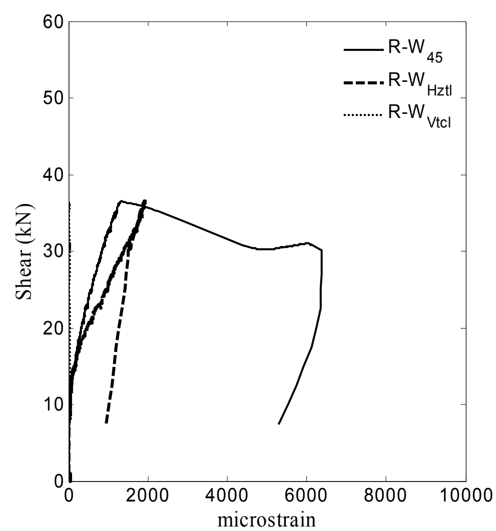

(d) Strains in the West-side Rosette LVDTs

Figure 11.2: Experimental shear-deflection curve for Specimen B0.0%

11.2.2 Specimen B0.5%

Specimen B0.5% was constructed with the same details as Specimen B0.0% but contained fibre reinforcement in a quantity of 0.5% by volume of concrete. It was expected that the addition of fibres would lead to an increase in the maximum shear capacity of the beam while also improving the crack control in the specimen.

The same loading sequence used in the testing of Specimen B0.0% was used in the testing of this specimen. Figure 11.3 summarizes the major events that occurred during the testing of this beam. The first signs of cracking occurred at a load of 10 kN (V = 5 kN), with a couple of hairline cracks appearing in the constant moment region of the beam. At a load of 42 kN (V = 21 kN), the first crack formed outside the constant moment region. The first flexural-shear cracks began to clearly form on the West shear-span of the beam at a load of approximately 62 kN (V = 31 kN). At a load of 70 kN (V = 35 kN) a flexural-shear crack formed on the East side of the beam. This crack would eventually develop into the shear crack that led to the shear failure of the specimen. In fact, at a load of approximately, 86 kN (V = 43 kN) a sudden shear crack formed on the East side of the beam extending to both support locations, resulting in a shear failure soon thereafter with a sudden loss in load carrying capacity.

Figure 11.4 (a) shows a plot of the shear load that was applied to the specimen versus the corresponding midspan deflection. The failure occurred at load of 96 kN (V = 48 kN) with a corresponding midspan deflection of approximately 7.8 mm. Although the fibres have allowed the beam to reach an improved level of shear resistance, the fibres were not sufficient in quantity to allow the beam to reach its flexural capacity, and therefore this specimen experienced a brittle shear failure

Figure 11.4 (b) shows the measured strains in the longitudinal steel reinforcement. Due to the fact that the specimen showed a brittle shear response, failure occurred prior to the yielding of the longitudinal reinforcement. For instance, the measured strain in the longitudinal reinforcement at mid-span reached a maximum tensile strain of approximately 2082 $\mu\varepsilon$.

The measured concrete strains in the East side and West side rosettes are shown in Fig. 11.4(c) and 11.4(d) respectively. A comparison of the strain measurements shows that the failure occurred on the East side of the beam as evident by the large jump in strains in the LVDT that was placed at 45^{o} in this location. This LVDT showed a maximum concrete strain of 8000 με, a value which is slightly higher than the measurements observed in the critical rosette of Specimen B0.0%

The maximum crack width just prior to the brittle shear failure was 0.2 mm for the main flexural-shear crack in the East shear span, while the largest flexural crack reached a maximum value of 0.3 mm at midspan. The shear crack after failure was 1 mm.

Load stage	V (kN)	Mid-span Δ (mm)	
L2	4	0.23	- First hairline cracks appear in the constant moment region
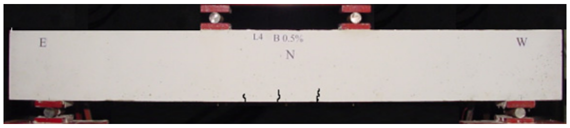			
Load stage	V (kN)	Mid-span Δ (mm)	
L8	21	2.21	- First cracks appear outside the constant moment region
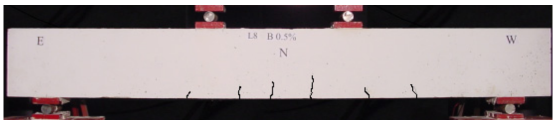			
Load stage	V (kN)	Mid-span Δ (mm)	
L13	31	3.68	- Flexural-shear crack beginning to form on the W-side of the beam
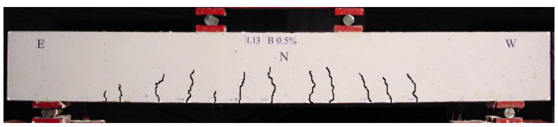			
Load stage	V (kN)	Mid-span Δ (mm)	
L15	35	4.34	- Flexural-shear crack beginning to form on the E-side of the beam
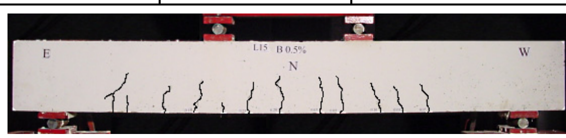			
Load stage	V (kN)	Mid-span Δ (mm)	
L19	43	5.79	- Shear crack forming on the E-side of the beam
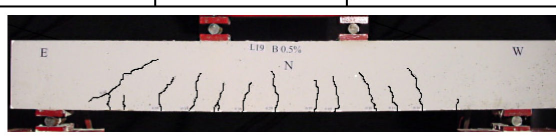			
Load stage	V (kN)	Mid-span Δ (mm)	
L22	48	7.82	- Extension of the shear crack on the E-side of the beam, with shear crack forming on W-side. - Peak capacity reached
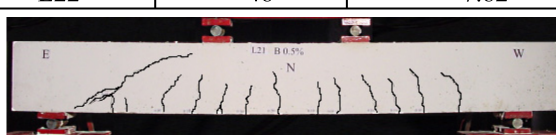			
Load stage	V (kN)	Mid-span Δ (mm)	
Failure	48	7.82	- Specimen fails
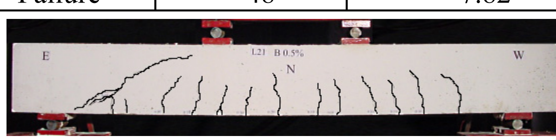			

Figure 11.3: Major events for specimen B0.5%

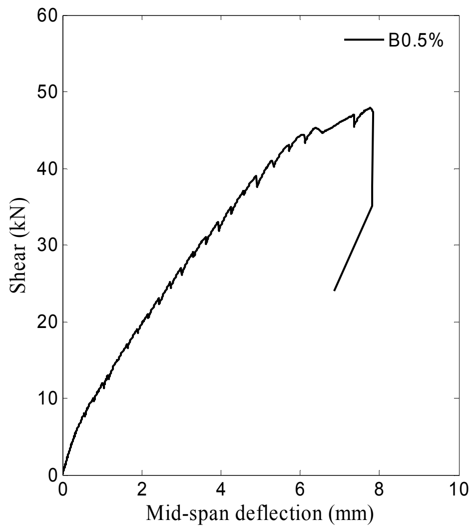

(a) Shear-load versus mid-span deflection

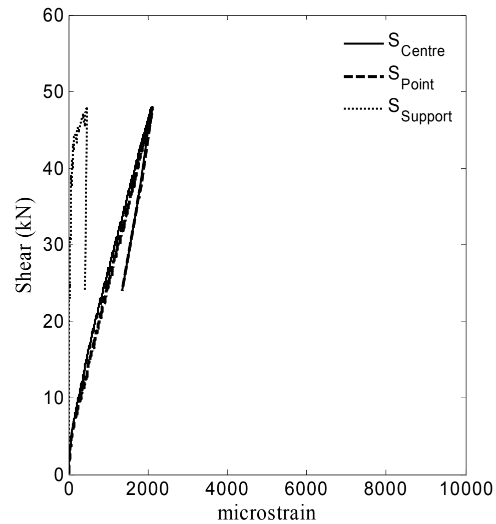

(b) Tensile strains in the longitudinal reinforcement

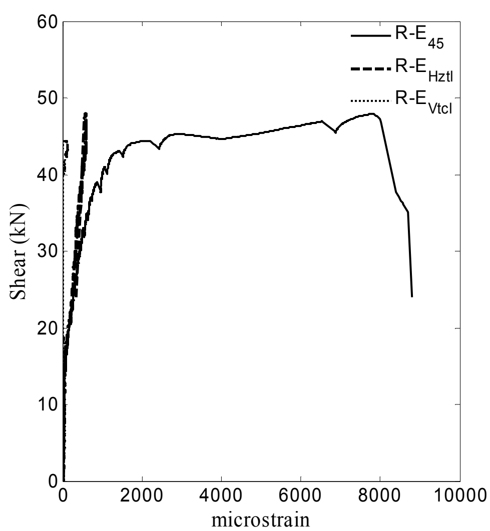

(c) Strains in the East-side Rosette LVDTs

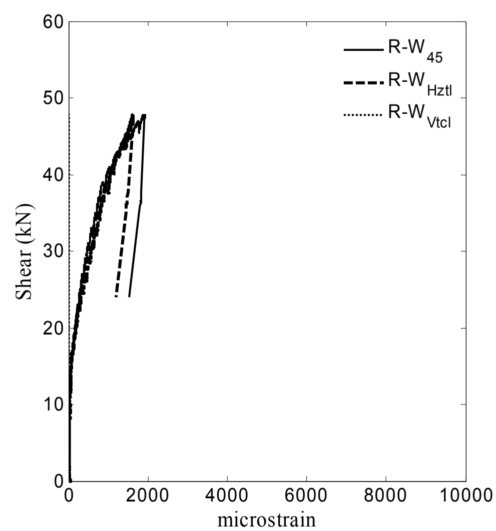

(d) Strains in the West-side Rosette LVDTs

Figure 11.4: Experimental shear-deflection curve for specimen B0.5%

11.2.3 Specimen B1.0%

Specimen B1.0% had the same details as Specimen B0.0% but was constructed with a concrete that had a fibre content of 1% by volume. In addition to improving the shear capacity of the beam and crack control, it was expected that this fibre content would be sufficient to transform the failure mechanism of the specimen from a brittle shear failure to a ductile flexural failure.

Figure 11.5 summarizes the major events that occurred during the testing of this specimen. In accordance with observations made during the testing of the two previous specimens, the first signs of cracking were observed near the mid-span of the beam at a load of 12 kN (V = 6 kN). Therefore, one can conclude that the addition of fibres does not significantly affect the cracking strength of the concrete at this fibre quantity (this was also observed in the tensile test series).

At a load of 42 kN (V = 21 kN), the first crack forms outside the constant moment region. The first flexural-shear cracks began to clearly form on the West shear-span of the beam at a load of approximately 58 kN (V = 29 kN). At a load of 94 kN (V = 47 kN) a sudden shear crack formed on the East side of the beam. However, although the shear crack formed suddenly, it did not lead to a loss in load carrying capacity. Rather, the fibres were able to control the shear cracks and sustain load for significantly large deflections. As loading continued it was noted that many of the cracks showed a “forking” cracking pattern close to the tensile face of the member.

Subsequent to this event, the beam was able to reach its flexural capacity, with flexural yielding of the longitudinal reinforcement at midspan. At this stage the flexural cracks began to grow with increasing load, with the shear cracks now stabilizing at a crack width of 1 mm for the remainder of the test. At a mid-span deflection of 18 mm, signs of crushing were observed on the compression side of the beam at mid-span. Soon thereafter the load began to drop in a stable manner. The test was stopped at a deflection of 32 mm, when the capacity of the specimen reached 85% of its peak resistance.

Figure 11.6 (a) shows a plot of the shear load that was applied to the specimen versus the corresponding midspan deflection. The maximum sustained load was 113 kN (V = 57 kN) and the capacity of the beam dropped below 85% of this maximum resistance at a mid-span deflection of approximately 32 mm, with a displacement ductility of 3.1. As in Specimen B0.5%, the fibres have allowed the beam to reach an improved level of shear resistance. However in contrast to the observations made in B0.5%, the fibres were sufficient in quantity in order to allow the beam to reach its flexural capacity, and therefore this specimen experienced a ductile flexural failure

Figure 11.6 (b) shows the measured strains in the longitudinal steel reinforcement. Since this specimen displayed a ductile flexural response, yielding of the longitudinal reinforcement occurred, with the development of the yield plateau and some strain hardening before failure. At the end of testing the measured strain in the longitudinal reinforcement at mid-span reached a maximum value of approximately 14000 με.

The measured concrete strains in the East side and West side rosettes are shown in Fig. 11.6(c) and 11.6(d) respectively. A comparison of the strain measurements shows that both shear spans experienced shear cracking as demonstrated by the significant strains measured by the diagonal LVDTS. These LVDTs showed a maximum concrete strain of 3500 με, and 5800 με respectively.

The maximum crack widths were 0.5 mm (flexural) and 0.7 mm (shear) when the specimen reached its peak capacity. At failure the largest flexural crack reached a maximum value greater than 4 mm at midspan, while the main shear crack at failure had a width of 1 mm.

<table>
<tr><td>Load stage</td><td>V (kN)</td><td>Mid-span Δ (mm)</td><td rowspan="3">- First hairline cracks appear in the constant moment region</td></tr>
<tr><td>L2</td><td>6</td><td>0.43</td></tr>
<tr><td colspan="3">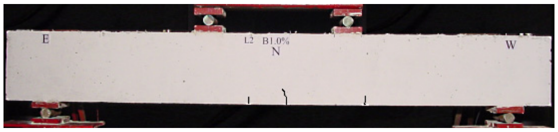</td></tr>
<tr><td>Load stage</td><td>V (kN)</td><td>Mid-span Δ (mm)</td><td rowspan="3">- First cracks appears outside the constant moment region</td></tr>
<tr><td>L8</td><td>21</td><td>2.44</td></tr>
<tr><td colspan="3">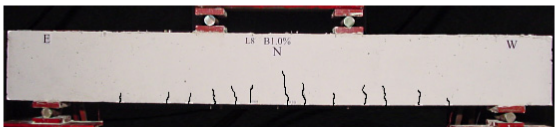</td></tr>
<tr><td>Load stage</td><td>V (kN)</td><td>Mid-span Δ (mm)</td><td rowspan="3">- Flexural-shear crack beginning to form on the W-side of the beam</td></tr>
<tr><td>L12</td><td>29</td><td>3.66</td></tr>
<tr><td colspan="3">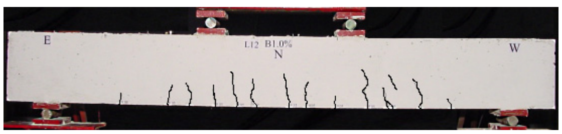</td></tr>
<tr><td>Load stage</td><td>V (kN)</td><td>Mid-span Δ (mm)</td><td rowspan="3">- “Forking” cracks beginning to form
- Shear crack suddenly forms on the E-side of the beam</td></tr>
<tr><td>L21</td><td>47</td><td>6.94</td></tr>
<tr><td colspan="3">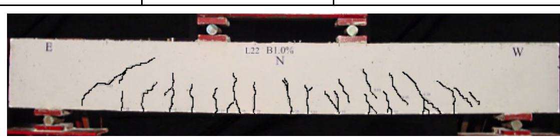</td></tr>
<tr><td>Load stage</td><td>V (kN)</td><td>Mid-span Δ (mm)</td><td rowspan="3">- Flexural yielding at midspan
- Peak capacity reached</td></tr>
<tr><td>L25</td><td>57</td><td>10.5</td></tr>
<tr><td colspan="3">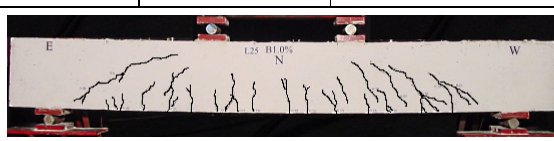</td></tr>
<tr><td>Load stage</td><td>V (kN)</td><td>Mid-span Δ (mm)</td><td rowspan="3">- Signs of crushing on the compression side of the beam at midspan
- Flexural cracks (>2 mm)</td></tr>
<tr><td>L32</td><td>57</td><td>13.60</td></tr>
<tr><td colspan="3">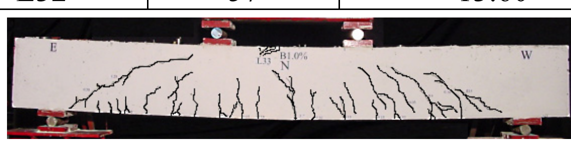</td></tr>
<tr><td>Load stage</td><td>V (kN)</td><td>Mid-span Δ (mm)</td><td rowspan="3">- Failure of specimen (capacity drops to 85% of peak value)</td></tr>
<tr><td>Failure</td><td>51</td><td>32</td></tr>
<tr><td colspan="3">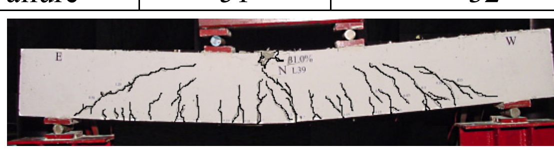</td></tr>
</table>

Figure 11.5: Major events for specimen B1.0%

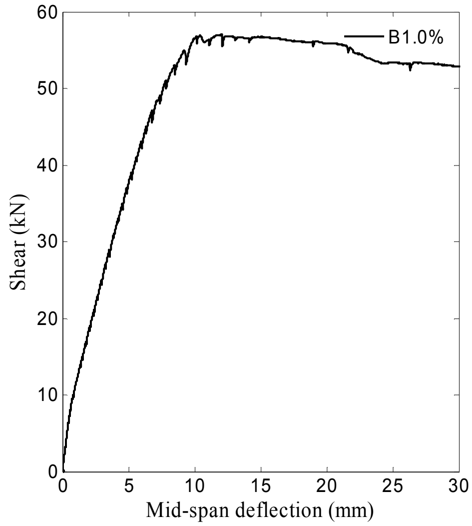

(a) Shear-load versus mid-span deflection

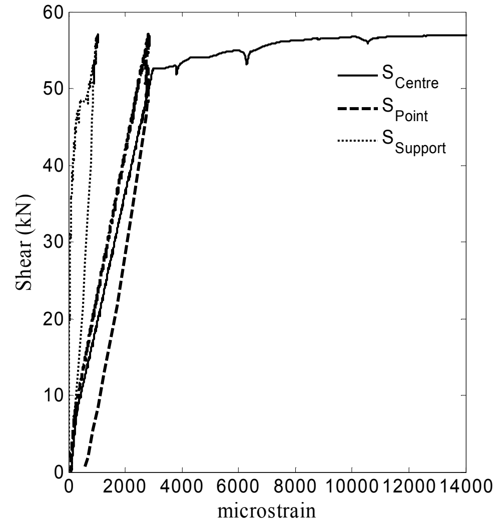

(b) Tensile strains in the longitudinal reinforcement

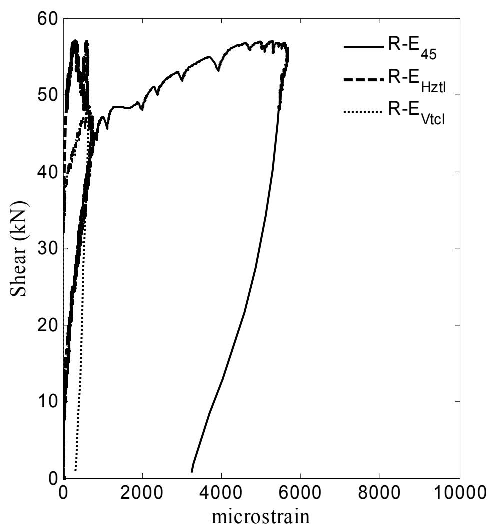

(c) Strains in the East-side Rosette LVDTs

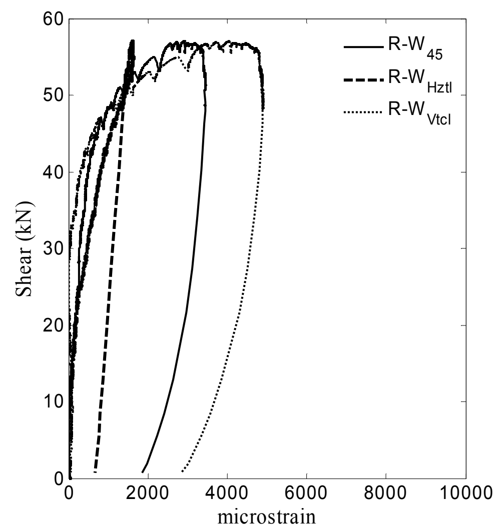

(d) Strains in the West-side Rosette LVDTs

Figure 11.6: Experimental shear-deflection curve for specimen B1.0%

11.2 Comparison and Analysis of the Results

11.3.1 Effect of the fibres on shear resistance and member response

A comparison of the values for the maximum shear capacities, V_{exp} , of all the specimens is given in Table 11-1. A comparison of the load-deflection responses for the various specimens is shown in Fig. 11.7(a). By examining these results one can make two main conclusions: (1) the addition of fibres increases the shear resistance of a shear-deficient beam, and (2) the addition of a sufficient amount of fibres can transform the brittle failure response of a shear deficient beam into a flexural failure.

Table 11-1: Maximum shear and deflection for the various beam specimens

Beam specimen	% Fibres	Maximum Shear capacity V_{exp} (kN)	Increase in Resistance $\frac{(V_{exp} - V_{exp_{0\%}})}{V_{exp_{0\%}}}$	Deflection at Maximum Resistance Δ_{exp} (mm)	Maximum Deflection Δ_{max} (mm)
B0.0%	0.0	36.5	---	4.8	4.8
B0.5%	0.5	47.5	30 %	7.8	7.8
B1.0%	1.0	56.5	55 %	10.6	31.8

Specimen B0.0% showed a behaviour that is characteristic of shear-critical beams in that the response showed a brittle and sudden shear failure at relatively low load and deflection.

In terms of improving shear resistance, the addition of 0.5% fibres has increased the capacity of the beam by 30% (when compared to Specimen B0.0%). Furthermore the specimen was able to sustain 1.65 times as much deflection before failure.

Likewise, the addition of 1% fibres has resulted in an increase of 55% in the resistance of the beam. The deflection at maximum resistance showed a two-fold increase when compared to the deflection obtained for the plain reinforced concrete member.

The comparison of the specimen responses shows that although the addition of fibres in a quantity of 0.5% has allowed the beam to reach an improved level of shear resistance, this quantity of fibres was not sufficient in order to avoid a brittle shear failure. On the other hand the addition of fibres in a quantity of 1% transformed the failure response into a ductile flexural failure. What's more, the mid-span deflection for this member was nearly 32 mm at failure (an increase of nearly 700% over the maximum mid-span deflection of the specimen that was constructed without fibres) due to the more ductile failure mode associated with this specimen.

11.3.2 Effect of the fibres on controlling crack widths

Figure 11.7(b) shows a comparison of the maximum shear crack widths in the various beams as a function of load. From this plot one can see that the addition of fibres leads to a better control of crack widths. At a given load level, when compared to the results associated with the RC specimen constructed without fibres, the crack widths were smaller and developed in a more controlled manner in the case of the SFRC specimens (with the 1% fibre content providing the best results).

Furthermore, while the plain concrete member was only able to resist a shear crack width of approximately 0.05 mm before the brittle shear failure occurred, for the specimen constructed with 1% fibres, the shear cracks developed in a steady and controlled manner in both shear spans before the main shear crack reached a maximum width of 1 mm. The result for Specimen B0.5%, although not as dramatic, showed that the beam was able to resist a maximum crack width of nearly 0.2 mm prior to the formation of the shear failure mechanism, giving slight warning that failure of the beam was immanent.

In terms of flexural cracking, one can see that in the case of the beams that experienced a brittle shear failure (B0.0% and B0.5%), the flexural cracks were still relatively small (< 0.3 mm) when failure occurred. This is problematic since the shear cracks developed very suddenly, giving no warning of the impending brittle shear failure. On the other hand, the 1% fibre quantity allowed the beam to reach flexural yielding, and therefore a steady and controlled increase in the flexural crack widths was observed for this specimen. This allowed one to have sufficient warning that the failure of the beam was occurring.

11.3.3 Effect of the fibres on cracking patterns

Figure 11.7(d) compares the amount of cracks that were developed in the two shear spans as well as the constant moment regions of the specimens. Figure 11.8 shows a comparison of the crack patterns for the three tested specimens.

Specimen B0.0% contained neither fibres nor any shear reinforcement, and hence this specimen displayed comparatively large crack widths and crack spacings. The moderate fibre content in Specimen B0.5%, led to reductions in crack widths. However this fibre content did not significantly alter the spacing between the cracks.

The most impressive result is attributed to Specimen B1.0%. The higher fibre content that was used in this specimen led to both reductions in crack spacing and crack widths. Furthermore the addition of fibres in this specimen led to a more diffused cracking pattern. For instance, in addition to reductions in crack widths, "forking" crack patterns were observed, with the development of many secondary cracks that grew out of the primary cracks. These cracking patterns which are a consequence of the bridging action of the fibres (and resulting improvements in tension stiffening) resulted in the reductions in observed crack widths. Furthermore, as a result, even when the main shear crack formed, the beam was still able to resist further load due to the ability of the fibres to transmit stresses between the cracks, and hence the shear capacity of the member was able to increase further until the full flexural resistance of the beam was attained.

11.3.4 The use of fibres to replace traditional transverse reinforcement

From these results, it is evident that fibres can have a positive influence on controlling crack formation, and increasing shear resistance. Furthermore, if a sufficient quantity of fibres is added to the concrete matrix this can lead to a transformation in the failure mode of shear deficient beams allowing the beam to achieve its full flexural capacity thereby avoiding a brittle shear failure.

Hence, from the results of this experimental program, one can conclude that the addition of a sufficient quantity of fibres can partially substitute for conventional transverse reinforcement. This could lead to improvements in constructability and to potential savings in associated material and labour costs.

However, the results also showed the importance of selecting the most efficient fibre quantity for a given beam, which we may call the “critical” fibre content. Adding fibres in a quantity lower than the critical content, results in a beam that does not show a ductile failure response. On the other hand, adding fibres beyond the critical content, will not lead to an increase in resistance. Rather beyond this critical fibre content, the addition of fibres will lead to improvements in ductility and crack control. Hence, it is important for the design engineer to be able to select the most appropriate fibre content in order to provide a safe design, while also minimizing material costs.

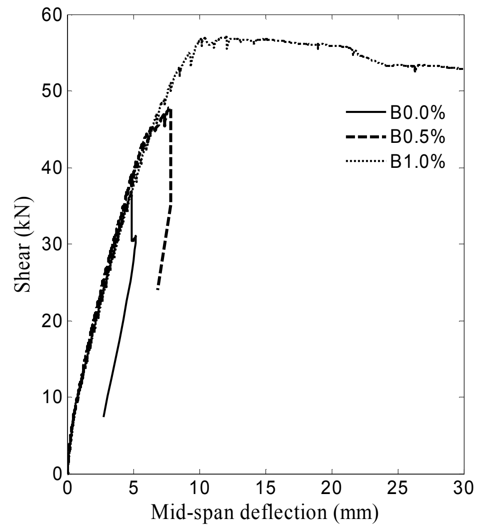

(a) Comparison of the member responses

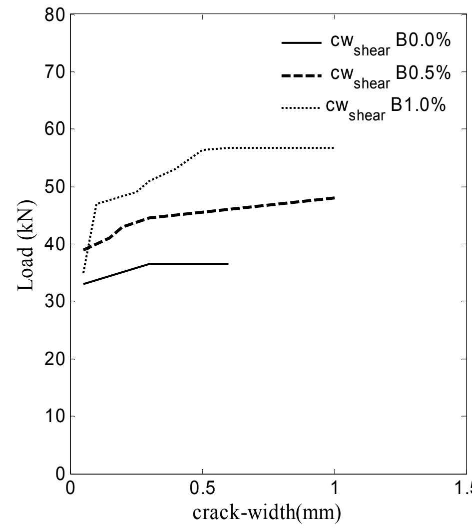

(b) Comparison of maximum crack widths (shear)

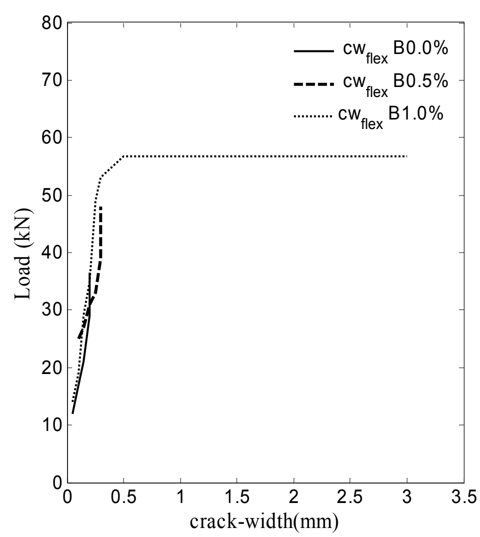

(c) Comparison of maximum crack widths (flexural)

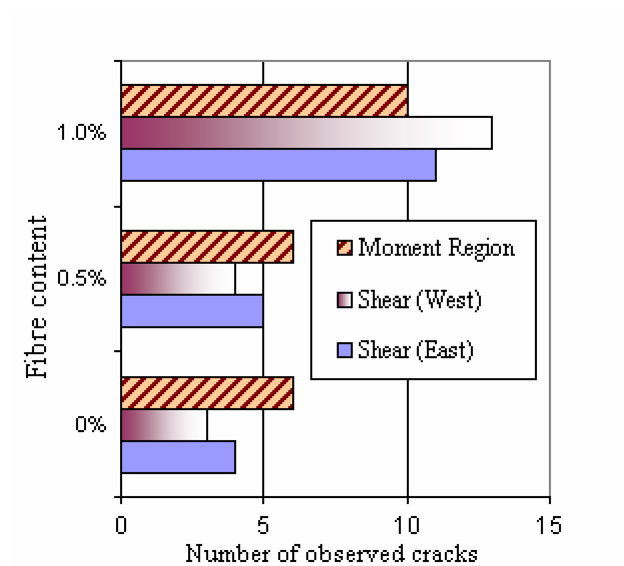

(d) Comparison of number of cracks in each specimen.

Figure 11.7: Comparison of the Experimental results

<table>
<tr><td>0% fibres</td><td>- Large crack widths
- Large spacing between cracks</td></tr>
<tr><td colspan="2">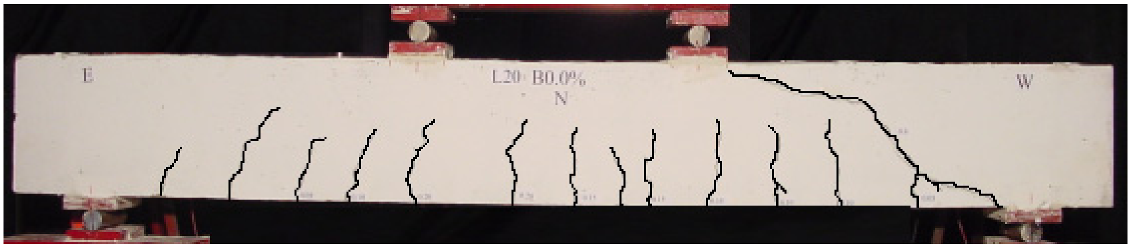
</td></tr>
<tr><td>0.5% fibres</td><td>- Reduced crack widths at equivalent load stages
- Similar spacing between cracks</td></tr>
<tr><td colspan="2">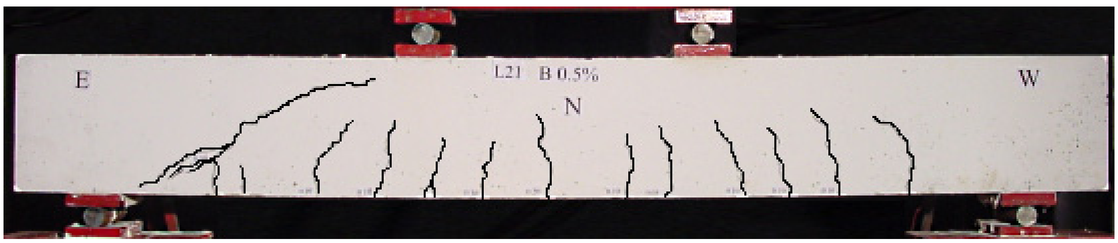
</td></tr>
<tr><td>1% fibres</td><td>- Reduced crack widths at equivalent load stages
- Development of flexural cracks in a steady and stable manner
- Reduced spacing between cracks
- “forking” cracking patterns</td></tr>
<tr><td colspan="2">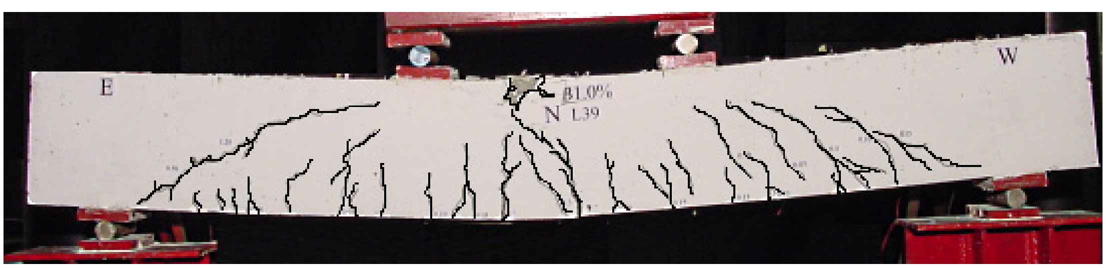
</td></tr>
</table>

Figure 11.8: Comparison of cracking patterns at failure for the specimens

Chapter 12 Modelling the Influence of Fibres in Beams Containing SFRC

12.1 Chapter Overview

In this chapter, a model is presented for the prediction of the maximum shear resistance of beams containing SFRC. Section 12.2 to 12.4 present a method for predicting the shear strength of SFRC beams. Section 12.5 compares the experimental results to those predicted using the model. In Section 12.6, the design equations are validated using experimental results available in the literature.

12.2 Model for Evaluating the Shear Resistance of SFRC Beams

There are several empirical relationships that have been proposed in the literature to predict the shear strength of SFRC (Li et al., 1992, Ashour et al., 1992, Mansur et al., 1986). In this study a model is presented in order to get an accurate prediction of the shear resistance of such fibre reinforced structural elements.

It is reasonable to assume that the improvement in the shear resistance of SFRC beams arises due to the much improved post-cracking tensile resistance of the concrete when fibres are added to the matrix. Hence, one can infer that the shear resistance of a SFRC beam can be equivalent to the expected shear resistance of a traditional reinforced concrete beam plus the additional shear resistance provided by the fibres due to the improved post-cracking resistance of the SFRC

Section 12.3 presents several methods that can be used in order to obtain the expected contribution neglecting the fibres, while Section 12.4 presents the model for predicting the fibre contribution. In order to compute the contribution of the fibres to shear resistance, the model uses a simple iterative procedure.

12.3 Predicting the Shear Resistance of RC Beams

There are several methods that can be used in order to compute the expected shear resistance of RC beams constructed without fibres. In this study, the modified compression field theory (MCFT) as well the general method described in the CSA Standard can be used in order to obtain an estimation of the shear resistance of the beams neglecting the effect of the fibres, V_{no}. These prediction methods are detailed further in the sections that follow.

12.3.1 MCFT method

One of the more effective and rational methods that can be used for the evaluation of the shear resistance of RC beams is the "modified compression field theory" (MCFT) (Collins et al., 1996). The more convenient way to solve the equilibrium, compatibility and stress-strain relationships of the MCFT theory is to use a computer program (Collins et al., 2006). In this study, the program Response 2000, which was developed at the University of Toronto by Bentz (2000) is used for this purpose. The quantity $V_{n\,MCFT}$ is the shear resistance that is computed using this approach.

12.3.2 CSA general method

The analytical method presented in the CSA Standard (CSA, 2004) for the evaluation of the nominal shear capacity of RC beams is given by Eq. 12-1.

$$V_n = V_c + V_s \qquad 12\text{-}1$$

Where the concrete and transverse steel contributions to shear strength, V_c and V_s, are computed using Eq. 12-2 and 12-3.

$$V_c = \phi_c \lambda \beta \sqrt{f_c'}\, b_w d_v \qquad 12\text{-}2$$

$$V_s = \frac{\phi_s A_v f_y d_v \cot\theta}{s} \qquad 12\text{-}3$$

The value β accounts for the ability of the concrete to transmit tensile stresses between the cracks and is limited by the ability to transmit shear stresses across cracks by aggregate interlock. The angle θ is the angle of inclination of the diagonal compressive stresses to the longitudinal axis of the member (CSA, 2004).

The CSA standard gives several different procedures for calculating the factor β and the angle θ. In the simplified method, θ is taken to be 35^{o} while β is computed according to the simplified relationships presented in Clause 11.3.6.3 of the 2004 CSA Standard.

In addition to the simplified design method, the 2004 CSA standard includes a "general design method" based on the equations of the modified compression field theory (MCFT). This "general method", which is presented in Clause 11.3.6.4 of the 2004 CSA standard, allows one to compute the θ and β values using simplified equations that have been derived based on the MCFT. The relationships take into account the effects of axial load and bending moment on the shear capacity. The details regarding this method are discussed further in Section 2.53 of the Literature Review.

For the purpose of predicting the nominal shear resistance of the beams, the material resistance factors for concrete and steel, ϕ_c and ϕ_s are taken as 1.0. The quantity $V_{n\,CSA}$ is used to represent the shear resistance that is computed using this approach.

12.4 Predicting the Shear Resistance of SFRC Beams

12.4.1 Iterative procedure

The influence of the fibres on the shear resistance of the beams can be related to their pullout strength. The expected maximum pullout strength of a single fibre, $F_{pullout}$, can be accurately estimated using Eq. 9-3 which was presented in Chapter 9. The effective number of fibres per unit area, N_{fibres}, for fibres randomly oriented in three dimensions can be calculated using Eq. 6-5 that was presented in Section 6.4.1 of this thesis.

Shear forces in a beam will cause diagonal tensile stresses to develop which will in turn cause inclined cracks that will result in fibre pullout. However as illustrated in Fig. 12.1, the shear stresses in a beam will result in crack slip, and hence it is expected that there will be a reduction in the pullout efficiency of the fibres when compared to the pullout in the case of pure tensile loading. In order to account for this phenomenon, a shear factor, α_v (where $\alpha_v = 0.83$) is used to scale the pullout resistance of the fibres ($\alpha_v F_{pullout}$), as they resist tension at the crack while undergoing a shear deformation (see Fig. 12.1(b)). This factor on the pullout resistance was empirically determined by comparing the predicted shear strengths using the procedure in this section with the experimental results from this study and from other researchers (see references in Table 12-3).

From the free-body diagram in Fig. 12.2 for an SFRC beam with a crack inclination, θ, one can compute the influence of the fibres on the shear resistance of the beam. If one considers that the fibres are perpendicular to the cracking plane, then the fibre contribution to shear resistance, V_{fib}, can be computed using Eq. 12-4

$$V_{fib} = \left(N_{fibres} \times \alpha_v F_{pullout}\right) \times b_w d_v \times cot\,\theta \qquad 12\text{-}4$$

Where b_w represents the width of the beam (in mm) and the value d_v is computed using Eq. 12-5, where d represents the effective depth of the beam (in mm).

$$d_v = 0.9d \qquad 12\text{-}5$$

The expected angle of inclination, θ, of the principal compressive stresses in the concrete (which can be used to approximate the angle to be formed by the shear crack) can be calculated using the procedure outlined in Clause 11.3.6.4 of the 2004 CSA Standard. Equation 12-6 is used to calculate the angle of inclination, θ, of the diagonal compressive stresses:

$$\theta = (\varepsilon_x \times 7000) + 29^\circ \qquad 12\text{-}6$$

The quantity, ε_x, is the longitudinal strain at mid-depth of the cross-section. For the case of moment and shear:

$$\varepsilon_x = \frac{\left(\frac{M}{d_v}\right) + V}{2 \times E_s \times A_s} \qquad 12\text{-}7$$

An iterative solution is necessary to solve for the shear capacity because one of the main parameters, ε_x, is a function of the shear V. In order to solve for the shear capacity, the shear, V, in Eq. 12-7 can initially be taken as the maximum expected shear resistance of the beam neglecting the effect of fibres (V_{no}). For the loading configuration used in this study, Eq. 12-8 can be used in order to compute the corresponding moment in the beam, M at a distance d/2 from the maximum moment, where a represents the shear span of the beam:

$$M = V \times \left(a - \frac{d}{2}\right) \qquad 12\text{-}8$$

Using the initial estimate, V_{no}, the strain, ε_x, the angle, θ and the fibre contribution to the shear resistance, V_{fib} can be estimated. This enables a new estimate of the shear resistance of the beam including the influence of the fibres to be determined using Eq. 12-9 as:

$$V_{nf} = V_{fib} + V_{no} \qquad 12\text{-}9$$

This procedure is repeated until a satisfactory conversion is attained for V_{nf}. The fibres will cause the shear resistance of the beam to increase, which will in turn cause ε_x and θ

to increase. The change in ε_x will cause a decrease in β which will in turn cause a decrease in the expected concrete contribution to shear resistance (V_{no}). Furthermore the increase in θ will lead to a reduction in the expected fibre contribution to the shear resistance (V_{fib}). Hence an iterative approach should be used to arrive at a correct estimate of V_{nf}. This procedure is summarized in the flowchart shown in Fig. 12.3.

It is assumed that the contribution of the fibres to the flexural capacity is negligible. Therefore it is noted that in predicting the shear resistance it is necessary to limit the predicted shear capacity such that the flexural capacity ($M_{\max}$) is not exceeded. Hence, V_{nf}, should be limited as shown in Eq. 12-10.

$$\text{If} \quad V_{nf} > \left[V_{max} = \left(\frac{M_{max}}{a} \right) \right] \xrightarrow{then} V_{nf} = V_{max} \qquad \text{12-10}$$

12.4.2 Semi-empirical procedure

The increase in shear resistance due to the positive influence of the fibres will cause an increase in both ε_x and θ. This will in turn cause a decrease in the concrete and fibre contributions to shear resistance.

In lieu of using the iterative procedure presented in the previous section, a semi-empirical equation can be used. It is noted that for a given increase in shear resistance, the relative increase in ε_x and θ will be more important in the case of a beam with a higher expected moment. Based on this assumption, Eq. 12-11 can be used to compute a "participation factor", κ_{eff}, that indirectly accounts for the expected decrease in the fibre and concrete contributions.

$$\kappa_{eff} = \left(\frac{1.77 \times V \times d_v}{M} \right)^{1.23} \qquad \text{12-11}$$

It is noted that κ_{eff} is assumed to be inversely proportional to $\frac{M}{Vd}$ which is equal to $\frac{a}{d}$.

Using this factor, the effective shear contribution of the fibres, $V_{fib,eff}$, can be computed using Eq. 12-12:

$$V_{fib,eff} = V_{fib} \times \kappa_{eff} \qquad 12\text{-}12$$

Thereafter, the shear resistance of the beam including the influence of the fibres can be calculated using Eq. 12-13.

$$V_{nf} = V_{fib,eff} + V_{no} \qquad 12\text{-}13$$

As discussed previously, V_{nf}, should not exceed the shear corresponding to the flexural resistance of the beam. Figure 12.4 outlines the steps involved using this approach.

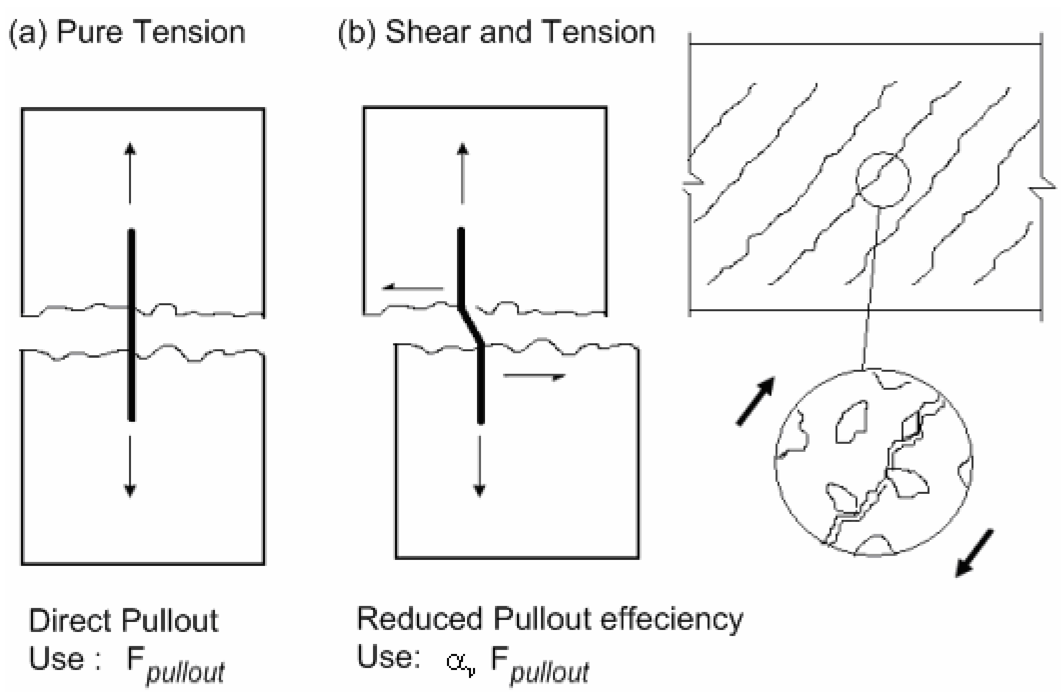

Figure 12.1: Pullout contribution in direct tension and the reduced pullout resistance in combined tension and shear

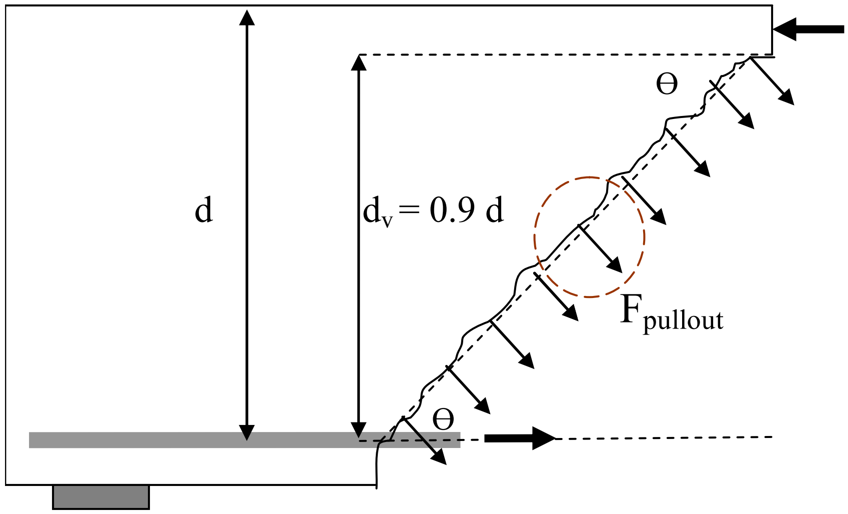

(a) Fibres crossing shear crack

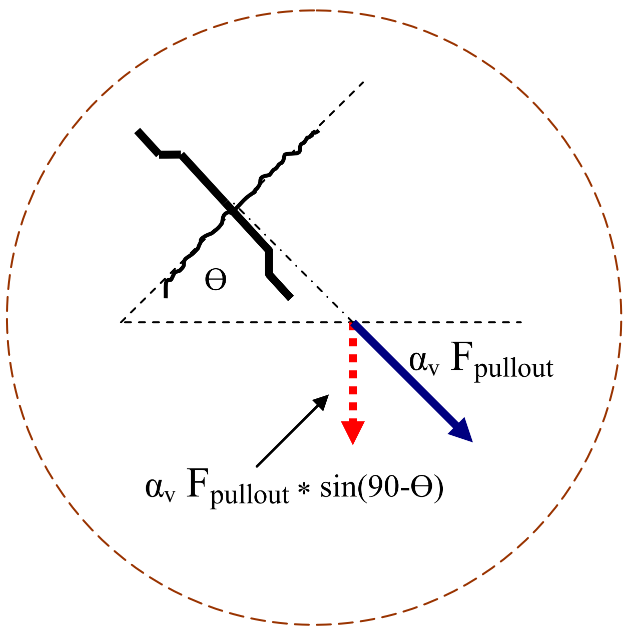

(b) Contribution of one fibre to shear resistance

$$V_{fib} = N_{fibers} \times \left[\alpha_v F_{pullout} \times sin(90-\theta)\right] \times \left(\frac{b_w d_v}{sin\,\theta}\right)$$

(c) Contribution of randomly oriented fibres to shear resistance

Figure 12.2: Fibre contribution to shear resistance as a function of fibre pullout

Step 1:

- Calculate $F_{pullout}$ using Eq. 9-3
- Calculate N_{fibres} using Eq. 6-5

Step 2:

Using $V = V_{no}$ and $M = V \times \left(a - \frac{d}{2}\right)$:

- Calculate ε_x using Eq. 12-7
- Calculate θ using Eq. 12-6

Step 3:

- Calculate V_{fib} using Eq. 12-4

Step 4:

- Obtain an initial estimate of the shear resistance $\{V_{nf}\}_i = V_{fib} + V_{no}$

Step 5: Iterative Procedure

Iterate to obtain the correct value of V_{nf}.

- Start with $\{V_{nf}\}_i$ from **step 4**.
- Revise the calculation for ε_x and θ by taking $V = \{V_{nf}\}_i$
- Revise calculation for β and calculate $V_{no} = V_{n\,CSA}$
- Revise calculation for V_{fib}
- Revise the calculation for the shear resistance of the beam $\{V_{nf}\}_{i+1} = V_{fib} + V_{no}$

Step 6: Check Accuracy

Compare $\{V_{nf}\}_{i+1}$ with $\{V_{nf}\}_i$ by calculating the error, $e = \left| \frac{\{V_{nf}\}_{i+1} - \{V_{nf}\}_i}{\{V_{nf}\}_i} \right|$

- If $e > 5\%$: Repeat **Step 5**, with $\{V_{nf}\}_{i+1}$
- If $e \leq 5\%$: then $V_{nf} = \{V_{nf}\}_{i+1}$
    - Check that flexural capacity is not exceeded using Eq. 12-10

Figure 12.3: Iterative procedure for obtaining the shear resistance of SFRC beams

Step 1:

- Calculate $F_{pullout}$ using Eq. 9-3
- Calculate N_{fibres} using Eq. 6-5

Step 2:

Using $V = V_{no}$ and $M = V \times \left(a - \frac{d}{2} \right)$:

- Calculate ε_{x} using Eq. 12-7
- Calculate θ using Eq. 12-6

Step 3:

- Calculate V_{fib} using Eq. 12-4

Step 4:

- Calculate the fibre contribution to shear resistance:
  $V_{fib} = \left(N_{fibers} \times \alpha_{v} F_{pullout} \right) \times \left(b_{w} \times d_{v} \right) \times cot(\theta)$

Step 5:

- Compute the participation factor : $\kappa_{eff} = \left(\frac{1.77 \times V_{n} \times d_{v}}{M_{n}} \right)^{1.23}$
- Calculate the effective fibre contribution to shear: $V_{fib,eff} = V_{fib} \times \kappa_{eff}$

Step 6:

- Calculate the shear resistance of the beam including the influence of the fibres
  $V_{nf} = V_{fib,eff} + V_{no}$

Figure 12.4: Steps involved in using the semi-empirical procedure to calculate V_{nf}

12.5 Strength Predictions

The proposed equations have been used to estimate the maximum shear capacities of the specimens that were tested in this experimental program. The results of this analysis are presented in Tables 12-1 to 12-3.

Table 12-1, shows the results of the analysis. One can see that there is good agreement between the actual and estimated results. Furthermore the model was able to predict that the addition of fibres in Beam B1.0% would lead to a flexural failure. Table 12-2 compares the results obtained using the semi-empirical equation to those obtained experimentally. It can be seen that this approach provides reasonably accurate predictions.

Table 12-1: Model predictions for the tested beams

Beam Specimen	Concrete contribution V_{no}	Predicted shear resistance V_{nf}	Experimentally obtained shear resistance V_{exp}	Accuracy $\left(\frac{V_{exp}}{V_{nf}}\right)$
B0.0%	30.8	30.8	36.5	1.19
B0.5%	29.8	44.0	47.5	1.08
B1.0%	29.0	59.1 … 53.3	56.5	1.06

Table 12-2: Empirical Model predictions for the tested beams

Beam Specimen	Concrete Contribution V_{no}	Fibre contribution to shear resistance $V_{fib_{eff}}$	Predicted shear resistance V_{nf}	Experimentally obtained shear resistance V_{exp}	Accuracy $\left(\frac{V_{exp}}{V_{nf}}\right)$
B0.0%	30.4	---	30.4	36.5	1.19
B0.5%	29.3	13.5	43.2	47.5	1.09
B1.0%	28.6	27.0	56.8 … 53.3	56.5	1.06

12.6 Validation with Results Available in the Literature

It should be noted that many of the experimental tests available in the literature present the results of beams that had a shear-span-to-depth ratio (a/d) less than 2.5. Such beams carry load by strut and tie action and in such cases the strength of the beams is strongly influenced by the details near the supports (Collins and Mitchell, 1997). Hence, the response of such beams should not be predicted using the same procedure as in the case of beams that have an a/d ratio that is greater than 2.5. Therefore in the present analysis only those beams that had a shear-span-to-depth ratio that was greater or equal to 2.5 were considered.

The procedures described in this chapter were used to predict the shear capacities of beams from 7 experimental studies. Table 12-3 and Fig. 12.5 and 12.6 present the results of this analysis. One can see that the predicted capacities obtained using the analytical model agree well with the experimentally obtained shear capacities (see Fig. 12.5).

Furthermore, the predictions obtained using the semi-empirical method compare very well with the experimental results (see Fig. 12.6).

Table 12-3: Model predictions for a wide range of experimental data available in the literature

Author	Beam I.D.	f'_c (Mpa)	v_f (%)	L_f (mm)	d_f (mm)	ρ (%)	b_w (mm)	h (mm)	d (mm)	$\frac{a}{d}$	V_{exp} (Mpa)	Iterative method		Semi-Empirical method	
												V_{nf} (Mpa)	$\left(\frac{V_{exp}}{V_{nf}}\right)$	V_{nf} (Mpa)	$\left(\frac{V_{exp}}{V_{nf}}\right)$
Montesinos et al. (2006)	B4	38.1	1	30	0.5	2.7	152	457	381	3.4	148.4	159	0.93	128	1.15
	B11	49.2	1	30	0.5	2.7	152	457	381	3.5	148.4	159	0.93	143	1.04
Rosenbusch (2002)	1.2/2	46.9	0.25	60	0.9	3.6	200	300	260	3.5	109.7	103	1.07	103	1.07
	1.2/3	43.7	0.51	60	0.9	3.6	200	300	260	3.5	120.1	123	0.97	116	1.03
	1.2/4	48.3	0.76	60	0.9	3.6	200	300	260	3.5	155.0	147	1.05	134	1.15
	2.2/2	40	0.25	60	0.9	1.2	200	300	260	2.5	81.6	76	1.07	85	0.96
	2.2./3	38.7	0.76	60	0.9	1.2	200	300	260	2.5	107.1	97	1.10	97	1.10
	2.4/2	40	0.25	60	0.9	1.8	200	300	260	2.5	107.6	88	1.22	96	1.12
	2.4/3	38.7	0.76	60	0.9	1.8	200	300	260	2.5	144.0	127	1.13	139	1.03
	2.6/3	41.2	0.25	60	0.9	1.8	200	300	260	4	82.2	78	1.05	76	1.08
	2.6/3	40.3	0.76	60	0.9	1.8	200	300	260	4	117.0	99	1.19	99	1.19
Cucchiara et al. (2004)	A10	41.2	1	30	0.5	1.9	150	250	219	2.8	96.4	81	1.19	86	1.13
	A20	41.2	2	30	0.5	1.9	150	250	219	2.8	103.3	115	0.90	115	0.90
Ashour et al. (1992)	B/4/0.5/A	92	0.5	60	0.8	2.8	125	250	215	4	63.0	72	0.87	58	1.09
	B/4/1.0/A	92	1	60	0.8	2.8	125	250	215	4	84.0	80	1.05	74	1.13
	B/4/1.5/A	92	1.5	60	0.8	2.8	125	250	215	4	94.0	80	1.17	80	1.17
	B/6/0.5/A	92	0.5	60	0.8	2.8	125	250	215	6	47.0	53	0.88	45	1.05
	B/6/1.0/A	92	1	60	0.8	2.8	125	250	215	6	50.0	53	0.94	53	0.94
	B/6/1.5/A	92	1.5	60	0.8	2.8	125	250	215	6	53.0	53	0.99	53	0.99

Author	Beam I.D.	f'_c (Mpa)	v_f (%)	L_f (mm)	d_f (mm)	ρ (%)	b_w (mm)	h (mm)	d (mm)	$\frac{a}{d}$	V_{exp} (Mpa)	Iterative method		Semi-Empirical method	
												V_{nf} (Mpa)	$\left(\frac{V_{exp}}{V_{nf}}\right)$	V_{nf} (Mpa)	$\left(\frac{V_{exp}}{V_{nf}}\right)$
Lim et al. (1992)	A0.5/3.5	34	0.5	30	0.5	1.2	152	254	221	3.5	45.2	42	1.08	42	1.08
	A1.0/3.5	34	1	30	0.5	1.2	152	254	221	3.5	47.0	42	1.12	42	1.12
	B0.5/3.5	34	0.5	30	0.5	2.4	152	254	221	3.5	49.4	63	0.79	61	0.81
	B1.0/3.5	34	1	30	0.5	2.4	152	254	221	3.5	67.4	77	0.87	77	0.87
Mansur et al. (1986)	B0.5	24.2	0.5	30	0.5	1.4	150	225	197	2.8	52.5	45	1.16	46	1.13
	B0.75	24.2	0.75	30	0.5	1.4	150	225	197	2.8	60.0	52	1.17	54	1.11
	B1.0	24.2	1	30	0.5	1.4	150	225	197	2.8	65.0	57	1.13	57	1.13
	C0.5	24.2	0.5	30	0.5	1.4	150	225	197	3.6	45.0	42	1.06	38	1.16
	C0.75	24.2	0.75	30	0.5	1.4	150	225	197	3.6	47.5	45	1.07	45	1.07
	C1.0	24.2	1	30	0.5	1.4	150	225	197	3.6	50.5	45	1.13	45	1.13
	D0.5	24.2	0.5	30	0.5	1.4	150	225	197	4.4	38.0	37	1.04	34	1.11
	D0.75	24.2	0.75	30	0.5	1.4	150	225	197	4.4	41.0	37	1.12	37	1.12
	D1.0	24.2	1	30	0.5	1.4	150	225	197	4.4	44.0	37	1.21	37	1.21
Belghiti (2007)	BB 0.5	21.3	0.5	30	0.55	1.3	300	500	438	1.4	154.3	187	0.87	162	0.95
	BB 1.0	19.6	1	30	0.55	1.3	300	500	438	1.4	198.0	249	0.81	219	0.90
	BA 0.5	21.3	0.5	30	0.55	1.3	300	500	438	1.4	244.4	252	0.97	252	0.97
	BA 1.0	19.6	1	30	0.55	1.3	300	500	438	1.4	244.3	249	0.98	249	0.98

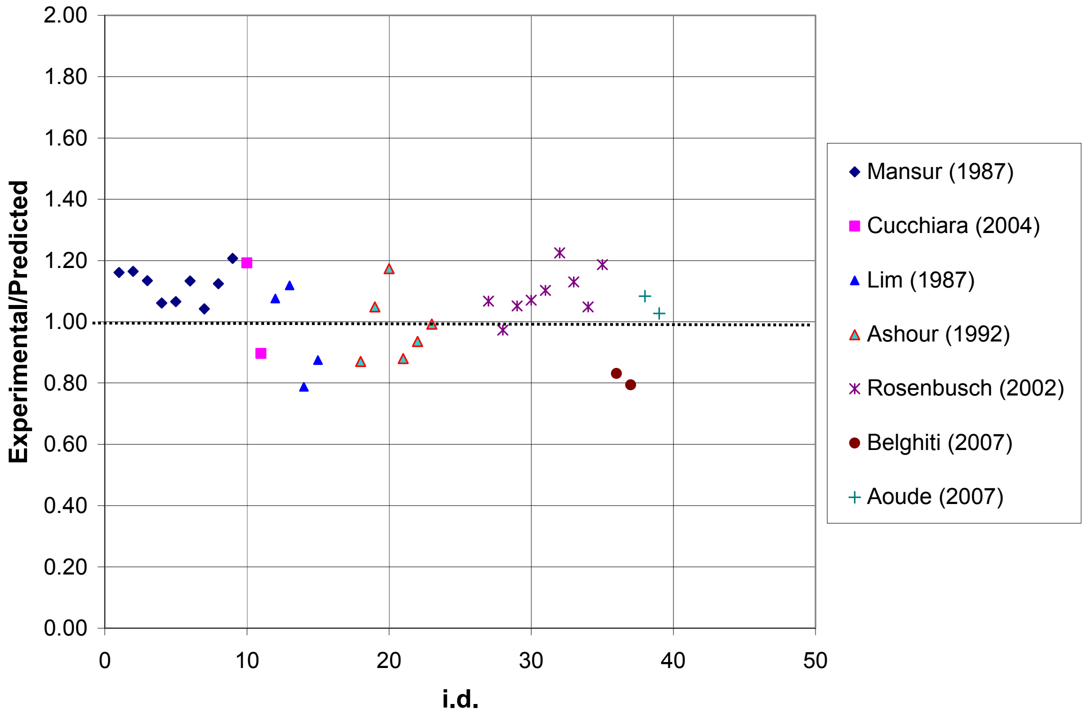

(a) Ratio of experimental and predicted shear capacities

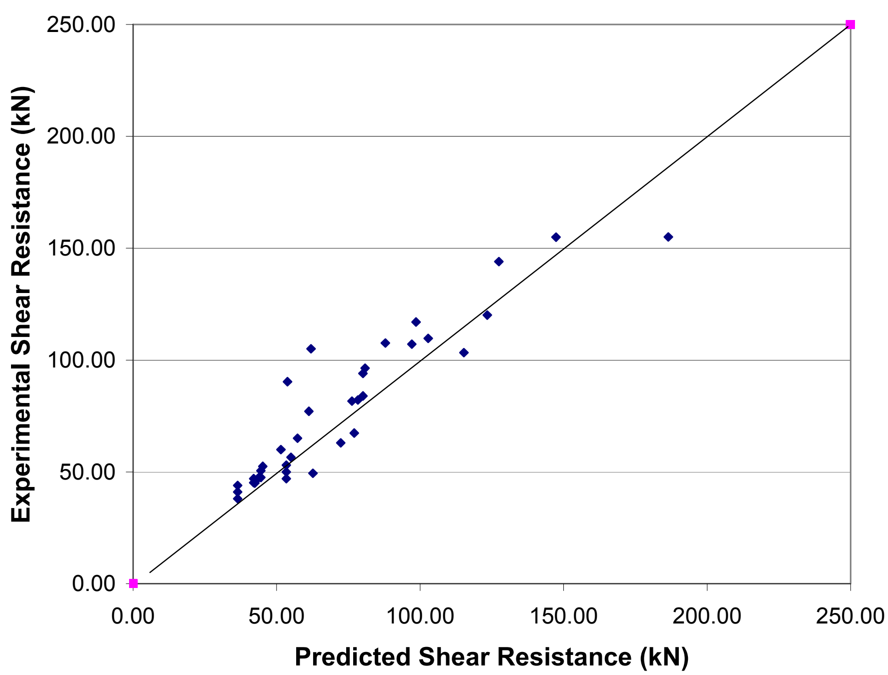

(b) Experimental versus predicted shear capacities

Figure 12.5: Accuracy of the iterative analytical method

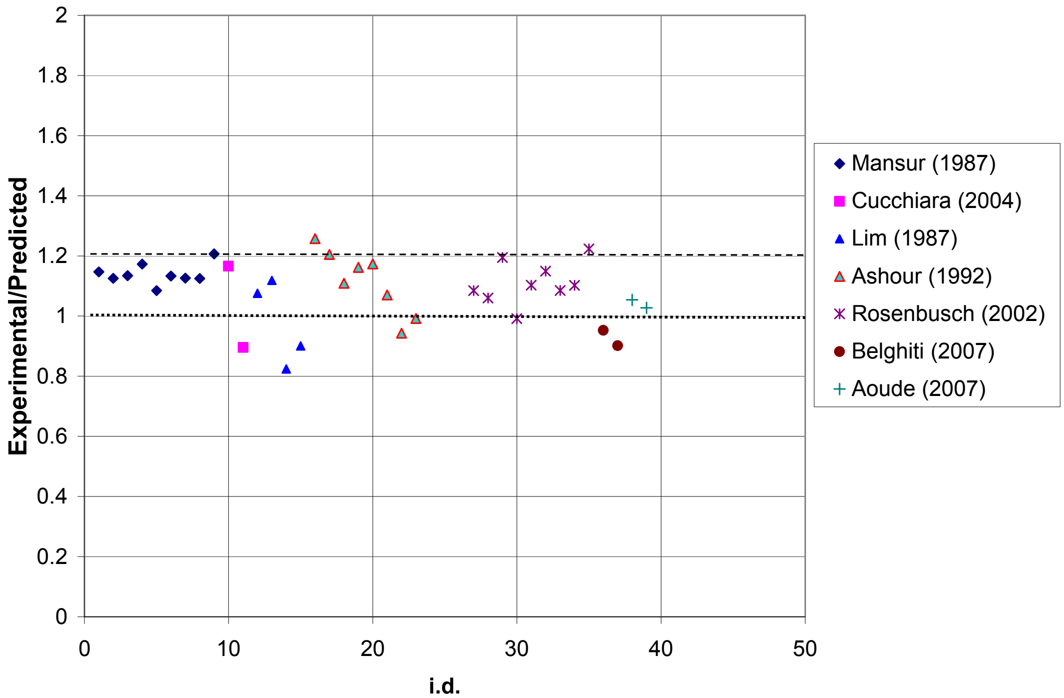

(a) Ratio of experimental and predicted shear capacities

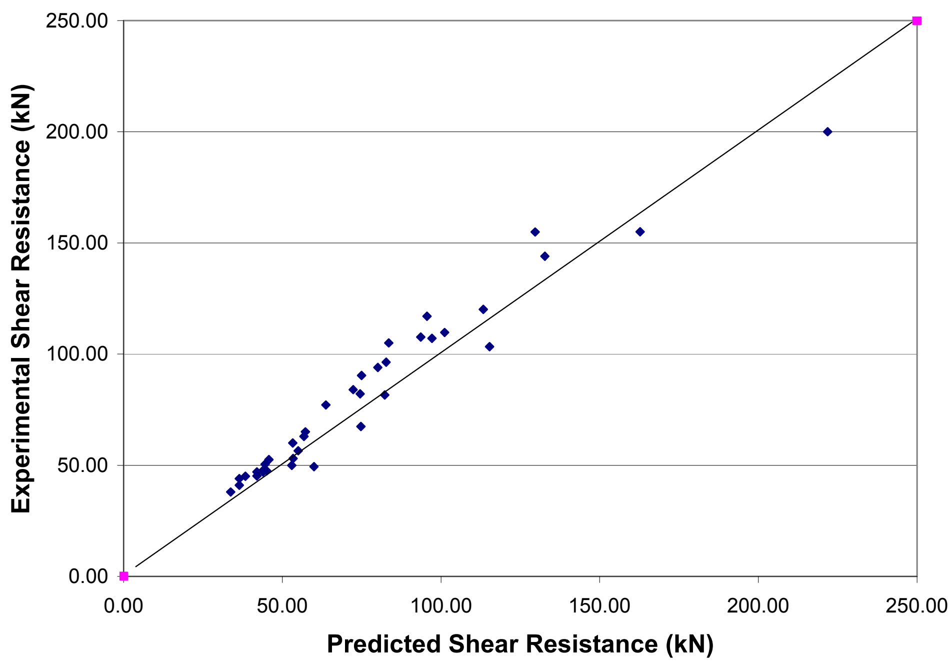

(b) Experimental versus predicted shear capacities

Figure 12.6: Accuracy of the semi-empirical method

12.7 Concluding Remarks

A procedure for predicting the influence of fibres on the shear capacity of beams was presented. This method uses an approach where the procedure in the General Method of the CSA Standard is adjusted for the presence of fibres based on the pullout strength of fibres in shear. The approach accounts for the influence of shear, moment and the contribution of the fibres. The method provides reasonably accurate predictions for a wide variety of beams tested in this research program and by other researchers. A semi-empirical method was also developed to estimate the beneficial effects of fibres on shear capacity.

Chapter 13 Conclusions

The purpose of this research program was to perform an experimental and analytical study on the performance enhancements from the use of steel-fibre reinforced concrete in reinforced concrete members. The conclusions based on the experimental and analytical programs are summarized below.

13.1 Experimental Program

13.1.1 Column specimens

Thirteen specimens constructed using plain and fibre reinforced concrete and containing varying amounts of transverse reinforcement were tested under pure axial compression loading. In addition seven companion specimens constructed without cover were also tested. These tests examined the influence of several parameters, including the effect of fibres on confinement, cover spalling and bar buckling. In addition a SCC concrete mix was used in an attempt to improve the workability of the SFRC. From this series of tests the following conclusions can be made:

(i) An addition of moderate amounts of fibres to SCC can lead to an adequately workable concrete mix. However, there is a limiting fibre content, above which the SCC mix can lose much of its workability leading to reduced fibre efficiency

(ii) The addition of steel fibres in reinforced concrete columns can lead to improvements, including the following enhancements:
- An increase in peak load carrying capacity of the column
- A significant improvement in the post-peak response of the column
- A transformation of sudden cover spalling into a gradual mechanism

(iii) The results showed that fibres can partially substitute for the transverse reinforcement in RC columns

13.1.2 Tension specimens

Three specimens containing varying amount of fibres were tested under pure tensile loading in order to examine the influence of fibres on tension stiffening. From this series of tests the following conclusions can be made:

(i) The addition of fibres improves the tension stiffening response of the concrete

(ii) The inclusion of fibres leads to improvements in crack control

(iii) The influence of the fibres on the tensile response was isolated and it was observed that the enhancement provided by the fibres can be linked to the expected pullout response of the fibres

13.1.3 Beam specimens

Three beam specimens containing varying fibre contents were tested in order to investigate the influence of steel fibres on the structural response of RC beam elements. From the results of this series of experiments, the following conclusions can be made:

(i) The addition of steel fibres enhances the maximum shear capacity of RC beams

(ii) An addition of a sufficient quantity of fibres leads to an improved ductility and can result eliminating brittle shear failures in shear deficient beams

(iii) A sufficient quantity of fibres can be used in order to partially substitute for conventional transverse reinforcement

(iv) The inclusion of fibres leads to improvements in crack control (with reductions in crack widths and crack spacings)

13.2 Analytical Program

Analytical models for the prediction of the behaviour of structural elements constructed with SFRC were developed:

(i) A model that can predict the compressive load-strain response of columns constructed with SFRC was developed. The model takes the following parameters into account:
   - The influence of the fibres in improving the peak load carrying capacity using an empirical equation that is a function of the confining effect provided by the randomly oriented fibres
   - The influence of fibres in improving the post-peak resistance of the columns based on the material stress-strain curve of SFRC
   - The influence of the fibres in delaying cover spalling

(ii) A model that can predict the tension stiffening curve of SFRC based on the pullout response of hooked-end steel fibres was presented.

(iii) A procedure that can be used to predict the maximum shear resistance of beams constructed with SFRC was presented. The influence of the fibres in improving the shear resistance is computed based on the pullout resistance of fibres in the situation of combined tension and shear.

13.3 Future Research

Suggestions for future research are given below:

(i) An experimental program on the reversed cyclic loading response of columns constructed with steel fibre reinforced concrete to examine the influence of cyclic loading on the ductility and response of SFRC columns

(ii) The behavioural models presented for the prediction of the compressive load-strain response of SFRC columns could be implemented in a computer program

(iii) Based on further experimental tests, expressions that can be used to introduce the influence of fibres in reducing the required hoop spacing in RC columns could be developed and implemented in codes of practice

(iv) The tension stiffening model could be implemented in a program that uses the MCFT method to calculate the response of RC beams subjected to shear

(v) Further fibre typologies could be used to examine the influence of fibre geometry on the response of structural members constructed with SFRC

Statement of Originality

The original contributions described in this thesis include:

(i) Thirteen full-scale specimens were tested in pure axial compression to assess the benefits of using steel fibres on the performance of columns. These specimens were constructed with and without fibres and contained varying amounts of transverse reinforcement consistent with column detailing requirements for different ductility levels.

(ii) Seven full-scale column specimens, constructed without cover and containing various amounts of fibres and transverse reinforcement, were tested in order to examine the influence of fibres on core confinement and cover spalling in SFRC columns

(iii) Tests were conducted on three specimens tested under pure axial tensile loading in order to study the influence of steel fibres on tension stiffening. The test specimens were constructed with different fibre contents.

(iv) Three full-scale beam specimens constructed without web reinforcement but containing various fibre contents were tested under four-point loading in order to study the influence of fibres on the shear resistance of RC beams.

(v) Analytical models that can be used to compute the complete load-strain response of SFRC columns were presented and used to predict the response of the column specimens that were tested in the experimental program

(vi) An analytical model that can be used to predict the tension stiffening response of SFRC was presented and validated using the experimental results from the tension test series

(vii) A procedure that can be used to predict the shear resistance of SFRC beams was developed. An additional simple empirical equation was also presented. Both methods were used to predict the shear capacities of the beams tested in this experimental program. In addition the models were also validated using a wide range of test data available in the literature

References

ABRISHAMI, H. H. & MITCHELL, D. (1997) Influence of steel fibers on tension stiffening. *ACI Structural Journal,* 94 (6)**,** 769-776.

ALWAN, J. M., NAAMAN, A. E. & HANSEN, W. (1991) Pull-out work of steel fibers from cementitious composites: Analytical investigation. *Cement and Concrete Composites,* 13 (4)**,** 247-255.

ARMELIN, H. S. & BANTHIA, N. (1997) Predicting the flexural postcracking performance of steel fiber reinforced concrete from the pullout of single fibers. *ACI Materials Journal,* 94 (1)**,** 18-31.

ASHOUR, S. A., HASANAIN, G. S. & WAFA, F. F. (1992) Shear behavior of high-strength fiber reinforced concrete beams. *ACI Structural Journal* 89 (2)**,** 176-184.

ASTM (1998) *C 1018: Standard test method for flexural toughness and first crack strength of fiber reinforced concrete* Philadelphia, American Society of Testing and Materials.

ASTM (1998b) *C 1399: Test method for obtaining average residual-strength of fiber-reinforced concrete,* Philadelphia, American Society of Testing and Materials.

BAE, S., MIESES, A. M. & BAYRAK, O. (2005) Inelastic buckling of reinforcing bars. *Journal of Structural Engineering,* 131 (2)**,** 314-321.

BANTHIA, N. & MINDESS, S. (1995) *Fiber Reinforced Concrete: Modern developments,* Vancouver, University of British Columbia Press.

BANTHIA, N. & MINDESS, S. (2004) Toughness characterization of fiber-reinforced concrete: which standard to use? *Journal of Testing and Evaluation,* 32 (2)**,** 138-42.

BANTHIA, N. & TROTTIER, J.-F. (1995) Test methods for flexural toughness characterization of fiber reinforced concrete: some concerns and a proposition. *ACI Materials Journal,* 92 (1)**,** 48-57.

BARROS, J. A. O. & FIGUEIRAS, J. A. (1999) Flexural behavior of SFRC: Testing and modeling. *Journal of Materials in Civil Engineering,* 11 (4)**,** 331-338.

BEKAERT (2007) Dramix steel fibres, http://www.bekaert.com/BUILDING , accessed May 3 2007.

BELGHITI, M. E. (2007) Shear behaviour of SFRC beams. *Department of Civil Engineering* Montreal, McGill University.

BENTZ, E. C. (2000) RESPONSE 2000: Reinforced concrete sectional analysis program. 1.05 ed. Toronto.

BENTZ, E. C. & COLLINS, M. P. (2006) Development of the 2004 Canadian Standards Association (CSA) A23.3 shear provisions for reinforced concrete. *Canadian Journal of Civil Engineering,* 33 (5)**,** 521-534.

BISCHOFF, P. H. (1983) Response of prestressed concrete tension members. *Department of Civil Engineering* Montreal, McGill University.

BISCHOFF, P. H. (2001) Effects of shrinkage on tension stiffening and cracking in reinforced concrete. *Canadian Journal of Civil Engineering,* 28 (3)**,** 363-374.

BISCHOFF, P. H. (2003) Tension stiffening and cracking of steel fiber-reinforced concrete. *Journal of Materials in Civil Engineering,* 15 (2)**,** 174-182.

BJERKLI, L., TOMASZEWICZ, A. & JANSEN, J. (1990) Deformation properties and ductility of high strength concrete. *Proceedings of the Second international symposium on utilization of high strength concrete.* Berkeley.

CAMPIONE, G. (2002) The effects of fibers on the confinement models for concrete columns. *Canadian Journal of Civil Engineering,* 29 (5)**,** 742-750.

CASSANOVA, P. (1996) Bétons renforcés de fibres métalliques: Du matériau à la structure. *Division Bétons et Ciments pour Ouvrages d'art* Paris, Ecole Nationale des Ponts et Chaussées.

CEB-FIP (1978) *Model code for concrete structures: CEB-FIP International recommendations,* Paris, Comité Euro-International du Béton.

CHANVILLARD, G. & AITCIN, P.-C. (1996) Pull-out behavior of corrugated steel fibers qualitative and statistical analysis. *Advanced Cement Based Materials,* 4 (1)**,** 28-41.

CMRI (2007) Hooked end steel fibres used in SFRC beam-column joint test, http://www.engineering.sdsu.edu/~sfrc, accessed May 1 2007.

COLLINS, M. P., BENTZ, E. C. & MITCHELL, D. (2006) Ch. 4: Shear and Torsion. *CAC Concrete Design Handbook.* Ottawa, Cement Association of Canada.

COLLINS, M. P. & MITCHELL, D. (1991) *Prestressed concrete structures,* Englewood Cliffs, Prentice Hall Inc.

COLLINS, M. P. & MITCHELL, D. (1997) *Prestressed concrete structures,* Toronto, Response Publications.

COLLINS, M. P., MITCHELL, D., ADEBAR, P. & VECCHIO, F. J. (1996) General shear design method. *ACI Structural Journal,* 93 (1)**,** 36-45.

CSA (2004) *CSA A23.3-04: Design of Concrete Structures,* Mississauga, Canadian Standards Association.

CUCCHIARA, C., LA MENDOLA, L. & PAPIA, M. (2004) Effectiveness of stirrups and steel fibres as shear reinforcement. *Cement and Concrete Composites,* 26 (7)**,** 777-786.

CUSSON, D. & PAULTRE, P. (1995) Stress-strain model for confined high-strength concrete. *Journal of Structural Engineering,* 121 (3)**,** 468-477.

DHAKAL, R. P. (2006) Post-peak response analysis of SFRC columns including spalling and buckling. *Structural Engineering and Mechanics,* 22 (3)**,** 311-330.

DUPONT, D. (2003) Modelling and experimental validation of the constitutive law and cracking behavior of Steel Fiber Reinforced Concrete. *Department of Civil Engineering.* Heverlee, Catholic Universty of Leuven.

FIELDS, K. & BISCHOFF, P. H. (2004) Tension stiffening and cracking of high-strength reinforced concrete tension members. *ACI Structural Journal,* 101 (4)**,** 447-456.

FOSTER, S. J. (2001) On behavior of high-strength concrete columns: Cover spalling, steel fibers, and ductility. *ACI Structural Journal,* 98 (4)**,** 583-589.

FOSTER, S. J. & ATTARD, M. M. (2001) Strength and ductility of fiber-reinforced high-strength concrete columns. *Journal of Structural Engineering,* 127 (1)**,** 28-34.

FOSTER, S. J., LIU, J. & SHEIKH, S. A. (1998) Cover spalling in HSC columns loaded in concentric compression. *Journal of Structural Engineering,* 124 (12)**,** 1431-1437.

GANESAN, N. & RAMANA MURTHY, J. V. (1990) Strength and behavior of confined steel fiber reinforced concrete columns. *ACI Materials Journal,* 87 (3)**,** 221-227.

GRUNEWALD, S. (2004) Performance-based design of self-compacting fibre reinforced concrete. *Department of Structural and Building Engineering.* Delft, Delft University of Technology.

GRUNEWALD, S. & WALRAVEN, J. (2001) Parameter-study on the influence of steel fibers and coarse aggregate content on the fresh properties of self-compacting concrete. *Cement and Concrete Research,* 31 (12)**,** 1793-1798.

GURJAR, A. (2004) MIx design and testing of self-consolidating concrete using florida materials. Daytona Beach, The Florida Department of Transportation.

HANNANT, D. J. (1978) *Fibre cements and fibre concretes,* New York, John Wiley and Sons.

HSU, L. S. & HSU, C.-T. T. (1994) Stress-strain behavior of steel-fiber high-strength concrete under compression. *ACI Structural Journal* 91 (4)**,** 448-457.

IMAM, M., VANDEWALLE, L. & MORTELMANS, F. (1995) Shear-moment analysis of reinforced high strength concrete beams containing steel fibres. *Canadian Journal of Civil Engineering,* 22 (3)**,** 462-470.

IMAM, M., VANDEWALLE, L., MORTELMANS, F. & VAN GEMERT, D. (1997) Shear domain of fibre-reinforced high-strength concrete beams. *Engineering Structures,* 19 (9)**,** 738-747.

JOHNSTON, C. (2001) *Fiber-reinforced cements and concretes,* Amsterdam, Gordon & Breach.

JSCE (1984) *Standrad SF-4: Method of test for flexural tougness and first crack strength of fiber reinforced concrete*, Japan Society of Civil Engineers.

KANI, G. N. J. (1964) Riddle of shear failure and its solution. *American Concrete Institute Journal,* 61 (4)**,** 441-467.

KENT, D. C. & PARK, R. (1971) Inelastic behavior of reinforced concrete members with cyclic loading. 4 (1)**,** 108-25.

KHAYAT, K. H. & ROUSSEL, Y. (2000) Testing and performance of fiber-reinforced, self-consolidating concrete. *Materials and Structures,* 33 (230)**,** 391-397.

KHUNTIA, M., STOJADINOVIC, B. & GOEL, S. C. (1999) Shear strength of normal and high-strength fiber reinforced concrete beams without stirrups. *ACI Structural Journal,* 96 (2)**,** 282-289.

KOEHLER, E. & FOWLER, D. (2003) Summary of concrete workability test methods. Austin, International Center for Aggregates Research, University of Texas at Austin.

KUTZING, L. (2000) Trafahigkeitsermittlung stahlfaserverstarkter Betone (in German). Stuggart, University of Leipzig.

KWAK, Y.-K., EBERHARD, M. O., KIM, W.-S. & KIM, J. (2002) Shear strength of steel fiber-reinforced concrete beams without stirrups. *ACI Structural Journal,* 99 (4)**,** 530-538.

LEE, C.-D. (1990) Consitutive modelling and flexural analysis of steel fiber reinforced concrete for structural apllications. *Department of Civil and Environmental Engineering.* Ann Arbor, Michigan State University.

LEGERON, F. & PAULTRE, P. (2003) Uniaxial confinement model for normal- and high-strength concrete columns. *Journal of Structural Engineering,* 129 (2)**,** 241-252.

LI, B., PARK, R. & TANAKA, H. (1994) Strength and ductility of reinforced concrete members and frames constructed using high strength concrete. Christchurch, Department of Civil Engineering, Uinversity of Canterbury.

LI, V. C. (2002) Large volume, high-performance applications of fibers in civil engineering. *Journal of Applied Polymer Science,* 83 (3)**,** 660-686.

LI, V. C., WARD, R. & HAMZA, A. M. (1992) Steel and synthetic fibers as shear reinforcement. *ACI Materials Journal,* 89 (5)**,** 499-508.

MAAGE, M. (1977) Interaction between steel fibers and cement based matricies. *Materials and Structures,* 10 (59)**,** 297-301.

MANDER, J. B., PRIESTLEY, M. J. N. & PARK, R. (1984) Seismic design of bridge piers. Christchurch, Department of Civil Engineering, Uinversity of Canterbury.

MANDER, J. B., PRIESTLEY, M. J. N. & PARK, R. (1988) Theoretical stress-strain model for confined concrete. *Journal of Structural Engineering,* 114 (8)**,** 1804-1826.

MANSUR, M. A., CHIN, M. S. & WEE, T. H. (1999) Stress-strain relationship of high-strength fiber concrete in compression. *Journal of Materials in Civil Engineering,* 11 (1)**,** 21-29.

MANSUR, M. A., ONG, K. C. G. & PARAMASIVAM, P. (1986) Shear strength of fibrous concrete beams without stirrups. *Journal of Structural Engineering,* 112 (9)**,** 2066-2079.

MASSICOTTE, B., MOSSOR, B., FILIATRAULT, A. & TREMBLAY, S. (1998) Compressive strength and ductility of steel fiber reinforced concrete columns. *ACI Special Publication SP182.* Farmington Hills, American Concrete Institute.

MINELLI, F. (2005) *Plain and fiber reinforced concrete beams under shear loading: Structural behavior and design aspects,* Brescia, Starrylink Editrice.

MITCHELL, D. & COLLINS, M. P. (1974) Diagonal Compression Field Theory: A rational model for structural concrete in pure torsion. *Journal of the American Concrete Institute,* 71**,** 396-408.

MITCHELL, D. & PAULTRE, P. (2006) Ch. 11: Seismic Design. *CAC Concrete Design Handbook.* Ottawa, Cement Association of Canada.

MORSCH, E. (1905) Bending tests on reinforced concrete beams (Biegungsversuche mit Armierten Betonbalken). *Schweizerische Bauzeitung*.

MUGURUMA, H., NISHIYAMA, M. & WATANABE, F. (1993) Stress strain curve for concrete with a wide range of compressive strengths. *Proceedings of Symposium on high strength concrete.* Lille-hammer.

NAGASHIMA, T., SUGANO, S., KIMURA, H. & ICHIKAWA, A. (1992) Monotonic axial compression test on ultra-high-strength concrete tied columns. *Proceedings of the World conference on earthquake engineering.* Madrid.

NAMMUR, G., JR. & NAAMAN, A. E. (1989) Bond stress model for fiber reinforced concrete based on bond stress-slip relationship. *ACI Materials Journal,* 86 (1)**,** 45-57.

NARAYANAN, R. & DARWISH, I. Y. S. (1987) Use of steel fibers as shear reinforcement. *ACI Structural Journal,* 84 (3)**,** 216-227.

NATARAJA, M. C., DHANG, N. & GUPTA, A. P. (1999) Stress-strain curves for steel-fiber reinforced concrete under compression. *Cement and Concrete Composites,* 21 (5)**,** 383-390.

NRCC (2005) *National Building Code of Canada* Ottawa, Canadian Comission on Building and Fire Codes, National Research Council of Canada (NRCC).

OZYILDIRIM, C. & LANE, D. S. (2003) Final report: Evaluation of self-consolidating concrete. Charlottesville, Virginia Transportation Research Council.

PARK, R., PRIESTLEY, M. J. N. & GILL, W. (1982) Ductility of square confined concrete columns *American Society of Civil Engineers, Journal of the Structural Division,* 108 (nST4)**,** 929-950.

PARRA-MONTESINOS, G. J., WIGHT, J. K., DINH, H. & LIBRRECHT, A. (2006) Shear strength of fiber reinforced concrete beams without stirrups. Ann Arbor, Uinversity of Michigan.

PAULTRE, P., KHAYAT, K. H., LANGLOIS, A., TRUDEL, A. & CUSSON, D. (1996) Structural performance of some special concretes. *Proceedings of the 4th International symposium on the utilization of high performance concrete.* Paris.

POPOVICS, S. (1973) Numerical approach to the complete stress strain curve of concrete. *Cement and Concrete Research,* 3 (5)**,** 583-599.

RAMESH, K., SESHU, D. R. & PRABHAKAR, M. (2003) Constitutive behaviour of confined fibre reinforced concrete under axial compression. *Cement and Concrete Composites,* 25 (3)**,** 343-350.

RAZVI, S. R. & SAATCIOGLU, M. (1999) Confinement model for high-strength concrete. *Journal of Structural Engineering,* 125 (3)**,** 281-288.

RICHART, F. E., BRANDTZAEG, A. & BROWN, R. L. (1928) Study of the failure of concrete under combined compressive stresses. *University of Illinois Engineering Experiment Station Bulletin,* 26 (12)**,** 102.

RICHART, F. E., BRANDTZAEG, A. & BROWN, R. L. (1929) Testing the failure of plain and spirally reinforced concrete in compression. *Contract Record and Engineering Review,* 43 (33)**,** 939-941.

RILEM (2002) Rilem TC 162-TDF: Test and design methods for steel fibre reinforced concrete - Bending test. *Materials and Structures,* 35 (253)**,** 579-582.

ROSENBUSCH, J. & TEUTSCH, M. (2002) Trial beams in shear. Technical Uinversity of Braunshweig.

ROSSI, P. (1998) *Les bétons de fibres métalliques,* Paris, Presses de l'Ecole nationale des ponts et chaussées.

SCOTT, B. D., PARK, R. & PRIESTLEY, M. J. N. (1982) Stress-strain behavior of concrete confined by overlapping hoops at low and high strain rates *Journal of the American Concrete Institute,* 79 (1)**,** 13-27.

SHARMA, A. K. (1986) Shear strength of steel fiber reinforced concrete beams. *Journal of the American Concrete Institute,* 83 (4)**,** 624-628.

SHARMA, U., BHARGAVA, P. & KAUSHIK, S. K. (2005) Comparative study of confinement models for high-strength concrete columns. *Magazine of Concrete Research,* 57 (4)**,** 185-197.

SHEIKH, S. A. & UZUMERI, S. M. (1980) Strength and ductility of tied concrete columns. 106 (5)**,** 1079-1102.

SHEIKH, S. A. & UZUMERI, S. M. (1982) Analytical model for concrete confinemnt in tied columns. *American Society of Civil Engineers, Journal of the Structural Division,* 108 (ST12)**,** 2703-2722.

VECCHIO, F. J. & COLLINS, M. P. (1986) Modified compression field theory for reinforced concrete lements subjected to shear *Journal of the American Concrete Institute,* 83 (2)**,** 219-231.

WAGNER, H. (1929) Metal beams with very thin webs *Zeitschrift fur Flugtechnik und Motorluftschiffahr,* 20 (8-12).

YONG, Y.-K., NOUR, M. G. & NAWY, E. G. (1988) Behavior of laterally confined high-strength concrete under axial loads *Journal of Hydraulic Engineering,* 114 (2)**,** 332-351.